Study on eco-hydro-geomorphological effects of sediment replenishment for efficient river habitat restoration

LIN JIAQI

2023

Acknowledge

I would like to thank Prof. Dr. Tetsuya Sumi, professor of Socio and Eco Environment Risk Management laboratory, Water Resources Research Center, Disaster Prevention Research Institute, Kyoto University for providing me with the opportunity to start my PhD study in his laboratory. He continuously encourages me and is always willing to assist my research in any way. Without his efforts in contact with river offices, I can not have the chance to learn about Japanese river systems and obtain sufficient data to continue my research.

I would like to say a special thank to Assoc. Prof. Dr. Sameh Ahmed Kantoush, my direct supervisor, in Socio and Eco Environment Risk Management laboratory, Kyoto University. He is always willing to conduct brainstorming with me and we together raise lots of novel research viewpoints. He always forgives my mistakes and encourages me to insist on my research directions. Without his help and enlightening, I can not come through the most difficult periods in numerical simulations. He advised me to publish more papers and participate in more international conferences and workshops for enhancing my scientific thinking. I am sure we will have more opportunities to collaborate in the future.

I would like to express my deep thanks to Assoc. Prof. Dr. Yasuhiro Takemon for his valuable suggestions in ecological analysis and field survey. His experience in using measuring instruments such as drones helps me to collect accurate topographical data in the field. Discussion with him is helpful for me to expand my research in aquatic habitats.

I would like to thank Mrs. Obara, Mrs. Ibaraki, and Mrs. Morimoto, secretary of our laboratory, for their help on my daily life and traveling. They are always kind and patient to listen and solve my issues.

I would like to thank all labo members for their support of my PhD study. Special thanks to Dr. Chen, my friend and colleague, he helped me a lot with the numerical model establishment. And Mr. Mahmood, his suggestions on image treatment and analysis are significant for my research. Also, I would like to express my sincere thanks to Dr. Saber for teaching me the knowledge regarding ArcGIS.

Special thanks to Mr. Yamazaki, the manager of technical affairs, DPRI, Kyoto University. His supports in the installation of cameras and turbidity meters were significantly helpful for me to collect the field data.

My sincere thanks are also extended to Dr. Brousse Guillaume from EDF, France. My numerical model was improved thanks to his advice and discussions. His support in sharing data on the Buëch River is much appreciated as well.

My PhD research is financially supported by the Japan Science and Technology Agency (JST SPRING).

In the end, I would like to express my gratitude to my father, LIN HAI, my mother, JIAN XIAODONG, and my girlfriend, PAN JIAO for their support, and encouragement in my life and study.

Table of contents

List of figures

List of tables

List of symbols

x,y: Coordinates on the moving image

X, Y, Z: Coordinates on the actual image

A_1, A_2, A_3, A_4, B_1, B_2, B_3, B_4, C_1, C_2, C_3: The coefficients that are utilized to transfer the coordinates between rectified images and GCPs

q_i: Calculated flow discharge at segment i

$Q_i{}^o$:

V_i: Depth-average flow velocity at segment i

V: Depth-average flow velocity

h_i: Water depth at segment i

H: Water depth

B: width of the segment

v_i: Surface flow velocity at segment i

V_s: Surface flow velocity

α: The coefficient of the rate between surface flow velocity to average flow velocity

n: Manning's roughness

S_f: Head loss slope

u_*: Friction velocity

g: The acceleration of gravity

ε_s: The dissipation rate at the water surface

κ: Von Karman constant

τ_{ij}: SGS stress tensor

$\bar{S}_{ij}$: SGS strain rate tensor

Δ: Size of the interrogation area

C_s: Model constant of the Large Eddy PIV method for dissipation estimate

U_i, U_j: Surface velocity in the direction i and j (i and j for 2D PIV measurements)

Q^E: Estimated flow discharge by LSPIV and STIV

Q^O: Observed flow discharge from Nagayasuguchi dam

$\bar{Q}_{i,i-1}$: The average magnitude of the flushing flow between two time steps

$\Delta t_{i,i-1}$: The interval of the time step

N: The total number of all possible types of units (including macro-units and sub-types)

NT_{GU}: The total number of types of macro units

N_{GU}: The total number of quantities of macro units

L: The length of the study reach

σ_v, σ_d: The standard deviation of flow velocity and water depth

μ_v, μ_d: The mean value of flow velocity and water depth

z_{i_y}: The bed level at node I in one year

n_i: The number of survey points that the substrates belong to the type i

n_{total}: The total number of survey points

n_s: The total number of individuals of one specie

n_{st}: The total number of individuals of all species

y_i: The measured data

f_i: The simulated data

$\overline{f_i}$: The mean value of simulated data

b_i: The value of baseline

Δt: time step in TELEMAC simulation

ν: Velocity diffusivity

φ: Angle of repose

θ_{cr}: Critical classes shield parameter

β_2: The parameter for deviation

α_{sc}: Associated coefficient for secondary currents effects

α_s: The ratio of roughness height

d_a: Active layer thickness

ω_s: Settling velocity

$k_s{}'$: Roughness height

Abbreviations

SR: Sediment replenishment

PIV: Particle image velocimetry

LSPTV: Large Scale Particle Tracking Velocimetry

SSIV: Surface Structure Image Velocimetry

LSPIV: Large Scale Particle Image Velocimetry

STIV: Space-Time Image Velocimetry

STI: Space-time images

ADCP: Acoustic Doppler Current Profiler

DPI: Dots per inch

FPS: Frame per second

PTZ: Pan-tilt-zoom

GCPs: Ground control points

IA: Interrogation area

TKE: Dissipation rate of surface turbulence

LOW: Law-of-Wall

POM: Particulate organic matter

LR: Length of bed aggradation

PR: The persistence of SR

WR: The eroded width

BRI*: Bed Relief Index

EDF: National Hydraulics and Environment Laboratory of Electricité de France

RM: River miles in km

TR: Transported ratio

TFWV: Total flushing water volume

GU: Geomorphic units

GUS: Geomorphic units survey

GUSI-R: Richness index of geomorphic units survey

GUSI-D: Density index of geomorphic units survey

HMID: Hydro-morphological Index of Diversity

BCI: Bed change index

H value: Diversity index for fish

MQI: Geomorphological Quality Index

rMQI: Revisited Geomorphological Quality Index

2D: 2-dimensional

GSD: Grain size distribution

D10: The corresponding particle size when the cumulative percentage reaches 10%

D30: The corresponding particle size when the cumulative percentage reaches 30%

D50: The corresponding particle size when the cumulative percentage reaches 50%

D90: The corresponding particle size when the cumulative percentage reaches 90%

RMSE: Root-Mean-Square Error

NSE: The Nash-Sutcliffe number

BSS: Brier Skill Score

DEM: Digital elevation map

FSC: Free surface gradient compatibility

CS: Cross section

SSC: Suspended sediment concentrations

SC: Simulated scenarios

Abstract

Dam as a common hydraulic structure, have already been constructed worldwide for the mitigation of floods or generation of power. Sediment is trapped due to the exist of such structures, further resulting in the deficit problem of sedimentation load at downstream reach. The lack of sediment can give rise to several adverse impacts, for instance, bed amouring, riverbed degradation, and deterioration of habitat quality and diversity. Corresponding countermeasures related to the supply of additional sediment have been widely developed as well, including sediment flushing, sediment sluicing, sediment bypass tunnel, and sediment replenishment. In this study, sediment replenishment (SR) is the restoration strategy that is discussed and investigated in detail. It is a common approach that supplies additional sediment employing artificial deposits or injections to the restoration of downstream geomorpho-ecology. The replenishment characteristics, for instance, flushing flow, replenishment locations and volume, the grain size distribution of placed sediment, and the downstream hydro-geomorpho-ecological characteristics, such as riverbed substrates and level, habitat structures, flow patterns, are considered to investigate the implementation of replenishment and its corresponding downstream responses.

The Naka River, which is located in the Tokushima prefecture, Japan, is the selected study area for this study. Continuous SR has been conducted here since 2009, and the accumulated replenished volume is around 1 million m^3. The long-term implementation of SR leads to significant alterations in sediment dynamics and flow regimes, which is valuable for the investigation of downstream impacts.

In the first part of the study, we conducted field measurements of gravel bars, suspended sediment concentration (SSC) and flow patterns in the Naka River to compensate for the deficit of measured data. BASEGRAIN was utilized to measure the grain size distribution of gravel bars by high-quality photos. Coarsen and finer tendency of grains can be founded spatially and temporally due to the differences in erosion and deposition areas along the meandering channel. A turbidity meter was installed at 3 km downstream of the SR site to measure the variation of sediment concentration during releasing period. A counterclockwise relationship was observed between measured SSC and releasing discharge from Nagayasuguchi dam. LSPIV and STIV were further used for real-time measurement of flow patterns. The STIV was proved as more reliable for the measurement of flow velocity and

discharge. The LSPIV can be used for the measurement of water depth through surface turbulent structures, while the results are not accurate due to the limitation of data and cameras.

In the second part of the study, we developed a comprehensive approach to assess the implementation of SR and its downstream hydro-geomorpho-ecological responses. Despite the Naka River, the Buëch River in France was also utilized for the assessment and an integrated comparison of SR works was conducted. Regarding the approach, the transported ratio (TR) and total flushing water volume during flushing (TFWV) was developed to investigate the relationship between SR erosion and flushing flow. Then, several indicators or aspects, such as the Geomorphic Units Survey (GUS), the Hydro-geomorphological Index of Diversity (HMID), the BCI value of bed level changes, the riverbed substrates, and the Fish Diversity Index (H value), were considered to evaluate the riverine impacts. The replenishment projects in both two rivers can be considered as successful cases since positive responses of downstream geomorpho-ecology were observed, for instance, promoting the formation of habitat structures, solving amouring issues, and enhancing the habitat diversity and suitability. Potential interrelationships are also developed between each indicator. The newly formatted riffles are beneficial for the increase of the H value, while an opposite phenomenon is observed for HMID. It is recommended to maintain suitable amounts of sediment supply combined with flushing flow to restore the downstream reach under long-term consideration.

In the third part of the study, we established a two-dimensional model to simulate the hydro-geomorphological changes with the implementation of SR in the Naka River based on TELEMAC-2D coupled with Gaia. The model was then utilized to simulate several scenarios to investigate the optimization strategies of SR by considering replenishment erosion and downstream responses.

Regarding the current arrangement of the SR site, numerical results show that the higher magnitude of flushing flow can promote the erosion of SR sediment. However, it is not an efficient way since the increasing rate of TR is only about 2% if the flushing magnitude is enlarged by 100%. The riverbed aggradation and degradation are promoted by higher flushing flow and higher HMID value can be observed. Nevertheless, extremely higher flushing flow may not beneficial for the maintenance of riffles, which means that the GUSI-D and H values may be reduced and it is harmful to the habitat quality. Furthermore, increasing the percentage of finer sediment in SR material can significantly promote SR erosion (TR increases by 10%). However, the promotion of downstream hydro-geomorphology is limited between the different sizes of SR sediment as the simulated period is short. Despite this, introducing a second flood pulse can further facilitate the TR by about 1.5%.

Nevertheless, the promotion of the HMID is limited (less than 5%) due to the different geomorphological alterations along the reach.

Considering the new arrangement of the SR site, the application of double stockpiles at both sides of banks can increase the eroded volume and transported volume at the SR site (TR increase of 10%). Combined with double flood pulses, the mobilization of SR sediment is promoted, which is beneficial for the enhancement of habitat suitability away from the SR site.

The findings of the study enhance the understanding of relationships between SR implementation and its downstream hydro-geomorpho-ecological impacts. It can then consequently assist the design and optimization of SR projects in the Naka River. In the future, the conclusions and recommendations can be considered as the reference for the design of guidelines for river restoration by SR.

Key words: *River restoration, Sediment replenishment, hydro-geomorpho-ecological changes, image-based velocimetry, numerical simulation, TELEMAC-2D*

Chapter 1. Introduction and Research Framework

1.1. Hydro-geomorpho-ecological responses due to dam construction

Dams as common hydrological structures have already been widely constructed around the world for various purposes, for instance, irrigation, hydropower generation, flood mitigation, and water supply. Regardless of such different objectives, sediment is trapped by all of the dams, which may lead to significant alterations at upstream and downstream reaches. Specifically, at upstream reach, riverbed aggradation occurs due to the trapped sediment, which results in the reduction of reservoir capacity, and further influence the dam capacity on power generation, water supply, and management of flood risk (Alemu, 2016; Fan & Morris, 1992; Schleiss, Franca, Juez, & De Cesare, 2016). While at downstream reach, G. M. Kondolf (1997) has revealed that due to the alterations of flow regime and reduction of sediment load by dam construction, the downstream water can be described as 'hungry water', which means the sediment deficit issues. Such deficit problems will directly influence the downstream water quality, temperature, riverbed formation, and flow regime (Sameh A Kantoush & SUMI, 2010).

Figure 1-1 illustrated the possible effects due to the sediment deficit problem caused by dam construction (S. Kantoush, Sumi, Kubota, & Suzuki, 2010). The effects of dam construction can be summarized into three aspects, including hydrological impacts, such as alteration of flood magnitude and frequency, flow releasing period and quantity, and seasonal flow changes (Ligon, Dietrich, & Trush, 1995); Geomorphological impacts, including riverbank instability, river channel incision, river width adjustment, bed amouring and broken to bridges and embankment (Batalla, 2003; G. M. Kondolf, 1997; Mörtl & De Cesare, 2021); Ecological impacts, for example, reduction of geomorphic units (riffle, pool, and bar structures) (Ock, Gaeuman, McSloy, & Kondolf, 2015), loss of gravels for spawning grounds (G Mathias Kondolf & Wolman, 1993), and adverse impacts on nutrient balance of food system (Ock & Takemon, 2010).

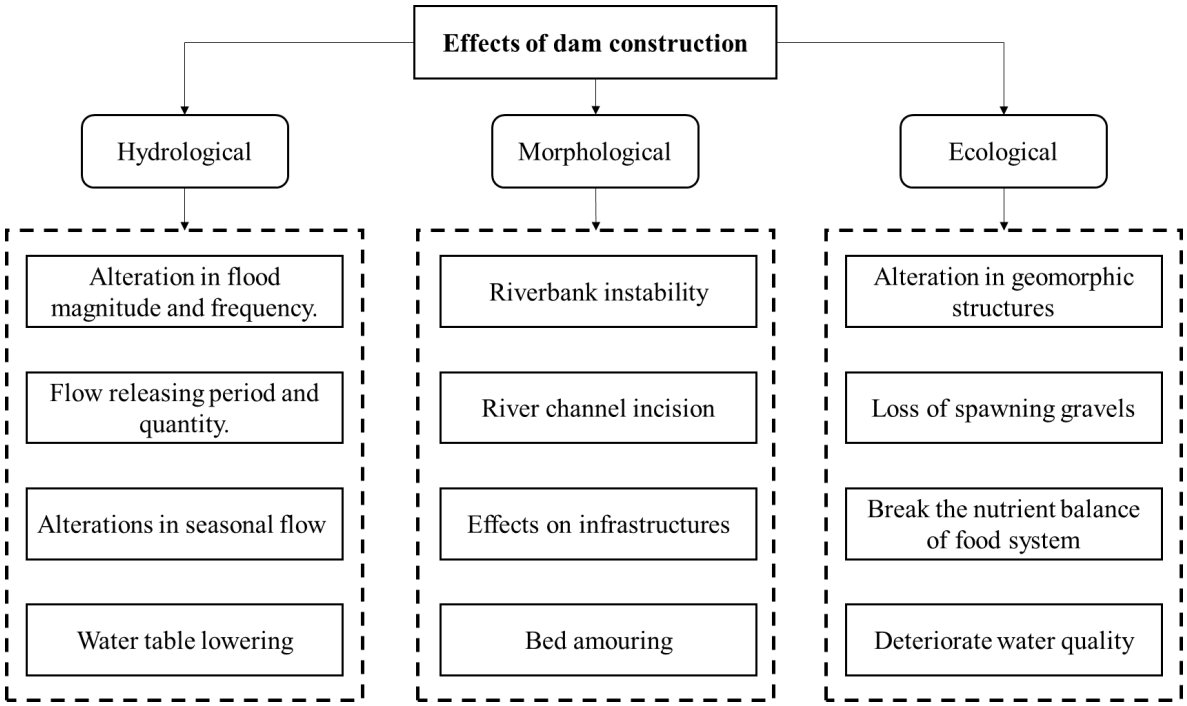

Figure 1-1 The summarized impacts due to the sediment deficit problem caused by dam construction on river hydro-geomorpho-ecology (S. Kantoush et al., 2010).

1.2. Restoring the dam impacts by Sediment replenishment

It is worthwhile to notice that integrated management of sediment in river basins should be implemented to restore the continuity of sediment transportation and provide additional sediment to fix the sediment deficit problems. Various management strategies have already been developed around the world, for instance, promoting sediment transportation by flushing flow (sediment flushing) (Sameh Kantoush, Sumi, Suzuki, & Murasaki, 2010), or providing an additional pathway for sediment transportation (sediment sluicing and sediment bypass tunnel)(Sameh Kantoush & Sumi, 2016; Koshiba, Miura, & Sumi, 2022). Despite this, a novel approach called sediment replenishment (SR) has already been implemented in Japan, Europe, and the USA, which restores the sediment transportation by an artificial supply of additional sediment to downstream reach (S. Kantoush et al., 2010; G. M. Kondolf, J. Toby Minear, 2004; Lin, Kantoush, Sumi, & Takemon, 2021; Stahly, Franca, Robinson, & Schleiss, 2019). According to different sediment sources, topography, objectives, and magnitude of flow, the scale of replenishment and implemented methods are varied (Ock, Sumi, & Takemon, 2013).

In this study, we will focus on restoring the adverse impacts of dam construction through the implementation of SR. Figure 1-2 shows the state of the art of SR and its potential responses to downstream reaches. To be specific, SR is a restoring approach, which utilizes the trapped sediment from upstream to artificially replenish to downstream reaches. For different replenishment projects, various characteristics can be investigated, including different replenished methods (stockpile or injection), the different grain sizes of replenished sediment (fine or coarse), different locations and shapes of the replenished stockpile, different flushing flow (magnitude and frequency) (S. Kantoush et al., 2010). The additional sediment supply will directly lead to some geomorphological changes, for instance, riffle, pool, bar formation, and channel adjustment. Such alterations may have a further influence on habitat quality and diversity. The mentioned characteristics above are the current research gaps in investigating and understanding SR implementation and its corresponding responses to downstream hydro-geomorpho-ecology. Therefore, it is worthwhile to better understand the inner relationships between each characteristic for conducting an efficient and sustainable SR project.

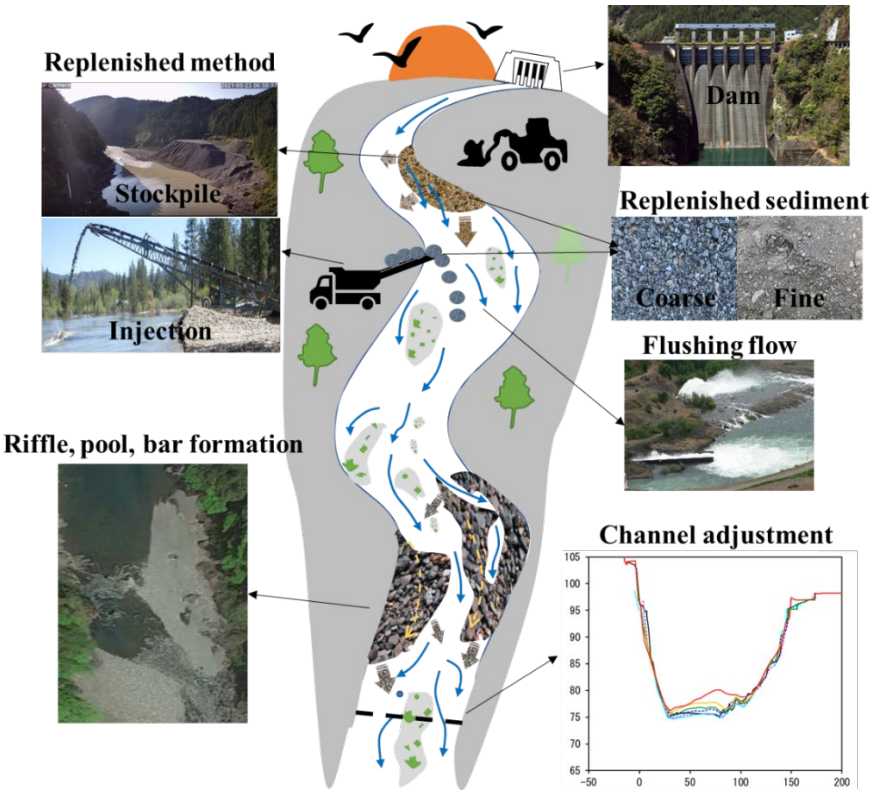

Figure 1-2 The state of the art of SR and its potential responses to downstream reaches.

1.3. Research questions and objectives

Considering the implementation of SR and its impacts on downstream hydro-geomorpho-ecology, several scientific questions and objectives can be developed:

Research questions:

1. What are the differences in SR in the world? For instance, different grain size distribution, placed method and volume, and bank erosion process of placed sediment.
2. What is the main controller of the erosion process of SR?
3. How SR enhances the downstream hydro-eco-geomorphology? The problem can be analyzed based on 4 aspects:

- Bar, pool, and riffle formation at downstream reach.
- Alterations in riverbed substrates.
- Degradation and aggradation on the riverbed.
- Habitat quality based on alteration of species quantities and diversity.

4. What is a successful SR project and how to efficiently implement it?

Objectives:

1. Summarize the information on typical SR projects around the world.
2. Analyze and understand the erosion process of SR under different hydrological conditions, placed volumes, and locations.
3. Evaluate the hydro-geomorph-ecological responses due to the implementation of SR.
4. Investigate the strategies to optimize SR implementation.

1.4. Research Methodology

Figure 1-3 depicts the flow chart of the research methodologies and main objectives. In the beginning, literature reviews related to SR concepts, implemented projects, and riverine hydro-geomorpho-ecology were conducted to investigate the research gaps. Then, required data regarding the replenishment site and downstream reaches were collected from previous research and reports. Additional data was necessary to be collected after the preliminary data collection, and we conducted image-based velocimetry for flow patterns measurement and an on-site field survey for gravel bar measurement. After that, a comprehensive assessment approach was developed for the evaluation of

the erosion process and downstream impacts of SR. Several assessment indicators were determined based on the available data. In the end, we developed a 2D numerical model for hydrodynamics and sediment transportation (TELEMAC-2D coupled with Gaia) to understand the erosion process of replenishment and downstream geomorphological changes. Several scenarios were designed to analyze the influence of different flushing flow, replenished material, placed volume, and locations based on the previous assessment approaches so that countermeasures can be investigated for optimization of SR.

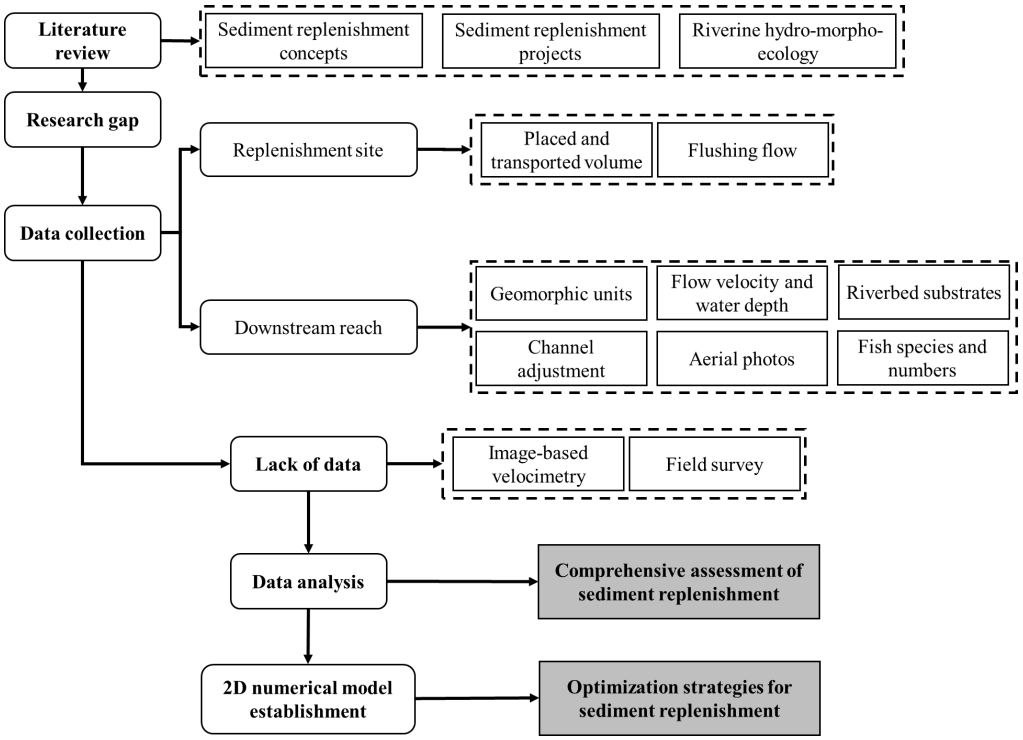

Figure 1-3 Flow chart of the research methodologies and main objectives

1.5. Outline of the thesis

The thesis contains seven chapters which can be divided into six parts: chapter 1 is the introduction and research methodology; chapter 2 is the backgrounds and literature reviews of SR; chapter 3 is the field measurement of additional data, including gravel bars and flow patterns; chapter 4 is the comprehensive assessment of SR based on the collected data; chapter 5 and 6 is the numerical model

establishment and scenarios design for optimization of SR projects; chapter 7 is the conclusions, recommendations, and future works. The connections between each chapter are shown in Figure 1-4.

Chapter 1 depicts an introduction of potential hydro-geomorpho-ecological impacts due to the construction of dams and a novel countermeasure, SR. Several replenishment characteristics should be investigated to efficiently restore the downstream hydro-geomorpho-ecology. After that, the research questions, objectives, and outline of the thesis are presented at the end.

Chapter 2 summarizes the state of the science related to SR implementation, assessment, and modeling. A brief introduction of SR is provided at the first. Then, typical replenishment projects around the world are summarized and a comprehensive comparison is conducted. Assessment approaches of replenishment efficiency and downstream hydro-geomorpho-ecology are investigated, and several valuable indicators and indices are founded. In the end, previous research on numerical and physical models related to SR reproducing is summarized.

Chapter 3 presents the field measurement of flow patterns and gravel bars that conducted by ourselves. Firstly, the study area, the Naka River, is introduced including its previous replenishment works, sediment sources, and operation of flushing flow. Then, the necessity of collecting additional data on flow measurement, SSC and grain sizes is discussed. The grain size of four gravel bars is measured by an image-based approach, BASEGRAIN, and an analysis of its alterations is discussed as well. The SSC is measured based on the installed turbidity meter in 2022. The non-intrusive velocimetry method is then utilized to measure the real-time flow patterns near the replenishment site.

Chapter 4 develops a comprehensive approach to assess the SR works in the Naka River, Japan, and the Buëch River, France. Several indicators are utilized to evaluate the erosion of the replenishment site and the downstream hydro-geomorpho-ecology. Then, the mitigation of promoting the erosion process of the replenished stockpile and the inner relationships between replenishment and downstream responses are discussed respectively. In the end, we conducted a comparison of SR works between two target rivers based on the previous assessment results.

Chapter 5 presents the establishment of a 2D numerical model to simulate the SR works in the Naka River based on TELEMAC-2D coupled with Gaia. Sensitivity analysis is conducted based on the variation of several numerical and physical parameters. Due to the limitation of available data, the best model parameters are set to evaluate the erosion process of the replenished stockpile and downstream geomorphological changes based on the results of sensitivity analysis.

Chapter 6 discusses the SR strategies that consider the erosion process of replenished stockpiles and downstream responses. Different scenarios related to various magnitudes and frequencies of flushing flow, grain sizes of replenished material and locations, and volumes of replenished stockpile are designed and simulated by utilizing the models developed in chapter 5. The performance of scenarios is evaluated based on the developed assessment approaches in chapter 4. The results can be used to optimize the SR works in the Naka River.

Chapter 7 summarizes the conclusions of the research and provides several directions for future works. Recommendations for optimization and design of SR works are also depicted at the end.

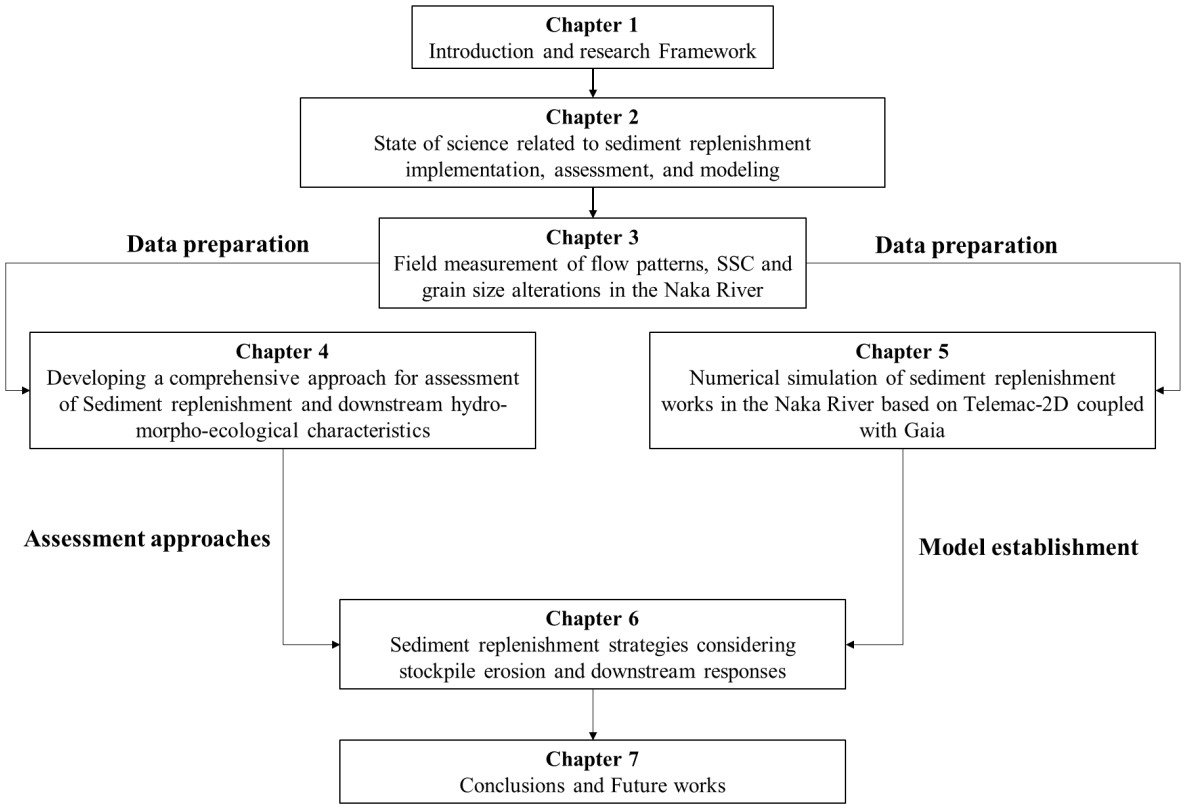

Figure 1-4 The outline of the chapters and their inner connections

Chapter 2. State of science related to Sediment replenishment implementation, assessment, and modeling

2.1. Introduction of SR

Due to the construction of dams, amounts of sediment were trapped in upstream, which decreases reservoir storage capacity and raises the risk of flooding for the residents (G. M. Kondolf, 1997). Simultaneously, at the downstream reach, the issue of sediment deficit will occur, which will result in significant geomorphological changes, including riverbed incision, riverbank instability, and armoring bed (Tetsuya Sumi & Kantoush, 2010). Furthermore, the number of habitat structures, such as riffles, bars, and pools, is reduced, which is harmful to the food web and spawning grounds of aquatic habitats (Ock, Kondolf, Takemon, & Sumi, 2013). Sediment transportation is a significant aspect that requires to be enhanced. To tackle such adverse impacts, SR (or called gravel augmentation), as one typical restoration technique, is conducted which aims to recover the downstream geomorphology and aquatic habitat by supplying additional sediment (Ock, Sumi, et al., 2013). The principle of implementing SR is to recreate pristine sediment transportation and promote the diversity of downstream geomorphology (L. S. Sklar et al., 2009). Specifically, part of the upstream coarse material is excavated and transported by trucks or conveyors to the downstream areas below dams. The sediment can be alternatively placed at the bank side as a stockpile, or just directly injected into the river, and finally eroded and transported by natural or artificial floods (S. Kantoush et al., 2010) (Figure 2-1)

Figure 2-1 The process of SR implementation from the excavation site to the replenishment site (S. Kantoush et al., 2010).

From the previous study and research, the volume of replenishment sediment should consider the sediment budget and calculate the required amounts of sediment for restoring the spawning grounds (D. Gaeuman, Krause, A., 2013). However, sediment transportation is a long-term process and it is not reasonable to equalize the calculated volume from the sediment budget to the placed volume of replenishment material (D. Gaeuman, Krause, A., 2013). The transport capacity under various regulated flows should be considered to place the adaptable volume for SR (Elena Battisacco, 2016). Despite this, the grain size of the replenishment sediment is also significant for ecological restoration. The replenished sediment is usually finer than the substrates of the riverbed to establish appropriate spawning grounds for fish (D. Gaeuman, 2008) (Wheaton, Pasternack, & Merz, 2004). Moreover, the replenished sediment should be scoured and deposited at the desired locations, which needs further consideration of the replenishment sites and implementing methods (D. Gaeuman, Krause, A., 2013). To be specific, current implementation approaches can be classified into four types (Ock, Kondolf, et al., 2013) (Figure 2-2). The low-flow stockpile is the common approach utilized from the 1970s to efficiently create pool and riffle tails by replenishing fine sediment (Ock, Kondolf, et al., 2013) (Figure 2-2 (a)). The time required for restoration is short since the sediment is eroded and transported during normal flow. However, the in-channel placement may increase the river turbidity and influence the downstream habitat quality. Regarding the high-flow stockpile, the fine or medium gravels are placed at the bank side of channel and will be scoured during high flow period (Figure 2-2 (b)). It is suitable for large dams where the flushing flow is higher and the flushing duration is short. Moreover, this method also can economically place considerable volume of sediment if the desired volume of excavation from upstream sediment sources is extremely high. The capability for altering riverbed is also higher than the low-flow stockpile. Nevertheless, the location of the placement is limited. For the point bar stockpile, the coarse sediment is placed at the low flow and bank simultaneously which aims to create the point bar at the downstream specific locations (Figure 2-2 (c)). The limitation is the restriction of transportation and erosion process at the bend of the meandering rivers. With the high-flow injection method, it is a common approach utilized in the Trinity River, USA to directly inject coarse sediment into the river channel during high flow by heavy equipment (Krause, 2012) (Figure 2-2 (d)). The advantage of this approach is that the sediment can be efficiently transported to downstream and the transported volume can be easily controlled as well. The limitation of the method is the dangerous working conditions and the high cost (G. M. Kondolf, J. Toby Minear, 2004). The characteristics of each methods were summarized in Table 2-1.

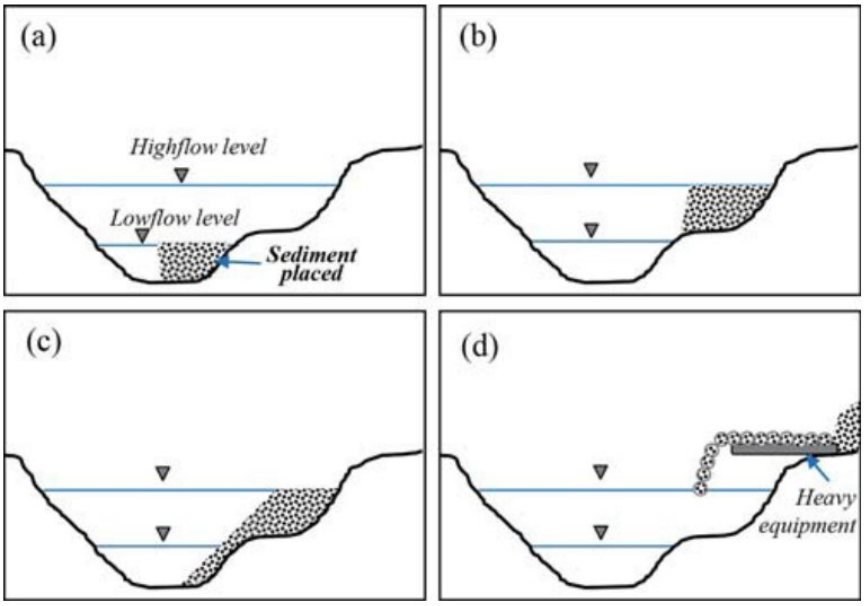

Figure 2-2 The different implementation methods for SR. (a) Low-flow stockpile. (b) High-flow stockpile. (c) Point bar stockpile (d) High-flow injection (Ock, Sumi, et al., 2013).

Table 2-1 The characteristics of different implementation approaches of SR (Ock, Kondolf, et al., 2013) (G. M. Kondolf, J. Toby Minear, 2004).

	Low-flow stockpile	**High-flow stockpile**	**Point bar stockpile**	**High-flow injection**
Flow condition during replenishment	Low flow	High flow	Low and high flow	High flow
Main function	Riffles or pool tails	Channel adjustment	Point bar generation	Same functions as low and high-flow stockpile
Erosion rate of replenished sediment	Low	High	Medium	High
GSD of replenished sediment	Fine	Fine to medium gravels	Coarse gravels	Coarse gravels
Restoration responses	Direct	Long-term	Direct	Direct
Turbidity problem	High	Medium	Low	Low

2.2. Overview of SR works around the world

SR as a typical approach for river restoration has already been implemented at various river basins worldwide, for instance, Uda River (SA Kantoush & Sumi, 2011), Naka River (Lin et al., 2021), and Kizu River (Ock, Kondolf, et al., 2013) in Japan, Buëch River (Guillaume Brousse et al., 2019), Sarine River (Stahly et al., 2019), and Old Rhine River (Paquier et al., 2018) in Europe, and Trinity River (D. Gaeuman, 2014) in USA. For each river, the implementation approach, the GSD of replenishment sediment, the location of replenishment, and the targets are varied. Successful and unsuccessful outcomes of downstream responses were obtained. In this section, the summarized information on replenishment characteristics of several typical replenishment projects was reviewed and a comparison of replenishment information was conducted in Table 2-2.

2.2.1. SR implemented in Japan

In Japan, currently, there are nearly 500,000 numbers of dams, and sediment management issues have already been investigated for several years. To mitigate the sediment deficit problems, several sediment supply approaches have already been implemented at several dams in Japan, including sediment flushing, sediment sluicing, sediment bypass tunnel, and SR (Sameh Ahmed Kantoush et al., 2018) (Figure 2-3). It can be noticed that SR as the most common strategy, has been utilized in 50% of the sediment management projects in Japan. Replenishment material varied from fine to medium coarse sediment (D50 ranged from 0.2 mm to 20 mm) depending on the sediment sources and the requirements for restoration of downstream geomorphology (T. Sumi & Kantoush, 2011) (Figure 2-4). The targets of replenishment were varied, including prevention of riverbed degradation, improvement of fish habitat, and disposal of sediment accumulated at the check dam. Here we summarized details information on typical replenishment projects from previous research in Japan, including:

- Akiha dam (Tenryu River)

The Akiha dam project was a typical high-flow stockpile project. The replenished sediment was placed on top of the bed protection works. According to the pre-investigation, the deposits would begin to be submerged at a flow rate of 400 m^3/s and would be fully submerged at 1500 m^3/s. Several subsequent SR projects were conducted from 1998 to 2001 (Okano, Kikui, Ishida, & Sumi, 2004).

Sediment was excavated from the upstream of the check dam, which contained 67% gravel and 29% sand.

- Murou dam (Uda River)

The project was conducted below Murou dam in the Uda river from 2006 to 2010, which aims to investigate the linkage between flushing flow, erosion process, as well as grain size distribution (Figure 2-5). Specifically, both natural flow and artificial flow were utilized in the project to figure out their differences in transported volumes and travel distance. Furthermore, the RUBEE-Tag and Passive TI-rfID were utilized to track the bed load movement during replenishment (SA Kantoush & Sumi, 2011).

- Nunome dam (Nunome River)

The SR was conducted as an experiment in the Nunome dam from 2004 to 2009. The placed volume varied from 190 m^3 to 720 m^3 and the D50 of placed sediment was around 0.4 mm. The low-flow stockpile was utilized and replenished sediment was scoured by natural flood from the upstream dam (Figure 2-5). The main targets of the project were to investigate the erosion process of the replenishment stockpile and the environmental issues at downstream reach (Sameh Kantoush, Sumi, & Kubota, 2010).

- Managawa Dam (Kuzuryu River)

The SR combined a flexible dam operation that has been conducted at the Managawa dam in the Kuzuryu River since 2000. The high-flow stockpile was implemented here to replenish coarse sediment with a flushing flow of around 500 m^3/s to 2700 m^3/s (Figure 2-5). Restoration of downstream flow and sediment regimes was the main target of the project (Matsushima, Hyodo, Shibata, & Shimizu, 2018).

- Nagayasuguchi dam (Naka River)

Since 1991, SR began to be conducted at six locations downstream of the Nagayasuguchi dam in the Naka River (Figure 2-5). As usual, a high-flow stockpile was utilized to replenish the considerable volume of sediment (around 1.7 million m^3 in total) with flushing flow varied from 500 m^3/s to 5000 m^3/s. The project aims to dispose of the trapped sediment upstream and restore the downstream geomorpho-ecology at the same time (Lin et al., 2021).

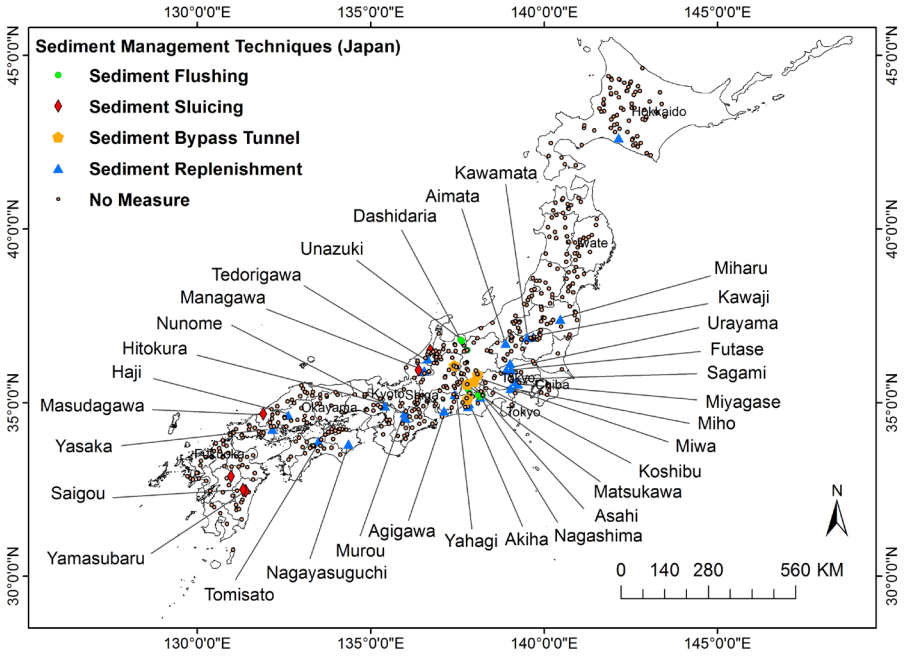

Figure 2-3 The sediment management strategies implemented in Japan, including sediment flushing, sediment sluicing, sediment bypass tunnel, and SR (Sameh Ahmed Kantoush et al., 2018)

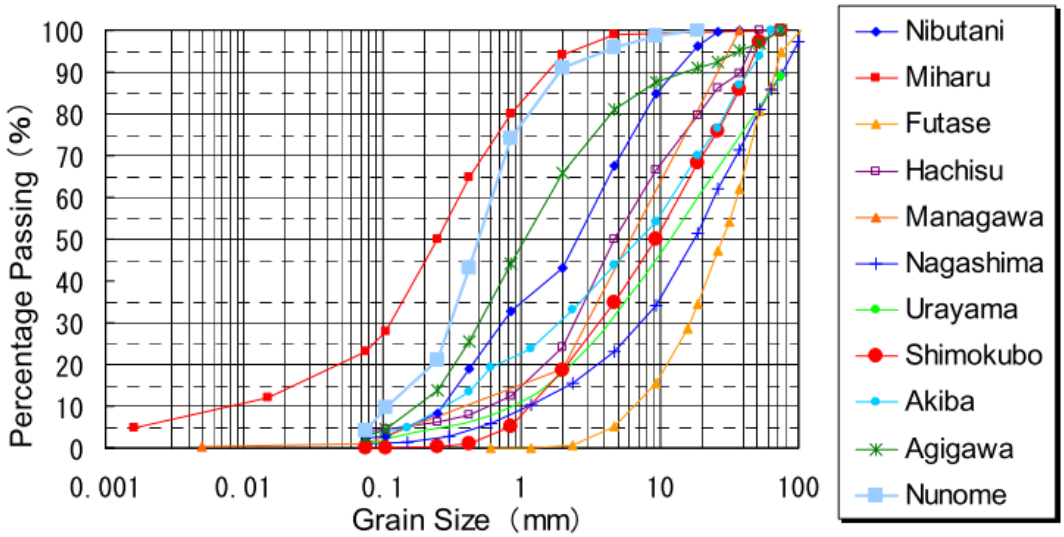

Figure 2-4 The grain size distribution of replenishment material utilized in Japan (T. Sumi & Kantoush, 2011).

Figure 2-5 Typical SR projects implemented in Japan, including Murou dam (SA Kantoush & Sumi, 2011), Managawa dam (Matsushima et al., 2018), Nunome dam (Sameh Kantoush, Tetsuya Sumi, & Akira Kubota, 2010), and Nagayasuguchi dam (Lin et al., 2021).

2.2.2. SR implemented in Europe

In Europe, SR is also the common management strategy for river restoration below dams. Gravel augmentation is the usual name of the project since the replenished sediment is usually coarse gravel. Main projects have started to be conducted in France, Germany, and Switzerland since 2010 utilizing the stockpile approach. Several novel implementation approaches were used which were different from the Japanese works. Here four projects were summarized, including:

- Rossens Dam (Sarine River)

The replenishment was conducted at Rossens Dam in the Sarine River, which is located in western Switzerland. Despite the normal single stockpile, four parallel deposits were placed at the bank side with a total volume of around 1000 m^3 (Figure 2-6). A one-time flushing occurred in 2016 with a peak discharge of around 190 m^3/s and a duration of around 24 hours. The main target of the replenishment was to fix the channel incision and disconnection of the floodplain in the Sarine River (Stahly et al., 2019).

- Kembs Dam (Old Rhine River)

To enhance the fluvial ecosystem downstream of the Kembs dam, gravel augmentation was conducted at three locations from 2010 to 2016. The D50 of augmentation material ranged from 12 mm to 112 mm, which was much coarser than Japanese projects. The key findings of the project were the adaptable location for the promotion of the erosion process of the stockpile. It was founded that artificial deposits should be placed in concavity zones instead of convexity zones since the bed shear stress is higher (Paquier et al., 2018).

- Sylvenstein Dam (Isar River)

Artificial insertion of sediment was conducted at three potential locations downstream of the Sylvenstein dam from 1995 to 2013. The annual total volume of placed sediment was around 10,000 m^3 and the flushing flow varied from 500 m^3/s to 900 m^3/s. The project aims to fill the deficit of bedload due to the construction of dams and dispose of the considerable volume of excavated sediment (2,800,000 m^3) from upstream tributaries (Heckmann, Haas, Abel, Rimböck, & Becht, 2017).

- Saint-Sauveur Dam (Buëch River)

Due to the construction of the Saint-Sauveur dam in 1992, channel incisions occurred at several locations downstream. SR was first conducted in 2016 to restore the damage to the active channel (Guillaume Brousse et al., 2019). Three stockpiles (called berms) were placed at the left bank, right bank, and channel central with one secondary channel established to promote the erosion process of sediment (Figure 2-6). In 2018, a mitigation of the replenishment site was conducted to move the scoured material from a low erosion area to a high erosion area.

Figure 2-6 The SR projects implemented in Europe. Left: Sarine River in the Switzerland (Stahly et al., 2019). Right: Buëch River in France (Guillaume et al., 2018).

2.2.3. SR implementation in USA (Trinity River)

The famous SR project (or gravel augmentation) in the USA was implemented in the Trinity River, located in northern California. It should be the first country that conducted gravel excavation and augmentation (since 1912). Continuous replenishment utilizing various implementation methods (low-flow stockpile, high-flow stockpile, high-flow injection (Figure 2-7)) was recorded from 1977 (G. M. Kondolf, J. Toby Minear, 2004). Several targets were considered in the project, including riffle construction and maintenance, coarse sediment disposal, side channel creation, and spawning grounds generation (G. M. Kondolf, J. Toby Minear, 2004). An integral monitoring system has already been established by TRRP (Trinity River Restoration Program) regrading the geomorphic responses as well as ecological restoration downstream of the Lewiston dam.

Figure 2-7 High-flow injection as the replenishment approach implemented in the Trinity River (Krause, 2012).

Table 2-2 The information on SR projects around the world, including river name, dam name, country, Implementation method, year of SR implementation, and D50 of replenished material, placed volume, and flushing flow.

River	Dam	Country	Implementation method	Year	D50 (mm)	Placed volume (m^3)	Flushing flow (m^3/s)	Source
Tenryu River	Akiha dam	Japan	High-flow stockpile	99-05	25	2000 - 10,000	500 - 4400	Okano et al. (2004)
Uda River	Murou dam		Low-flow stockpile	06-10	1	90 - 280	12	SA Kantoush and Sumi (2011)
Nunome River	Nunome dam		Low-flow stockpile	04-09	0.4	100 -720	80	Sameh Kantoush, Tetsuya Sumi, and Akira Kubota (2010)
Kuzuryu River	Managawa dam		High-flow stockpile	03-12	25	100 - 980	30 - 370	Matsushima et al. (2018)
Naka River	Nagayasuguchi dam		High-flow stockpile	09-now	7	40,000 - 390,000	500 - 5000	Lin et al. (2021)
Sarine River	Rossens dam	Switzerland	Low-flow stockpile (multiple locations)	16	39	10,000	190	Stahly et al. (2019)
Old Rhine River	Kembs dam	France, Germany	High-flow stockpile	10-16	12 - 112	-	-	Paquier et al. (2018)
Isar River	Sylvenstein dam	Germany	High-flow stockpile	95-98, 09, 13	50	1500 - 6700	110 - 350	Heckmann et al. (2017)
Buëch River	Saint-Sauveur dam	France	Low-flow stockpile (multiple locations)	16, 18	21	43500	265 - 300	Guillaume Brousse et al. (2019)
Trinity River	Lewiston dam	USA	High-flow and low-flow stockpile, high-flow injection	72-11	50 - 120	70 - 3000	5 - 300	G. M. Kondolf, J. Toby Minear (2004)

2.3. *Assessment of SR and river hydro-geomorpho-ecology*

The assessment of SR and its downstream impacts on riverine hydro-geomorpho-ecology is the crucial part to understand the conduct of a successful SR. Several parameters should be considered to implement a successful replenishment (Figure 2-8). Specifically, replenishment characteristics including placed volume, flushing discharge, and GSD of placed sediment should be investigated. While at the downstream reach, the flow characteristics (flow velocity and water depth), geomorphological characteristics (bed aggradation or degradation, riverbed substrates), and ecological characteristics (quantity and diversity of fish species, water quality, distribution of habitat structures) should be discussed in detail (SA Kantoush & Sumi, 2011).

It is essential to utilize indicators or indices as an efficient tool to evaluate these characteristics and understand whether replenishment projects are successful or not. Regarding replenishment characteristics, there is rare research that develops an integrated approach for evaluation. The majority of the research recorded and determined the placed volume, transported volume, and flushing flow, and no further analysis of relationships was conducted (Sameh Kantoush, Tetsuya Sumi, & Akira Kubota, 2010; S. Kantoush et al., 2010; G. M. Kondolf, J. Toby Minear, 2004; Okano et al., 2004). Despite this, E. Battisacco, Franca, and Schleiss (2016) developed several analyzed indicators to understand the replenishment characteristics and channel geomorphology based on the physical model. Moreover, Elena Battisacco (2016) and Friedl (2017) investigated the influence of replenishment geometry, locations, GSD of sediment, and flushing flow through laboratory tests, and a valuable conclusion was obtained regarding the efficient transport of more sediment to downstream reach.

For the assessment of downstream hydro-geomorpho-ecology, amounts of scale-based indicators and indices have already been developed to assist the management of river restoration. Several integrated systems combining amounts of sub-indicators were established to comprehensively evaluate the riverine environment. To be specific, M. Rinaldi, Surian, Comiti, and Bussettini (2013) developed the Geomorphological Quality Index (MQI) to analyze the hydro-geomorphological condition of Italian streams. The index comprehensively considered 28 sub-indicators regarding channel continuity, channel pattern, channel adjustment, riverbed substrates, and vegetations (M. Rinaldi et al., 2013). Moreover, González del Tánago, Gurnell, Belletti, and García de Jalón (2015) utilized

similar indicators of MQI to integrally assess the flow regime, geomorphic conditions, and riparian environmental quality in the UK. Ioana-Toroimac, Zaharia, and Minea (2015) revised and updated the current MQI method and developed the rMQI system, which additionally considers the impacts of human pressure. Despite these synthetical approaches, vast of indicators for part of the hydro-geomorpho-ecology was also existed and widely utilized. For instance, the Geomorphic Units Survey (GUS), which focus on the classification of different habitat structures and analyze the alterations by considering several indictors regarding to diversity and richness (Belletti et al., 2015). Gostner, Alp, Schleiss, and Robinson (2012) established the hydro-geomorphological index of diversity (HMID), which aims to investigate the geomorphic impacts on physical diversity. Furthermore, the Shannon-Wiener index of diversity (Shannon, 2001) was widely used to calculate fish diversity, for instance, in the Ganga basin, India (Lakra et al., 2010).

In summary, a comprehensive assessment of SR and its responses to downstream requires the assistance of indices and indicators. Depending on the differences between rivers and the availability of data, suitable evaluation methods are varied. Adaptable indicators and indices should be selected from previous research or developed by ourselves to establish an integrated system for SR evaluation.

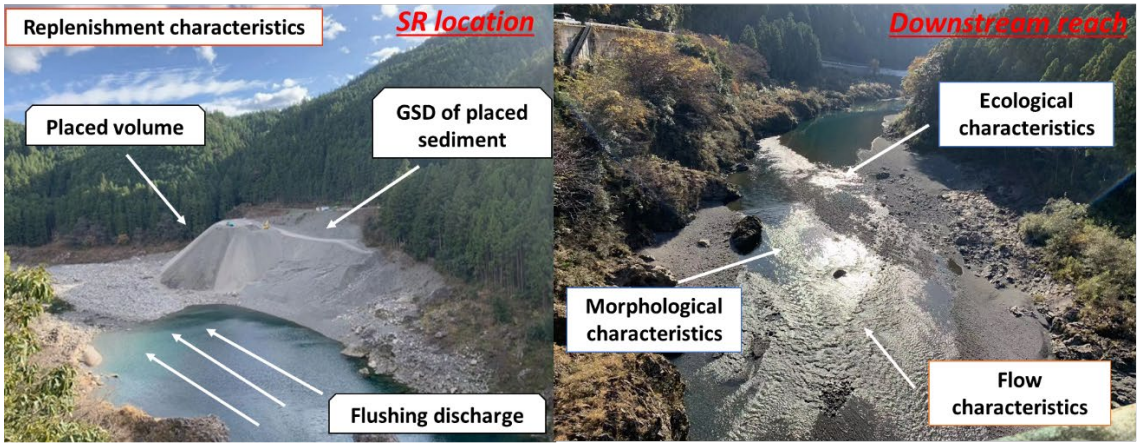

Figure 2-8 The characteristics that should be considered to assess the SR project.

2.4. Experimental models for simulation of SR

Numerical models for reproducing SR were widely developed to investigate the lateral erosion of replenishment stockpiles and the downstream geomorphological changes. Specifically, two-dimensional models were preferred for most cases of replenishment modeling since a good agreement

between flow regime, sediment transportation, and computational time was expected (Cordier et al., 2019). Reproducing the lateral erosion process is the key point to establishing a well numerical model for SR. Several modeling of lateral erosion have already been developed for cohesive or non-cohesive banks (Bosa, Petti, & Pascolo, 2018; Massimo Rinaldi, Mengoni, Luppi, Darby, & Mosselman, 2008; Xiao, Zhou, & Yang, 2016). The majority of the research emphasized that the angle of repose of sediment was the essential factor in accurately reproducing the process of lateral erosion (Vonwiller, Vetsch, & Boes, 2018). Several numerical models combined with flume experiments (Physical model) were conducted to investigate the lateral erosion of SR (Juez, Battisacco, Schleiss, & Franca, 2016; Vonwiller et al., 2018). Despite the investigation of lateral erosion, numerical models can also assist to design efficient SR projects for river restoration on a reach scale. For instance, Hiroshi and Parker (2012) developed a two-dimensional numerical model to investigate the impacts of SR on river restoration and a physical model to verify the results. They made concluded that replenishment at upper riffles is more efficient for scouring more sediment from the replenishment site (Hiroshi & Parker, 2012). Furthermore, Cajot, Schleiss, Sumi, and Kantoush (2012) also developed a 2-D numerical model for the Nunmoe River to evaluate the impacts of SR on downstream habitat diversity. established a 2-D numerical model to simulate the erosion process of artificial deposits and experimental tests were implemented to verify as well. Sameh Ahmed Kantoush et al. (2018) developed a numerical study to investigate the strategy for the production of spawning grounds for Ayu-fish in the Tenryu River. Moreover, Pasternack, Wang, and Merz (2004) established a 2-D numerical model to design the spawning gravels of replenishment in the Mokelumne river, California.

The summary of the numerical model and physical model for SR was illustrated in Table 2-3. It can be noticed that rare researchers utilized a numerical model for reproducing the SR and the application of the physical model is still the dominant method for the investigation of replenishment. Nevertheless, the physical models are limited to reproducing the downstream impacts of replenishment along a large scale of reach. The numerical model is more economic and efficient to investigate the lateral erosion process and sediment transportation of SR if sufficient and accurate data of geomorphology and an adaptable numerical tool are prepared and selected.

Table 2-3 Summary of physical and numerical models for simulating SR.

Source	Experimental method		Target	
	Physical model	Numerical model	Lateral erosion and sediment transportation	Downstream responses
Pasternack et al. (2004)		√		√
L. Sklar et al. (2009)	√			√
Cajot et al. (2012)		√		√
Hiroshi and Parker (2012)	√	√		√
Elena Battisacco (2016)	√		√	√
Juez et al. (2016)	√	√	√	
Vonwiller et al. (2018)	√	√	√	
Sameh Ahmed Kantoush et al. (2018)		√		√

Chapter 3. Field measurement of flow patterns, SSC, and grain size alterations of bars in the Naka River

3.1. Introduction of the management strategy for SR implementation in the Naka River

The Naka River in Japan was selected as the study area to process our research regarding SR. The continuous replenishment works with an extreme volume of placed sediment were unique and thus significant downstream responses were expected. In this section, detailed information on sediment management strategy including SR works, sediment sources, and dam operation of Nagayasuguchi in the Naka River was revealed.

3.1.1. SR works

The Naka River Basin is located in the Tokushima Prefecture. The total drainage area is around 874 km^2, and the total length of the river reach is around 125 km (Figure 3-1). Continuous SR was started to be conducted in 1991 at six locations downstream of the Nagayasuguchi dam and Kawaguchi dam (Figure 3-1). Due to the management of the Naka River Office, the replenishment sites were mitigated and only the two sites near Kohama bridge (downstream of Nagayasuguchi dam) were maintained as the replenishment locations since 2010. And since 2016, only one site downstream of the Kohama bridge was kept. In this paper, the replenishment works after 2010 at two locations near Kohama bridge were investigated and the detailed information on placed volume and transported volume was shown in Table 3-1.

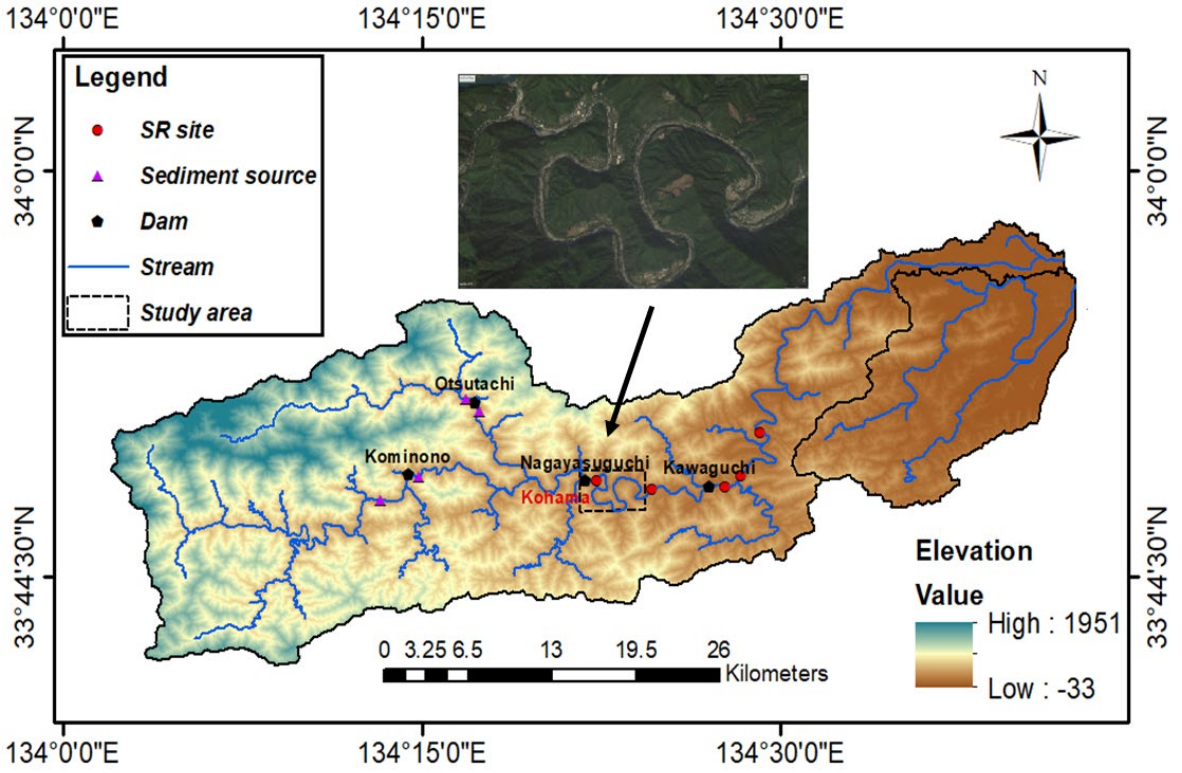

Figure 3-1 The Location map of the Naka River Basin, including the SR sites, sediment sources, dams, and study area.

Table 3-1 The summary of placed volume and transported volume at two replenishment sites upstream and downstream of Kohama Bridge from 2010 to 2020.

Year	Kohama upstream		Kohama downstream	
	Placed volume (m^3)	Transported volume (m^3)	Placed volume (m^3)	Transported volume (m^3)
2010	84,200	53,000	41,800	64,000
2011	19,000	70,000	88,800	117,000
2012	57,800	3,000	41,400	50,000
2013	50,300	33,000	138,300	32,000
2014	20,200	137,000	188,400	143,000
2015	17,300	15,000	105,170	147,000
2016	-	-	106,170	20,000
2017	-	-	28,330	80,000
2018	-	-	65,000	47,000
2019	-	-	5,514	50,000
2020	-	-	167,200	15,000

3.1.2. Sediment sources of replenishment

The sediment sources of replenishment in the Naka River were mainly from the upstream reaches of the Otsutachi dam and Kominono dam (Figure 3-2). Sediment source 1 is located at the otsutachi dam, which provided the majority of sediment (2 million m^3 since 2004) for replenishment in the Naka River. The considerable sediment was caused by the significant landslide that happened in 2004 (Figure 3-3). Currently, reliable protection work has already been done to maintain the stability of the slide, and additional sediment is placed on the right bank of the river channel and ready for transportation (Figure 3-3). Some extremely large gravels and cobbles have already been classified to ensure the requirements of the replenishment sediment. Moreover, in the downstream area, the quantity of sediment deposition is also considerable due to the high sediment concentration of flushing from upstream reach. Recently, the excavation work is continuously processed to reduce the flooding risk during the rainy season (Figure 3-4). In summary, sediment excavation at Otsutachi dam can not only dissolve the additional sediment from the landslide and reduce the flooding risk in the downstream area but also supply sufficient fine sediment for replenishment work. Besides, the distance from the replenishment site is around 10 km, which means that cost of sediment transportation is affordable. Therefore, it is the most reliable sediment source and we can do further research to optimize the excavation and transportation here.

Regarding sediment source 2, the same problem of huge sediment deposits occurred. Removal work of sediment has been conducted here as well. The river office utilized a dredging machine on the boat to remove the sediment during the summer season instead of direct excavation here.

Despite the 2 current places, upstream of Kominono dam was considered as another potential location for sediment supply. Specifically, due to the sediment trapping by the dam, amounts of sediment were deposited here. Comparing the riverbed level between 1965 and 2020, significant aggradation can be observed with a depth of more than 15 m (Figure 3-5). The current distance between the riverbed to the tail of the bank is only around 5 m, which means that severe inundation of the surrounding residential area may happen under significant flood. Though the excavation is needed, issues still exist. Firstly, compared to replenished sediment placed at Kohama, sediment at Kominono was coarser and the coarse gravels (range from 100 mm to 150 mm) was dominant (Figure 3-6). Furthermore, the distance to the replenishment site is long and it is not an economic choice. That may be the main reason why the river office tends to excavate and place the sediment in the nearby mountains instead of using it for replenishment.

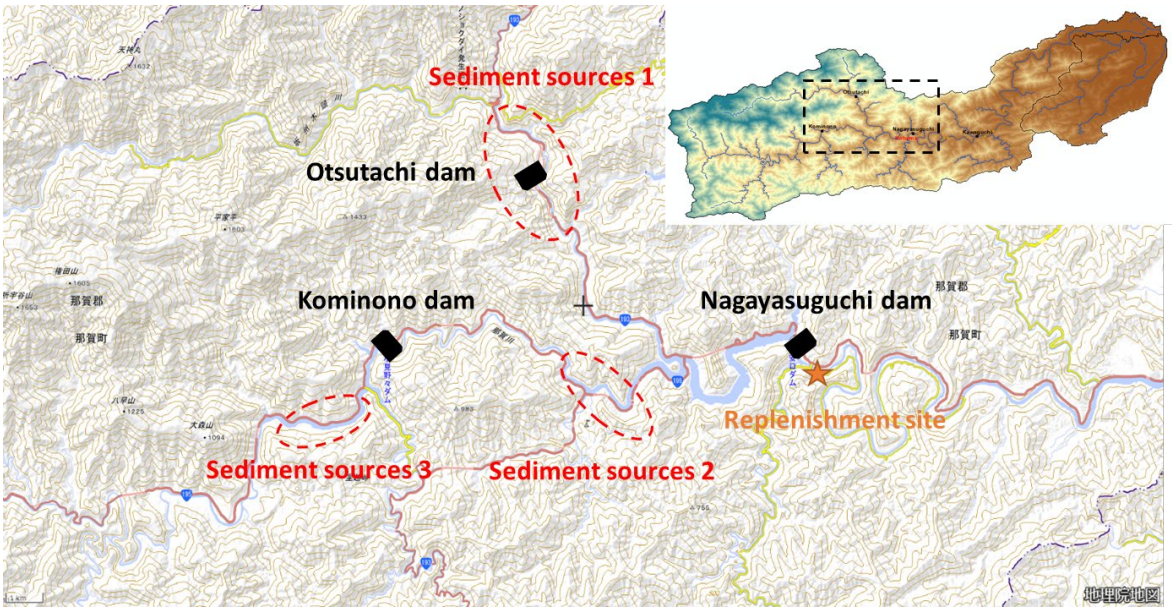

Figure 3-2 The locations of sediment sources upstream of Nagayasuguchi dam.

Figure 3-3 The sediment sources upstream of Otsutachi dam. Left figure: The landslide of the mountain. Right figure: The sediment for replenishment including classification.

Figure 3-4 The sediment excavation downstream of Otsutachi dam.

Figure 3-5 The potential sediment sources upstream of Kominono dam shows significant bed aggradation. Left figure: Photo in 1965 (from the report of Naka River). Right figure: Photo in 2020.

Figure 3-6 The comparison of sediment between Kominono (potential sediment source) and Kohama (current replenishment sediment)

3.1.3. Operation of Nagayasuguchi dam for flushing of replenished sediment

The Nagayasuguchi dam was located 1 km upstream of the replenishment site at Kohama (Figure 3.1), which aims to reduce the downstream flood risk and supply water for agriculture and hydropower stations. The releasing flow of Nagayasuguchi dam is the dominant part of SR implementation since it is the direct flushing flow to erode the sediment. The high flow season usually begins in April and ends in October while the low flow season usually lasts 5 to 6 months from November to the next year March. The regulation of releasing period mainly depends on the precipitation in the upstream area. During the rainy period, if the water level of the storage exceeds the level for pre-releasing (218.70 m), the dam will release flow to the downstream area. It is obvious that the period with high precipitation is corresponding to the releasing period in 2018 (Figure 3-7).

The current operation of Nagayasuguchi dam may not suitable for continuous SR at the downstream area as the magnitude and duration of flushing flow mainly depend on the precipitation. Significant variations of releasing flow and duration between each year from Nagayasuguchi dam can be observed from 2010 to 2020 (Table 3-2). The Naka River experienced extreme typhoons in 2011,2014 and 2015, where significant releasing flow occurred with a magnitude greater than 4000 m^3/s, while medium flood events happened in 2012, 2018, and 2019 (releasing flow around 2000 m^3/s to 3000 m^3/s). Despite this, the releasing duration also varied annually from 29 days to 71 days depending on the precipitation period. The differences in flushing flow result in the variation of transported volume at the replenishment site and thus affect the restoration of downstream geomorpho-ecology. It can be noticed that a deficit of flushing flow occurred in the recent two years (2020, 2021) and the corresponding transported volume was limited. It is worthwhile to consider releasing additional flow with a small magnitude (less than 400 m^3/s) to enhance the sediment transportation of the replenishment site and promote the effects of downstream restoration.

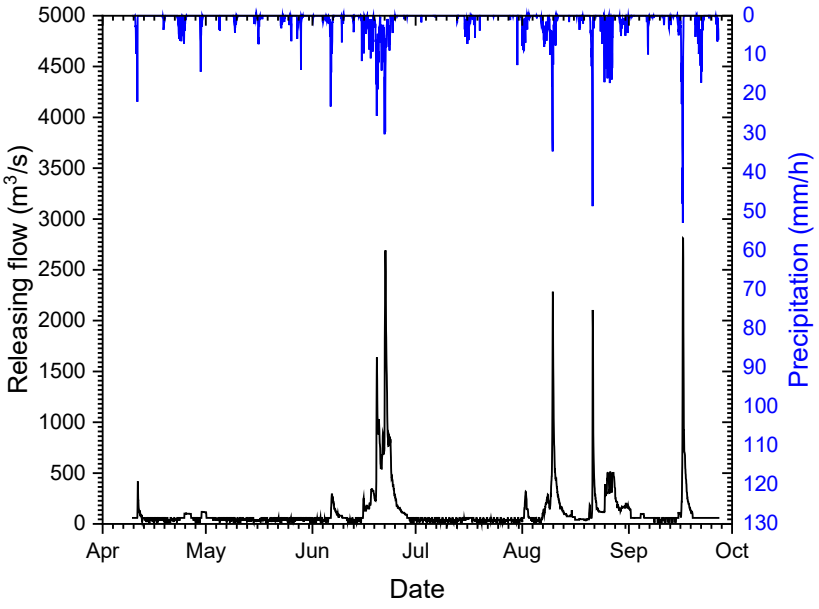

Figure 3-7 The releasing flow and precipitation at Nagayasuguchi dam in 2018.

Table 3-2 The inflow, releasing flow, and releasing duration at Nagayasuguchi dam from 2010 to 2020.

Year	Inflow (m^3/s)	Releasing flow (m^3/s)	Total Duration (day)
2010	113 - 1080	176 -1198	47
2011	117 - 4494	92 - 4113	58
2012	88 - 2112	79 - 2006	61
2013	126 - 1382	90 - 1644	29
2014	79 - 5758	68 - 5465	40
2015	102 - 5238	129 - 4594	52
2016	99 - 1286	90 -1225	59
2017	120 - 1551	125 - 1559	40
2018	102 - 3636	101 - 2878	71
2019	91 - 3850	99 -3295	37
2020	135 - 1005	147 - 1006	51
2010	120-1023	105 - 920	32

3.2. Motivations of conducting additional field survey in the Naka River

The geomorphological changes caused by the implementation of SR were the common investigating aspect that was widely discussed in several replenishment projects, for instance, the grain size of substrates and bars, the adjustment of channels, and the formation of habitat structures (D. Gaeuman, Krause, A., 2013; S. Kantoush et al., 2010). Such alterations help understand the impacts of SR and provide valuable references for further optimization of the river restoration works. In the Naka River, the relevant survey of downstream geomorphological patterns has already been conducted since 2010. Specifically, the bathymetric survey of 70 cross sections from Nagayasuguchi dam to Kawaguchi dam with an interval of 200 m was implemented from 2010 to 2017. Moreover, grain size measurements of several gravel bars and riffles were also conducted by grid approaches. However, such a survey was lacking in recent years from the river office and it is worthwhile to continuously conduct it by ourselves to better understand the geomorphological changes. Due to the limitation of instruments and the role of the River office, our field measurements of geomorphological parts mainly focused on the grain size of gravel bars. A novel approach for measurement of grain size through photos by BASEGRAIN was utilized since it is more accurate and simple than the traditional method. The measured results were compared to the previous measurement from the River office to investigate the impacts of SR on the grain size of bars. Furthermore, turbidity is another essential issue that should be considered in the aquatic ecosystem. We installed a turbidity meter 3 km downstream of the SR site to measure the SSC from May to October 2022.

Besides the downstream geomorphological changes, as mentioned before, the characteristics of replenishment, for instance, flow patterns around the replenishment site, is another crucial part to understand the erosion process of the stockpile. Generally, such flow patterns are measured and collected from gauges or instruments. Specifically, the rating curves are usually used for the estimation of flow discharge with the assistance of water level measurement (Dottori, Martina, & Todini, 2009). Furthermore, current meters are commonly utilized in river gauges for flow velocity measurement around the world due to their lower price and convenience. Another high-accuracy approach called Acoustic Doppler Current Profiler (ADCP) is also widely used for conducting flow area yet it is more expensive and time-consuming. However, Such approaches can not be utilized in the Naka River due to several points: (1) there are no river gauges downstream of the Nagayasuguchi dam, which means that the data of flow patterns can not be directly collected; (2) the magnitude of flushing flow for replenishment is higher in the Naka River (greater than 1000 m^3/s), and the

traditional method for flow velocimetry is difficult to implement since the operator can not access the river and control the field equipment in a particular situation (Hauet, Creutin, & Belleudy, 2008). To overcome such difficulties and limitations, non-intrusive velocimetry using an image-based approach is developed and utilized in the Naka River to measure the real-time flow patterns and enhance the investigation of SR erosion during such extreme flood conditions. Additionally, the measured velocity from the image-based approach can also be used for calibration and validation of the 2-dimensional numerical model to investigate the downstream geomorphological changes.

3.3. Field measurement of downstream gravel bars

3.3.1. Introduction of BASEGRAIN

BASEGRAIN is an image-based approach for the measurement of fluvial non-cohesive gravels through a granulometric investigation based on the MATLAB code (Detert & Weitbrecht, 2013). It is widely used for the analysis of grain sizes in both riverine and coastal areas, for instance, Rhine River (Chardon, Piasny, & Schmitt, 2021), Mimikawa River (Takechi, Aragaki, & Irie, 2021), and Mihama Coast (Kiku, Nakamura, & Mizutani, 2017). The outlines of grains can be detected automatically from photos after several pre-processes, including detection and filtering by double grayscale threshold approach and watershed algorithms (Detert & Weitbrecht, 2013). Compared to the traditional grid method and sieving method, the BASEGRAIN approach can obtain similar results efficiently and economically. However, the quality of analysis results from BASEGRAIN is highly dependent on the resolution of the photos, the angle of shooting, and the distance between the camera and the grains. Hence, it should be carefully to take the photos of grains in order to get an acceptable result.

3.3.2. Materials and methods

During our four times field surveys of the Naka River, a total of four gravel bars were investigated, located around 1 km (gravel bar 1), 1.5 km (gravel bar 2), 3 km (gravel bar 3), and 11 km (gravel bar 4) downstream of the replenishment site (Figure 3-8). At each gravel bar, we measured the GSD from the bar head to the bar tail with various intervals depending on the length of the bar.

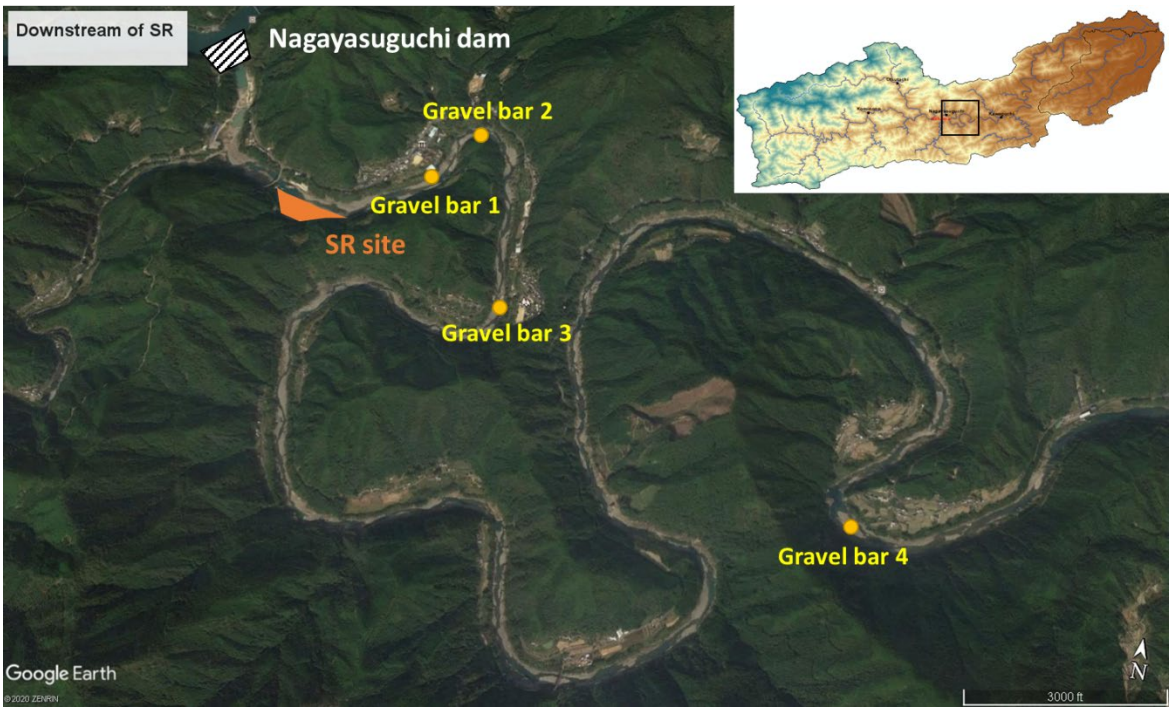

Figure 3-8 The measured locations of four gravel bars during the field survey in the Naka River.

At each gravel bar, several photos were taken to manually compare the alterations of GSD and measure the GSD based on BASEGRAIN. Specifically, the photos were taken from the iPhone with 3024 pixels to 4032 pixels (72 dpi). The distance between the camera and the ground was maintained at around 1 meter and the shooting angle is 90 degrees to avoid errors and enhance accuracy. A meter was placed to help us set the scale of the photo for the calculation of the grain size. During the analysis, several parameters should be adjusted to obtain the acceptable outline of the grains, such as gray-thresh value, size of the median filter, and minimal size of the grain. After the analysis from the BASEGRAIN, it is also required to manually check some grains with errors through tools of departing, merging, and blanking. After several trials and adjustments of the parameters, an acceptable result of BASEGRAIN analysis is shown in Figure 3-9. It can be noticed that the result is still not good since some grains with dark color can not be successfully detected. Despite this, small grains under the big rocks can not be analyzed as well. It can be expected that the analyzed results from BASEGRAIN are overestimated since such loss and errors in small grains. Nevertheless, the BASEGRAIN can be considered a useful tool to roughly know the overall grain size of grains.

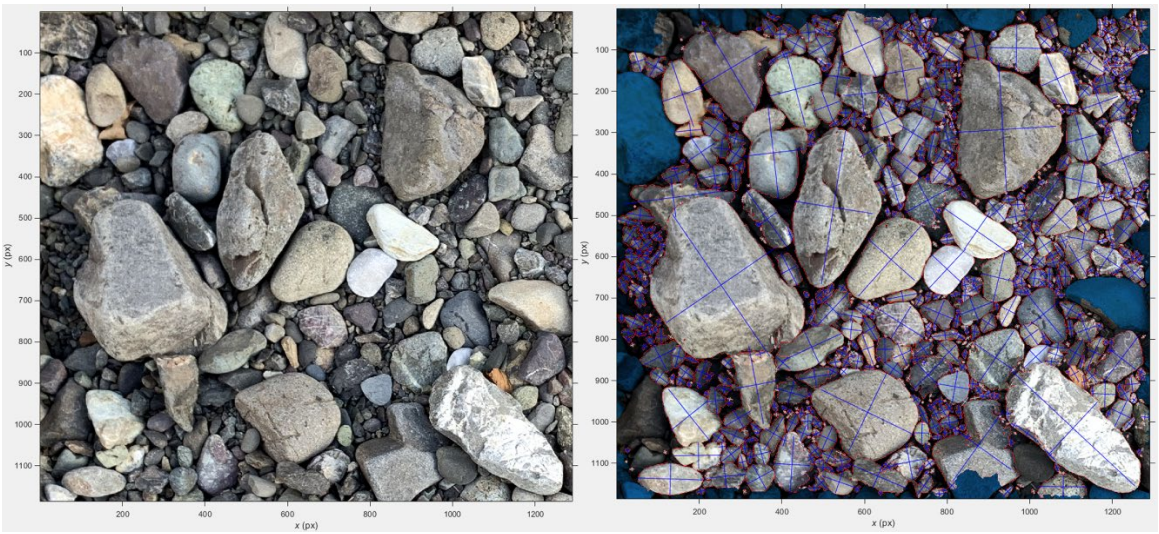

Figure 3-9 The analyzed result of BASEGRAIN. Left figure: original photo. Right figure: analyzed the result of grains by BASEGRAIN.

3.3.3. Results of grain size measurement

3.3.3.1. Gravel bar 1

The gravel bar 1 was located 1 km downstream of the replenishment site and we conducted the measurement during our first field survey on December 2020. From the bar head (0 m), we measured six points with an interval of 10 m to investigate the longitudinal changes in grain size along the bar (Figure 3-10). Due to the limitation of BASEGRAIN, only results at four locations (0 m, 20 m, 40 m, 60 m) can be determined. Slightly different substrates distribution can be observed along the bar from head to tail. Specifically, small gravels (2 cm to 5 cm) were the dominant grains at the bar hear (Figure 3-11, 0 m). While the number of small gravels was reduced and the percentage of cobbles (>20 cm) was increasing with the increasing distance from the bar head (Figure 3-11, 20 m, 40 m). Nevertheless, same some gravel can be founded under the large cobbles near the bar tail (Figure 3-11, 60 m). The results determined from the BASEGRAIN also show the same phenomenon (Table 3-3). The grains at bar head were much finer than those at the middle and tail of the bar. Furthermore, the grain size was similar among the middle and tail of the bar (20 m, 40 m, and 60 m) and only some differences in D10 can be observed at 60 m.

Despite this, the grain size measurement at the middle area of the same gravel bar from the previous field survey was included here to discuss the temporal alterations (Figure 3-12). Due to the limitation

of data, only detailed measurements in 2017 can be founded from the River office. It can be noticed that the grains in 2017 were finer than in 2020 due to the lack of small to median gravels (5 mm to 40 mm). Based on the grain size of replenished material in 2014 (dash line in Figure 3-12), it can be expected that the SR provided the majority of such gravels to the downstream reach. Therefore, the deficit of sediment supply from the replenishment site may occur in recent years to lead to such a shift of GSD at gravel bar 1.

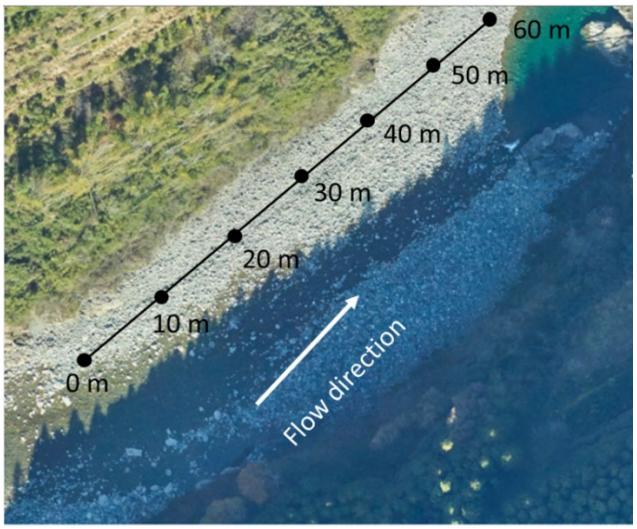

Figure 3-10 The measured points at gravel bar 1 (the meters means the distance from the bar head)

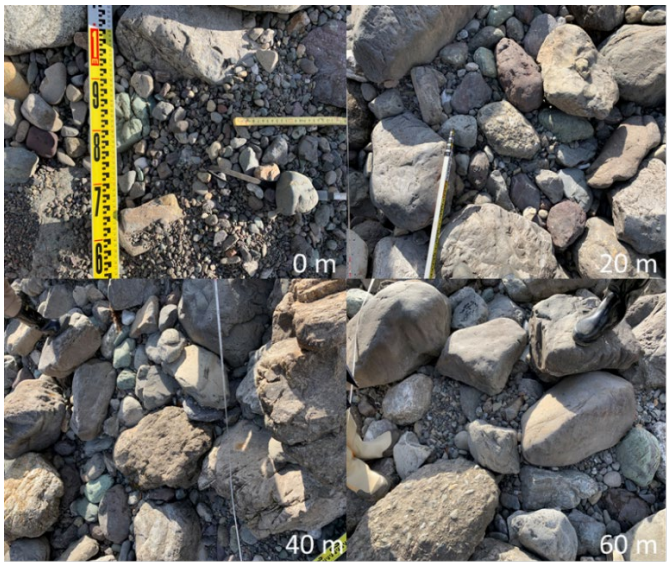

Figure 3-11 The photos of grain distribution at 0 m, 20 m, 40 m, and 60 m at gravel bar 1 in 2020 field survey.

Table 3-3 The results of grain size determined from the BASEGRAIN at four locations at gravel bar 1 (including four representative grain sizes D10, D30, D50, and D90).

Distance from the bar head	0 m	20 m	40 m	60 m
D10 (mm)	10.2	31.2	34.5	21.9
D30 (mm)	7.9	108.8	110.3	108.3
D50 (mm)	17.5	169.5	162.3	156.3
D90 (mm)	35.8	236.2	256.2	261.5

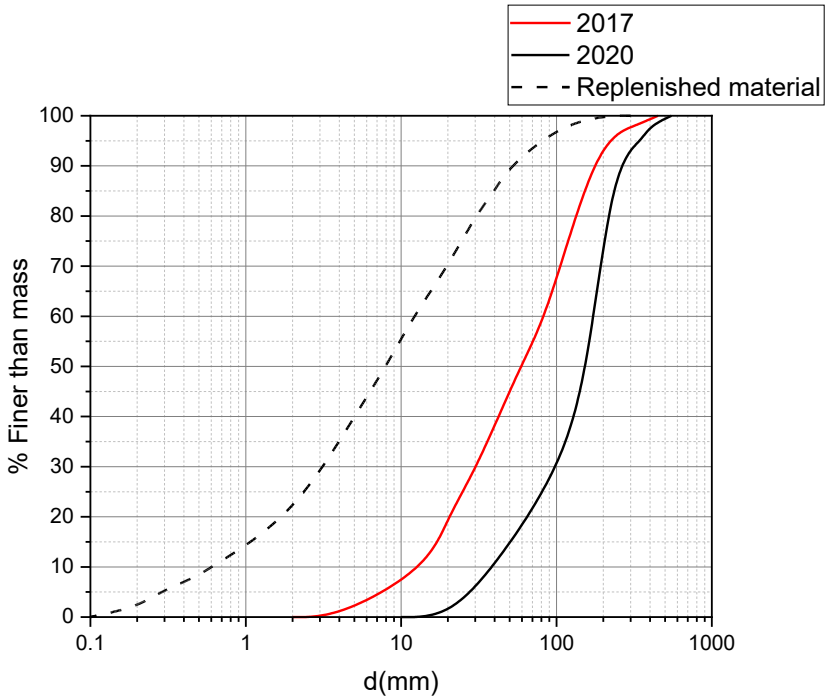

Figure 3-12 The comparison between the previous field survey from River Office (2017) and our field survey (2020) at the middle area of gravel bar 1. The grain size of replenished material in 2014 was also included to show the influence of SR.

3.3.3.2. Gravel bar 2

Gravel bar 2 was located 1.5 km downstream of the replenishment site and the field measurement was implemented during the same field visit at gravel bar 1 (December 2020). We measured four points from the bar head to bar tail with an interval of 10 m since the bar was shorter than the previous one (Figure 3-13). It was a typical point bar located at the inner side of the curve channel and finer sediment can be founded to be deposited here (Figure 3-14). To be specific, from the bar hear to the bar tail, the number of small gravels (5 cm to 10 cm) was reduced. Despite this, some extremely large

cobbles (20 cm to 30 cm) can be founded near the bar tail which was not observed at the bar head. The results from BASEGRAIN reveal no significant differences in grain size from bar head to bar tail (Table 3-4). Only the D90 was increased by around 25% at 20 m and 30 m due to the exist of large cobbles.

The comparison between the previous survey in 2017 and our field measurement in 2020 at the middle area of gravel bar 2 was shown in Figure 3-15. The percentage of finer gravels was increasing in 2020 since the curve was shifted to the left side. It can be expected that replenished sediment was more likely to be deposited here, which assisted the formation of a point bar at the inner bank of the meandering channel.

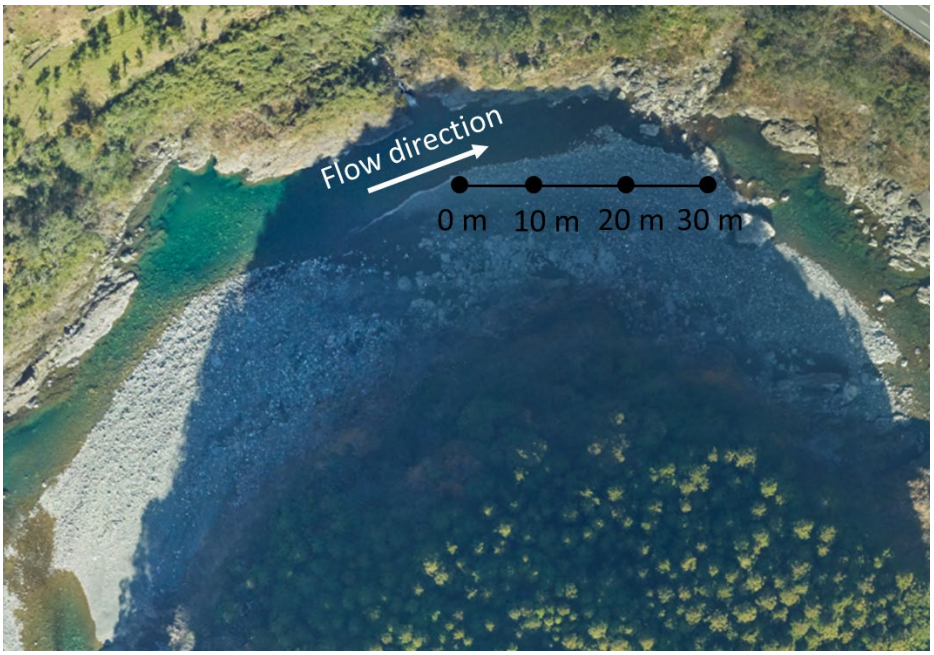

Figure 3-13 The measured points at gravel bar 2 (the meters mean the distance from the bar head).

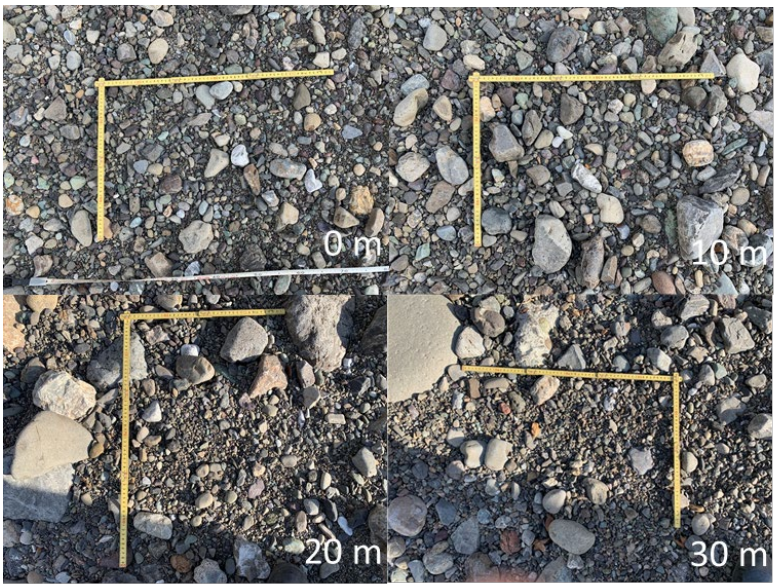

Figure 3-14 The photos of grain distribution at 0 m, 10 m, 20 m, and 30 m at gravel bar 2 in the 2020 field survey.

Table 3-4 The results of grain size determined from the BASEGRAIN at four locations at gravel bar 2 (including four representative grain sizes D10, D30, D50, and D90).

Distance from the bar head	**0 m**	**10 m**	**20 m**	**30 m**
D10 (mm)	4.2	4.1	4.4	4.6
D30 (mm)	8.3	9.2	8.1	11.4
D50 (mm)	23.5	21.3	24.4	24.6
D90 (mm)	54.2	45.3	70.5	72.2

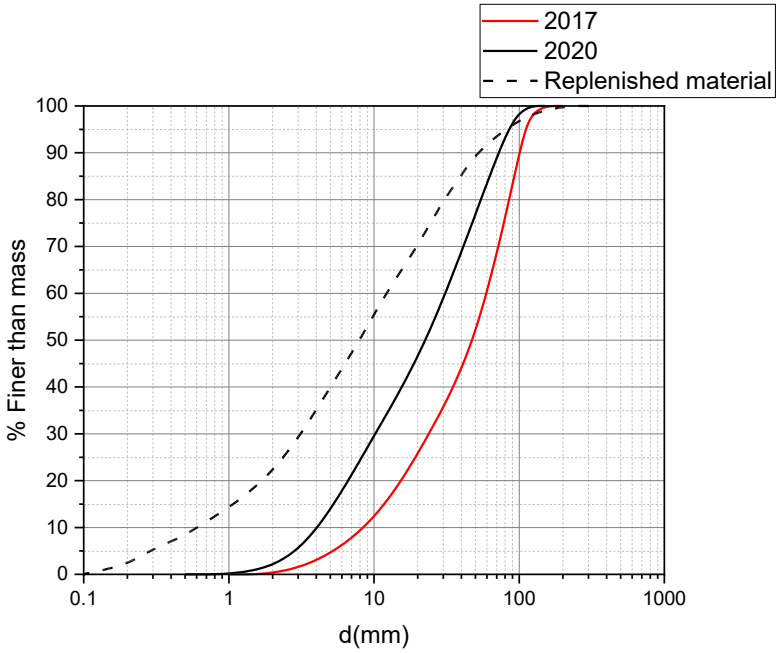

Figure 3-15 The comparison between the previous field survey from River Office (2017) and our field survey (2020) at the middle area of gravel bar 2. The grain size of replenished material in 2014 was also included to show the influence of SR.

3.3.3.3. Gravel bar 3

The gravel bar 3 was located around 3 km downstream of the replenishment site. It was also a point bar created at the inner bank of the meandering channel. Due to the length of the bar being too long, we only measured the grain size within a 30 m area from the bar head to the middle part (Figure 3-16). According to the photos, the coarse gravels and large cobbles (greater than 30 cm) were the dominant grain types at gravel bar 3 (Figure 3-17). Moreover, less small to medium gravels can be founded below the cobbles at all of the survey points. The analysis results of BASEGRAIN show a similar grain size distribution at 0 m, 10 m, and 20 m (Table 3-5). However, the number of large cobbles was reduced, which lead to a reduction of grain size at 30 m.

The previous measurements conducted in 2008, 2011, and 2017 near 20 m were included to investigate the impacts of SR at gravel bar 3 (Figure 3-18). Specifically, the armoring problem was efficiently solved by replenishment since more small to median gravels were deposited here. However, the lack of such median sediment tended to be occurred in recent years (2017 and 2020). The supply

volume from the replenishment site was reduced and the grain size of replenished sediment may alter to lead such changes at gravel bar 3.

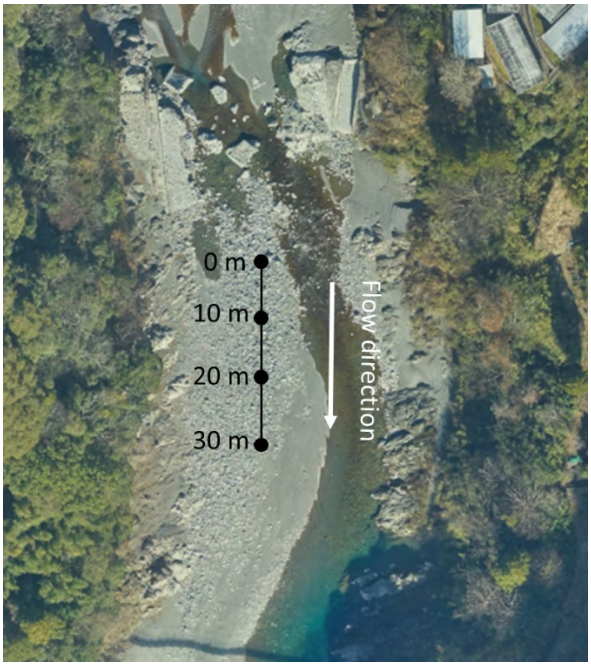

Figure 3-16 The measured points at gravel bar 3 (the meters mean the distance from the bar head).

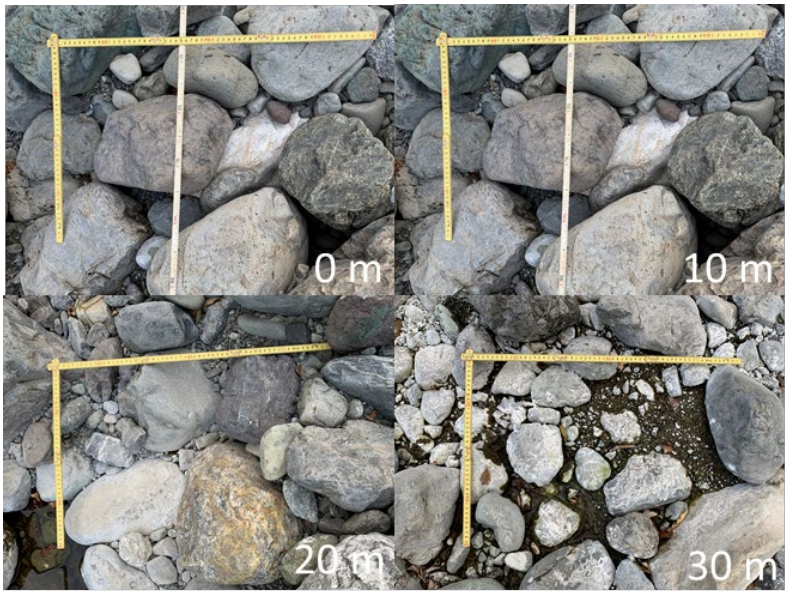

Figure 3-17 The photos of grain distribution at 0 m, 10 m, 20 m, and 30 m at gravel bar 3 in 2020 field survey.

Table 3-5 The results of grain size determined from the BASEGRAIN at four locations at gravel bar 3 (including four representative grain sizes D10, D30, D50, and D90).

Distance from the bar head	0 m	10 m	20 m	30 m
D10 (mm)	8.7	8.8	8.2	8.4
D30 (mm)	34.5	24.5	33.9	26.6
D50 (mm)	95.5	90.5	86.6	64.2
D90 (mm)	187.2	192.3	172.3	127.8

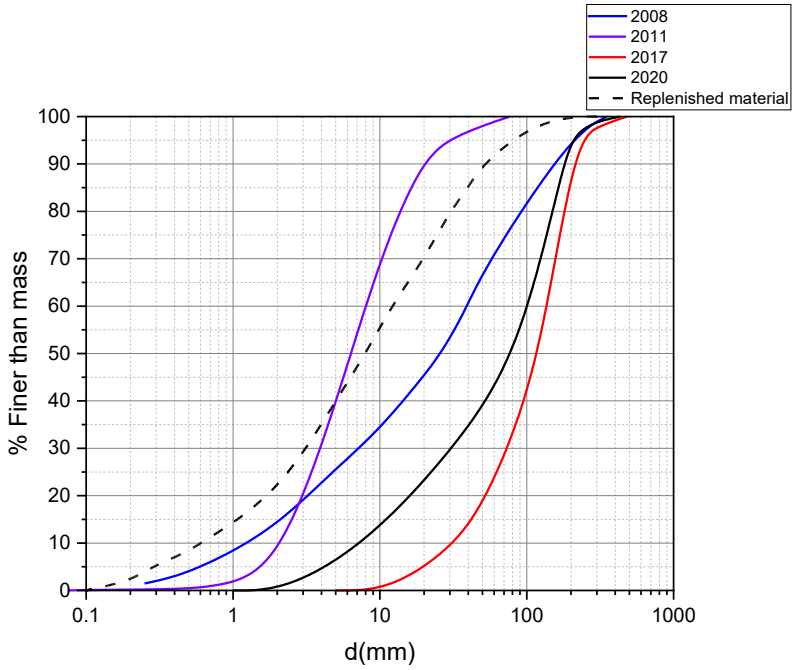

Figure 3-18 The comparison between the previous field survey from River Office (2008, 2011, and 2017) and our field survey (2020) at 20 m in gravel bar 3. The grain size of replenished material in 2014 was also included to show the influence of SR.

3.3.3.4. Gravel bar 4

The gravel bar 4 was located around 12 km downstream of the replenishment site. Upstream of the bar, there was a deep pool with a depth greater than 10 m (based on 2017 bathymetry). The survey was conducted during our field survey in 2022 with an interval of 10 m, and the GSD of each 20 m was calculated to investigate the variations of grains (Figure 3-19). According to the photos, it can manually be observed that the majority of the large gravels and cobbles occurred at the bar head and the middle part (Figure 3-20). However, such gravels and cobbles were rarely founded at the bar tail, which means that lower bed shear was expected here to restrict the transportation of finer grains.

According to the results of GSD measurement, the bar tends to be finer from head to tail, which is the common grains sorting phenomenon that has already been proved by Ashworth (1996).

The time variation of grain sizes was analyzed based on the previous survey in 2010 and 2017 (Figure 3-21). Specifically, the bar tended to be finer from 2010 to 2017, while becoming coarser from 2017 to 2022. According to the on-site photos (Figure 3-20), the bar was highly influenced by the replenishment since small to median gravels were the dominant grains here (similar to replenished sediment). Hence, such tendency of finer or coarser may have a direct correlation to the quantity of transported sediment from the replenishment site. Considering the rare appearance of flood events in recent years, less sediment supply from the replenishment site can be expected, which leads to the coarsening of the gravel bar here.

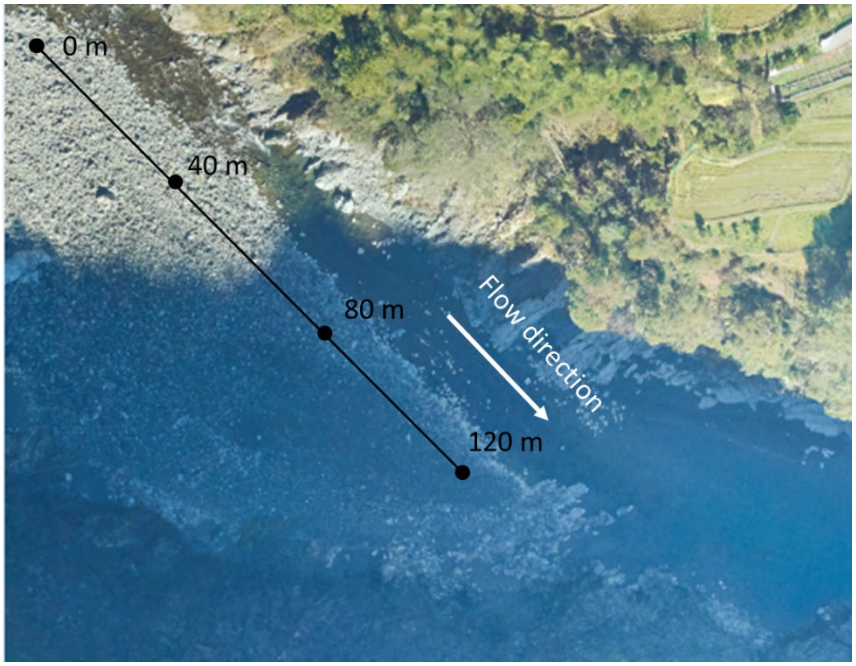

Figure 3-19 The measured points at gravel bar 4 (the meters mean the distance from the bar head).

Figure 3-20 The photos of grain distribution at 0 m, 40 m, 80 m, and 120 m at gravel bar 4 in the 2022 field survey.

Table 3-6 The results of grain size determined from the BASEGRAIN at four locations at gravel bar 4 (including four representative grain sizes D10, D30, D50, and D90).

Distance from the bar head	**0 m**	**40 m**	**80 m**	**120 m**
D10 (mm)	17.4	18.8	17.6	8.5
D30 (mm)	33.6	46.2	38.4	18.3
D50 (mm)	54.2	82.5	64.6	34.2
D90 (mm)	147.8	192.2	154.3	74.5

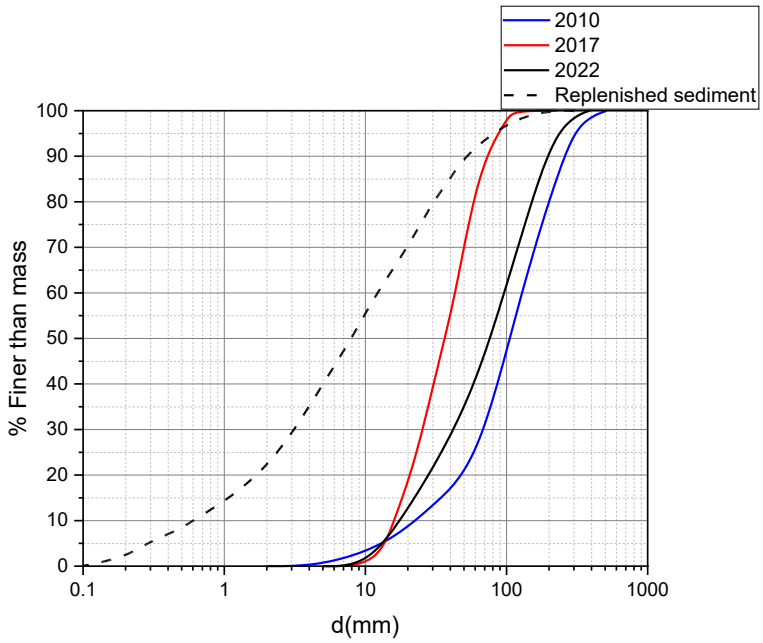

Figure 3-21 The comparison between the previous field survey from River Office (2010 and 2017) and our field survey (2020) at the middle area in gravel bar 4. The grain size of replenished material in 2014 was also included to show the influence of SR.

3.3.4. Discussion and conclusion of gravel bar alterations

According to our field survey and previous survey from the river office, both temporal and spatial variations of grain sizes and distributions can be founded. To be specific, the spatial alterations of bars (for instance, from bar head to bar tail) have close correlations to the variations of flow velocity and bed shear stress (Babej, Máčka, Ondrejka, & Peterova, 2016). Some finer grains were founded at the bar head of gravel bar 1, which means that bed shear stress and velocity may reduce here. The increasing channel width and capacity from upstream to gravel bar 1 may be the crucial reason that leads to such aggradation at the bar head. For gravel bar 2, uniform distribution of similar finer grains was observed along the entire bar from head to tail. It can be expected that gravel bar 2 was a newly formed bar due to the sediment supply from the replenishment site since the grain size distribution was close to the replenished sediment. The bar location may be the vital reason to cause such formation as significant aggradation usually occurs at the convex bank of the meandering channel (Izumi & Aoki, 2012; Lageweg et al., 2015). Regarding bar 3, the same aggradation of finer sediment can be observed in the middle area since the channel becomes meandering from the middle to the bar

tail. In the contrast, majority of the bar 4 was located at the concave bank of the channel, which means that the flow velocity and erosion were greater and boundary stress was higher (Stoesser, Ruether, & Olsen, 2010). Therefore, rare distribution of finer sediment was observed at the bar head and middle area. And deposition was expected to occur near the bar tail since a small pool was located at the downstream area and the flow velocity and shear stress will be decreased.

Regarding the temporal alterations of bars, the same coarsening tendency can be observed at gravel bar 1 and gravel bar 4 from 2017 to recent years (2020 and 2022). The reduction of sediment supply from replenishment sites in recent years significantly raised the grain sizes here since higher erosion can be expected in those areas during floods. Nevertheless, the opposite tendency of grain size alterations can be observed in gravel bar 2 and gravel bar 3 as those locations can be recognized as deposited areas (near the convex bank). Moreover, compared to the year before replenishment (2008), more median-size sediment (5 mm to 40 mm) was deposited at gravel bar 3 to enrich the sediment ranges in 2011.

In summary, the spatial alterations of gravel bars in the Naka River follow the principle of aggradation and degradation in a meandering river. The higher numbers of the meandering area cause the unique formations of bars, riffles, and pools, which can be further investigated based on a detailed geomorphic survey.

3.4. Field measurement of SSC by turbidity meter

3.4.1. Introduction of turbidity meter

The installed turbidity meter is Infinity-ATU75W2-USB, which utilized 4 pieces of batteries and the maximum measured period is around 5 months. The installed location is 3 km downstream of the SR site (Figure 3-22). We utilized brackets, anchors, bolts, and steel bands to fix the protected pipe (Figure 3-22). The turbidity meter was hung inside the pipe with a steel wire.

The turbidity meter recorded the data every 15 mins. At each recorded period, a total of 3 values were recorded with an interval of 1 min. The average value of those recorded values was calculated as the representative SSC at each reading time. Due to the angle of the installed meter is around 30 degrees instead of 90 degrees, the sediment may be stuck at the bottom, and some errors occurred in the

recorded values (extremely higher values or negative values). Those errors should be deleted to ensure the availability of the data.

Figure 3-22 Top figure: the installed location of the turbidity meter in the Naka River. Bottom figure: the photo of the turbidity meter and the installed method.

3.4.2. The results of the measured SSC

The measured period of the SSC is from 16th May to 14th October 2022. The measured SSC in mg/l and the releasing discharge from Nagayasuguchi dam were shown in Figure 3-23. It can be noticed that the SSC was increased during the flood events. Higher releasing flow not only increased the volume of sediment input from upstream but also promoted sediment transportation at downstream reach.

The extreme flood event that occurred in September was selected to analyze the inner relationship between discharge and SSC (the black circle in Figure 3-23). It can be observed that the occurrence of peak value for SSC was always delayed with the peak value of discharge (left figure in Figure 3-24). The difference in peak timing leads to the counter-clockwise hysteresis in the discharge-SSC relationship (right figure in Figure 3-24), which has already been investigated and proved in the Mad River watershed (Javed, Hamshaw, Rizzo, & Lee, 2019) and the Na Borges basin (Estrany & Garcia, 2005).

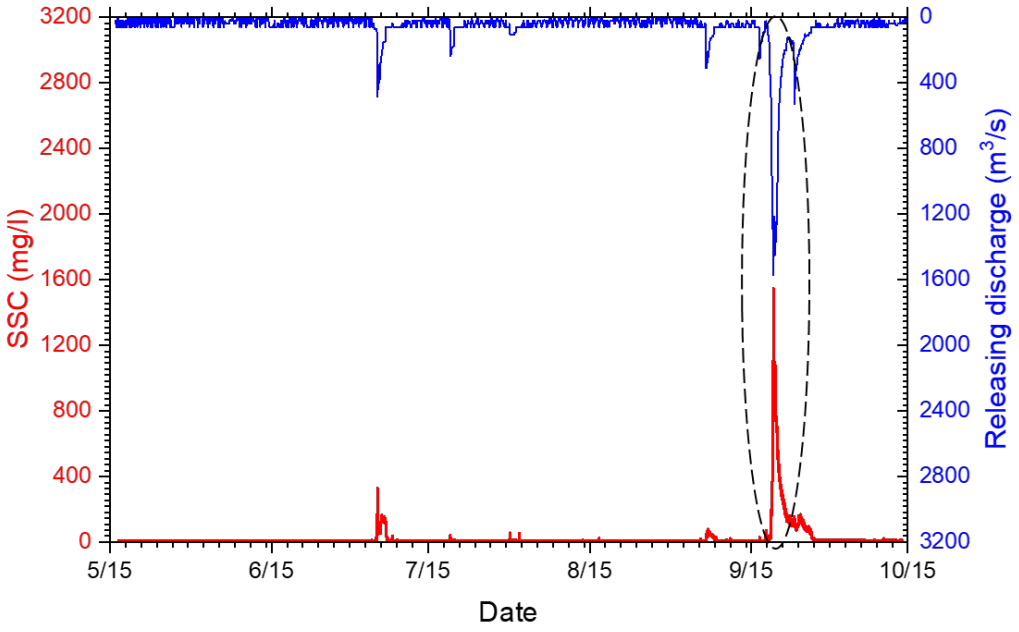

Figure 3-23 The measured SSC by the installed turbidity meter and the releasing discharge from Nagayasuchi dam in 2022. The black circle represents the target flood event for analyzing the inner relationships.

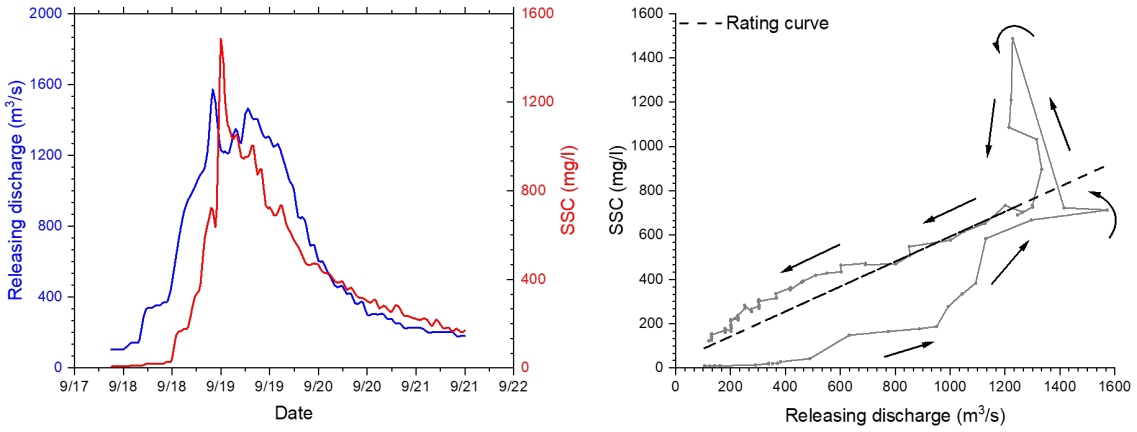

Figure 3-24 Left figure: the time series of releasing discharge and SSC during the flood event in September 2022. Right figure: the discharge-SSC relationship shows the hysteresis.

3.5. Real-time measurement of flow patterns through the image-based approach

3.5.1. Backgrounds of the image-based approach

The non-intrusive velocimetry utilizing an image-based approach is widely used for river gauges around the world. Specifically, the surface velocity can be determined according to the particle tracking and image intensity from the validated images captured from cameras (Fleet, 2012). This approach has already been conducted for around 30 years at several rivers with various types of cameras. Particle image velocimetry (PIV) was the first image-based approach that developed in the mid-1990s, which relied on the analysis of correction among tracers on the water surface (Fujita & Komura, 1994). Moreover, several evolving techniques for correlation-based dynamics were also developed, including Large Scale Particle Image Velocimetry (LSPIV) developed by Fujita, Muste, and Kruger (1998) and Large Scale Particle Tracking Velocimetry (LSPTV) by Brevis, Niño, and Jirka (2011). Furthermore, novel methods based on the investigation of image intensity were established as well, such as Space-Time Image Velocimetry (STIV) (Fujita, Watanabe, & Tsubaki, 2007) and Surface Structure Image Velocimetry (SSIV) (Leitão, Peña-Haro, Lüthi, Scheidegger, & de Vitry, 2018). These non-intrusive approaches have already been successfully utilized for the

calculation of instantaneous flow velocity with errors of less than 20% (Al-mamari, Kantoush, Kobayashi, Sumi, & Saber, 2019; Fujita, Notoya, Tani, & Tateguchi, 2019; Kim et al., 2008; Sun et al., 2010).

Despite this, it is also important to note that the visible features on the river surfaces are the signature of riverbed alterations and related turbulences that the PIV technique can utilize by the Large Eddy approach (Sheng, Meng, & Fox, 2000). Lewis and Rhoads (2015) evaluated the surface turbulence for a natural flow based on the PIV approach. Johnson and Cowen (2017) have utilized the dissipation rate of surface turbulence (TKE) to calculate the water depth without the assistance of an extra bathymetric survey. The approach was further promoted by Jin and Liao (2019), and the final results showed good agreement with the field survey in the application in the Milwaukee River. Moreover, Kobayashi et al. (2022) investigated the variations of flow velocity and dissipation rate of TKE around river training structures and further investigate its linkage to aquatic habitat formation.

Nevertheless, applying an image-based method to measuring river flow still exist its challenges and difficulties. The lack of surface seedings, such as floatable objects, bubbles, and ripples, will lead to an underestimate of flow velocity in the application of the LSPIV approach (Harpold, Mostaghimi, Vlachos, Brannan, & Dillaha, 2006). Additionally, the quality of images (resolution) and the angle of cameras also directly affect the validity of the images, and fair values should be determined to improve the accuracy of results (Fujita et al., 2017). Hence, several pre-enhancement techniques should be utilized to enhance the quality of photos and outcomes.

3.5.2. Materials and methods of the image-based approach

In this study, we utilized the LSPIV and STIV to measure the real-time flow patterns, including surface flow velocity, flow discharge, and water depth near the replenishment site during two flood events that occurred in 2021. The results can assist us to understand the flow conditions near the replenishment site, which is the crucial part to investigate the erosion process of replenished sediment. Furthermore, the results of surface flow velocity can also be utilized as the calibrated data for our numerical model establishment in Chapter 5.

3.5.2.1. Installation of cameras

To collect the required images for LSPIV and STIV, a PTZ (Pan-tilt-zoom) camera with the solar panel was installed on the Kohama bridge, at 45 m above the channel (Figure 3-25). To fix the camera

on the bridge, Yamazaki san from the Technical support of DPRI helped us to design the installation approach and prepare the required materials and tools. Finally, an integral design was generated by Yamazaki san and LIN, including the fixation of the solar panel and mounting part (Figure 3-26). The camera was successfully installed on April 2021 and started to record videos in May 2021. The videos can be transmitted to the PC by the 4G technique at the frame rate of 15 FPS (15 images per second). Then, the images can be extracted from the videos with a resolution of 2550×1440.

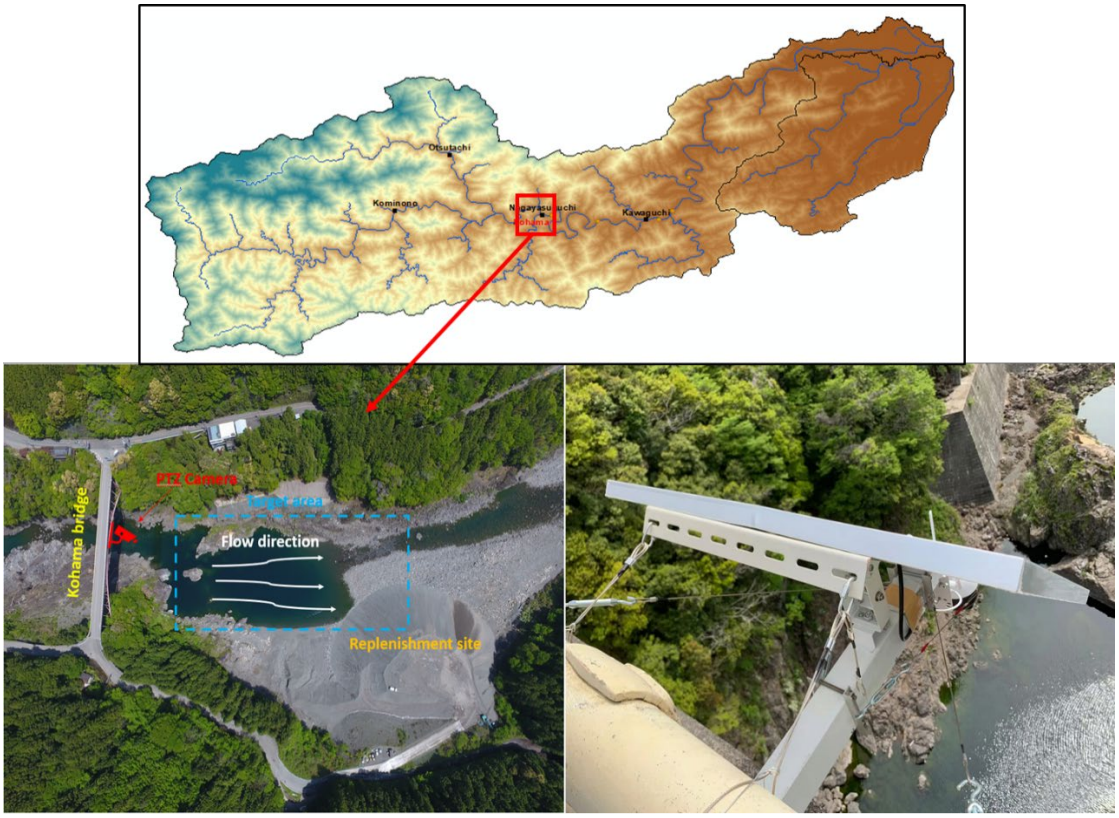

Figure 3-25 The location of camera installed on the Kohama bridge. The left figure shows the plan view of the camera location and replenishment site. The right figure shows the PTZ camera with solar panel.

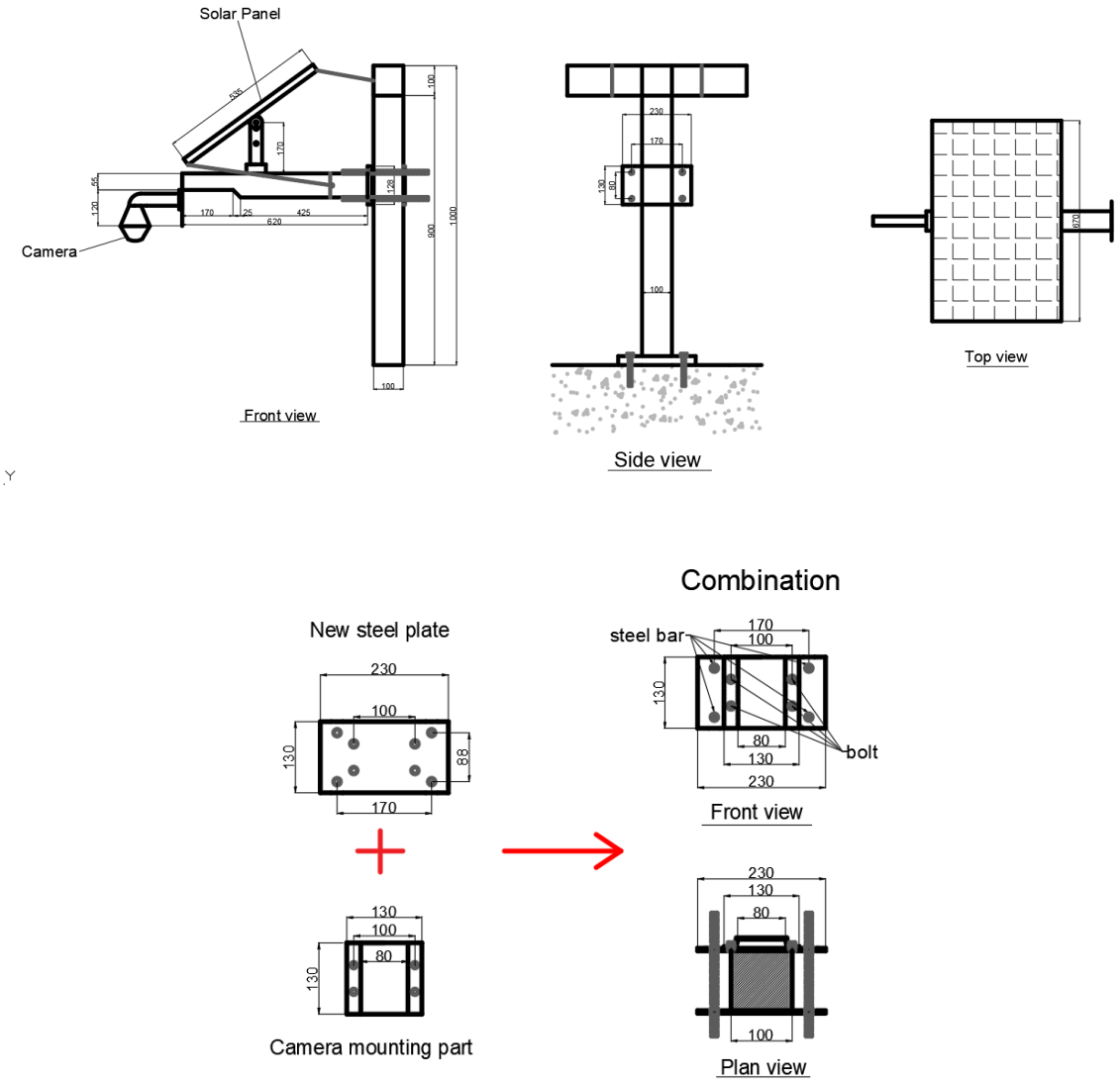

Figure 3-26 The integral design of camera installation on the Kohama bridge. The top figure shows the front view, side view, and top view of the whole camera composition. The bottom figure shows the detailed design of the mounting part.

3.5.2.2. Image processing

Figure 3-27 depicts the required steps for the image-based method utilized in the Naka River. Specifically, several videos were captured during the flood events, and frames were extracted by applying the Fudaa LSPIV, an open-source program (INRAE River Hydraulics, France). To carry out

the geometric correction of the frames, ground control points were set (orthorectification). After that, pre-treatment was conducted to improve the quality of the orthoimages. We made adjustments to several parameters, including resolution, size, and exposure rate. LSPIV and STIV can then be used, respectively, and several approaches regarding filtering and validation of the computed results were also utilized to enhance the results. Finally, based on the measurement of surface flow velocity, flow discharge can be estimated by bathymetric data and water levels, and water depth can be determined through the surface turbulence structures.

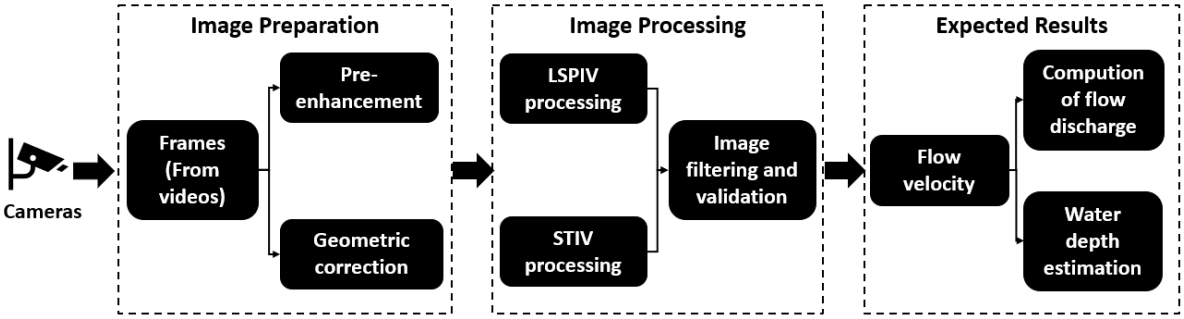

Figure 3-27 Flow chart of the image-based approach for flow measurement, including image preparation, image processing, and expected results.

3.5.2.3. Geometric correction

The images were captured at a 20 degrees oblique angle by the camera. To transfer the images from 3 dimensions to 2 dimensions, the geometrical modification was utilized based on various reference points suggested by Fujita et al. (1998). To be specific, it is a transferring process between the (x, y) coordinates on the moving image and the actual coordinates (X, Y, Z) on the actual image. During our field survey, only four ground control points (GCPs) were set on-site by a total station because of the topography's limitations (Red circle, Figure 3-28). Additionally, four extra GCPs were generated based on the topographical map in ArcGIS to increase the dependability of the ortho-rectified images (Yellow circle, Figure 3-28). Two of them are near the banks' edge. The other is on the rock in the channel's center.

In our study, the Perspective Projection transformation was applied to conduct image rectification using the X, Y, and Z coordinates of each GCP. The relationship between the rectified images and GCPs can be determined by:

$$x = \frac{A_1X + A_2Y + A_3Z + A_4}{C_1X + C_2Y + C_3Z + 1} \qquad y = \frac{B_1X + B_2Y + B_3Z + B_4}{C_1X + C_2Y + C_3Z + 1} \tag{3-1}$$

Where X, Y, and Z are the coordinates of GCPs, and x and y are the coordinates of rectified images. The coefficients A_1 to C_1 can be computed using the least-square approach for at least six known GCPs. The rectified photos for those places far from the camera loss of resolution due to the long distance between the camera and our GCPs (around 200m). To make surface seedings in certain locations more visible, image enhancement should be done.

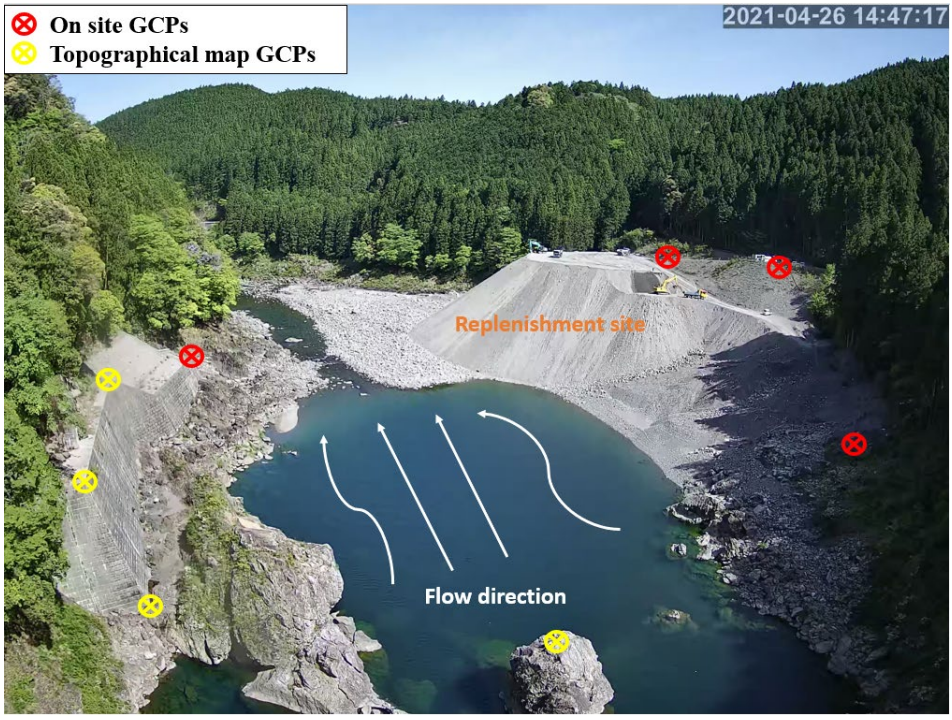

Figure 3-28 Location of ground control points. Red circle: GCPs set on-site by total station. Yellow circle: GCPs set by topographical map from ArcGIS.

3.5.2.4. Image enhancement

Prior to measurement, surface seeding density should be increased to enhance reliability and prevent underestimating of final LSPIV and STIV values (Harpold et al., 2006). However, the properties of seedings (colors, size, and shape) and environmental patterns (sunlight, shadow, and wind) may have

an adverse impact on the precise tracking of surface particles (Dal Sasso, Pizarro, Samela, Mita, & Manfreda, 2018). As seen in Figure 3-29 A, the floating debris, flow waves, and foams were not visible on the water's surface. Those seedings were challenging to track during the LSPIV and STIV processes, particularly in areas with low resolution and low flow along the riverbank (far from the camera).

To modify the features of the photographs, an image-enhancing operation should be carried out to lessen this negative influence. Here, batch processing was used to improve every frame using the open-source program ImageJ. To prepare for the next modification, the photos were first converted to RGB images. Then, to highlight the differences between tracers and water surfaces, the brightness and contrast were adjusted., At the same time, the riverbank's visibility was diminished by reducing the noise from the regional outflow. The exposure rate was then altered, further enhancing the sharpness of the surface waves and foam, and the window/level of the photos was modified. Eventually, smooth and sharp commends were applied to display the shape of the seedings. According to Figure 3-29 B, the quantities of visible seedlings were successfully increased after the enhancement, and more accurate results can be expected to obtain from subsequent LSPIV procedures.

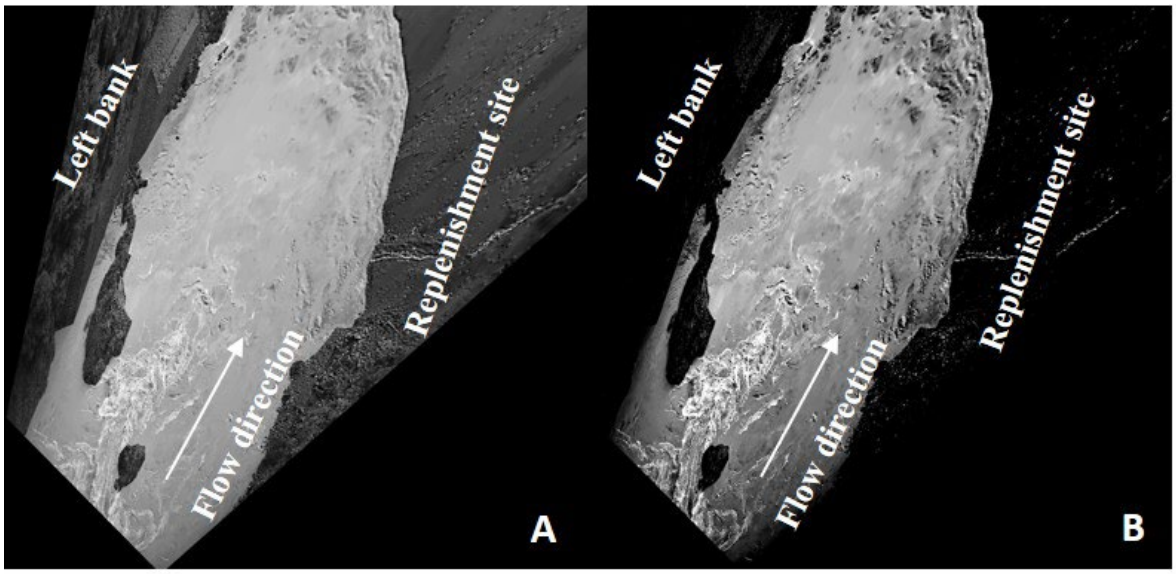

Figure 3-29 The results of image enhancement. A: Image after geometric correction without enhancement. B: Image after enhancement by ImageJ.

3.5.2.5. Procedure of LSPIV

Regarding the implementation of LSPIV, we used a commercial software called Dynamic studio (Dantec Dynamics A/S, Skovlunde, Denmark) to conduct the procedure of the cross-correlation, validations, filtering, and vector analysis of the improved images to measure flow velocity. Specifically, floating objects, riffles, and waves are examples of natural seedings that can depict the dynamic of surface flow. Cameras can record these surface seedings and display them on the image frames. It is possible to determine the representative velocity vectors for each particle by contrasting two photos taken at known intervals. The entire flow area can be subjected to vector analysis to get a velocity map (S. Kantoush & Schleiss, 2009).

In Dantec, at first, based on the FPS of the recorded video, we chose an appropriate time interval of 1/15 between two orthoimages. After that, the interrogation area (IA) should be built to ensure it is both large enough to contain all visible seedings inside it, and meanwhile, small enough to retain the scale of the interested region (Le Coz, Hauet, Pierrefeu, Dramais, & Camenen, 2010). In our research, an IA window with a size of 64 x 64 pixels and an overlap of 75% were chosen as the appropriate values for cross-correlation implementation. The image was filtered to remove some discontinuities at the edges of various noises using a recommended approach from Xu, Ling, and Zheng (2015), a Low-Pass Gaussian filter with a k value of 3. After the correlation between the chosen frames, the flow velocity vectors can be properly constructed (Figure 3-30 A). The undesirable vectors should then be removed, and two validation techniques were used to get reliable data for statistical analysis. In particular, range validation allows a vector map to be checked against a predetermined predicted range of velocities. To prevent unfavorable effects from disproportionate vectors, the min and max values of flow velocity are selected to be between -8 m/s and 8 m/s (rejected vectors in Figure 3-30 B). Then, those vectors that deviate too much from their neighbors were replaced using moving average validation. The average values of the neighbors were selected as the representative (replacement vectors in Figure 3-30, C) to improve the estimation of actual vectors. After validation, the vector map was smoothed using an average filter with an averaging area of 33 pixels, and all prior vectors were replaced with averaging values (Figure 3-30, D). Finally, we used vector statistics to derive statistics from several previously prepared velocity vector maps. The calculated mean velocity, variance, standard deviation, and skew can also be extracted from the maps. Additionally, for our interesting flow area, a scalar map of flow velocity distribution can also be produced.

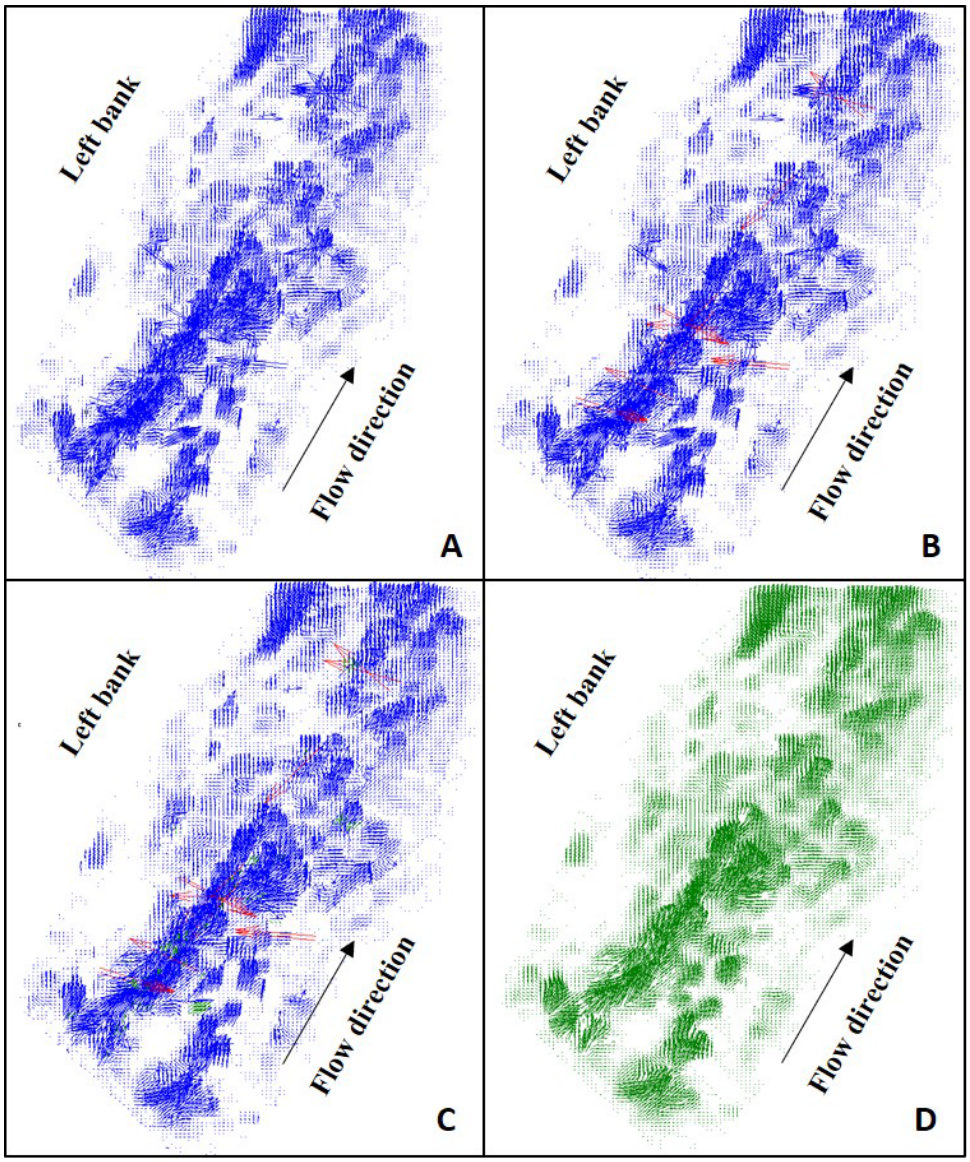

Figure 3-30 The results of flow vectors after conducting several correlations and validations. A: flow velocity vectors after cross-correlation. B: flow velocity vectors after range validation (red color is rejected vector). C: flow velocity vectors after moving average validation (green color means substituted vector). D: flow velocity vectors after the average filter.

3.5.2.6. Procedure of STIV

For a search line chosen in the flow direction, STIV establishes the space-time images (STI) using frames taken from videos (Fujita, Notoya, & Shimono, 2015). A trajectory can be created by examining the brightness change over time, and the angle of the inclination corresponds to the flow

velocity. To analyze the data using the STIV procedure, Hydro-STIV (Hydro Technology Institute Co., Ltd., Japan), a commercial software developed by the AI technology lab of Kobe University was used (Fujita, 2017; Fujita et al., 2019). Regarding the detailed procedure of Hydro-STIV, firstly, we established a survey line at the high flow location between a stable rock on the left side and the right bank. Then, along the survey line, 20 search lines were generated along the streamwise direction with the same interval of 3.5 m, and (Figure 3-31, A). The tilt angle is close to 20 degrees, and the horizontal distance between the camera and the survey line is about 70 meters. The plentiful and remarkable waves, riffles, and foams on the water's surface can significantly improve the STI and the trajectory's precision. After configuring the STI, Fourier correction was used to eliminate any external noise or static. Light pixels from STI can be removed by reducing the range of spatial and time filters, which will also reduce the analysis velocity. To minimize the negative effects of noise while yet maintaining the typical trajectory, two filters should be suitably tuned.

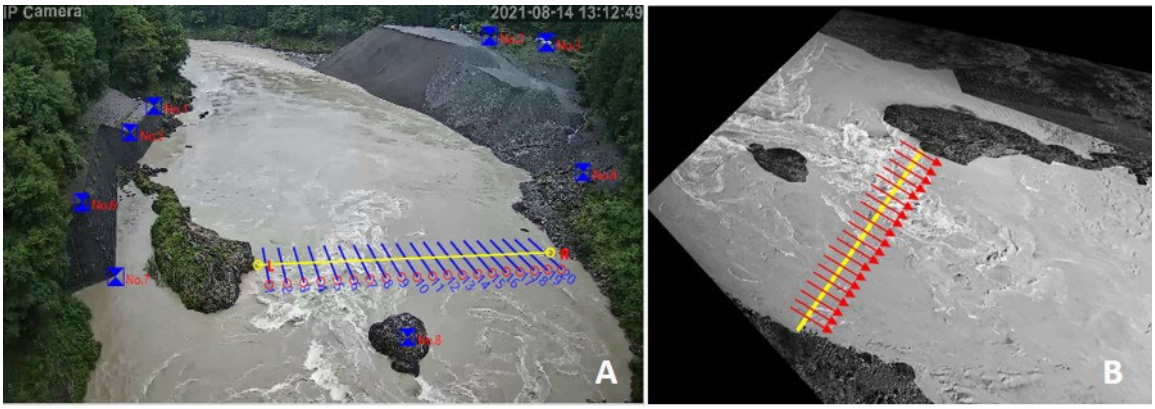

Figure 3-31 The interested survey line in STIV and LSPIV. A: The cross-sectional field with 20 search lines used in STIV. B: The same cross-sectional field with 20 segments used in LSPIV is shown on the orthoimage.

3.5.2.7. Computation of discharge

The identical cross-sectional field was chosen in STIV and LSPIV for analysis to compare the flow discharge from 2 image-based techniques (Figure 3-31 A and B). The selected cross-section was near the camera with high surface turbulence. Such presence of obvious natural seedings helped us to identify movable particles in both approaches. Real-time measuring data from Nagayasuguchi dam

(1.5 km upstream of the study region) was used for comparison and calibration of our results from LSPIV and STIV, respectively.

The bathymetry survey conducted in 2017 by the Naka River office provided cross-sectional data on the relevant field. The cross-section has 20 designated segments, and the following formulas can be used to determine the flow discharge for each segment:

$$q_i = \frac{V_i + V_{i+1}}{2} \cdot \frac{h_i + h_{i+1}}{2} \cdot B \tag{3-2}$$

Where h_i is the depth of the segment, and B is the width of the segment. V_i is the average flow velocity of the segment, which is equal to:

$$V_i = \alpha v_i \tag{3-3}$$

Where v_i is the surface velocity calculated by LSPIV and STIV, α is the coefficient of the rate between surface flow velocity to average flow velocity. It is a vital factor in predicting flow discharge and can differ greatly depending on the cross-section and the flood event (Gunawan et al., 2012). Due to the lack of an on-site measurement, 0.85 is roughly assumed in our research recommended by Creutin, Muste, Bradley, Kim, and Kruger (2003). Moreover, the water level is also crucial in the measurement of flow discharge. In our study, the water level was estimated through an image measuring tool created in the Hydro-STIV software. The pixel position at the water's edge detected from the image can be converted to the water level by calculating the actual length per pixel after establishing the GCPs and using the known height of the vertical structure (embankment at the left bank) (Figure 3-32).

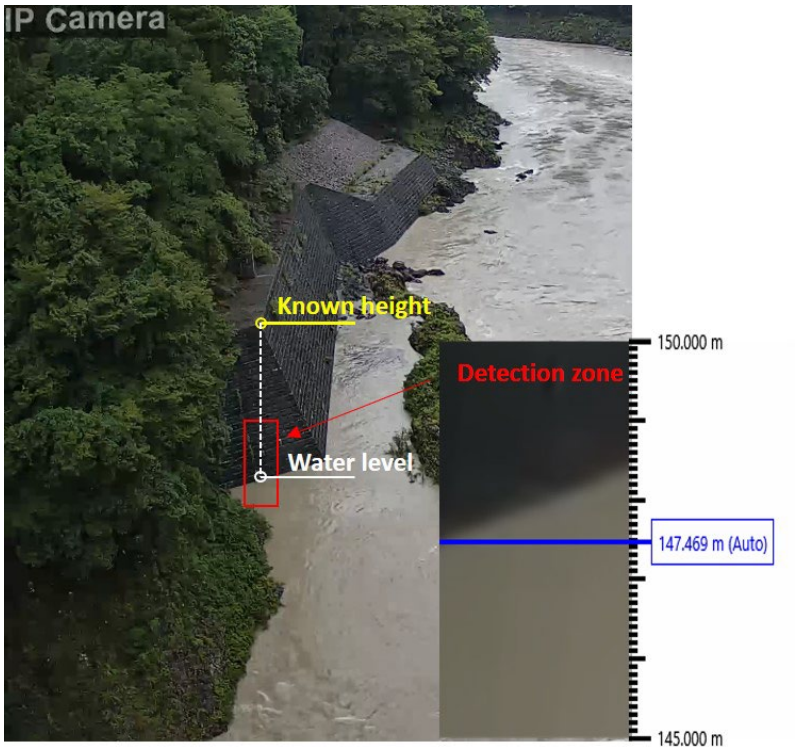

Figure 3-32 The approach utilized for estimating water level by the inner function of Hydro-STIV. The red square represents the detection zone at the edge of the embankment. The blue line represents the estimated water level.

3.5.2.8. Water depth estimation by surface turbulence

Jin and Liao (2019) first applied turbulent surface structures for determining water depth. They utilized the Large Eddy PIV approach, which converted an equation for estimating water depth by considering several surface flow parameters, including depth-averaged shear velocity, bed shear stress, and dissipation rate of turbulent kinetic energy (TKE). Specifically, the depth-averaged velocity was calculated using Manning's equation for the slice:

$$V = \frac{1}{n} H^{\frac{2}{3}} \sqrt{S_f} \tag{3-4}$$

Where n is Manning's roughness, which can be estimated as 0.03 for the natural channel with a clean, straight, and full stage (French & French, 1985). H is the water depth, and S_f is the head loss slope. Then, the momentum equation can be utilized to calculate the friction velocity u_* under the assumption of uniform flow:

$$u_* = \sqrt{gHS_f} \tag{3-5}$$

The relationship between bed friction and turbulence formation can be generated using the Law-of-Wall (LOW). It can be applied to the entire water area if we assume that the local dissipation rate of turbulent kinetic energy (TKE) is equal to the production of surface turbulence. Hence, we can compute the dissipation rate at the water surface as follows:

$$\varepsilon_s = \frac{u_*^3}{\kappa H} \tag{3-6}$$

Where κ is the von Karman constant, which is equal to 0.41 that estimated by Lo, L'Vov, Pomyalov, and Procaccia (2005). By combining Eq. 3-3, 3-4, 3-5, and 3-6

$$V_i = \alpha v_i \tag{3-3},$$

the water depth can be determined as:

$$H = \frac{(\alpha V_s)^2 n^2 g}{(\kappa \varepsilon_s)^{\frac{2}{3}}} \tag{3-7}$$

Where V_s is the surface flow velocity, which can be extracted from LSPIV. The PIV technique can also be used to determine the dissipation rate at the water surface ε_s. Specifically, the Large Eddy PIV approach, which was first established by Sheng et al. (2000), was utilized here to estimate the dissipation rate:

$$\varepsilon_s = -2\tau_{ij}\bar{S}_{ij} \tag{3-8}$$

Where τ_{ij} is the SGS stress tensor, which can be determined by applying the Smagorinsky model:

$$\tau_{ij} = -C_S^2\Delta^2\sqrt{2\bar{S}_{ij}\bar{S}_{ij}}\cdot\bar{S}_{ij} \tag{3-9}$$

Where C_S is the model constant, which should be calibrated by field measurement of flow patterns. Due to the fact that the objective of the study is to test the availability of utilizing the LSPIV approach to estimate the water depth, and meanwhile, we lacked the required field data to calibrate the results. Therefore, we utilized the water depth measured by Hydro-STIV to roughly calibrate the value of C_S , which is equal to 0.8 in our study. And Δ is the size of the interrogation area. By combining Eq. 3-8 and Eq. 3-9, the dissipation rate can be calculated as:

$$\varepsilon_s = 2\sqrt{2\bar{S}_{ij}\bar{S}_{ij}}\cdot C_S^2\Delta^2{\bar{S}_{ij}}^2 \tag{3-10}$$

Where $\bar{S}_{ij}$ is the SGS strain rate tensor, which equals to:

$$\bar{S}_{ij} = \frac{1}{2}\left(\frac{\partial\bar{U}_j}{\partial x_i} + \frac{\partial\bar{U}_i}{\partial x_j}\right) \tag{3-11}$$

In our study, all crucial factors were calculated using Matlab, a traditional mathematic instrument. From the experimental results of LSPIV, we deduced the surface velocity of two directions, U_i and U_j. The distribution of flow velocity, dissipation rate, and water depth in the research region can then be calculated using the Matlab code.

3.5.3. Results and discussion of the image-based approach

3.5.3.1. Stage measurement of releasing flow from Nagayasuguchi dam

To assess the accuracy of the image-based technique in the Naka River, data on flow discharge from the Nagayasuguchi dam (1.5 km upstream of the measuring region) was collected. The utilization of LSPIV and STIV was conducted during two flood events that occurred on 5/20 and 8/12 2021. Figure 3-33 displays the time series of the dam releasing flow from 5/20 to 5/23 and 8/12 to 8/17. The integrated process of flood events cannot be completely recorded due to the limitations on nighttime lighting and camera storage. The rising, peak, and recession of the flood occurrences were included in the period of image-based measurement, which is shown in Figure 3-33 as the red region. Following image-based analysis for the two flood occurrences, a video of 5 minutes in length was captured every 30 minutes. Based on the hydrographs of two flood events, it can be noticed that the releasing discharge peaked after numerous circulations of rising and falling stages. Furthermore, compared to a natural flood, the recession period may last for up to three days. The management and flood control of the Nagayasuguchi dam in the Naka River is remarkable in light of the aforementioned points.

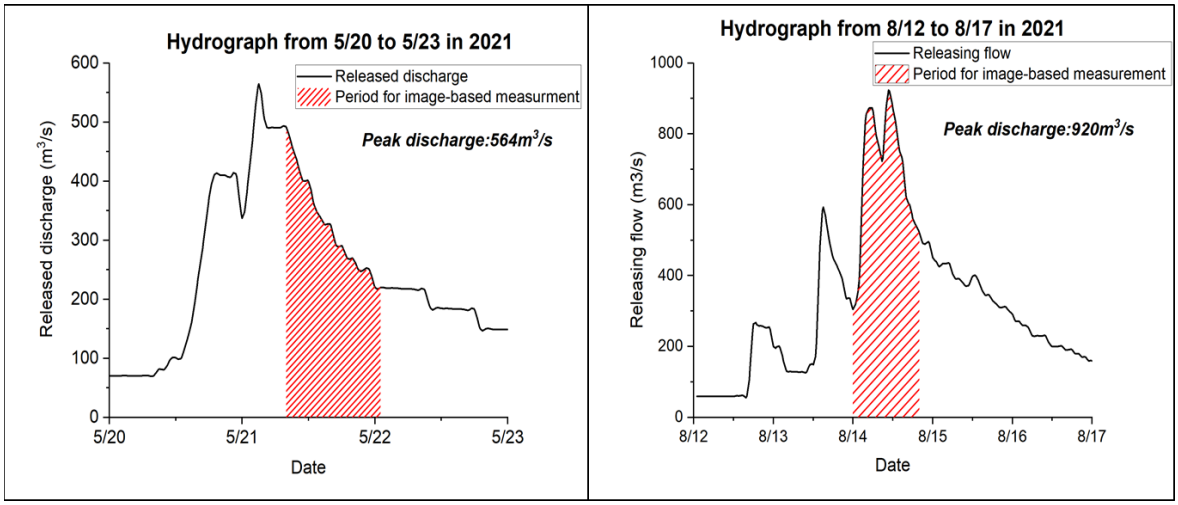

Figure 3-33 The time series of released flow from Nagayasuguchi dam during two flood events happened on 5/20 and 8/12 in 2021. A: flood event started on 5/20. B: flood event started on 8/12.

3.5.3.2. Experimental results of LSPIV

The surface velocity was shown as the vector maps utilizing LSPIV. To analyze the flow velocity distribution under different flow conditions, the flow vectors were analyzed and illustrated when releasing flow from Nagayasuguchi dam equaled to approximately 900 m^3/s and 700m^3/s on 8/14 and 500 m^3/s and 300 m^3/s on 5/21. Figure 3-34 below displays the matching scalar maps that include the magnitudes of surface velocity. It can be noticed that the scale of the map is slightly different since the angle of shooting is difficult to fix and the accuracy of the GCPs may not high. Regarding the results, it can be observed that the LSPIV can estimate the flow distribution and provide a 2-D flow map with a velocity greater than 1 m/s. However, errors with no velocity distribution can be seen in low-flow zones close to the riverbank, which is mostly because of the lack of obvious natural seedings.

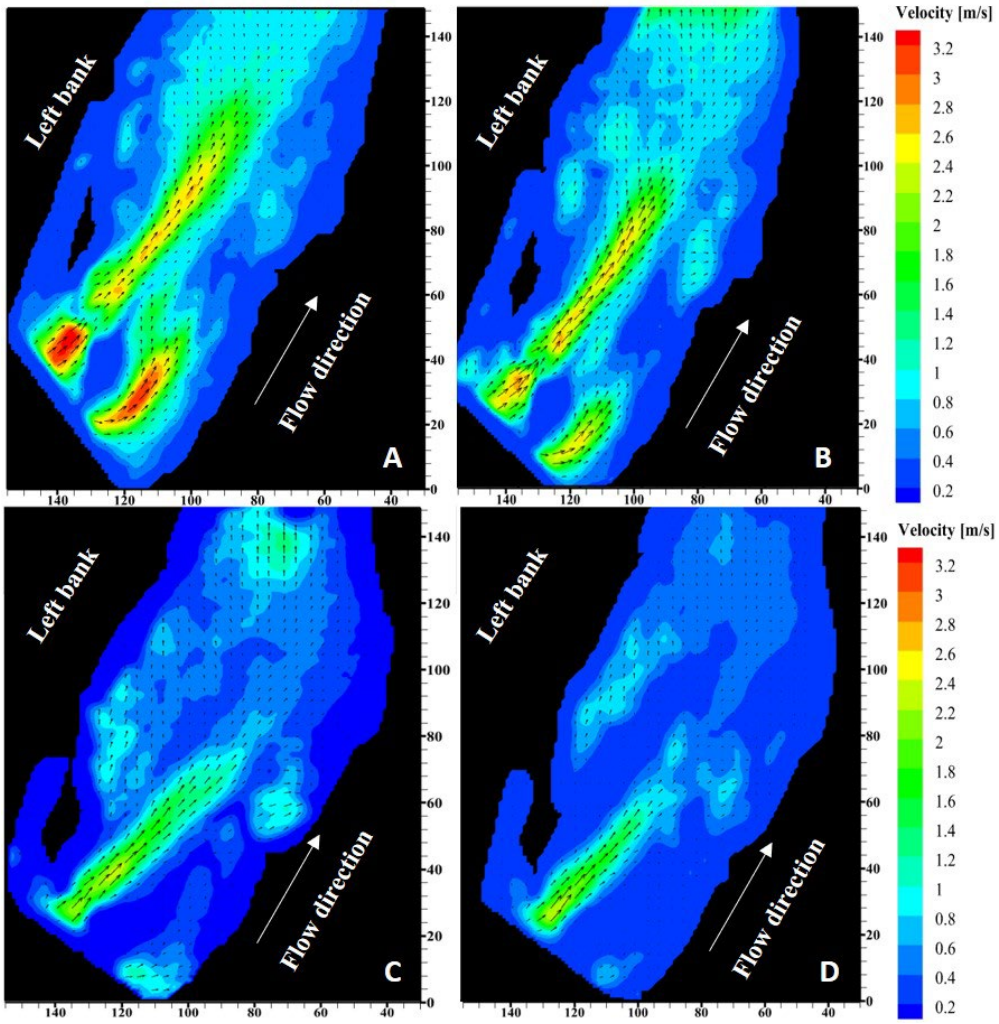

Figure 3-34 The distribution of surface flow illustrated by scalar map using LSPIV under four different releasing flows from Nagayasuguchi dam: A: 900 m^3/s, B: 700 m^3/s, C: 500 m^3/s, D: 300 m^3/s.

3.5.3.3. Experimental results of STIV

The Hydro-STIV was utilized to conduct the STIV processing of 2 flood events on 12th Aug and 21st May. Figure 3-35 illustrated the STIV result by showing the flow velocity of 20 search lines at the selected cross-section. Two rocks in the middle of the river caused a restricted channel to form, and a high-flow area with severe turbulence can be observed. Visible seedings were abundant here, which is advantageous for STI creation and analysis. The STIs at the high flow area (black square in Figure 3-35) under 4 releasing flows of approximately 900 m^3/s, 700 m^3/s, 500 m^3/s, and 300 m^3/s were illustrated respectively in Figure 3-35 B, C, D, and E. For all STIs, we can see the apparent distribution of inclined texture. By comparing the different STIs, the predicted flow velocity decreases with the increase of such inclination of texture. Moreover, the density of surface turbulence was significantly decreased with the reduction of releasing flow, thus causing a decrease in texture and surface velocity.

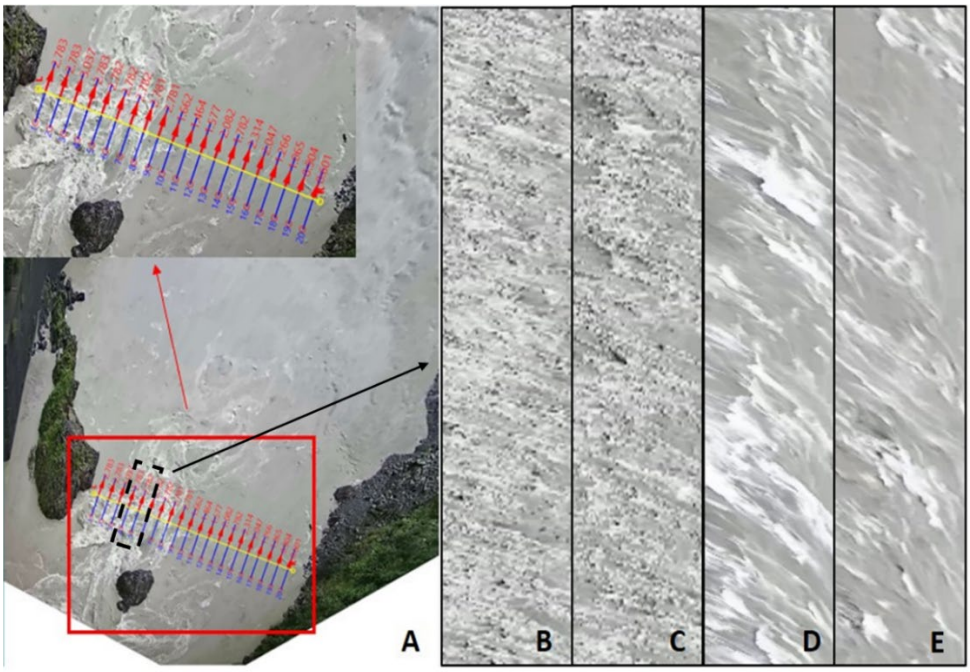

Figure 3-35 The example of STIV measurement with different STIs under different releasing flow from Nagayasuguchi dam. A: Example of calculated results from Hydro-STIV. B, C, D, and E: STIs under releasing flow of 900 m^3/s, 700 m^3/s, 500 m^3/s, and 300 m^3/s.

3.5.3.4. The comparison of surface velocity between STIV and LSPIV

The comparison of surface flow velocity was conducted between LSPIV and STIV under four releasing discharges at the same selected cross-section illustrated in Figure 3-31. Figure 3-36 shows the results of surface flow velocity estimated from two image-based approaches. It can be observed that both two methods display a similar trend of velocity distribution. In particular, we can observe the high flow area formed between two deep rocks (10 m to 25 m), then a static area that followed (25 m to 30 m), and another semi-high flow area close to the right bank (50 m-60 m).

In terms of the magnitude of surface velocity, the estimated results from STIV are higher than LSPIV except for the outcome during extremely high flow (900 m^3/s). Large tracers were produced at the water surface as a result of the significant turbulence generated by considerable upstream flow, which can improve the detection of LSPIV, while on the contrary, raising the uncertainty of STIV (Fujita et al., 2007). Furthermore, the results of LSPIV and STIV are quite comparable at the high flow area close to the left bank with peak velocity ranging from 2.3 m/s to 3.5 m/s. Additionally, for another flow area close to the right bank, the estimated velocity shows increasing discrepancies with a reduction of releasing flow while agreeing with higher upstream discharge. The peak difference occurred at 300 m^3/s, where STIV values are almost 30% higher than LSPIV values. Since this area can be distinguished as a static area under reduced upstream discharge, the absence of apparent seeds at the water surface can be considered the crucial reason to cause such differences. According to the actual image, only a few ripples were seen, and no visible foam or floating objects occurred there. Hence in the LSPIV, it is difficult to track these rare waves and riffles through the process of cross-correlation. However, STIV produced Space-Time Images (STI) for each survey line, resulting in a single, distinct image that included all the seeds. As a result, it is simple to produce trails that represent the velocity lines, and the results of surface velocity are more accurate than those of LSPIV at a low flow area.

In conclusion, both LSPIV and STIV approaches may accurately estimate flow velocity at a high flow area (flow velocity greater than 1.5 m/s). While the STIV technique is more reliable for the low-flow area because it requires less density of clear tracers for analysis. In the latter research on the numerical model, we preferred to utilize the estimated results from STIV as the source of calibration and validation since its higher feasibility under variable flow conditions and simple implementation procedures. In a word, the thorough application of non-intrusive velocimetry can assist us to

determine a more reliable velocity distribution map near the replenishing stockpile during flood events.

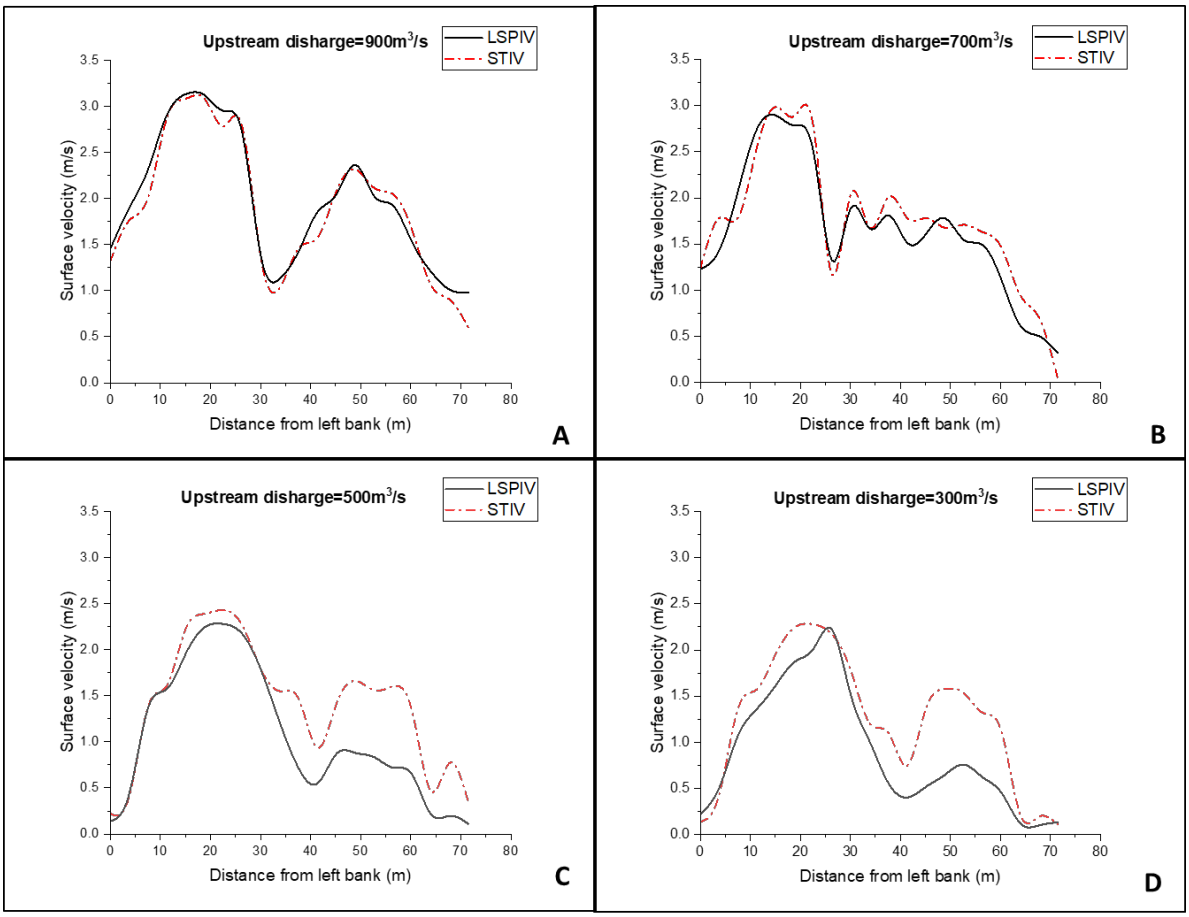

Figure 3-36 The comparison of surface velocity distribution along the selected cross-section determined by STIV and LSPIV under four releasing flows from Nagayasuguchi dam. A: 900 m^3/s, B: 700 m^3/s, C: 500 m^3/s, and D: 300 m^3/s.

3.5.3.5. The estimation of flow discharge by LSPIV and STIV

Figure 3-37 shows the measured discharge at the Nagayasuguchi dam and the computed flow rate determined by the distribution of flow velocity from LSPIV and STIV at the selected cross-section. On August 14, a severe flood event was observed, and a total of 11 data points were collected between

6 am to 4 pm with a one-hour interval. The release discharge from the dam increased starting at 2 am, peaked at 11 am with 920 m^3/s, and then reduced to 500 m^3/s at 10 pm.

To evaluate the performance of flow discharge estimation of two methods, we utilize the Root-Mean-Square Error (RMSE), which equals to:

$$\text{RMSE}\ (Q^E, Q^O) = \sqrt{\frac{1}{n}\sum_{i=1}^{n}\left(Q_i{}^E - Q_i{}^O\right)^2} \tag{3-12}$$

Where q_i is the estimated discharge from STIV and LSPIV, and q_i^o is the observed discharge from Nagayasuguchi dam.

In terms of the estimated magnitude of discharge, the results from STIV demonstrate significant agreement with the gauged flow, with an average difference of 26.3 m^3/s and RMSE of 31.0 m^3/s. Nevertheless, underestimation of flow discharge can be observed in LSPIV, with an average difference of 45.6 m^3/s and RMSE of 59.9 m^3/s. The incorrect computation of flow velocity may be the key factor contributing to this underestimate. As previously discussed, one disadvantage of LSPIV is that it cannot accurately estimate the flow velocity at a shallow flow area due to the absence of visible surface tracers. This influence is more crucial during the period of higher releasing flow since the water depth at this area is higher, and differences between actual and estimation are enlarged simultaneously. Nevertheless, the discrepancy may be reduced if the releasing discharge is great enough to generate clear tracers at the surface for velocity analysis. For instance, the difference is about 45 m^3/s at peak discharge (920 m^3/s), which is less than the typical level of differentials.

Furthermore, the precision of cross-sectional data may also have an impact on the dependability of discharge estimation. To improve our results, a precise bathymetric survey should be conducted. In a word, the image-based approach can be considered a dependable strategy to promote the discharge monitoring system in the Naka River.

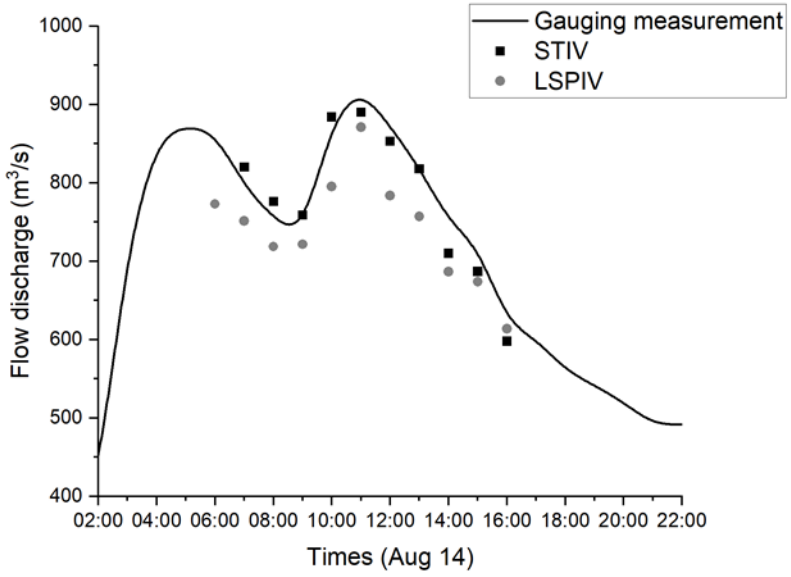

Figure 3-37 The comparison of flow discharge estimation by LSPIV, STIV, and gauging measurement from Nagayasuguchi dam on 8/14 from 6 am to 16 pm.

3.5.3.6. Dissipation rate and water depth estimation by LSPIV

Water depth was estimated based on Eq. 3-7, and the required data of flow velocity were extracted from the analysis of LSPIV. The model constant C_S was set to 0.8, and the manning coefficient n was equal to 0.03 for the natural channel. The ratio between surface velocity to depth-averaged velocity α was set to 0.85. The estimated water depth under four releasing flows was calculated and shown in Figure 3-38. Same to the results of LSPIV, visible tracks were successfully generated in that area with clear surface seedings between the two rocks. Furthermore, a reasonable shallow water area can be detected under 900 m^3/s and 700 m^3/s at the top of the scalar map, corresponding to the riffle area near the SR site (Figure 3-38, yellow circle). Nevertheless, unreasonable water depth estimation was also shown in the results as well. Specifically, water depth was extremely low in those areas with no visible seedings, for instance, near the river bank. Despite this, some overestimation of water depth can also be detected near the replenishment site and at the entrance of the flow (Figure 3-38, red circle). To be specific, based on the videos, the flow was separated here into two directions, and some adverse flow was generated near the replenishment site (right bank). Regarding the differences at the entrance, high turbulence flow can be observed, which will affect the results of water estimation as

well since we assume a uniform flow condition when calculating the momentum equation. Such complicated flow conditions will lead to some chaos on surface turbulence and thus, unreasonable results of water depth were determined.

Figure 3-39 shows the comparison of cross-section bathymetry estimation from image measurement function in Hydro-STIV and LSPIV analysis under four selected discharges. It shows that reasonable results of water depth can only be observed at the high flow area (5 m – 10 m from the left bank) under 500 m^3/s and 300 m^3/s. On the one hand, differences increase when the water depth is comparatively deep because the LOW can not be extended to the entire water column. It means that if we utilize Eq. 3-6 to determine the dissipation rate at the surface, errors will increase with the increase of water depth (Jin & Liao, 2019). On the other hand, visible seedings are also significant to the accuracy since water depth was calculated from the surface flow velocity. Hence, we can notice that relatively small values can be observed at the riverbank edges, especially under low upstream flow.

In summary, the application of TKE is limited by the applicable range of water depth, density of surface seedings, and flow condition. We have to say that only the small region shown in the white circle in Figure 3-38 can be trusted as the reasonable area to utilize the TKE for water depth estimation. Despite this, the approach still needs further investigation to enhance its accuracy. Data from field measurement is required to calibrate the parameters and coefficients, such as manning's n value, the model constant C_S and the depth-average velocity α. In a world, it can be considered as an alternative method to determine the water depth roughly near the replenishment site.

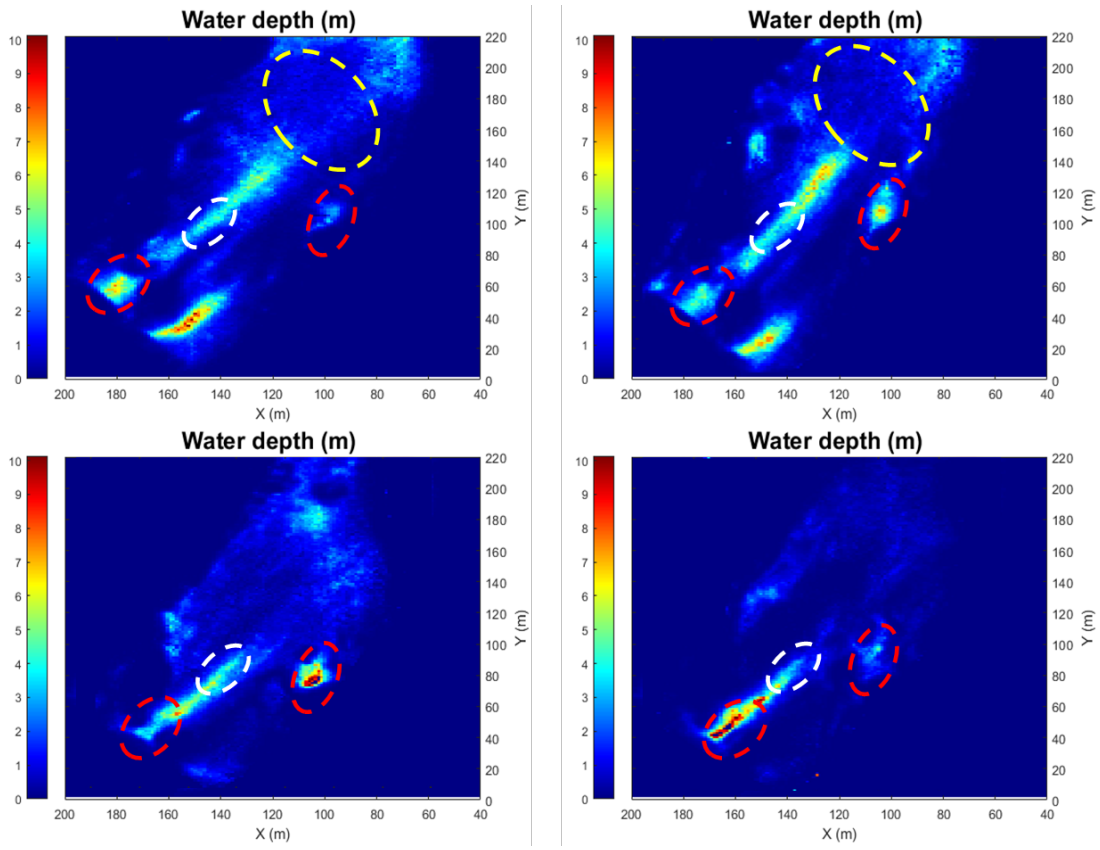

Figure 3-38 2-D scalar maps of estimated water depth under four different releasing flow based on the results of LSPIV. A: 900 m^3/s, B: 700 m^3/s, C: 500 m^3/s, and D: 300 m^3/s. The white circles represent the area with reasonable water depth. The yellow circles represent the downstream riffle area. The red circles represent the unreasonable area due to the chaos of turbulence.

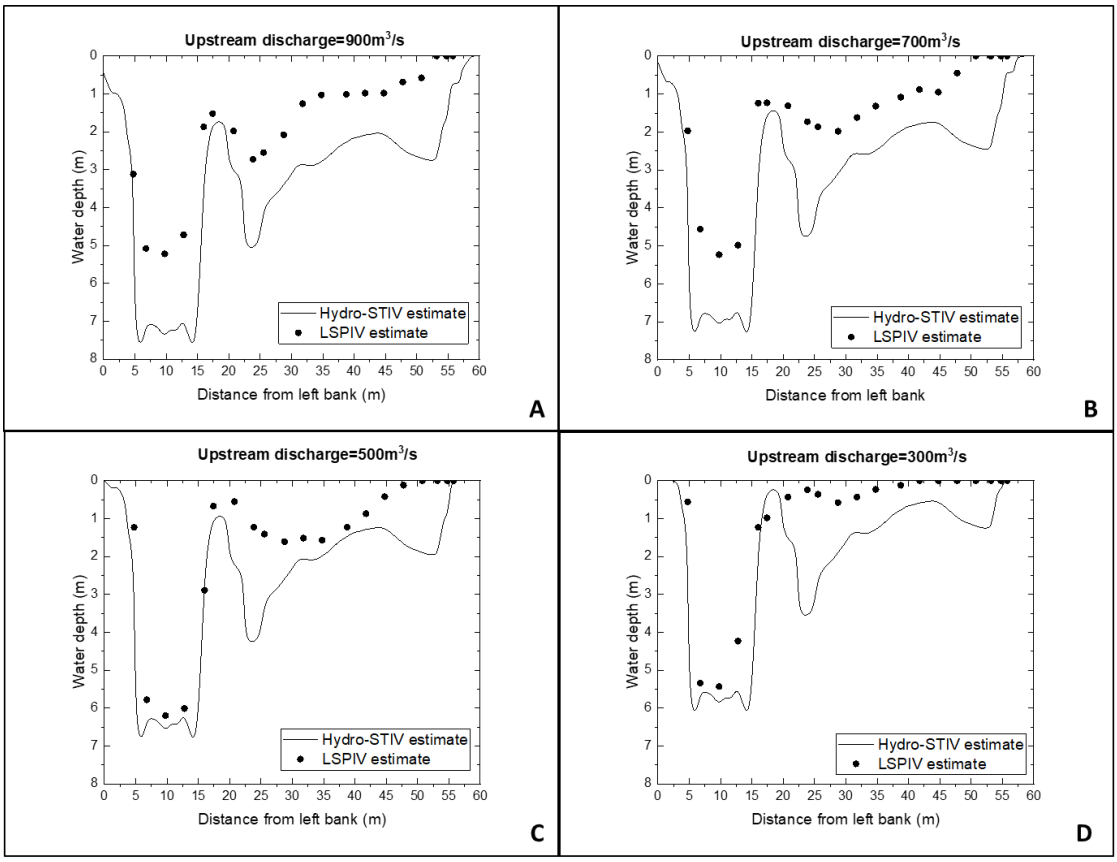

Figure 3-39 The comparison of water depth estimation from image measurement function in Hydro-STIV and LSPIV analysis under 4 selected discharges: A: 900 m^3/s, B: 700 m^3/s, C: 500 m^3/s, and D: 300 m^3/s.

3.6. Conclusion

Field measurement of downstream geomorphology is essential for the analysis of the impacts of SR. Previous data measured from the Naka River office may not sufficient due to the lack of surveys in recent years. To fill such gaps, we conducted four times of on-site surveys at four gravel bars downstream of the replenishment site from 2020 to 2022 to measure the grain size variations. The measured results were valuable for us to understand the spatial and temporal alterations of gravel bars due to the implementation of SR. Despite this, there are no motoring gauges of flow patterns, for instance, flow velocity and water depth, that are distributed in our study area, which restrict the investigation of the erosion process of replenishment and the establishment of numerical models. To overcome such missing hydrological data, image-based velocimetry was selected as a suitable

approach to measure the real-time flow patterns near the replenishment site. Two reliable image-based approaches, LSPIV, and STIV were utilized to measure the surface flow velocity, and further calculate the flow discharge and water depth based on a bathymetric survey. The main conclusions of this chapter are:

(1) The SR promotes the formation of several point bars at the convex of a meandering channel, for instance, the gravel bar 2 where the uniform distribution of fine sediment can be founded (Figure 3-14). For the rest bars, different coarsening and fining tendencies can be observed from bar head to bar tail depending on the specific locations of bars. Locations with lower flow velocity and bed shear stress may lead to more aggradation of fine sediment from the replenishment site and thus finer tendency of grains is expected (bar head of gravel bar 1). On the contrary, a higher dissipation area with great bed shear stress may cause coarsening of grains (gravel bar 4). Such differences in erosion and deposition area also lead to the temporal variation of grain size. Fining or stable tendency of grain size can always be detected as those aggraded areas annually since the replenished sediment is the source of the bar. Nevertheless, the erosion area may be more sensitive to the variation of sediment supply from the replenishment site.

(2) The installed turbidity meter can successfully measure the SSC for 5 months. Based on the analysis of the discharge-SSC relationship, the peak value of SSC occurred after the appearance of discharge, which leads to a counter-clockwise hysteresis that is shown in Figure 3-24. In the future, the measured SSC can be utilized to calibrate the numerical model.

(3) The LSPIV and STIV were utilized to measure the real-time flow velocity near the replenishment site. The LSPIV is more complicated and is more sensitive to the density of clear seedings on the water surface. Nevertheless, STIV can provide us reasonable flow velocity at both high flow and low flow areas, and thus more accurate calculation of flow discharge was obtained. Therefore, STIV should be considered as the main velocimetry and we utilized it to measure flow velocity at the Mizaki bridge (6 km downstream of the replenishment site) as well as to prepare more data for numerical model calibration and validation in Chapter 5.

(4) The TKE method can not provide us with an acceptable estimation of water depth in the Naka River due to several points, including:

Alternative locations at downstream reach with shallow water and less complex flow condition should be selected if we would like to obtain more accurate results of water estimation.

- The flow velocity determined from LSPIV is not accurate in those areas with less visible seedings.
- The flow condition is complex during flood events near the replenishment site and we can not assume it is a uniform flow to apply Eq. 3-4 to calculate the momentum.
- The water depth is high during flood events as well which may increase the error of calculating the dissipation rate using LOW.
- No measured data can be utilized to calibrate several parameters in the estimation, for instance manning's n value, the model constant C_S and the depth-average velocity α.

Alternative locations at downstream reach with shallow water and less complex flow condition should be selected if we would like to obtain more accurate results of water estimation.

Chapter 4. Developing a comprehensive approach for the assessment of Sediment replenishment and downstream hydro-geomorpho-ecological characteristics

4.1. Introduction

SR, as a common mitigation approach for river restoration, has already been implemented in Japan, America, and some European countries. For those river basins, the running of SR leads to some positive impacts on downstream reach, for instance, the reproduction of shallow geomorphic units (riffle, rapid, and run) (Lin et al., 2021), recovery of the riverbank incision and instability (Paquier et al., 2018). However, adverse impacts should also be considered, such as the increasing turbidity at downstream reach due to the utilization of the in-channel stockpile method for replenishment (Ock, Sumi, et al., 2013). The differences in implantation characteristics, such as implementation methods of replenishing, flushing flow, the placed volume of sediment, as well as the grain size of the scouring sediment are the main reasons that generate successful or unsuccessful outcomes.

The current research gaps are the lack of a comprehensive approach to assess the downstream responses of SR to judge whether the projects are successfully conducted or not. There is rare research that mentioned the relationships between the characteristics of SR (volume, grain size, arrangement, and injection method), flow conditions, and the downstream morph-ecological responses. Previous research mainly emphasized the geomorphological and ecological parts of SR solely. For instance, the alteration of river cross sections, riverbed substrates, and habitat structures are the three common aspects that have always been investigated for downstream geomorphology (Sameh Kantoush, Tetsuya Sumi, & Akira Kubota, 2010). While for ecology, the key points are the characteristics of habitat quality, such as water temperature, turbidity, and POM (Particulate organic matter). Hence, we still need to create a simple and integrated method to fill the blank among river geomorphology, aquatic habitat, and characteristics of SR.

Regarding our study area, in the Naka River, amounts of data on downstream geomorphology and ecology have already been collected, including the cross-section, the riverbed substrates, the distribution of geomorphic units, and the numbers of fish species and benthos. The impacts of implementing SR were analyzed through simple comparison and summary of the raw data, and we realized that it is not clear to show the long-term impacts of the SR along the reach.

While in the Buëch River, the assessment of the replenishment projects is more integrated and scientific. For the erosion of the replenishment stockpile, the persistence of SR (PR), the eroded width (WR), and the length of bed aggradation (LR) are considered (Guillaume Brousse et al., 2019). Moreover, the Bed Relief Index (BRI*) and the Shannon index were utilized to evaluate the SR effect on physical habitat diversity and quality (Molon, 2019). The utilization of various indicators is essential for the assessment of the replenishment impacts and it should be applied in the Naka River to conduct a more distinct and comprehensive analysis.

In this section, we will first show the data collected in the Naka River and the Buëch River. Then, we will introduce our methodologies for the assessment of the replenishment, including the efficiency of the replenishment and the downstream hydro-geomorpho-ecological responses. After that, we will apply our methodologies to assess replenishment works in the two study areas, respectively. At the end, we will discuss and compare the results from both two rivers and judge whether the implemented replenishment works are successful or not.

4.2. Materials and Methods

4.2.1. Study area

The study area in the Naka River is the 12.0 km reach downstream of the replenishment site in Kohama since we would like to minimize the impacts of backwater from Kawaguchi dam (Figure 4.1). To investigate the impacts of SR along the distance, the study area was divided into 12 semi-reaches with an interval of 1 km (Figure 4-1).

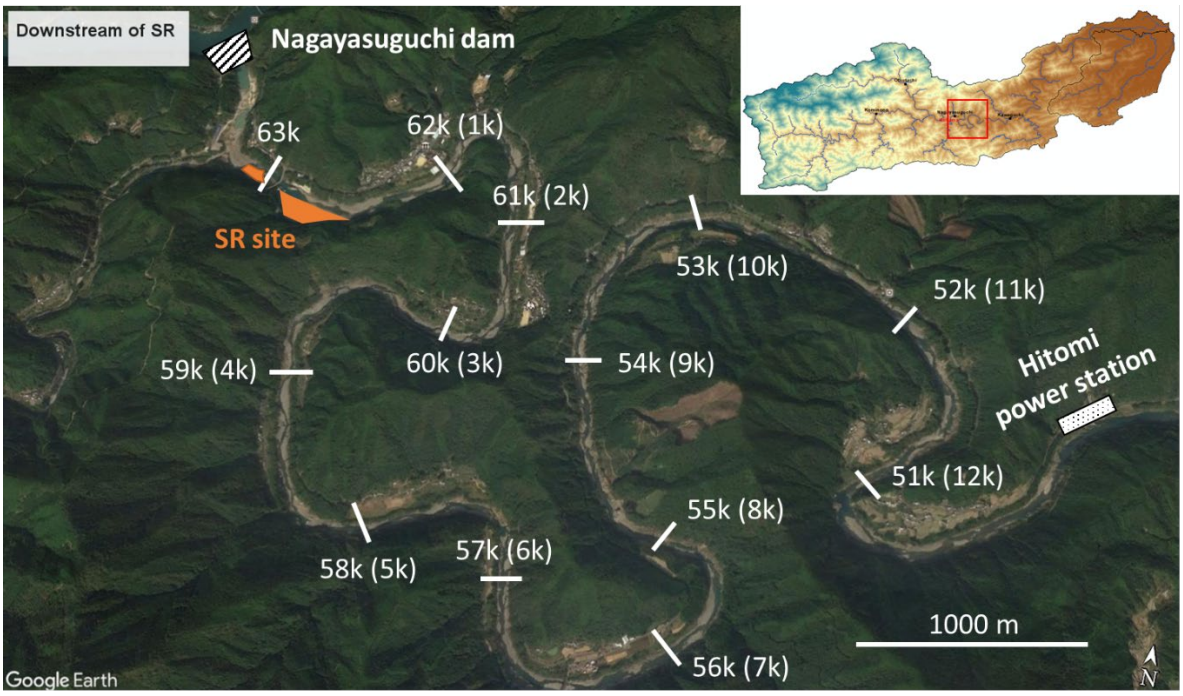

Figure 4-1 The study area in the Naka River for assessment of SR. The number means the river mile (distance from the SR site) in km.

Regarding the Buëch River, the study area is the 6 km reach downstream of the replenishment site in the Saint-Sauveur dam based on the previous research in the assessment of downstream responses (Guillaume Brousse et al., 2019) (Figure 4-2). Same to the Naka River, 6 semi-reaches were divided to spatially assess the downstream responses from replenishment.

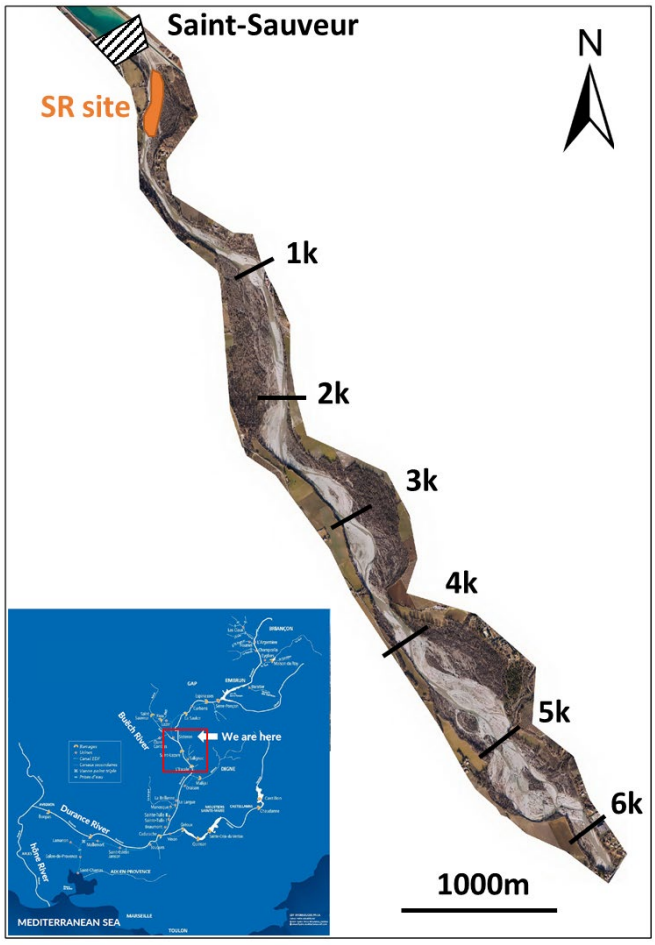

Figure 4-2 The study area in the Buëch River for assessment of SR (figure provided from EDF). The number means the distance from the SR site in km.

4.2.2. Data preparation

Figure 4-3 shows the collected data in time series in the Naka River. Table 4-1 shows detailed information on downstream hydro-geomorpho-ecological data in river miles (RM, in km). The cross-section was mainly collected from 2010-2017. Some additional bathymetric survey was conducted in 2003, 2008-2009, and 2019 in some locations. The geomorphic units were collected from 2010, 2014-2018, and the corresponding distribution of the units was also included. The riverbed substrates were collected dispersedly from 2007 to 2021. The water depth and flow velocity were collected in 2015, 2016, and 2020 during the normal flow period in spring and autumn. And the fish survey was mainly

conducted at the three spawning grounds located at 63k, 61k, and 51k. The aerial photos were collected in 2017 and 2019. It can be noticed that the survey conducted by the river office was scattered and not systematic, which increase the difficulties of the assessment works. The time series of each characteristic were summarized and prepared for the calculation of the analyzed indicators.

While for the Buëch River, the data was provided from the EDF (Électricité de France) in France and was summarized in Figure 4-4. The annually conducted same geomorpho-ecological survey for the 6 km study reach downstream of the Saint-Sauveur dam. The data on SR characteristics (placed volume and transported volume) was collected in 2016 and 2018 since they only conducted replenishment in these two years. The data of cross section was collected from 2016 to 2020 after the beginning of the replenishment. Data on the riverbed substrates was limited and only 2017 was available. The summary of the fish species was conducted from 2014 to 2018. And the aerial photos were available from 2016 to 2018. Data on the geomorphic units, flow velocity, and water depth was lacking, which means that some of the assessment methods can not be utilized here. However, the high-resolution aerial photos can assist us in manually creating the distribution of GU to fill the blank of the assessment.

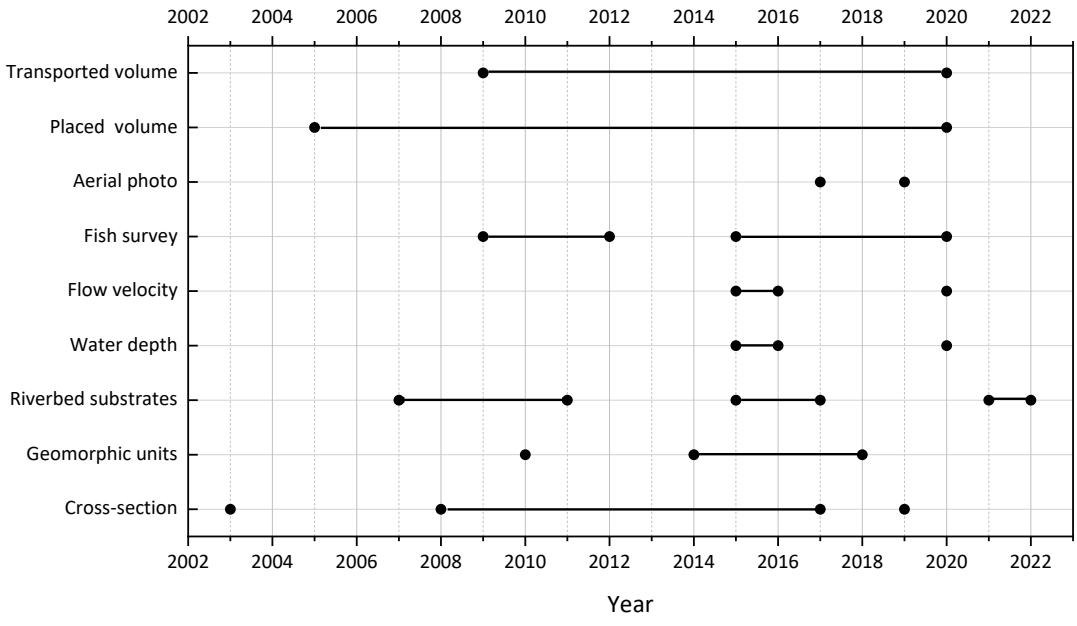

Figure 4-3 The collected data in time series for the Naka River

Table 4-1 The collected data of cross-section, geomorphic units, riverbed substrates, water depth, flow velocity, fish survey, and aerial photo downstream of the Nagayasuguchi dam from 63.0k to 50.0k in the Naka River.

<table>
<tr><th>RM (km)</th><th>Cross-section</th><th>Geomorphic units</th><th>Riverbed Substrates</th><th>Water depth</th><th>Flow velocity</th><th>Fish survey</th><th>Aerial photos</th></tr>
<tr><td>63-62</td><td rowspan="3">2003, 2008-2017</td><td rowspan="15">2010,2014-2018</td><td>2015-2016</td><td rowspan="2">2015,2016</td><td rowspan="2">2015,2016</td><td>2009-2012, 2015-2017</td><td rowspan="15">2017,2019</td></tr>
<tr><td>62-61</td><td rowspan="2">2007-2009,
2015-2017,2020</td><td>2015-2017</td></tr>
<tr><td>61-60</td><td rowspan="3">2015,2016,2020</td><td rowspan="3">2015,2016,2020</td><td>2010,2011
2015-2017</td></tr>
<tr><td>60-59</td><td>2003,2010-2017,2019</td><td rowspan="3">2015-2016</td><td rowspan="6">2015-2017</td></tr>
<tr><td>59-58</td><td rowspan="2">2003,2010-2017</td><td rowspan="5">2015,2016</td><td rowspan="5">2015,2016</td></tr>
<tr><td>58-57</td></tr>
<tr><td>57-56</td><td rowspan="2">2003,2010-2017,2019</td><td>2007, 2008,2015,2016
2011,2021</td></tr>
<tr><td>56-55</td><td rowspan="4">2015,2016</td></tr>
<tr><td>55-54</td><td rowspan="2">2003, 2008-2017</td></tr>
<tr><td>54-53</td></tr>
<tr><td>53-52</td><td rowspan="2">2003,2010-2017,2019</td><td rowspan="3">2015,2016,2020</td><td rowspan="3">2015,2016,2020</td></tr>
<tr><td>52-51</td></tr>
<tr><td>51-50</td><td>2003, 2008-2017</td><td>2010, 2013,2015-2017,2022</td><td>2012, 2015-2020</td></tr>
</table>

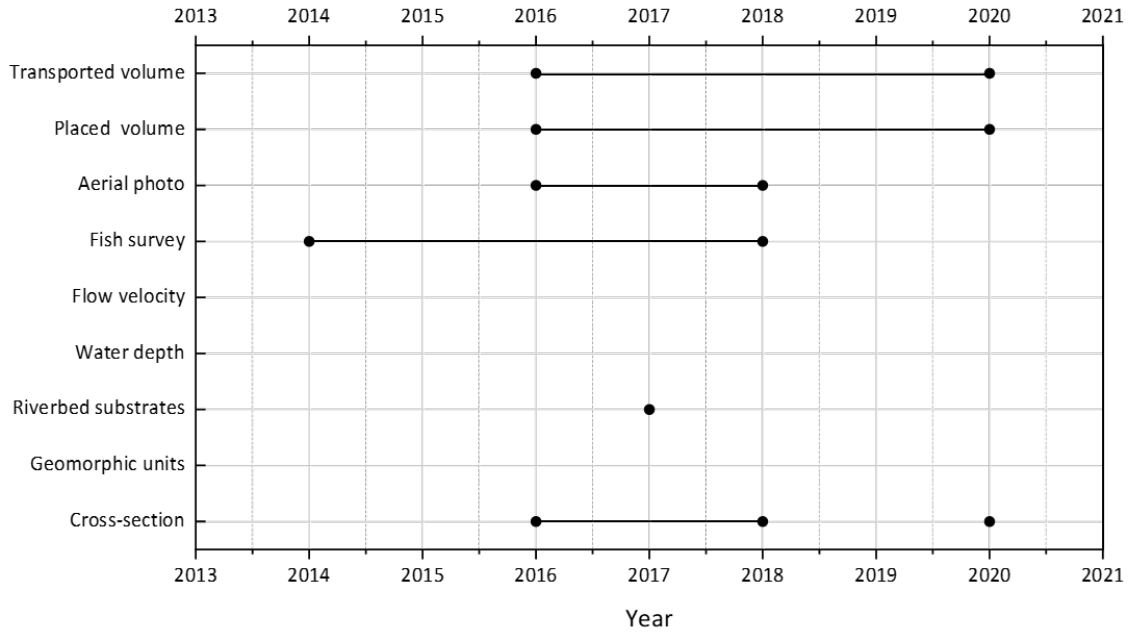

Figure 4-4 The collected data of SR characteristics, cross-section, riverbed substrates, fish survey, and aerial photo 6 km downstream of the Saint-Sauveur dam in the Buëch River.

4.2.3. Introduction of assessment methodology

4.2.3.1. Outline of the assessment framework

A unified methodological approach for the assessment of the riverine system during SR was developed. First of all, as shown in Figure 4-5, the efficiency of the SR for transporting the scouring sediment under different flushing flows was discussed based on two newly discovered parameters called the transported ratio (TR) and the total flushing water volume (TFWV). Meanwhile, several indicators for riverine assessment from the literature have been utilized to intuitionally present the downstream responses of SR, for instance, the Geomorphic Units Survey (GUS) (Belletti et al., 2015), the Hydro-geomorphological Index of Diversity (HMID) (Gostner et al., 2012), and Fish Diversity Index (H value) (Lakra et al., 2010) (Figure 4-6). Moreover, two basic aspects of river geomorphology, channel adjustment, and riverbed substrates were considered as well to analyze the reasons for indicators alterations.

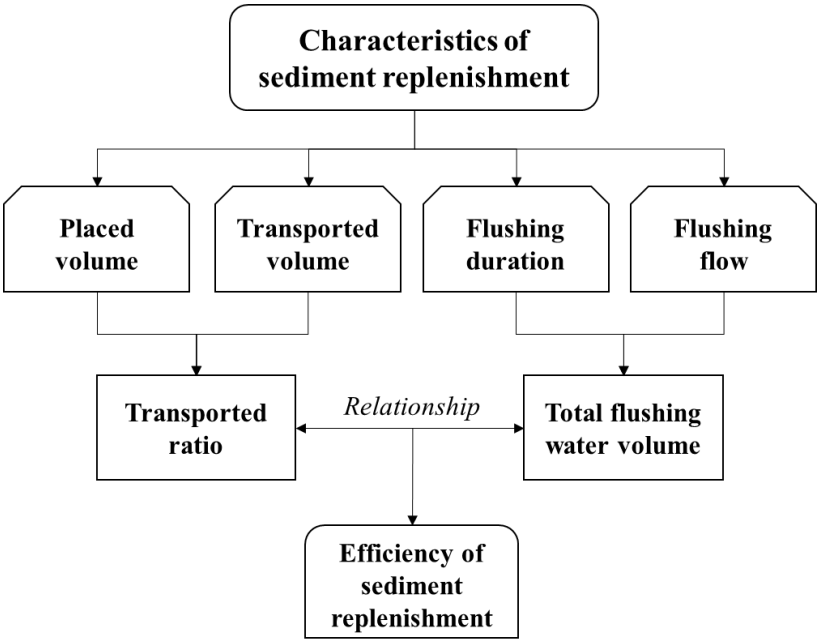

Figure 4-5 The flow chart for assessment of the efficiency of the SR considering the transported ratio and representative flow.

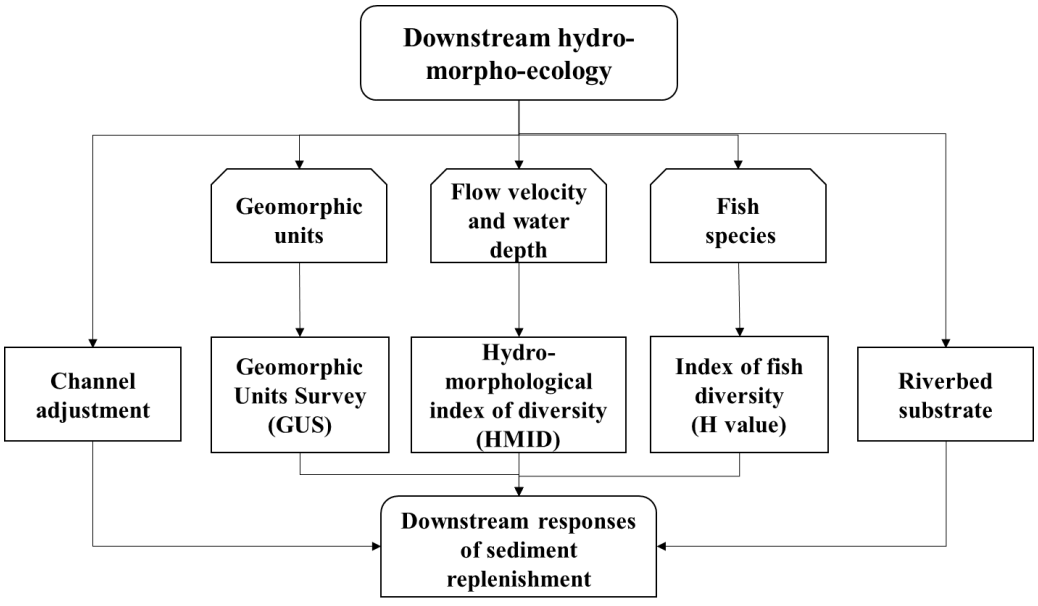

Figure 4-6 The flow chart for assessment of the downstream response due to the implementation of SR

Due to the lack of required data, our assessment approach can not be entirely applied to the Buëch River. The HMID and riverbed substrates were not analyzed since there was no sufficient data on flow velocity, water depth, and grain size. The plan for utilizing our assessment method for two rivers is shown in Table 4-2.

Table 4-2 The plan of utilizing each assessment approach in the Naka River and the Buëch River

Assessment approaches	Naka River	Buëch River
SR efficiency	√	√
GUS survey	√	√
HMID	√	
Channel adjustment	√	√
Riverbed substrates	√	
Fish diversity	√	√

4.2.3.2. Erosion efficiency of replenished sediment

The erosion efficiency of replenished sediment is not easy to define and calculate. The placed and transported volume of the stockpile, and the corresponding flushing flow magnitude and duration are 4 key points that affect the performance of the replenishing. Previous research may only focus on how much sediment is transported downstream and persisted at the replenishment site, for instance, the ratio of persistent sediment developed by Elena Battisacco (2016). It is logical for some projects in which the flushing flow is low and not fluctuant with significant differences, for instance in the Buëch River, France (Guillaume et al., 2018), and the Uda River (SA Kantoush & Sumi, 2011) and Nunome River (Ock, Kondolf, et al., 2013), Japan. However, in the Naka River, flushing flow during flood season is varied from 500 m^3/s to 5000 m^3/s due to the influence of typhoons. Moreover, the volume of placed sediment is another vital factor. Compared to other projects in Europe and Japan, the placed sediment in the Naka River is significantly larger, with an average volume of around 200,000 m^3. The differences in the flushing flow and placed volume lead to the variation of the submergence of the replenishing stockpile, and thus, different erosion rates and processes of the sediment may occur (Elena Battisacco, 2016).

Therefore, it is necessary to comprehensively analyze the efficiency of the SR by considering both the volume of sediment and the flushing flow. To reach such a goal, we calculated the total flushing water volume during the flushing period (TFWV, in m^3):

$$\mathrm{TFWV} = \sum_{i=1}^{n} \overline{Q}_{i,i-1} * \Delta t_{i,i-1} \tag{4-1}$$

Where, $\bar{Q}_{i,i-1}$ is the average magnitude of the flushing flow between two time steps in m^3/s, and $\Delta t_{i,i-1}$ is the interval of the time step in seconds.

While for the assessment of transported volume from the replenishment site, we utilized a simple indicator, transported ratio (TR), which equals to:

$$\mathrm{TR} = \frac{\text{Transported volume } (m^3)}{\text{Accumulated placed volume } (m^3)} * 100 \tag{4-2}$$

The relationship between these two factors can reveal to us how to reach the maximum SR efficiency with a suitable duration and magnitude of flushing flow.

4.2.3.3. Geomorphic Units Survey

The geomorphic units are the linkage between river geomorphology and habitat structures. The aquatic species can be influenced by the alteration of the surrounding topography, water depth, and flow velocity (Maddock, 1999). To classify the geomorphic units along the stream, the field survey coupled with remote sensing (aerial photos) is the common approach (M. Rinaldi et al., 2013). The detailed flow patterns and bathymetric of each unit can be measured on-site, and the shape and area of the units can be determined through GIS.

To simply analyze the data of the geomorphic units, the Geomorphic Units Survey (GUS) was considered, which is a common classification and assessment system utilized in European countries (Belletti et al., 2015). The system first classifies the macro-units at the reach (riffle, pool, puddle,

etc.), and then several subtypes of each macro unit (forced pool, scoured pool, etc.) are recognized if a detailed geomorphic survey is required. For our study, we only considered the first level of classification (macro units) since the data is limited. Two sub-indicators, the GUS Richness index (GUSI-R) and GUS Density index (GUSI-D) were applied in our study, which can be calculated by:

$$\mathrm{GUSI-R} = \sum \frac{\mathrm{NT_{GU}}}{N} \tag{4-3}$$

$$\mathrm{GUSI-D} = \sum \frac{\mathrm{N_{GU}}}{\mathrm{L}} \tag{4-4}$$

Where, NT_{GU} and N_{GU} are the total number of types and quantities of macro units within the investigated reach respectively. While *N* is the total number of all possible types of units (including macro-units and sub-types) within the reach. Due to the fact that we only considered the macro units in our study, the *n* is equal to N_{GU} here. *L* is the length of the study reach. For instance, the $NT_{GU} = 4$ since there are four types of units in the reach (rapid, run, pool, and puddle), while $N_{GU} = 7$ since the total number of units equals seven (Figure 4-7).

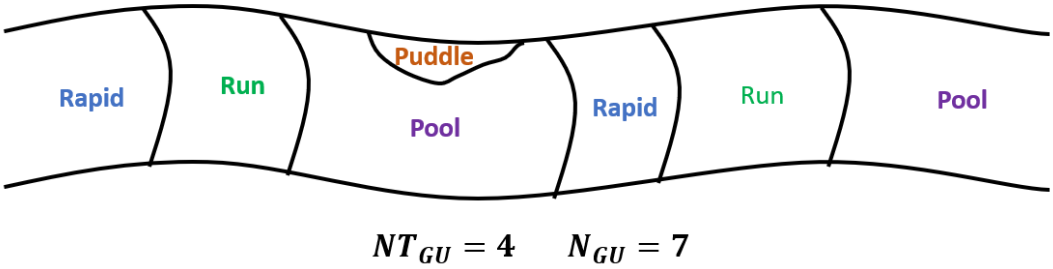

Figure 4-7 Example of how to calculate $\mathrm{NT_{GU}}$ and $\mathrm{N_{GU}}$ in a reach.

In the Naka river, the distribution of geomorphic units along the reach was generated by aerial photos and GIS from the river office. A total of five types of geomorphic units are considered, including pool, riffle (including rapid and run), toro, and puddle. While, in the Buëch River, the distribution was manually created by us using GIS and Autocad, and pool, rapid, run, and toro are investigated. Figure 4-8 shows a typical distribution of each geomorphic unit along a small reach. Table 4-3 illustrates the characteristics of each unit, including flow velocity, water depth, and bed substrates.

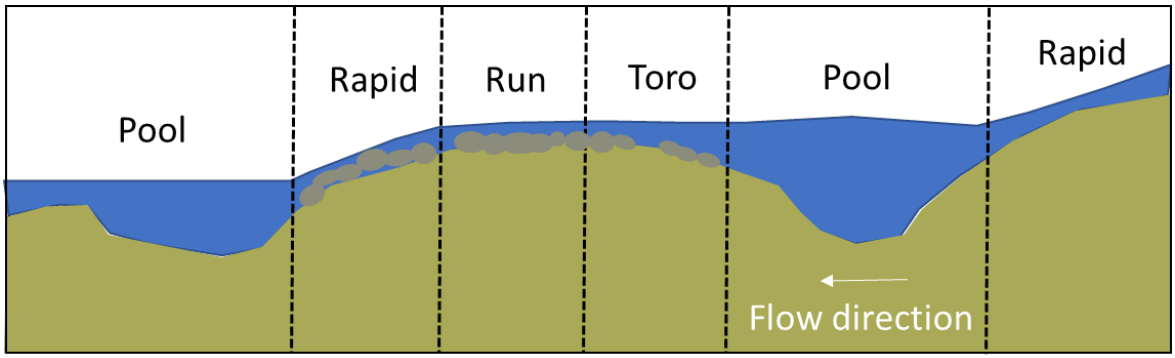

Figure 4-8 The figure that shows a typical spatial distribution of each geomorphic unit along a reach.

Table 4-3 The characteristics of each unit, including flow velocity, water depth, and bed substrates.

Characteristics	**Riffle**		**Toro**	**Pool**
	Rapid	**Run**		
Water depth	Shallow	Shallow	Little deep	Deep
Flow velocity	Fastest	Fast	Slow	Slow
Bed substrates	Floating gravels	Sinking gravels	Sandy gravel	Sand

4.2.3.4. Hydro-Geomorphological Index of Diversity

The Hydro-Geomorphological Index of Diversity (HMID) is a simple indicator to access the diversity and quality of the habitat structures (Gostner et al., 2012). It is based on the hydraulic measures of flow depth and velocity and their statistical parameters can be used to characterize the structural diversity of a river reach, which in turn is significant for habitat suitability of the aquatic and semi-aquatic region. (Gostner, Parasiewicz, & Schleiss, 2013). The indicator has already been successfully utilized in the Sarine River, Switzerland to access the impacts of SR in the downstream area (Stahly et al., 2019). The HMID can be calculated by:

$$\mathrm{HMID}_{\mathrm{Site}} = \left(1 + \frac{\sigma_v}{\mu_v}\right)^2 \cdot \left(1 + \frac{\sigma_d}{\mu_d}\right)^2 \quad (4\text{-}5)$$

Where σ_v, σ_d and μ_v, μ_d are the standard deviation and mean value of flow velocity and water depth within the investigated reach. As shown in Figure 4-9, a greater value of HMID (larger than 9) means the site is a geomorphological pristine site and can be considered as a reference for the restoration of gravel-bed rivers (Gostner et al., 2012). While a value less than 5 means the site is channelized and significantly altered by natural flow or artificial intervention.

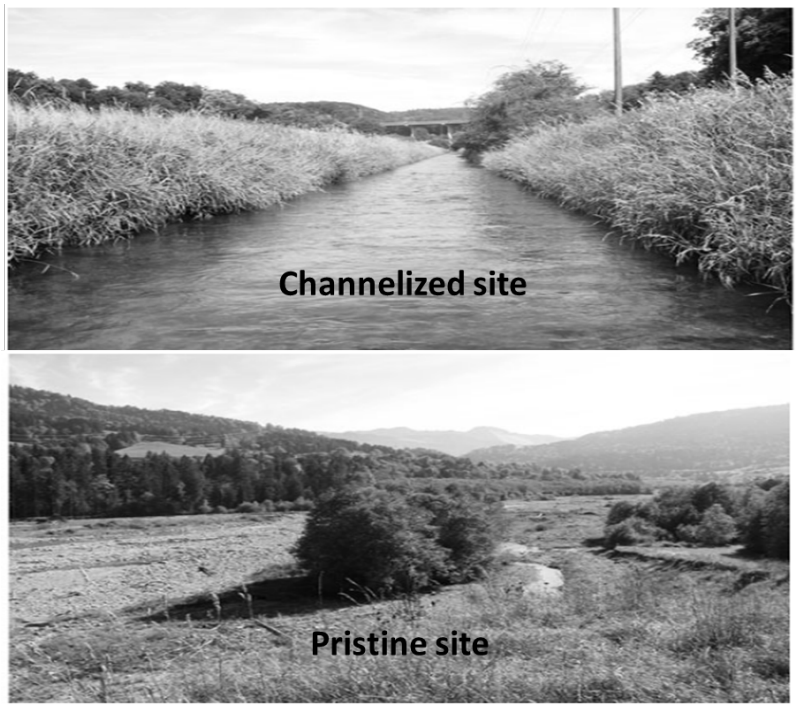

Figure 4-9 The examples of two study sites with different HMID values. The top one is a channelized site, in which the HMID value is less than 5. While the bottom one is a geomorphologically pristine site, which the HMID value greater than 9 (Gostner et al., 2012).

4.2.3.5. Channel adjustment

For the alteration of river geomorphology, the channel adjustment and riverbed substrates are two vital aspects that usually be discussed and analyzed together. Additional sediment supply from the replenishment site may let more riverbed aggradation occur, and at the same time, reduce the bed amouring issue (Friedl, 2017). In our study, we calculated the average bed level changes based on the BCI value utilized in many cases (Esmaeili et al., 2017). The calculation formula is:

$$\mathrm{BCI} = (\sum_{\mathrm{i}=1}^{\mathrm{n}} (z_{i_{y2}} - z_{i_{y1}}))/\mathrm{n} \tag{4-6}$$

Where $z_{i_{y2}}$ is the bed level at node i in next year, and $z_{i_{y1}}$ is the bed level at node i in the previous year.

4.2.3.6. Riverbed substrates

Regarding the riverbed substrate, we calculated the percentages of five types of substrates based on the field survey from the Naka river office, which can be determined as:

$$\text{Percentage of substrate for type i} = \frac{\mathrm{n_i}}{n_{total}} \times 100\% \tag{4-7}$$

Where n_i is the number of survey points that the substrates belong to the type i, and n_{total} is the total number of survey points in the study reach.

The classification of the substrates is shown in Table 4-4. The five types of substrates are sand (s), small gravel (m1), medium to large gravel (m2), small to large stone (m3), and rock (R).

Table 4-4 The classification of five types of substrates with different grain sizes (in mm) in the Naka River.

s	**m1**	**m2**		**m3**			**R**
Sand	Small gravel	Medium gravel	Large gravel	Small stone	Medium stone	Large stone	Rock
0.0074~2	2~20	20~50	50~100	100~200	200~500	>500	>500

4.2.3.7. Index of fish diversity

The variation of fish species and numbers is the straightforward way to investigate the quality of the spawning grounds in the river reach. We would like to utilize the Shannon-Wiener index of diversity (H value) to analyze the diversity of species (Lakra et al., 2010), which can be calculated as:

$$H = \sum_{i=1}^{n} \left(\frac{n_{si}}{n_{st}} \log 2 \left(\frac{n_{si}}{n_{st}} \right) \right) \quad (4\text{-}8)$$

Where, n_{si} is the total number of individuals of one specie, and n_{st} is the total number of individuals of all species. The calculation and analysis of the H value should be conducted in summer and autumn separately since the spawning season is a crucial pattern that affects the quantities and diversity of fish species (Overzee & Rijnsdorp, 2014).

4.3. Results

4.3.1. Erosion efficiency of replenished sediment

Regarding the Naka River, the analysis of SR efficiency was conducted at two replenishment sites upstream and downstream of the Kohama bridge from 2009 to 2020. The representative flow was calculated when the releasing discharge from the Nagayasuguchi dam was larger than 200 m^3/s (submergence of replenishing stockpile happened). The solid relationship between the TFWV and TR can be founded at the downstream site of Kohama (Figure 4-10).

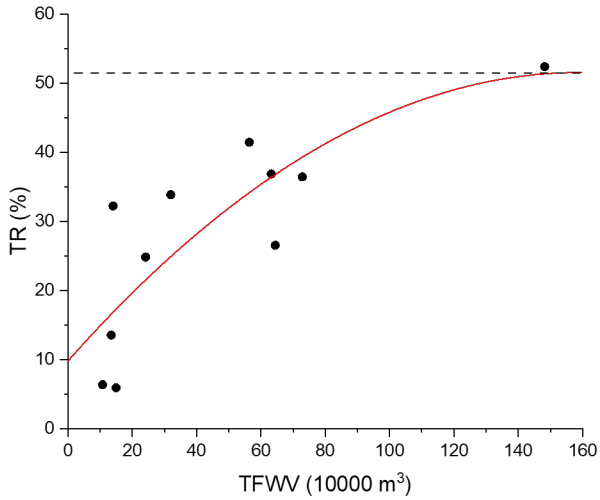

Figure 4-10 The relationship between TFWV and TR at the downstream site of Kohama in the Naka River.

The positive relationship between the two indicators (R square value equal to 0.7) represents that the flushing magnitude and duration are two essential parameters to drive the transportation of replenishing sediment. Nevertheless, the increasing speed of the TR value tends to be decreasing when the TFWV is greater than 800,000 m^3, and the TR value is nearly not increased when the TFWV is larger than 1,400,000 m^3, which is mainly due to the limitation of the erosion rate. With the sediment eroded from the stockpile, the channel configuration is increasing and the flow velocity near the replenishing site is reducing. The corresponding bed shear stress is reduced and the sediment is more difficult to be eroded (Elena Battisacco, 2016). Therefore, a threshold of flushing flow is occurred in replenishing the sediment, and a medium flow with adaptable flushing duration is more efficient for SR conducting.

To reduce the impact of the threshold and conduct more replenishment with the adaptable flow, an effective approach is to increase the number of replenishment sites. To analyze such influence, we summarized the data of TFWV and TR of both two sites by adding their value together. A comparison between a single site and multiple sites of SR is shown in Figure 4-11. Between 2010 to 2015, there were two sites of replenishment. Compared to the single site downstream, the TR value is increasing by around 10% with the same TFWV. It is a suitable countermeasure to divide the replenishing sediment and placed them at multiple downstream locations in the Naka River since the placed volume is higher.

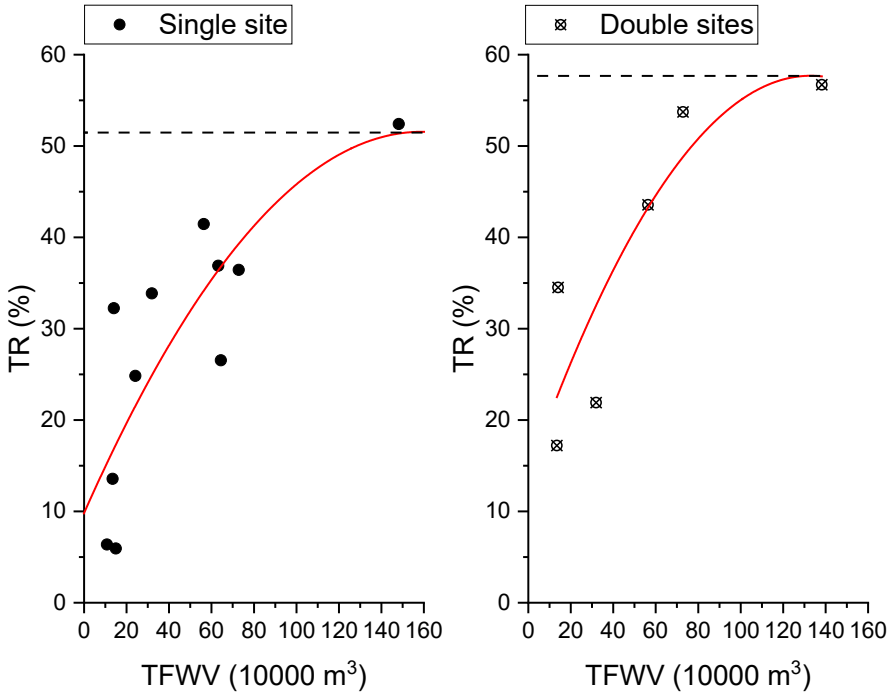

Figure 4-11 A comparison of single SR sites and multiple SR sites based on the information in the Naka River. Left figure: single SR site downstream of Kohama. Right figure: two SR sites both downstream and upstream of Kohama.

Regarding the Buëch River, SR was only conducted in 2016 and 2018, and the data for analysis of the relationship between TR and TFWV was very limited. The placed sediment, transported sediment, and corresponding TR from 2016 to 2018 is shown in Figure 4-12. It can be observed that a significant increase in TR value can be observed after the re-arrangement of the replenishment site in 2018 though the placed volume was smaller than the previous year. Here we need to discuss the re-design of replenishing shapes and locations in the Buëch River. During the first replenishing in 2016, three main berms were established for replenishing at the left bank (berm 2A and 2B), the central bank (berm 2C), and the right bank (berm 1) (Figure 4-13 left). The placed volume, transported volume, and TR value of each berm are determined in Table 4-5. Berm 1 and berm 2C are more efficient to transport more sediment downstream since the TR value reached nearly 60%. However, limited sediment was scoured downstream at berm 2A and 2B (TR only 10%), which was mainly due to the less flow in the secondary channel at the left bank. To mitigate such issue, sediment from berm 2A and 2B was moved to berm 2C and a new berm was created at the center with a volume of around

10000 m^3 (Figure 4-13 right). The movement of sediment from low flushing area to high flushing area is an efficient way to increase the TR value from 50% in 2016 to 83% in 2019 and thus can be proved as a successful strategy for replenishment implementation.

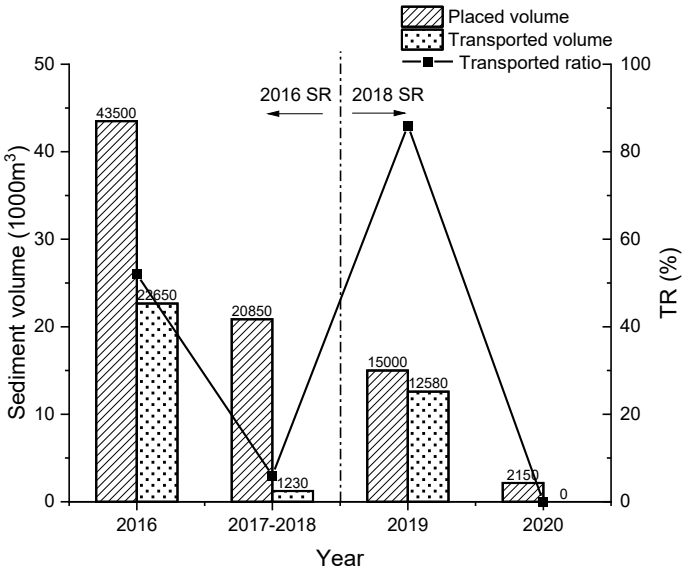

Figure 4-12 The placed sediment, transported sediment, and TR value in the Buëch River from 2016 to 2020.

Table 4-5 The placed volume, transported volume, and TR value of each berm in the first replenishment in 2016 in the Buëch River.

	Berm 1	**Berm 2A and 2B**	**Berm 2C**
Placed sediment (m^3)	12300	10000	21200
Transported sediment (m^3)	7000	1000	12500
TR	57%	10%	59%

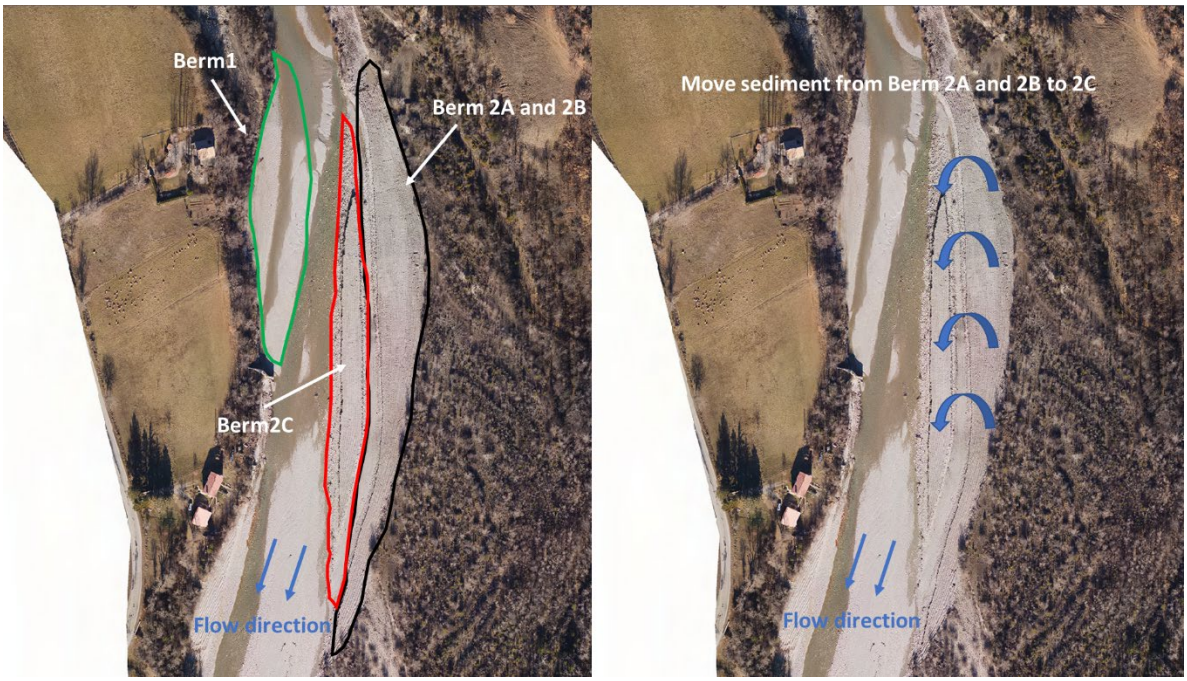

Figure 4-13 The design of the berm for replenishing in the Buëch River. The left figure shows the berm design in the first replenishment in 2016. The right figure shows the strategy of re-arrangement of the berm site in 2018 (photos provided by EDF).

4.3.2. Geomorphic units survey

Regarding the Naka River, we separated the downstream area into 12 reaches with an interval of 1 km. The GUS indicators were calculated respectively at each reach based on the geomorphic units survey conducted by the river office in Figure 4-14. The results of two indicators, GUSI-R and GUSI-D from 2015 to 2018 at each reach are shown in Figure 4-15. Significant alteration of both 2 indices can be observed from 2015 to 2016 at the middle of the reach (3 km to 8 km) with a difference of around 30%. Specifically, the GUSI-R was decreasing, which means that the types of units keep stable. On the contrary, the GUSI-D was increasing, which means the number of units was raising. Moreover, the average value of both GUSI indicators has close correlations to the variation of transported sediment from the replenishment site (Figure 4-16). GUSI-R decreased after the 2015 replenishment while GUSI-D shows the opposite trend. The significant transported sediment in 2015 (300,000 m^3) may be the main reason to cause such significant changes. Sediment from the replenishment site was derived by the flushing flow and accumulated at the middle reach after two years of flushing. The deposition of such sediment will significantly alter the formation and

distribution of habitat structures, for instance, creating new bars and riffles (Hyodo, 2015). Moreover, both GUSI-R and GUSI-D kept stable in the latter years, which may mainly be due to the reduction of transported sediment from the SR site (70,000 m^3 in 2017).

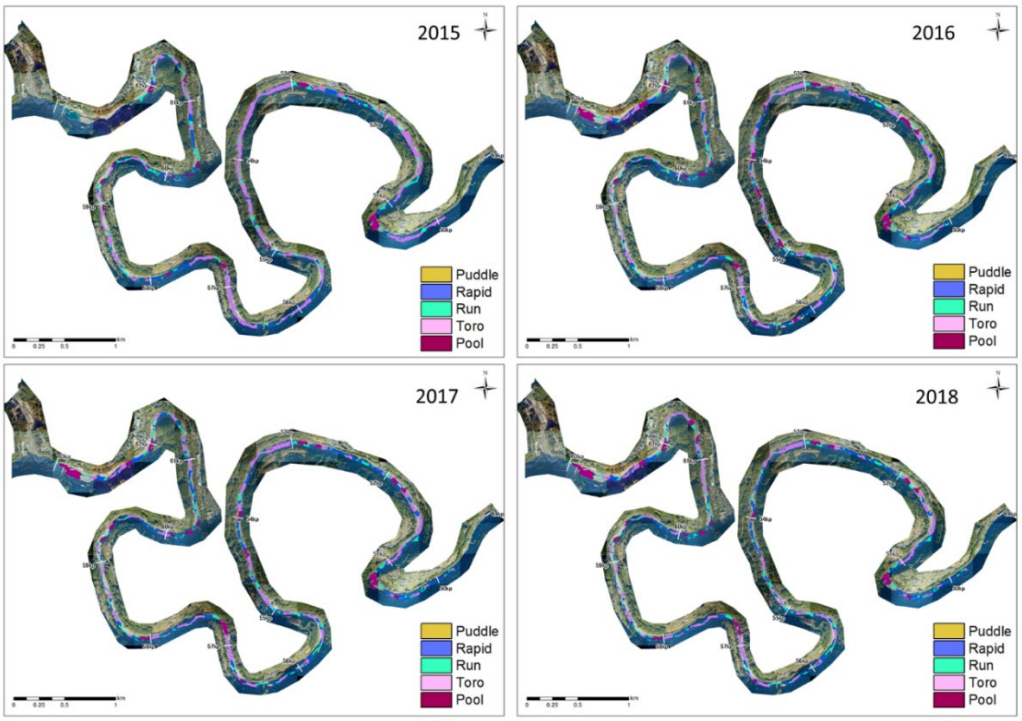

Figure 4-14 The geomorphic units survey conducted by the river office in the Naka River from 2015 to 2018.

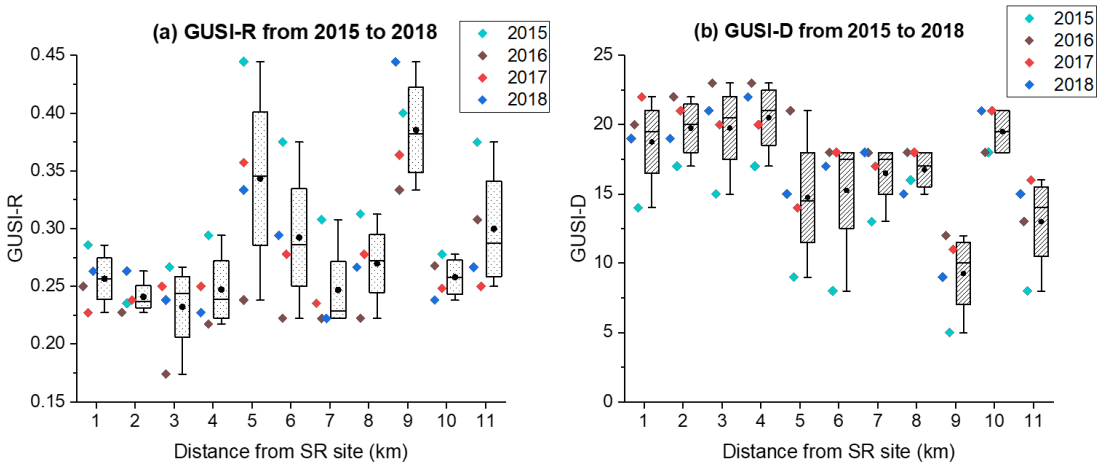

Figure 4-15 The GUSI-R and GUSI-D at 12 km downstream of the replenishment site in the Naka River from 2015 to 2018.

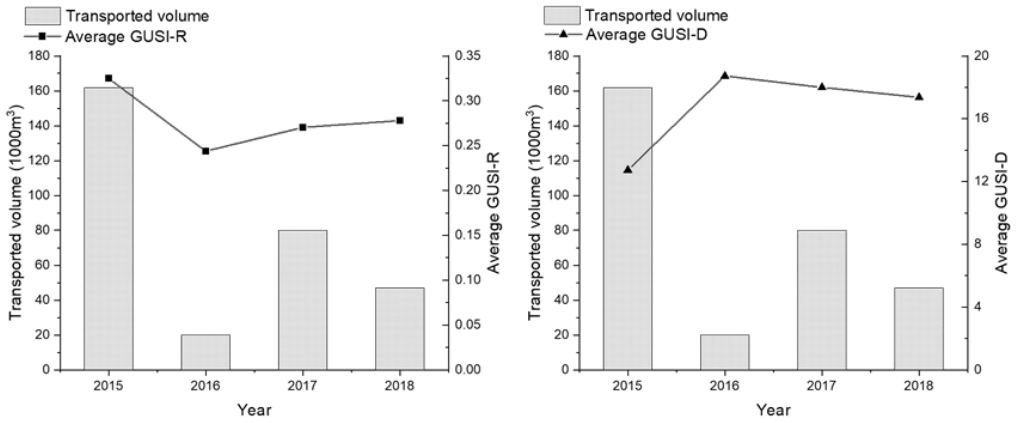

Figure 4-16 The relationship between transported volume and the average value of GUSI indicators in the Naka River. Left figure: GUSI-R. Right figure: GUSI-D

Despite this, such impacts due to the continuous sediment supply from the replenishment site can also be proved by determining the area changes of each geomorphic unit (Figure 4-17). Large and integral pools and toros were transferred to small runs and rapids, and the geomorphic units tended to be evenly distributed. Figure 4-18 shows the variation of geomorphic units at 9 km downstream of the replenishment site. It can be observed that clear transferring occurred from toros to rapids and runs. Based on the research from Morgan (2018), continuous sediment supply may break the integrated units into semi-units and therefore enhance the diversity of the habitat structures.

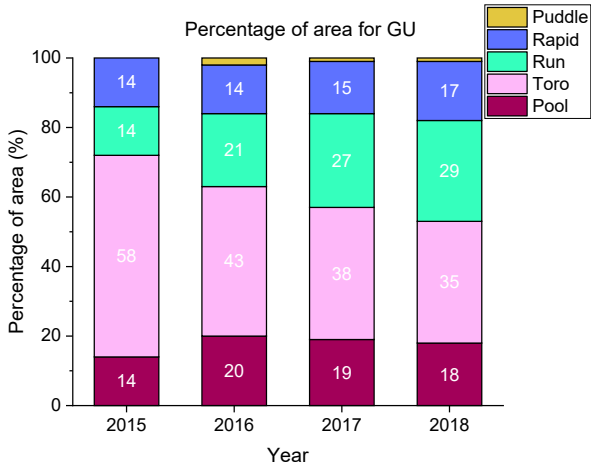

Figure 4-17 the percentage of area for different geomorphic units 12 km downstream of the replenishment site in the Naka River from 2015 to 2018.

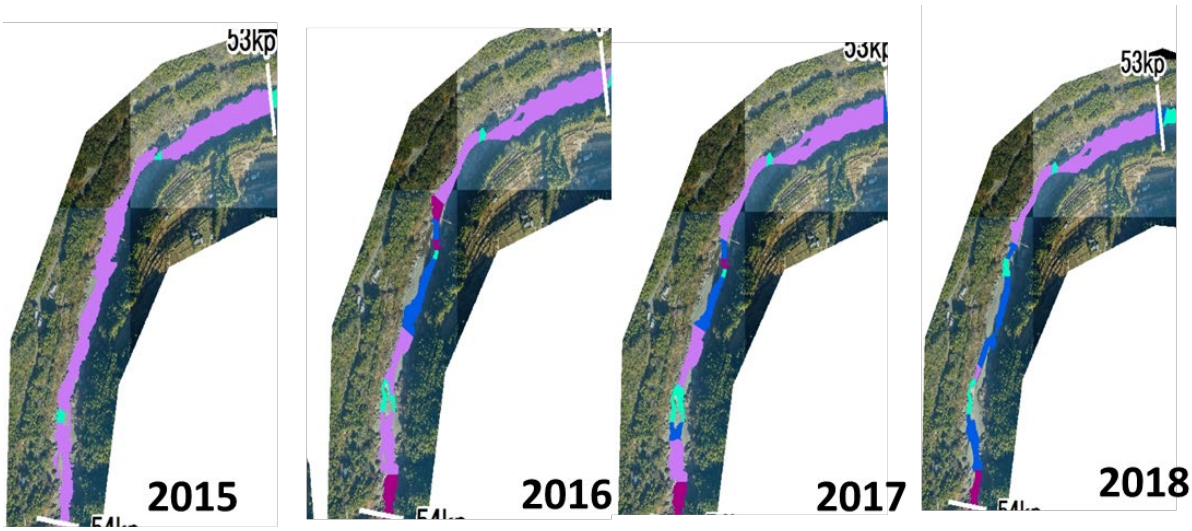

Figure 4-18 The distribution of geomorphic units at 9 km downstream of the replenishment site in the Naka River from 2015 to 2018.

For the Buëch River, the geomorphic units were manually classified from the high-resolution aerial photos from 2016 to 2018 (before the second replenishment in 2018) (Figure 4-19). The 6 km reach downstream of the replenishment site was selected as the study area. Same as the Naka River, two indicators of GUS were calculated with an interval of 1 km reach and the results were shown in Figure 4-20. The same trends of GUSI-R and GUSI-D occurred from 2016 to 2017 in the Buëch River, which means that the SR may lead to the same responses of geomorphic units in both two rivers. For the second year of replenishment (2018), the GUSI-D value decreased due to the lack of sediment supply from upstream. Some secondary channels located around 4-5 km disappeared which reduce the number of units and finally affect the value of GUSI-D.

Considering the area alterations of each unit, even distribution was also observed after the replenishment in 2016 (Figure 4-21). However, the distribution keeps stable between 2017 to 2018, which means that the downstream responses of replenishment to geomorphic units may stop. Compared to the Naka River, the scale of replenishment in the Buëch River was small and no continuous replenishment was implemented annually. The lack of such integrated management of sediment supply gives rise to such slow and indistinctive impacts on geomorphic units at downstream reach.

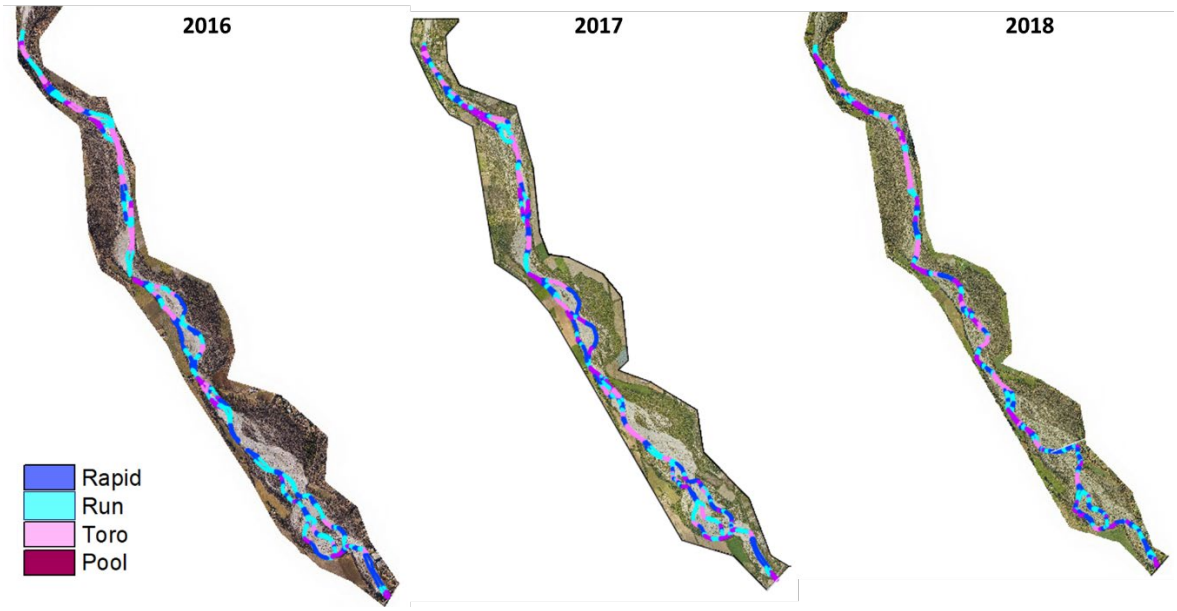

Figure 4-19 The distribution of geomorphic units 6 km downstream of the replenishment site in the Buëch River from 2016 to 2018.

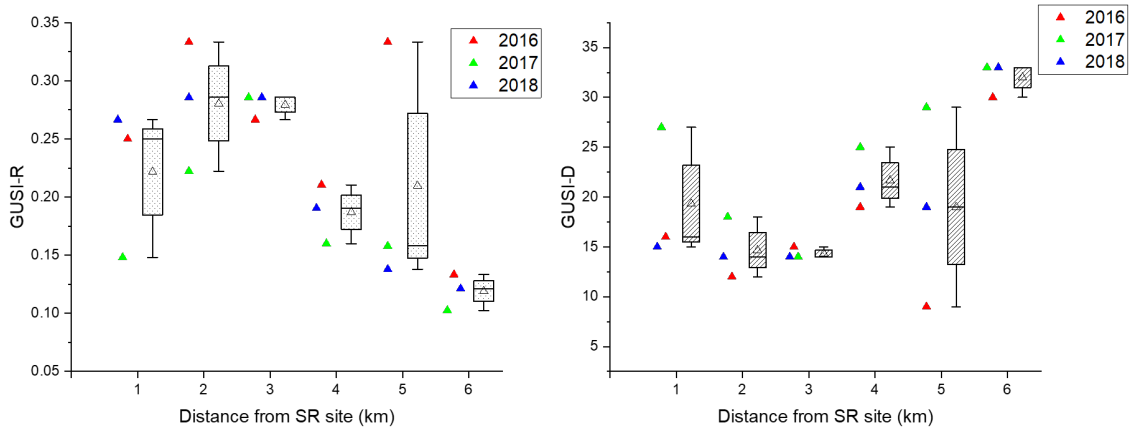

Figure 4-20 The GUSI-R and GUSI-D at 6 km downstream of the replenishment site in the Buëch River from 2016 to 2018.

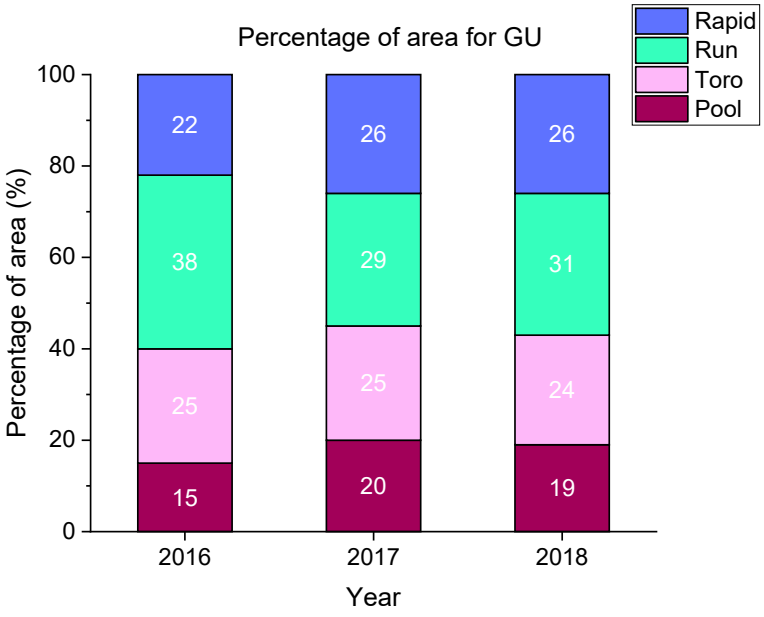

Figure 4-21 The percentage of area for different geomorphic units 6 km downstream of the replenishment site in the Buëch River from 2015 to 2018.

4.3.3. Hydro-Geomorphological Index of Diversity

The analysis of HMID was only conducted in the Naka River since there was no sufficient data on flow velocity and water depth in the Buëch River. The water depth and flow velocity during the normal flow period in the Naka River were measured up to 12 km downstream of the replenishment site in 2015 and 2016. While data is only available at two spawning grounds 2 to 3 km and 11 to 12 km downstream of the replenishment site in 2020. The results of the HMID value were shown in Figure 4-22 below. The HMID value was greater than 9 in the majority of the area, which means that the continuous implementation of SR was beneficial for reserving a geomorphological pristine site in the Naka River. Furthermore, increasing in HMID value can be founded from 2015 to 2016 at 7 km to 12 km downstream of the replenishment site. Specifically, the significant increase occurred at 11 and 12 km, with an average raising around 25% from 2015 to 2016. Despite this, all of the HMID values increased by around 10% to 30% from 2016 to 2020 at 4 locations.

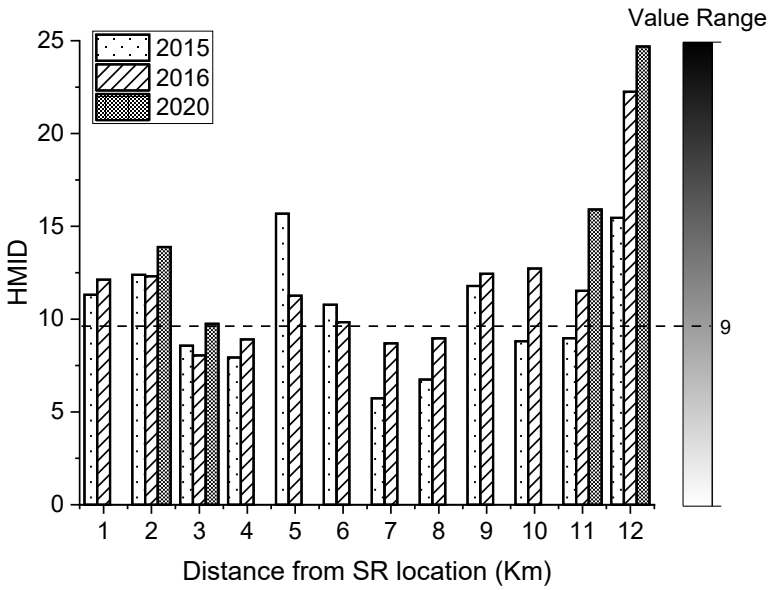

Figure 4-22 The HMID value in the Naka River up to 12 km downstream of the replenishment site in Naka River from 2015 to 2016, and 2020.

4.3.4. Channel adjustment

For the Naka River, the channel adjustment was calculated based on the bathymetric survey conducted from 2010 to 2017 up to 12 km downstream of the replenishment site. The alteration of average bed level changes between each year was summarized in Figure 4-23. Specifically, after the first replenishment implemented in 2010, the deposition occurred at the middle of the reach (3 km to 8 km) with an average value of around 1 meter, while erosion mainly occurred near the replenishment site (up to 2 km) in 2011. Moreover, the same trend of erosion and deposition happened from 2012 to 2011 with a less value of bed changes (less than 1 meter). An opposite tendency of geomorphological alteration happened from 2013 to 2012. Significant deposition can be observed near the replenishment site with an average value of around 0.7 meters. From 2014 to 2013, great geomorphological activity can be observed at the whole study reach, and deposition occurred at 90% of the locations with an average bed change of 0.8 meters. The locations where deposition occurred were reduced in 2015, while the magnitude increased. Some locations with significant bed aggradation (greater than 2 meters) can be observed at 1 km and 5 km. And in 2016, the deposition mainly occurred at the middle reach, which was quite similar to 2012. Nevertheless, higher erosion

can be observed near the replenishment site with an eroded depth of around 1.5 meters. On the contrary, deposition happened in 2017 at the location where erosion occurred in 2016, which means that some of the deposited sediment was transported downstream. Finally, considering the total changes from 2010 to 2017, bed aggradation occurred at most locations (greater than 90%) with an average magnitude of 1.5 meters. It can be concluded that the additional sediment supply from the replenishment site promoted the river bed aggradation in the Naka River.

Despite this, it can also be noticed that average bed level changes have a close correlation to the transported volume in the Naka River (Figure 4-24). We calculated the average bed level change of the whole study reach and found that the increase of sediment supply from the replenishment site directly will lead to more deposition occurring. The relationship between transported volume and average bed level change is also solid with an R square equaled 0.946.

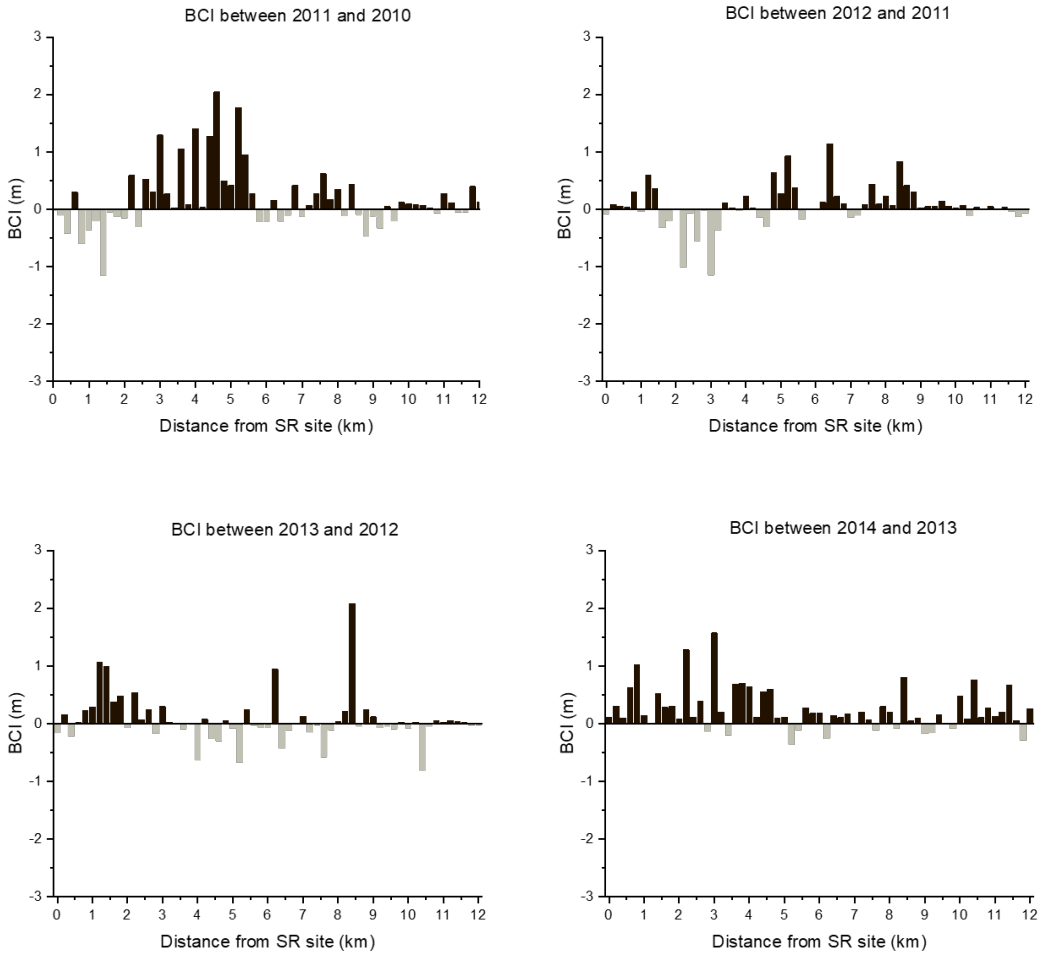

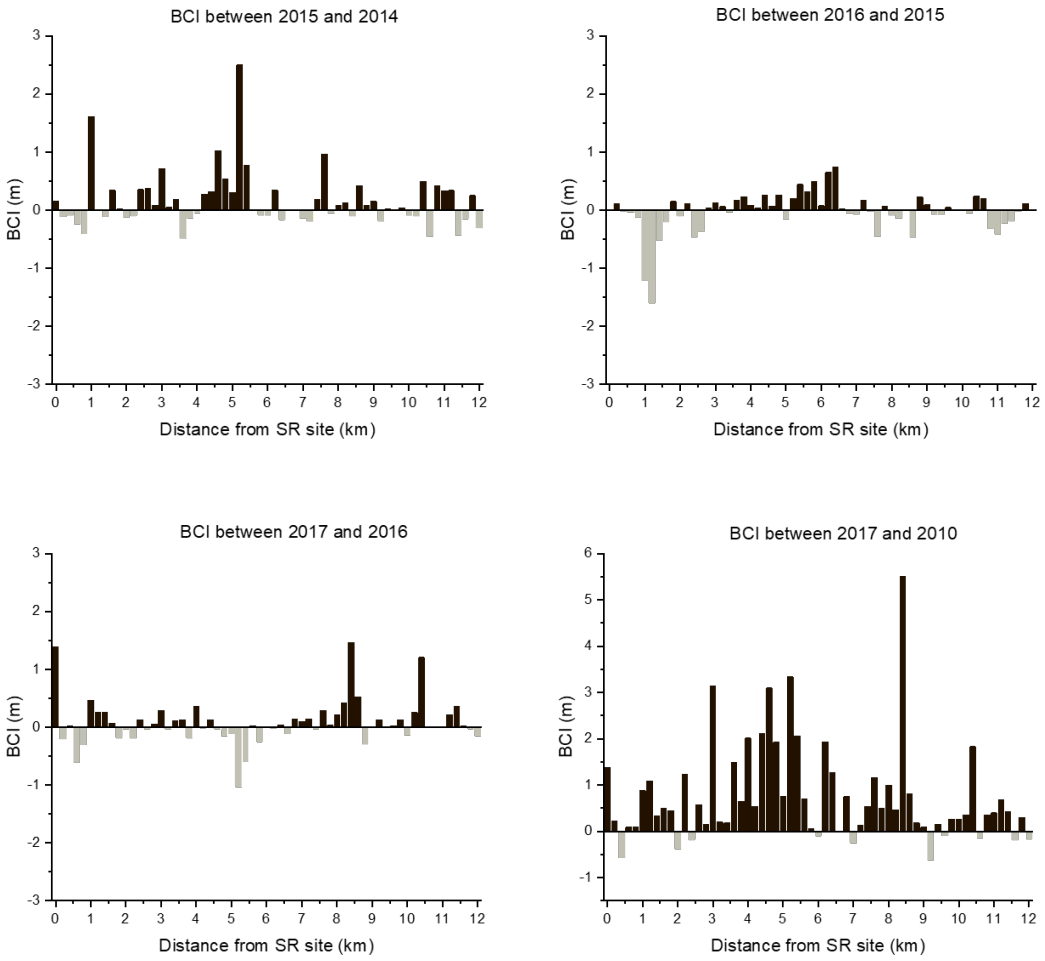

Figure 4-23 The alteration of BCI between 2010 to 2017 up to 12 km downstream of the replenishment site in the Naka River.

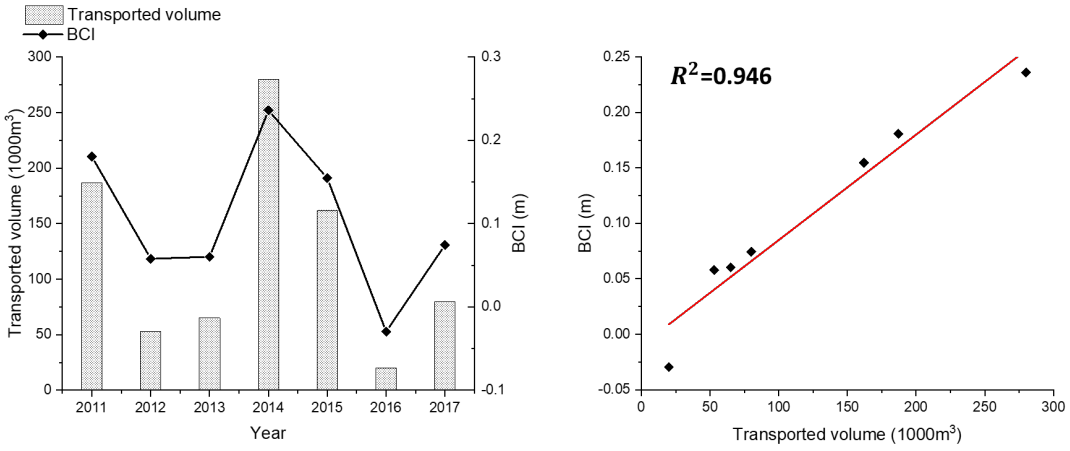

Figure 4-24 The analyzed results of BCI and transported volume in the Naka River from 2011 to 2017. Left figure: the results of the time series. Right figure: the results of the inner relationship.

The channel adjustment for the Buëch River was summarized from the first implementation of replenishment (2016) to 2020 (Figure 4-25). The timelines for calculating the alteration were: before the 2016 SR, after the 2016 SR, 2017, before the 2018 SR, after the 2018 SR, and 2020. To be specific, after the replenishment conducted in 2016, bed aggradation occurred at the majority of the locations, with a net change of around 0.2 meters, while erosion can be observed in the middle of reach between 2 to 4 km. In 2017, rare geomorphological alterations can be detected along the reach, and only some deposition around 0.15 meters happened near the replenishment site. Before the SR in 2018, significant erosion occurred near the replenishment site, which was the opposite in 2017. Moreover, aggradation with a small magnitude (average: 0.3 meters) can be seen at the majority of the reach after 0.5 km. And after the replenishment in 2018, an obvious alternative of aggradation and degradation can be observed at 1 km. Significant erosion occurred near the replenishment site while the rest reaches can be considered as aggradation. Furthermore, a similar distribution of aggraded and degraded reaches can be observed in 2020, which means that the characteristic of sediment transportation was not changed during that period. In summary, considering the four years' alteration, 90% of the reaches were aggraded with an average value of around 0.2 meters (max=0.5 m, min=0.01 m). The overall tendency of deposition and erosion was quite similar to that in the Naka River, which means that the geomorphological changes due to the conducting of SR were within our expectation.

Though the data is limited in the Buëch River, we can also observe the same positive relationship between transported volume and average bed level changes (Figure 4-26). Such promotion of riverbed deposition is one of the most direct impacts of SR to the downstream reaches.

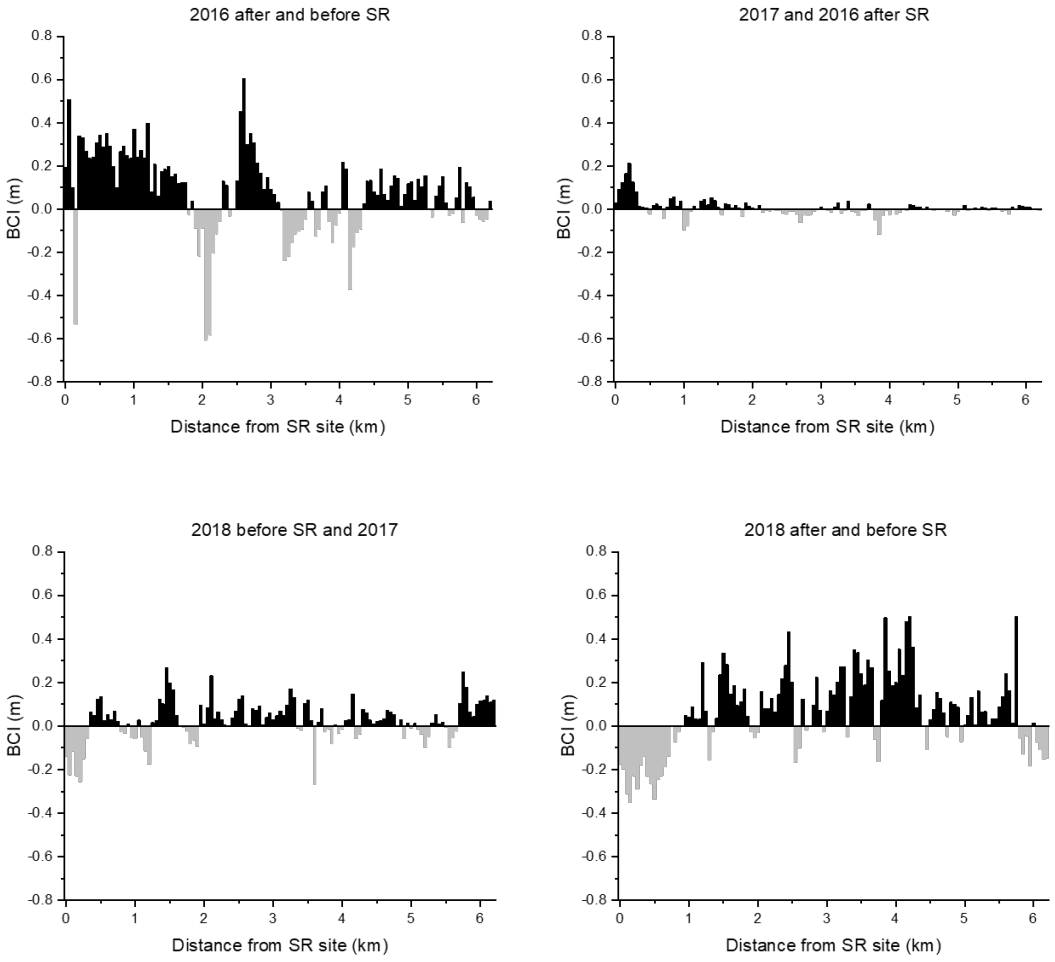

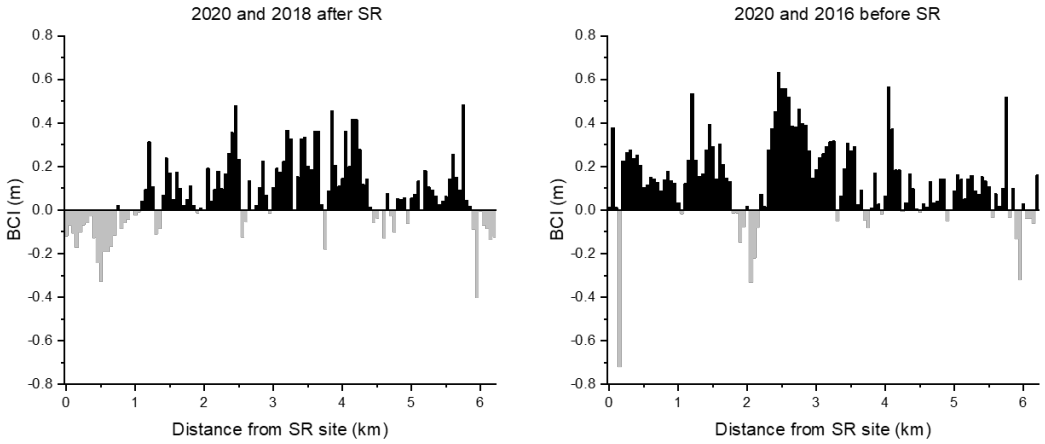

Figure 4-25 The alteration of BCI from 2016 before the SR to 2020 up to 6 km downstream of the replenishment site in the Buëch River.

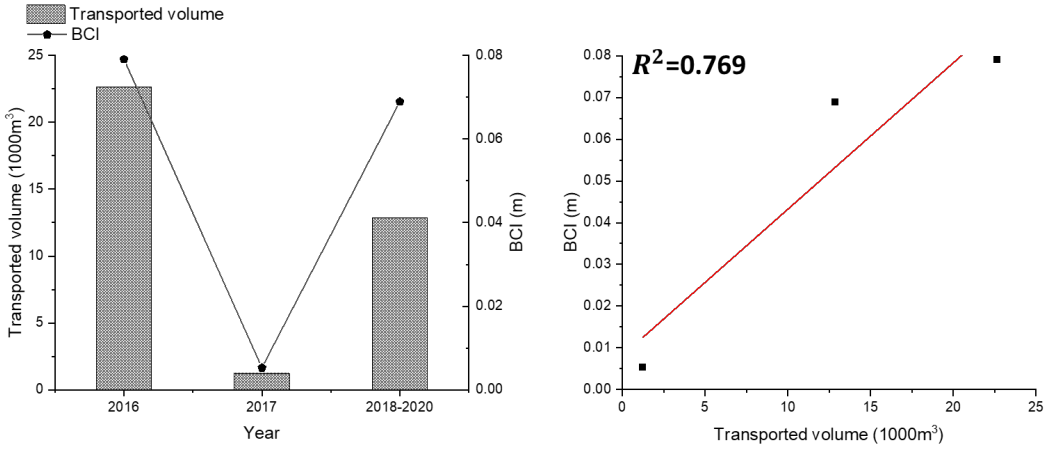

Figure 4-26 The analyzed results of BCI and transported volume in the Buëch River from 2016 to 2020. Left figure: the results of the time series. Right figure: the results of the inner relationship.

4.3.5. Riverbed substrates

The results of riverbed substrates were determined based on the field survey conducted in 2015 and 2016 in the Naka River. Results for the Buëch River can not be shown since only one year of data is available, which is not meaningful for analyzing the responses of SR. The calculated percentage of different sizes of substrates in 2015 and 2016 in the Naka River is shown in Figure 4-27. The

differences of each substrate between 2016 and 2015 at each reach were summarized in Table 4-6. It can be observed that the stones around 200 mm (m3) were dominant along the study area, with percentages ranging from 40% to 85%. On the contrary, the quantities of gravels (m1 and m2) were much less than stones (m3), with percentages ranging from 5% to 50%. In 2016, the percentage of gravels increased along the reach, especially the m1. An average raise of around 30% can be observed for m1 along the whole study reach. Despite this, the percentage of m2 slightly increased after 3 km with an average value of less than 10%. Such a significant increase in gravel may be mainly due to the supply of sediment from the replenishment site. The D50 of the replenished sediment in the Naka River was around 7 mm, which was corresponding to the range of grain size for m1 (2 mm to 20 mm). In contrast, the percentage of m3 decreased crucially along the reach, which peaked at 5 km to 6 km (45%). Such stones were transported by the high flushing flow between 2015 and 2016. Moreover, the distribution of the substrates was more even in 2016 at each reach, which means that the SR filled the lack of medium-sized sediment. The same responses of riverbed substrates can also be observed in replenishment projects conducted in the Nunome River (Sameh Kantoush, Tetsuya Sumi, & Akira Kubota, 2010).

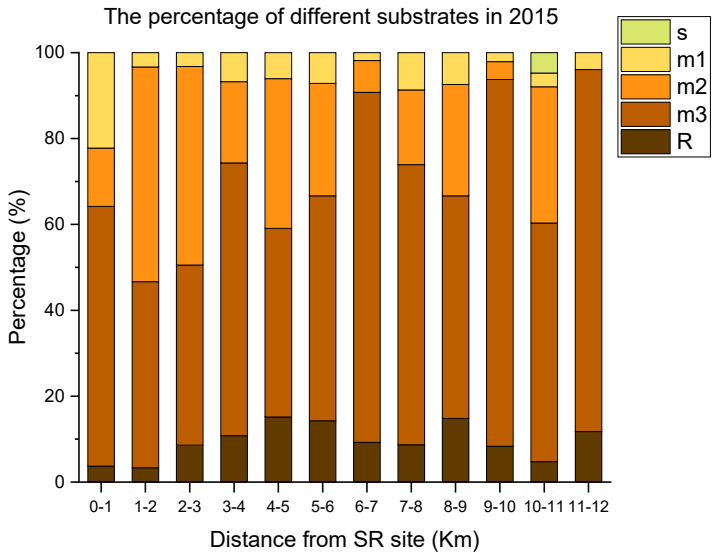

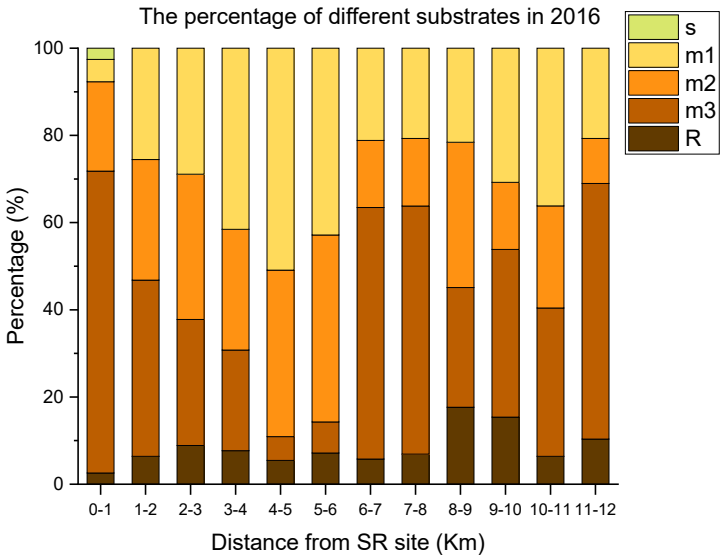

Figure 4-27 The percentage of different substrates along the 12 km reach in 2015 and 2016 in the Naka River

Table 4-6 The alteration of different substrates between 2016 to 2015 along the 12 km reach in the Naka River.

	R	m3	m2	m1	s
0-1k	-1%	9%	7%	-17%	3%
1-2k	3%	**-3%**	-22%	**22%**	0%
2-3k	0%	**-13%**	-13%	**26%**	0%
3-4k	-3%	**-40%**	**9%**	**35%**	0%
4-5k	-10%	**-38%**	**3%**	**45%**	0%
5-6k	-7%	**-45%**	**17%**	**36%**	0%
6-7k	-3%	**-24%**	**8%**	**19%**	0%
7-8k	-2%	**-8%**	-2%	**12%**	0%
8-9k	3%	**-24%**	**7%**	**14%**	0%
9-10k	7%	**-47%**	**11%**	**29%**	0%
10-11k	2%	**-22%**	-8%	**33%**	-5%
11-12k	-1%	**-26%**	**10%**	**17%**	0%

4.3.6. H value of fish diversity

For the Naka River, the time series of H values were calculated at three main spawning grounds, which were located 0.5 km, 2 km, and 11 km downstream of the replenishment site from 2009 to

2017 (Figure 4-28). Data between 2009 to 2011 was insufficient due to the lack of field surveys. Comparing the year before SR (2009 and 2010), the H value increased by 40% in 2015 at 0.5 km and 2 km during summer. Moreover, the H value also raised 30% from 2012 to 2015 at 11 km during summer. Such alterations may have a close relationship to the volume of transported sediment. Therefore, we generated the relationship between the average H value (average of Summer and Autumn) and transported volume (Figure 4-29). We can roughly analyze that the H value started to increase from the implementation of SR in 2010 at all spawning grounds. Such promotion of habitat quality stopped and adverse impacts can be observed after 2015 in the near two spawning grounds (0.5 km and 2 km). It can be noticed that the transported sediment started decreasing after 2015 (from 390,000 m^3 to 160,000 m^3), which may be the main reason to cause the turning points of the H value. A delay of such reduction occurred at 11 km (from 2016) which may be because sediment needs time to be transported to the site far away from the replenishment location.

Furthermore, a solid relationship can be generated between transported volume and to average alteration of H value with an R square equal to 0.781 (Figure 4-30) at 11 km spawning grounds. The increasing transported volume promoted the diversity of the spawning grounds (H value increasing). However, such efficiency of enhancement was decreasing because the transported volume was too high (larger than 350,000 m^3).

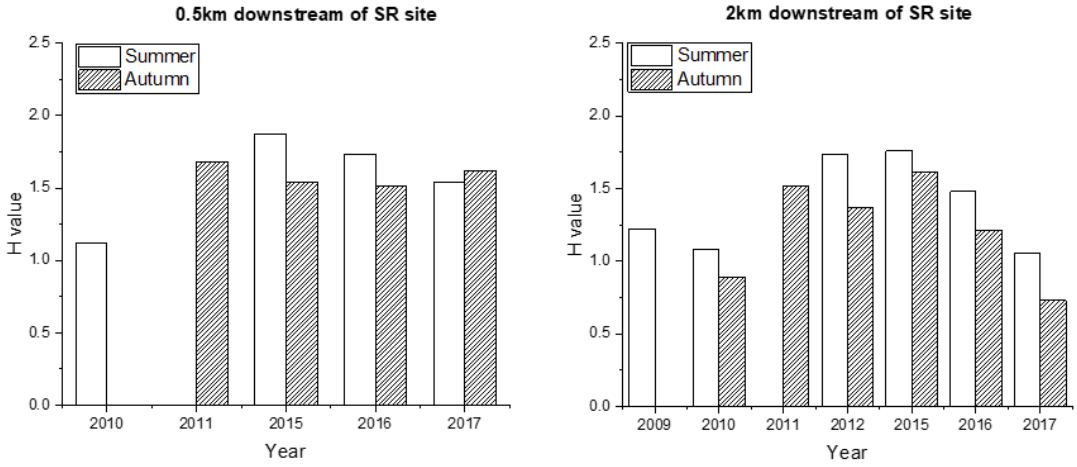

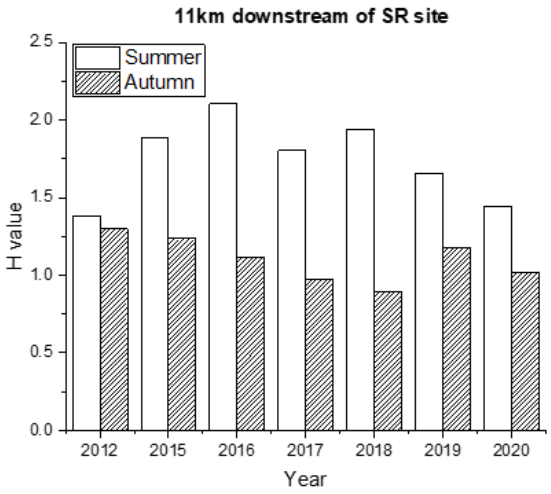

Figure 4-28 The results of H value at three spawning grounds located at 0.5 km, 2 km, and 11 km downstream of the replenishment site in the Naka River.

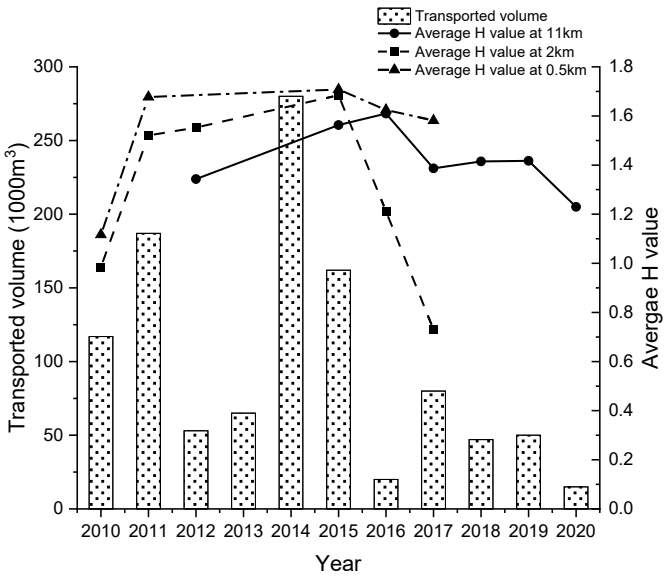

Figure 4-29 The relationship between the average H value at three spawning grounds and the volume of transported sediment from the replenishment site in the Naka River.

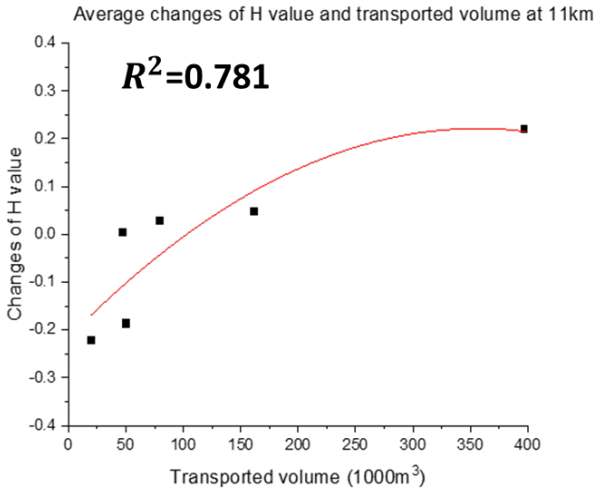

Figure 4-30 The relationship between transported volume and average changes of H value at 11 km in the Naka River.

The H value variation along the study reach from 2015 to 2016 was also summarized to spatially investigate the impacts of replenishment (Figure 4-31). From 2015 to 2016, decreasing occurred near the replenishment site while a small fluctuation (between 0.15 to -0.15) was observed at the rest area. However, declination can be detected in the whole study area between 2017 to 2016. The significant reduction of sediment supply to an extremely small volume (from 160,000 m^3 in 2016 to 20,000 m^3 in 2017) may weaken the habitat quality of the whole area.

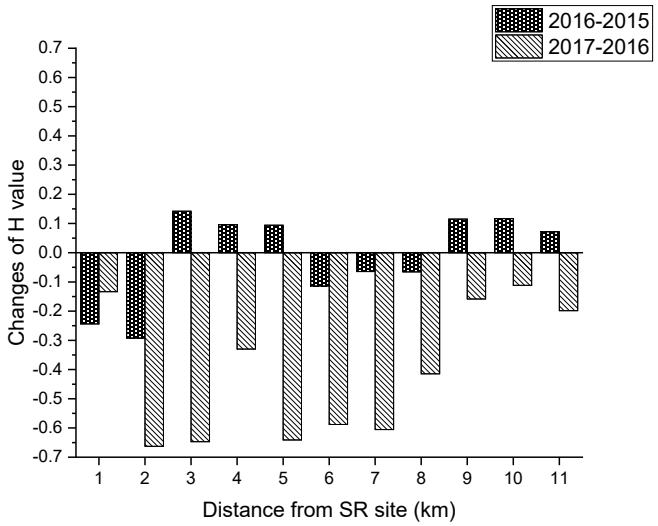

Figure 4-31 The alteration of H value with the distance from the replenishment site in 2015, 2016, 2017 in the Naka River.

The H value for the Buëch River was calculated at 6 km downstream of the SR site from 2014 to 2018 (before conducting the second replenishment) (Figure 4-32). It can be noticed that before 2016, the H value slightly increased by around 20% annually. However, a crucial growth of 30 % occurred after the replenishment in 2016 (from 1.5 to 2.0). The H value then fell back to the same level before replenishment in 2018. It can be expected that after the replenishment in 2018, the H value should increase if we have enough data to calculate.

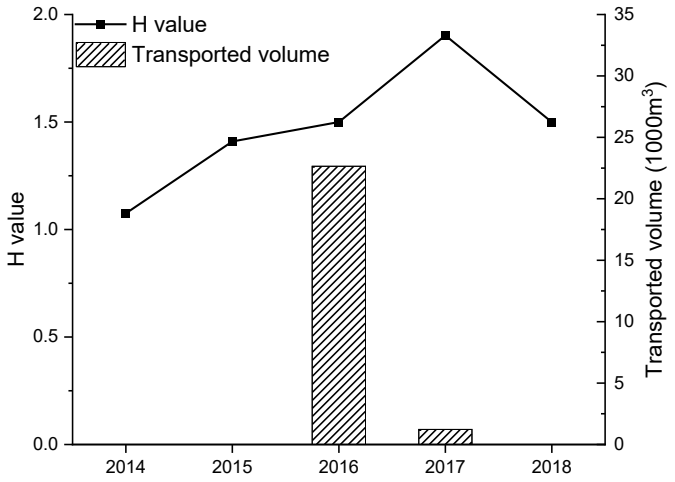

Figure 4-32 The results of the H value at 6 km downstream of the replenishment site from 2014 to 2018 in the Buëch River.

4.4. Discussion

4.4.1. The erosion process of replenished sediment

The strategy of implementing SR in the Naka River and the Buëch River is different due to the various sediment management approaches and basin sizes. For the Naka River, the replenishment stockpile is placed at the location where the channel is just widening from a narrow area. Based on the recorded video during the flood events in May 2021, the flow condition near the stockpile was summarized in

Figure 4-33. It can be observed that the high turbulence flow from the narrow channel was separated into two directions at the middle of the stockpile. A part of the water flowed downstream and was utilized to flush the stockpile. On the contrary, some reverse flow areas can be founded near the right side which was generated from another part of the inflow. A clear boundary of flow splitting can be recognized, which is also corresponding to the demarcation of the eroded and non-eroded area of the stockpile. However, if the inflow increases, some slight erosion will occur on the right side of the stockpile. Compared to the two flood events that occurred in 2021 with different inflows (May: around 490 m^3/s, August: around 900 m^3/s), there was nearly no erosion happened in May with a small inflow (Figure 4-34). Nevertheless, some sliding occurred at the surface of the stockpile and some small erosion occurred at the bottom after the flood in August (Figure 4-34). In summary, such splitting truly weakened the flushing capability of the inflow and may be one main reason that the TR value is lower in the Naka River. Die Moran et al. (2013) found that if the angle between the stockpile and the bank was less than or more than 90 degrees, the bank erosion process will be limited (Figure 4-35 B and C). While if the stockpile is perpendicular to the bank, stabilization of the stockpile may be weakened and more sediment will be scoured (Figure 4-35 A). Ishigaki (2004) also investigated the orientation of the stockpile and found that an angle larger than 90 degrees will weaken the stabilization of the stockpile and thus leads to more erosion. Despite this, the submergence of the stockpile is another key factor that affects the erosion process. Previously, the submergence ratio of the stockpile varied from 50% to 70% before 2019 since the releasing flow was higher (greater than 3000 m^3/s). However, there were fewer typhoons occurred in 2020 and 2021, and the submergence ratio was less than 30% due to the reduction of flushing flow (less than 1000 m^3/s). A higher submergence condition will promote the erosion process near the bank and thus more sediment will be scoured (Elena Battisacco, 2016). the re-design of the replenishment site by separating the placed sediment to multiple locations at the central, or left bank or some suitable locations downstream is resealable to conduct a high efficient replenishment works in the Naka River.

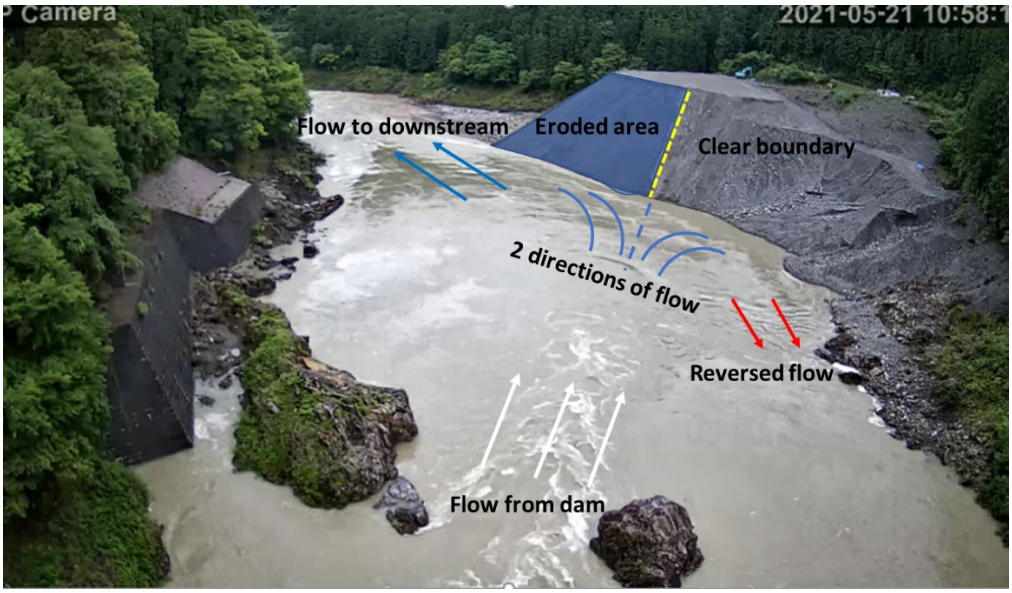

Figure 4-33 The flow condition near the stockpile based on the video recorded in May, 2021 in the Naka River.

Figure 4-34 The comparison of eroded area between flood events in May and August, 2021 in the Naka River.

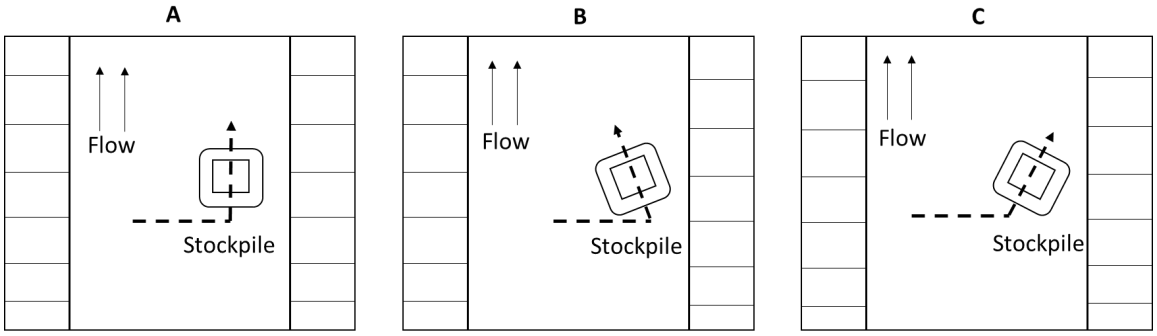

Figure 4-35 The different cases of stockpile orientation. A: angle equals 90°. B: angle less than 90°. C: angle greater than 90°.

For the Buëch River, the current strategy for removing sediment from the left bank to the central was proved as an efficient way to enhance the erosion process of the stockpile. The TR increased by around 50% from 2016 to 2018. However, there was still some sediment remaining at the site (Figure 4-36). Such sediment is difficult to be scoured since the submergence ratio was too high if the flood is coming. A submerged structure gives rise to less erosion than a part-submerged structure since the near-bank velocity is reduced and the corresponding shear stress is decreased as well (Die Moran et al., 2013). It can be concluded that one-time placement is not an efficient strategy to conduct SR. It is recommended to continuous supply sediment for reshaping the stockpile and maintaining a higher TR value in the Buëch River.

Figure 4-36 The remaining sediment at the replenishment site after the 2018 SR in the Buëch River.

4.4.2. The morph-ecological responses to the SR

Regarding the Naka River, based on the variation of GUSI indicators, it can be expected that the number of geomorphic units increased from 2015 to 2016 while maintaining stability between 2017 and 2018. The differences in sediment supply from the replenishment site may be the main reason that caused such alteration (Figure 4-16). Panel (2005) revealed that the variation of sediment input and transportation is one crucial point that causes hydrological and geomorphological changes, which in turn create new geomorphic units at downstream reach. Despite this, more riffles (rapids and runs) were created at the middle reach after 5 km (Figure 4-18) since the sediment was more likely to be accumulated or eroded here. Aggradation and degradation can also be observed in the corresponding area from 2015 to 2018 (Figure 4-23), which means that the SR may assist to transfer the geomorphic units from toro to riffle. Matsushima et al. (2018) also observed an increase in riffle area with the implementation of SR at the Managawa dam. Such alteration of geomorphology also leads to hydrological variations, for instance, alteration of flow velocity and water depth. The HMID represents the fluctuation of hydrological patterns, which shows variation from 5 km between 2015 to 2016 as well (Figure 4-22). The significant alteration at 11 km and 12 km resulted in the degradation of the riverbed and thus change the flow patterns. Despite this, it can be concluded that the amouring problem was well tackled by the SR implementation based on the results of riverbed substrates. More medium gravels were supplied to the whole study area and the discontinuous distribution of grain size was fixed. Such modification of the riverbed is one essential function of SR mentioned by G. M. Kondolf (1997), and Miyagawa, Sumi, Takemon, and Kobayashi (2017).

Moreover, the habitat quality was also enhanced by the replenishment according to the increase of H value from 2015 to 2016. However, it is worthwhile to notice that a continuous supply of adaptable volume of sediment is also vital to maintain the H value. The reduction of the H value occurred when the volume of sediment supply from the replenishment site decreased (Figure 4-29). The positive relationship between transported volume and H value at one spawning ground can prove such a viewpoint (Figure 4-30). A threshold may occur with the increasing transported volume, which means that an extreme volume of additional sediment supply may have adverse impacts on habitat quality. It can be concluded that the ecological responses are sensitive to the extreme alterations of sediment supply, for instance, implementing replenishment or not, or significant alteration of supply volume (Staentzel et al., 2020).

For the Buëch River, the same increase of GUSI-D occurred after the replenishment implemented in 2016 (Figure 4-20). The additional sediment supply increased the number of geomorphic units by splitting the large and integrated units (Morgan, 2018). While the response reduced in the second year since the remaining sediment at the replenishment site was small and there was no sufficient sediment supply downstream. Considering the alteration of the area of different units, more rapids were transferred from runs and the numbers of toros kept stable, which was different from the phenomenon in the Naka River. The replenishing material in the Buëch River (D50= 7 mm) was coarser than in the Naka River (D50= 7 mm). Such grain size of gravels tended to become the floating gravels and thus promote the formation of rapid. Furthermore, significant aggradation and degradation occurred after the 2016 replenishment (Figure 4-25), and the corresponding increase of GUSI-D happened in the whole study area as well (Figure 4-20). And after the second replenishment in 2018, significant geomorphological activities can also be detected. It can be expected that the number of geomorphic units will increase if we have data.

The alteration of habitat quality in the Buëch River was also sensitive to the additional sediment supply from replenishment. A significant reduction of H value happened in the second year of replenishment. It can be concluded that whether it is one-time replenishment or continuous replenishment, an adaptable sediment supply from the replenishment site is the key point to restoring the habitat structure and enhancing the habitat diversity.

The interrelationships between each assessed indicator are also essential to understand the relationship between geomorphology and ecology at downstream reach. Specifically, a solid relationship can be founded between HMID and GUSI indexes in the Naka River (Figure 4-37). The newly formatted riffles (run and rapid) and pools are not beneficial for the promotion of HMID, which leads to positive and negative relationships for GUSI-R and GUSI-D respectively. Nevertheless, opposite relationships can be founded for H value and GUSI indexes (Figure 4-38), which means that the increasing of riffles and pools can enhance the habitat quality. Furthermore, a negative relationship can be founded between HMID and H value with a R square of 0.14, which means that the inner connections between such indicators are not close (Figure 4-39). Therefore, the GUSI index should be considered as the most sensitive indicator to link the geomorphology and ecology in the analysis.

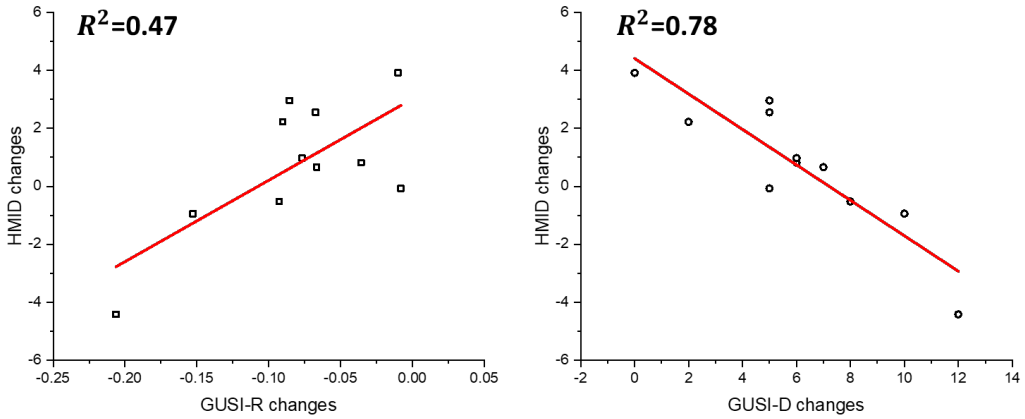

Figure 4-37 The interrelationship between HMID and GUSI index based on data of the Naka River. Left figure: GUSI-R changes and HMID changes. Right figure: GUSI-D changes and HMID changes.

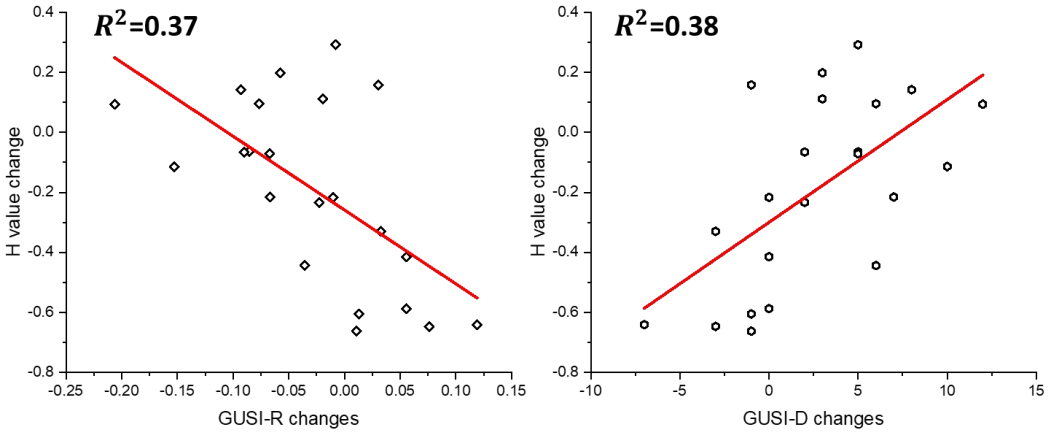

Figure 4-38 The interrelationship between H value and GUSI index based on data of the Naka River. Left figure: GUSI-R changes and H value changes. Right figure: GUSI-D changes and H value changes.

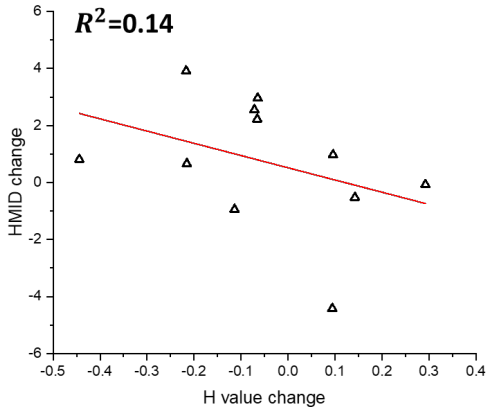

Figure 4-39 The interrelationship between H value and HMID based on data of the Naka River.

In summary, the geomorpho-ecological responses from the SR can be simplified into several parts (Figure 4-40). The flushing flow can be considered the driving force for sediment movement, including sediment erosion and transportation from the SR site and the original riverbed. Then, such alteration of sediment leads to several geomorphological changes, for instance, an increase numbers of geomorphic units, enriching the riverbed substrates (solving the amouring problem), and adjustment of the channel. Then, variations of assessment indicators can be observed, and GUSI indexes can be considered as the most sensitive indicator for assessment of downstream geomporpho-ecology as it has close correlations to the H value and HMID. Considering the objective, the restoration of the downstream hydro-geomorpho-ecology, optimal values of sediment supply and flushing flow is existed to maintain a better composition of geomorphic units at downstream reach, which can beneficial for the hydro-morphology (HMID>9) and ecology (higher H value) simultaneously. Based on the previous results, the optimal volume of sediment supply from SR is around 100,000 m^3 for the Naka River.

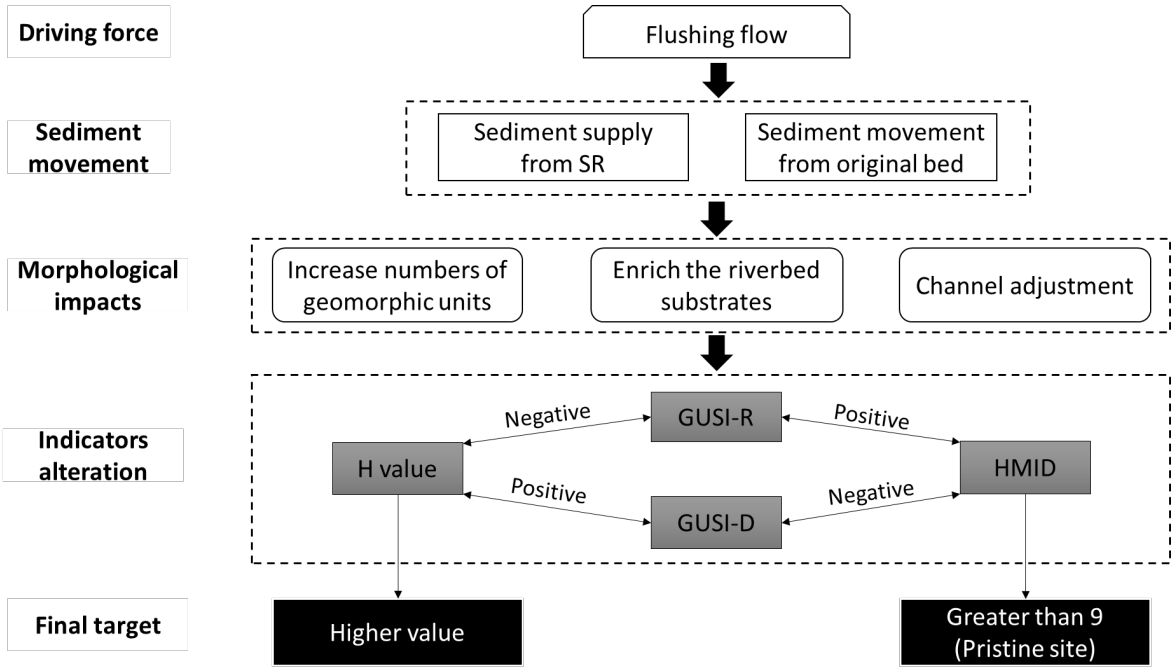

Figure 4-40 The summarized flow chart that shows the process of how SR leads to the downstream geomorpho-ecological responses and how to evaluate such responses.

4.4.3. The comparison of SR between the Naka River and the Buëch River

The comparison of replenishment implementation between the Naka River and the Buëch River was summarized in Table 4-7 based on all the analyzed indicators in the former part. For the replenishment characteristics, the Naka River utilized a single stockpile with considerable volume to conduct a continuous replenishment from 2010. In the contrast, the Buëch River implemented a one-time replenishment in 2016 and 2018 with less placed volume at the left, central, and right of the river channel. Moreover, compared to the Buëch River, the replenished gravels were much finer in the Naka River, which was mainly due to the differences in sediment sources upstream. Considering the TR value, the efficiency of replenishment in the Buëch River was higher than in the Naka River. The strategy of placing sediment at multiple locations with medium volume was one reason that promoted the erosion process in the Buëch River. Nevertheless, the higher flushing flow in the Naka River did not lead to a higher TR value, which may mainly be due to the considerable volume of placed sediment and the weakening of flushing capacity near the replenishment site.

Regarding the downstream geomorpho-ecological responses, the average value of GUSI-R in the Naka River was 25% higher than in the Buëch River, while an opposite phenomenon can be observed for GUSI-D. To explain it, the 1 km study reach in the Buëch River contains more geomorphic units than in the Naka River, which leads to the increase of N_{GU} and n. Thus, the GUSI-R is smaller and GUSI-D is higher in the Buëch River. The SR tends to create more numbers of geomorphic units in the Buëch River which may be due to the different channel configurations (Naka River: steep and meandering channel, Buëch River: straight and shallow channel). The average HMID value in the Naka River is greater than 9, which means that the geomorphological pristine sites kept well with the conducting of replenishment (Gostner et al., 2012). Furthermore, higher aggradation of the riverbed can be observed in the Naka River. The continuous implementation of replenishment with higher transported volume leads to more significant alteration of the river channel downstream. Finally, the H value at the spawning grounds of the two rivers does not show a great distinction. Similar enhancement of habitat quality and diversity is expected in both rivers.

Table 4-7 The comparison of replenishment characteristics and morph-ecological indicators between the Naka River and the Buëch River.

		Naka River	**Buëch River**
Replenishment characteristics	Implementation method	Single stockpile	Multiple stockpiles
	Replenishment date	From 2010 to now	2016 and 2018
	Placed volume (m^3)	130,000 to 390,000	2016: 43,500 2018: 15,000
	D50 of replenishment material (mm)	7	21
	Flushing flow (m^3/s)	400 to 5000	100 to 300
	TR value	5% to 50%	2016: 50% 2018: 87%
Geomorpho-ecological indicators (average)	GUSI-R	0.28	0.22
	GUSI-D	16.8	20.5
	HMID	11	-
	BCI (m)	Between 2017 to 2010: 0.84	Between 2020 to 2016: 0.18
	H value	At 11 km: 1.42	At 6 km: 1.47

4.5. Conclusion

In conclusion, a compressive assessment of SR works was conducted in the Naka River, Japan, and the Buëch River, France. The replenishment characteristics and downstream hydro-geomorpho-ecology were evaluated based on several simple indicators, including TR, TFWV, GUSI-R, GUSI-D, HMID, H value, BCI, and percentage of substrates. Data on the Naka River was collected from our field survey or provided by the Naka River Office. And data on the Buëch River was provided by the EDF (Électricité de France). However, a full assessment of replenishment works at two study rivers was difficult to conduct due to the lack of required data. The key findings of this chapter are:

(1) The efficiency of replenishment in the Naka River is not higher due to the location of the stockpile and the considerable volume of placed sediment. Future countermeasures with multiple replenishment sites and lower placed volume should be considered. In terms of the Buëch River, efficient replenishment works were successfully conducted due to the appropriate strategy of stockpile placement. Continuous SR with additional sediment input should be considered to effectively utilize the remaining sediment at the replenishment site.

(2) Regarding the downstream hydro-geomorpho-ecology, positive responses can be founded in both two study rivers. New geomorphic units (especially the riffles) were created (increasing of GUSI-D) and aggradation of the riverbed can be observed at the majority of the reaches with the additional sediment supply from the replenishment site. However, no new types of units are detected which leads to the reduction of GUSI-R. Such newly formatted riffles are beneficial for the habitat quality and thus lead to a promotion of H value. Yet, it can be noticed that the HMID has a negative correlation with the GUSI-D, which means that the riffles may not suitable for enhancing the hydro-geomorphological quality. Furthermore, the amouring problem was efficiently solved as more small to medium gravels were accumulated to fill the lack of such grains in the Naka River. For the consideration of restoring downstream hydro-geomorpho-ecology, continuous input of adaptable sediment combined with optimal flushing flow should be implemented.

(3) The replenishment works in the Naka River and the Buëch River can be recognized as successful projects as positive responses of downstream geomorpho-ecology were detected. However, modification of the replenishment strategy should be conducted to extend and enhance such beneficial responses. For the Naka River, due to the lack of flood events that occurred in recent years, the additional flow should be released to maintain the sediment

supply from the SR site (around 100,000 m^3 per year). For the Buëch River, it is recommended to implement continuous SR annually under the consideration of downstream restoration.

Chapter 5. Numerical simulation of sediment replenishment works in the Naka River based on TELEMAC-2D coupled with Gaia

5.1. Introduction

Based on previous results in the assessment of SR (chapter 4), the erosion process of the replenished stockpile and downstream hydro-geomorpho-ecological response are two crucial aspects that represent whether the restoration is successful or not. Several characteristics will influence the performance of replenishment works. Specifically, releasing flow as the driving force is the most significant characteristic that may directly influence the transported volume of replenished sediment, downstream aggradation, and degradation of the riverbed. Moreover, other characteristics, such as grain size of replenished material, replenished volume and locations should also be considered as the dominant characteristics in the investigation of SR.

Nevertheless, it is not integrated to investigate such crucial characteristics only based on field surveys and measurements since the data is very limited. To tackle it, numerical models have been widely utilized around the world to better understand the erosion process of replenished sediment and downstream geomorphological responses. It can not only assist us to investigate the hydrodynamics and sediment transportations, but also provide us valuable information on the optimization of replenishment works through designed scenarios. The previous study on numerical models related to SR has already been summarized in Section 2.4.

In this chapter, we establish a two-dimensional model to simulate the hydro-geomorphological changes with the implementation of SR in the Naka River. TELEMAC-2D as an open-source numerical tool has already been utilized to simulate the replenishment works in the Buëch River, France by Guillaume BROUSSE, Jodeau, and CORDIER (2022). We used their codes as a reference to conduct our model establishment in the Naka River. This chapter mainly focuses on sensitivity analysis to obtain the best model parameters. The expected results, for instance, the eroded volume of the replenishment site, the bed evolution, the flow velocity, and water depth at downstream reach can be used in the assessment of our replenishment works under different scenarios in Chapter 6.

5.2. Backgrounds of TELEMAC-2D and Gaia

5.2.1. TELEMAC-2D

TELEMAC-MASCARET is an open-source software for high-performance numerical simulations in the fields of hydrodynamics. MASCARET (1980) and TELEMAC (1987) were originally developed by the French National Laboratory for Water Conservancy and Environment, a subsidiary of EDF Group, and then integrated into TELEMAC-MASCARET and developed and maintained by six research teams from France, Britain, and Germany. Based on the finite element method, TELEMAC-MASCARET uses an irregular triangular mesh, allowing complex coastlines and estuaries to be depicted more accurately. TELEMAC-2D is one important function of TELEMAC-MASCARET, which utilized the depth-averaged free surface equation to solve the flow velocity and water depth in two dimensions (transversal and longitudinal directions). The tool can be coupled with several semi-models, including the sediment transport model (Sisyphe and Gaia), water quality model (Waqtel and Aed2), wave prediction model (Tomawac), and ice cover prediction model (Khione). Previous research has already proved that TELEMAC-2D can be successfully utilized in the simulation of river hydrodynamics, for instance in the Vietnamese Mekong Delta (Binh et al., 2022), in Isère River, France (Bel, Jodeau, Tassi, Claude, & Haddad, 2019), in Utvik River (Pavlíček & Bruland, 2019), and in "Gave de Pau" catchment (Yassine, Cassan, Roux, Frysou, & Pérès, 2022). Despite this, the TELEMAC model can be simulated in parallel mode, which means that we can obtain several results simultaneously. It is beneficial for saving simulated time in sensitivity analysis and forward research on scenarios.

5.2.2. Gaia

Gaia is the new coupled model of the TELEMAC-MASCARET system, which aims to simulate sediment transportation and bed evolution (erosion and disposition) (Audouin et al., 2019). It is developed based on the previous sediment transport model, Sisyphe, where several corrections and optimizations have been conducted. The Gaia can solve the sediment transport process in bedload transport (particles that direct contact with the riverbed), suspended load transport (particles that be transported by flow above the riverbed), or total load (both bedload and suspended load). Regarding the sediment type, cohesive sediment (silt or clay), non-cohesive sediment (gravel or sand), or mixed sediments (mud or sand mud mixtures) can be considered in the model. Moreover, the sediment sizes and composition can be designed manually by the users through the D50 of sediments and multiple

vertical layers of the riverbed. Despite this, several modifications related to bed slope effects, secondary current effects, and skin friction effects are also considered to assist the model calibration.

5.3. Evaluation of model performance

The model should be evaluated based on the differences between the simulated value and the measured value. In this chapter, three typical evaluation indicators are utilized:

The Root-Mean-Square Error (RMSE), which has already been utilized in Chapter 3 for analysis of the performance of LSPIV and STIV, the equation is:

$$\mathrm{RMSE} = \sqrt{\frac{1}{n}\sum_{i=1}^{n}(y_i - f_i)^2} \tag{5-1}$$

Where y_i is the measured value, f_i is the simulated value, and n is the total number of data points. A lower value of RMSE is expected since smaller differences between measured and simulated results are obtained.

The Nash-Sutcliffe number (NSE) is another reliable indicator for statistical analysis of model performance (McCuen, Knight, & Cutter, 2006), which can be determined by:

$$\mathrm{NSE} = 1 - \frac{\sum_{i=1}^{n}(f_i - y_i)^2}{\sum_{i=1}^{n}\left(f_i - \overline{f_i}\right)^2} \tag{5-2}$$

Where $\overline{f_i}$ is the mean value of measured data. A model with an NSE value near 1 means its predictive skill is better.

The Brier Skill Score (BSS) was developed for the evaluation of meteorological model performance, which predicts the model performance utilizing a baseline approach. It is widely utilized in research related to hydro-geomorphological simulation to assess the results of sediment erosion and deposition

across the entire domain (Aguirre, Bui, Giehl, Reisenbüchler, & Rutschmann, 2020; Linares, 2007; Yassine et al., 2022). The indicator can be calculated by:

$$\mathrm{BSS} = 1 - \frac{\frac{1}{n}\sum_{i=1}^{n}(f_i - y_i)^2}{\frac{1}{n}\sum_{i=1}^{n}(f_i - b_i)^2} \tag{5-3}$$

Where b_i is the value of the baseline. Because the score needs a baseline to calculate, it will be only utilized in the assessment of riverbed alterations (cross-section). Hence, b_i is the initial riverbed in our study. Table 5-1 shows the value range for the judgment of model performance based on BSS (Aguirre et al., 2020).

Table 5-1 The judgment of BSS values for evaluation of model performance

Performance of the model	**BSS value**
Excellent	0.5 – 1.0
Good	0.2 – 0.5
Reasonable	0.1 – 0.2
Poor	0.0 – 0.1
Bad	< 0.0

5.4. Develop a TELEMAC-2D model for clear water simulation

A reliable model of hydrodynamics is the base for further simulation of the sediment transport process. In this section, a TELEMAC-2D model was established for simulating the clear water situation (no sediment transport). The simulated results of flow velocity and water depth can be then input into the sediment transport model to calculate the bed shear stress and riverbed evolution. The simulated domain is similar to the study area in Chapter 4 (Figure 4-1), which started from Nagayasuguchi dam and ended at the Hitomi power station, with a total length of around 14 km. Regarding the model calibration and validation, we utilize the two recorded flood events in May and August that have already been depicted in Chapter 3 (Figure 3-33).

5.4.1. Model set up

The mesh was generated based on the triangle finite element method. To reduce the time of simulation, we utilized coarse mesh for the floodplain area with a grid size of 20 m, and fine mesh for the active channel with a grid size of 10 m. The replenishment site should be further refined with a grid size of 4 m since it is essential for our study. The final mesh contains 16384 nodes and 31160 elements. Then, the 2017 DEM data measured by Green Lidar (including the underwater part) provided by the Naka River office was utilized to interpolate the topographical value of the study domain (Figure 5-1).

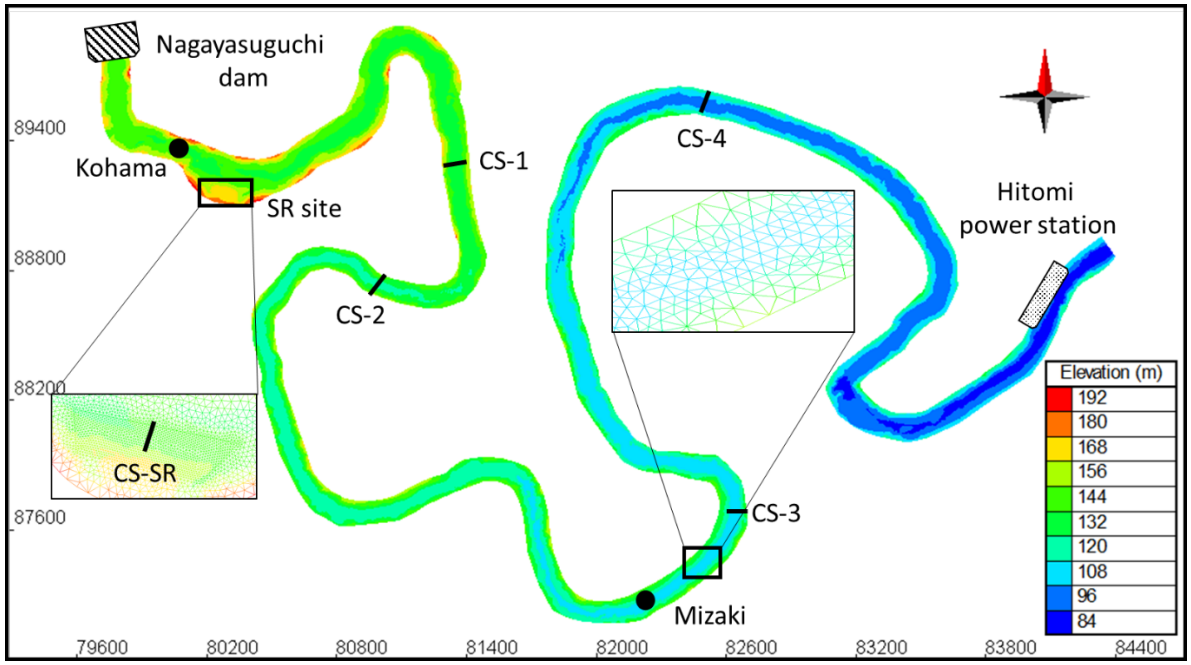

Figure 5-1 Geometric mesh of the study domain for TELEMAC-2D simulation based on 2017 DEM data.

5.4.2. Initial and boundary conditions

There are two boundaries in the domain. The upstream boundary is the releasing discharge from the Nagayasuguchi dam, while the downstream boundary is the prescribed water level near the Hitomi power station. Due to the lack of available data, the measured water level at the downstream boundary can not be obtained. Hence, we utilize the HEC-RAS, an open-source software for 1D hydrodynamics simulation, to roughly simulate the water level in our study domain. We use the same upstream

boundary in the Nagayasuguchi dam, while the downstream boundary is extended to the Kawaguchi dam since the water level here can be assumed as constant (94 m). The input bathymetric data is the same as the input data utilized in TELEMAC-2D (2017 DEM). The time series of the upstream boundary with flow discharge and downstream boundary with water level during two flood events, May and August 2021, is shown in Figure 5-2.

Regarding the initial conditions, a constant value of flow discharge and water level at two boundaries was simulated for 7 days to ensure a stable flow regime in the domain. Then, this pre-simulated result can be input as the initial conditions for the real simulation.

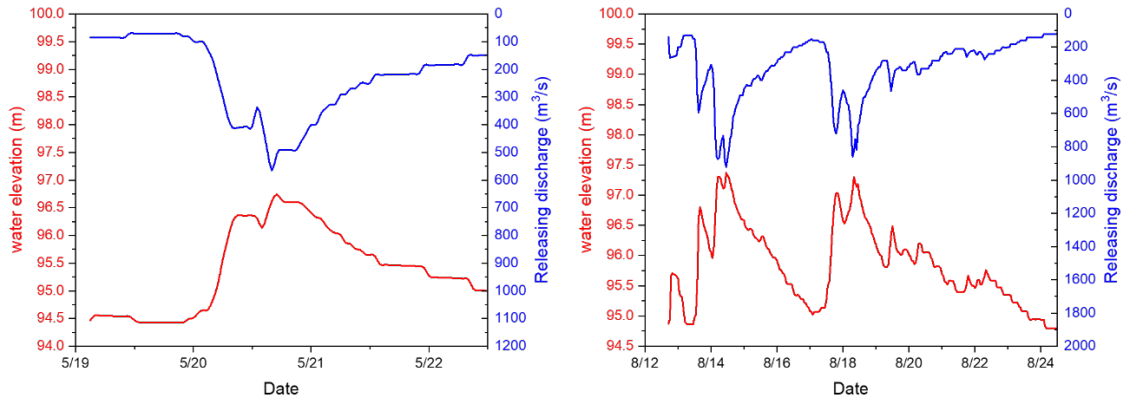

Figure 5-2 The boundary conditions of the study domain during two flood events in May and August 2021. Blue line: Upstream boundary with flow discharge from Nagayasuguchi dam; Red line: downstream boundary with water level calculated by HEC-RAS.

5.4.3. Sensitivity analysis

The sensitivity analysis is conducted based on the flood events that occurred in May 2021. Due to the lack of data, we can not obtain the 2021 DEM and we have to use the 2017 mesh for calibration. Hence, we have to assume that the alteration of bathymetry does not have significant impacts on the flow regime. Regarding the data of calibration, STIV has already been proven as a reliable tool to measure the surface flow in the Kohama based on previous research in Chapter 3. Additionally, we conduct STIV measurements in another location, Mizaki, which is located 7 km downstream of the replenishment site. Both measured results of surface velocity at two locations in the red square area

(shown in Figure 5-3) are times a ratio of 0.85 to calculate the corresponding depth-averaged velocity (Kim et al., 2008). Moreover, the water level simulated from HEC-RAS has also been considered an additional source for calibration of the flow regime in TELEMAC-2D.

Regarding the numerical parameters that were calibrated in TELEMAC-2D, we tested the time step (Δt), turbulence models, manning friction value (n), free surface gradient compatibility (FSC), and velocity diffusivity (ν). Around twenty-five tests were conducted to find the optimal value of each parameter. According to the trials, the time step is a very sensitive parameter that influences not only the simulated time but also the calculated flow regime. The time step was tested between 0.1 to 2 seconds. According to the results at Kohama (Figure 5-4), a larger time step (2 seconds) leads to an overestimate of water elevation and an underestimate of flow velocity during the high flow period. 0.5 seconds can be considered as an optimal value with a simulated time of 1 hour and RMSE around 0.04 m/s for flow velocity. The turbulence models were tested in the constant viscosity model, k-ε model, and Smagorinski model. No significant changes in flow velocity and water elevation can be observed when altering the models. However, utilizing the k-ε model and Smagorinski model increase around 20% of the simulated time since they are more complicated. To simplify our simulation, a constant viscosity model was selected. The manning friction value is another sensitive parameter that influences the flow regime. Due to the fact that no previous research or reliable data related manning coefficient in the Naka River, we have to use the value from other natural rivers as a reference. Arcement and Schneider (1989) revealed that the manning n value for flood plain can be varied from 0.01 to 0.2 depending on the types of vegetation. Because the trees and grass are the dominant vegetation of the floodplain in the Naka River, 0.05 was selected as the optimal value. While the friction value for the active channel has a close correlation to the grain size. Based on the previous survey, the average D50 of the riverbed should be around 20 mm, which corresponds to an n value of around 0.025 (estimated by the Manning-Strickler formula). Further tests of the n value for the active channel were conducted between 0.015 to 0.03. It can be observed that a higher manning friction value may lead to higher water elevation and lower flow velocity (Figure 5-5). In the end, 0.023 was selected as the optimum value. The free surface gradient compatibility and velocity diffusivity were also tested between 0.5 – 0.9 and 10^{-6} to 1.0, respectively. Nevertheless, they are not sensitive parameters and we utilize the default values in TELEMAC-2D.

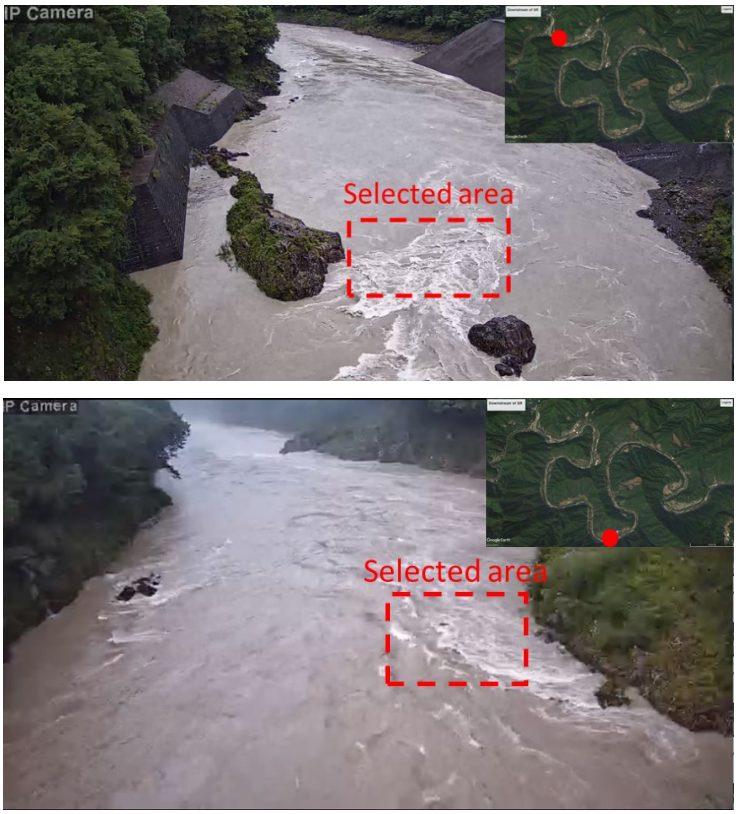

Figure 5-3 The measured locations of STIV for calibration and validation of hydrodynamics in TELEMAC-2D. The red squares represent the selected area for flow velocity calibration and validation. Top figure: Kohama. Bottom figure: Mizaki.

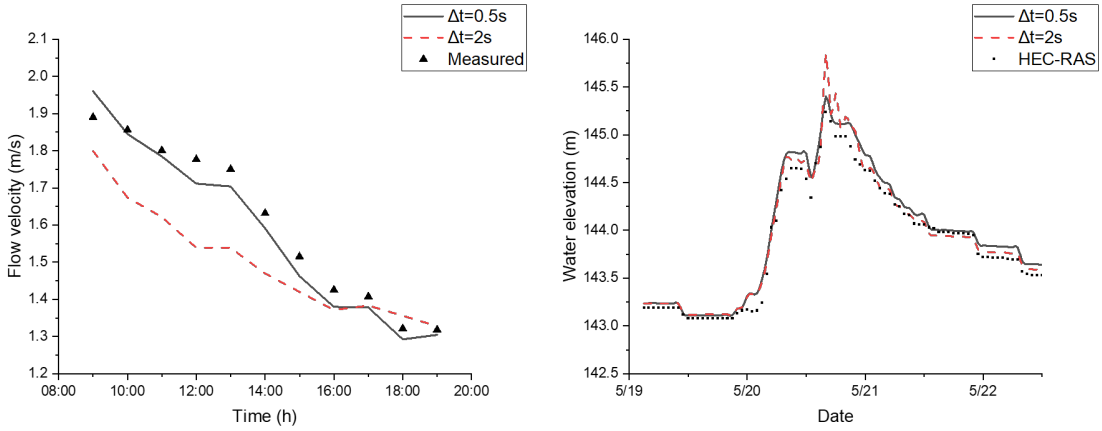

Figure 5-4 The flow velocity (on 5/21) and water elevation (during the flood event in May) at the Kohama under different time steps during.

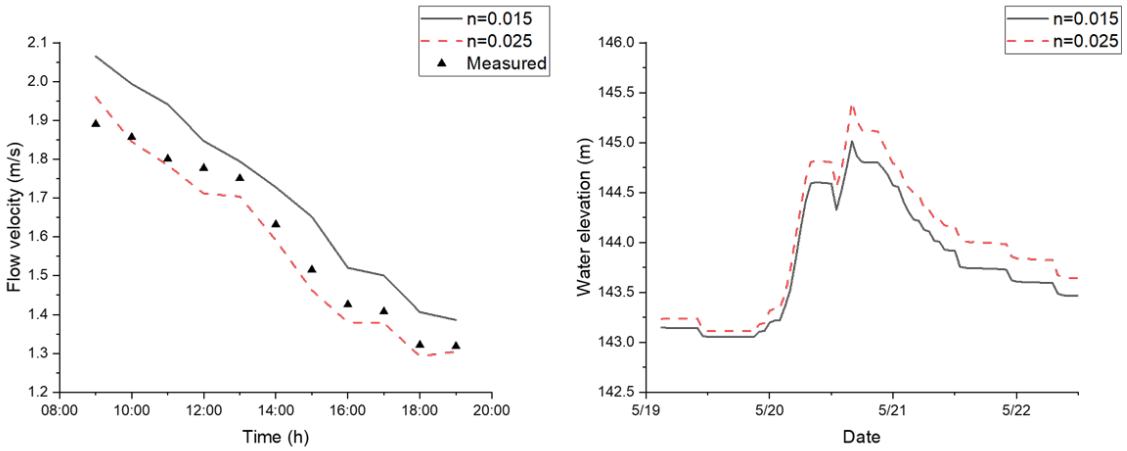

Figure 5-5 The flow velocity (on 5/21) and water elevation (during the flood event in May) at the Kohama under different manning friction values n.

5.4.4. Model validation

The optimal value of numerical parameters for hydrodynamics after calibration is shown in Table 5-2. Model validation is then conducted to test whether the numerical model can be utilized to simulate another event (a flood event in August). The comparison between simulated and measured flow velocity (STIV) on 8/14 from 6:00 to 16:00 at two locations (Kohama and Mizaki) was shown in Figure 5-6. Additionally, a 2D scalar map of flow velocity from TELEMAC-2D during the high flow period (11:00 on 8/14), and the comparison between simulated and measured velocity along the cross-section CS-V were shown in Figure 5-7. A high correlation can be founded at Kohama and Mizaki with lower RMSE (0.061 and 0.048) and higher NSE (0.939 and 0.889). While for flow velocity along the CS-V, the differences increase, which may be mainly due to the differences in bathymetry. The comparison of water elevation between HEC-RAS and TELEMAC-2D is illustrated in Figure 5-8. It can be noticed that the performance is worse than those in flow velocity simulation. Since our water level data is also obtained from simulation (HEC-RAS), we can not 100% trust it is correct. In the future, more reliable data is needed to finalize our validation process.

Table 5-2 The optimal value of numerical parameters for hydrodynamics after calibration

Δt (s)	Turbulence model	n		FSC	ν (m^2/s)
		Flood plain	Active channel		
0.5	constant viscosity	0.05	0.023	0.9	10^{-6}

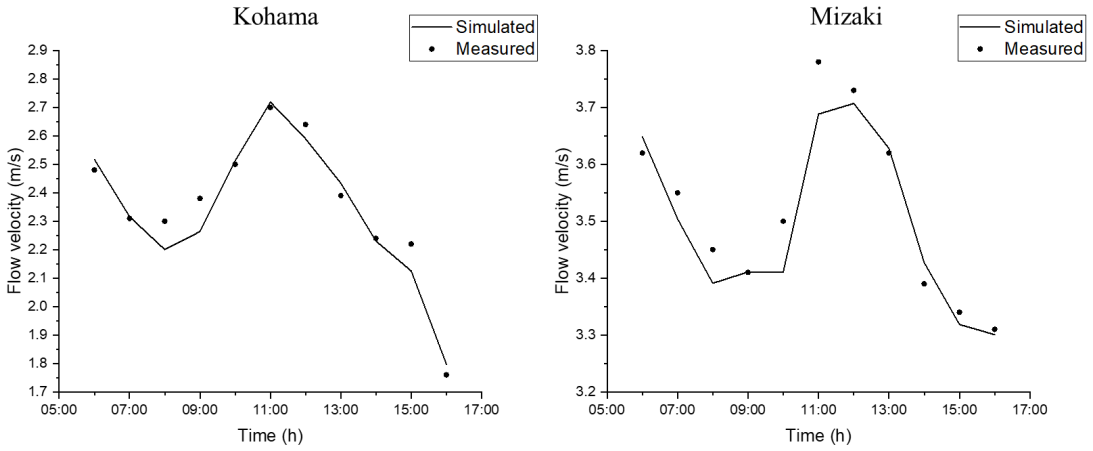

Figure 5-6 The comparison between simulated and measured flow velocity (STIV) on 8/14 from 6:00 to 16:00 at two locations (Kohama and Mizaki).

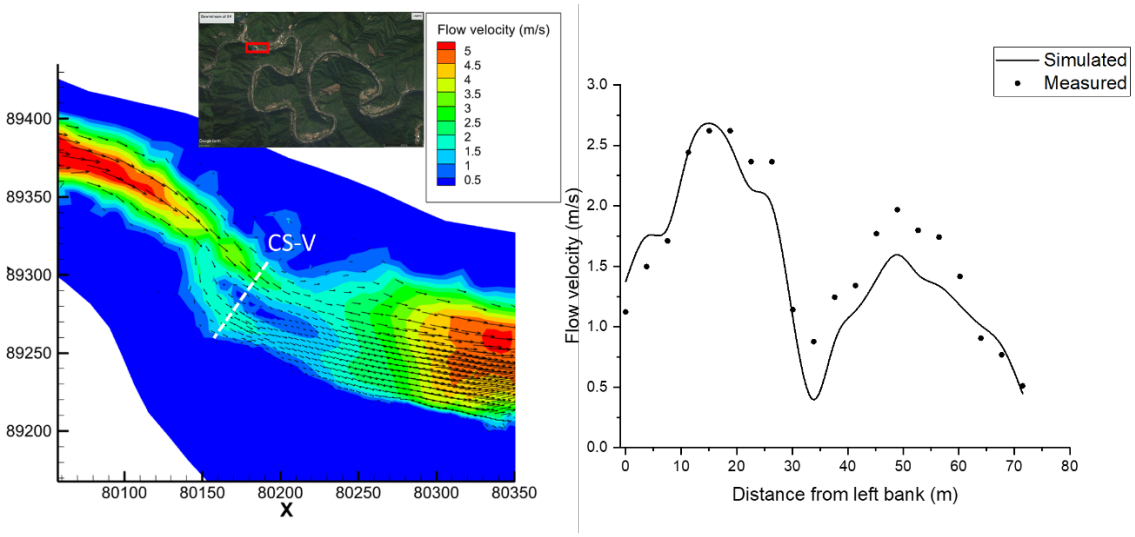

Figure 5-7 Left figure: The 2D scalar map of flow velocity from TELEMAC-2D at Kohama at 11:00 on 8/14. Right figure: the simulated and measured flow velocity at cross-section CS-V.

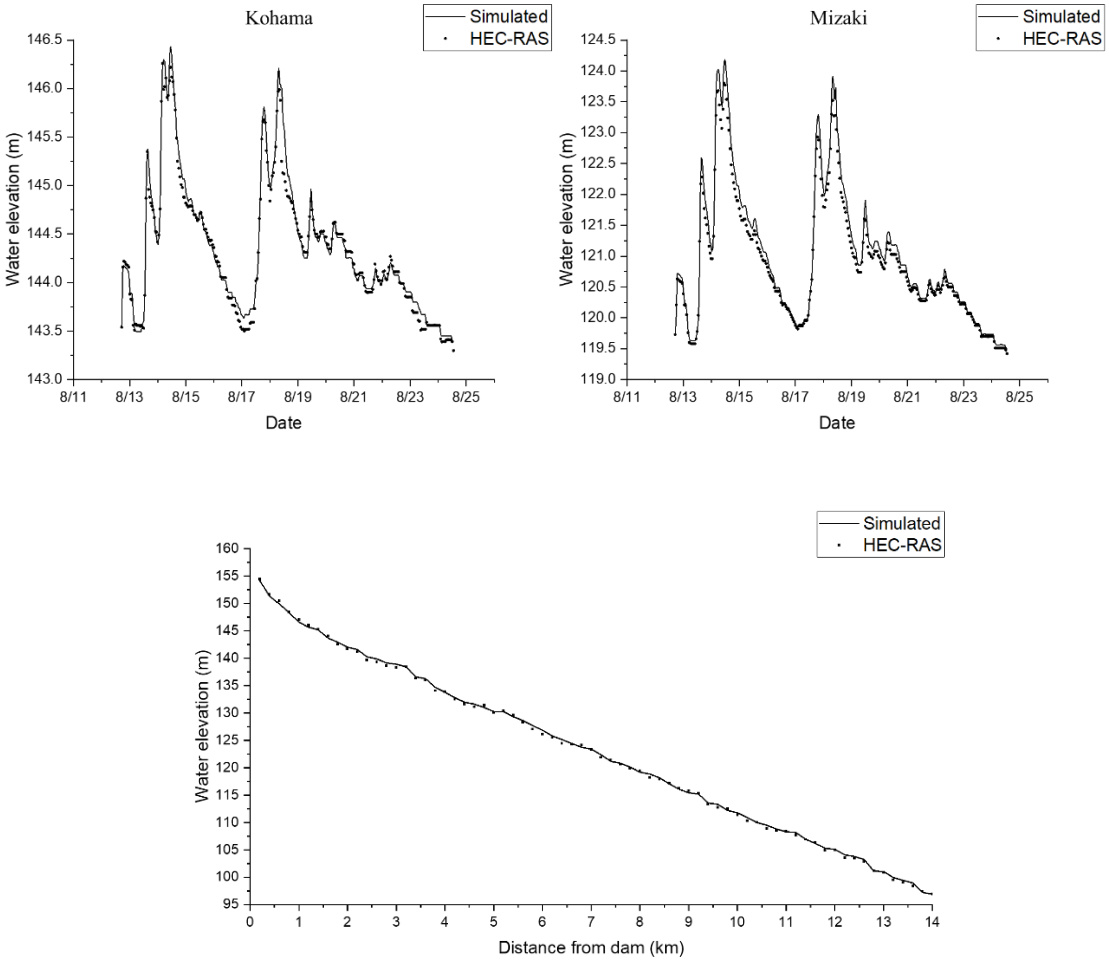

Figure 5-8 The comparison of simulated water elevation between TELEMAC-2D and HEC-RAS. Top figure: the time series of water elevation in Kohama and Mizaki. Bottom figure: typical water elevation in the longitudinal direction.

Table 5-3 The evaluation of model performance for TELEMAC-2D

	Flow velocity (m/s)			**Water elevation (m)**		
	Kohama	Mizaki	CS-V	Kohama	Mizaki	Longitude
RMSE	0.061	0.048	0.265	0.307	0.286	0.373
NSE	0.939	0.889	0.831	0.781	0.804	0.765

5.5. Establish a TELEMAC-2D model coupled with Gaia for the simulation of downstream geomorphology

5.5.1. Model set up

The established TELEMAC-2D is then coupled with Gaia to simulate the sediment transport and riverbed aggradation and degradation. We set up the same value of numerical parameters that have already been calibrated in the previous model for clear water except for the time step. Higher releasing flow during the simulated period increases the instability of the model, and we need to modify the time step to reduce such adverse impacts. Moreover, several additional settings related to Gaia simulation are also included to enhance our results, including:

- Erodible thickness

The erodible thickness is the thickness of sediment that can be eroded below the riverbed. The default value in Gaia is 100 m, which should be modified in our case. Because we utilized the Lidar profile to create our geometric mesh, detailed geomorphological patterns, especially the rocks, are included. Such rocks should be defined as non-erodible patterns to avoid unreasonable erosion occurring in the channel. Despite this, the floodplain area is also set up as non-erodible since it is composited of rocks and trees. The erodible thickness of the high dissipation area near the Nagayasuguchi dam and Hitomi power station is defined as 0.5 m to restrict extreme erosion. Then, 5 m is set up for the active channel and 10 m is defined for the replenishment site. The distribution of erodible thickness is shown in Figure 5-9.

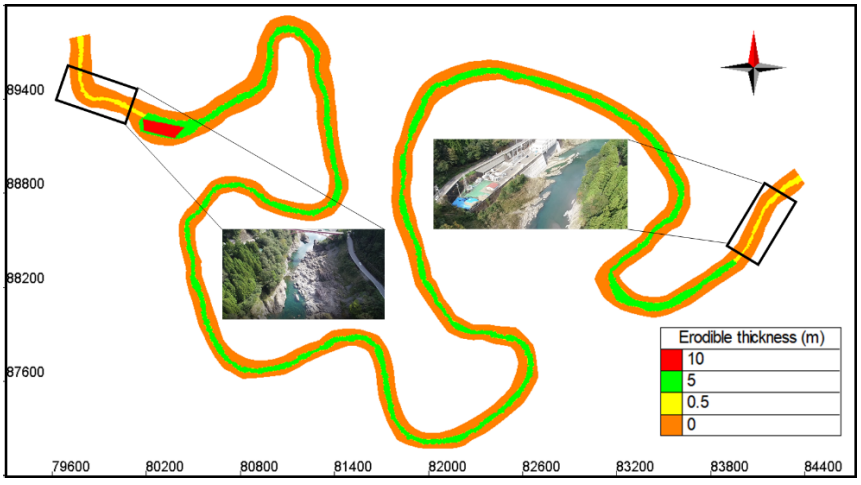

Figure 5-9 The spatial distribution of erodible thickness in the study domain

- Bank failure mode

The bank failure mode is important for simulating the erosion process of replenished material. In Gaia, the bank failure mode is called 'Maxslope', which is developed by El Kadi Abderrezzak, Die Moran, Tassi, Ata, and Hervouet (2016). The mode relies on the angle of repose (φ) to control the process of bank failure. Specifically, the slope of each element is compared to the angle of repose (φ) at each time step. The element is rotated around the axis to reach the angle of repose (φ) if the angle of the elements is higher than the angle of repose (φ). Then, a new surface is established based on the average height of adjacent elements, and the volume gained at the bottom half is equal to the volume at the top half (Figure 5-10) (El Kadi Abderrezzak et al., 2016). Nevertheless, one weak point of the mode is that it considers the same value of the angle of repose (φ) for the submerged and unsubmerged area. Generally, the angle of repose (φ) for submerged elements should be smaller than the unsubmerged elements. Such simple mode may lead to an underestimate of the eroded volume at the replenishment site.

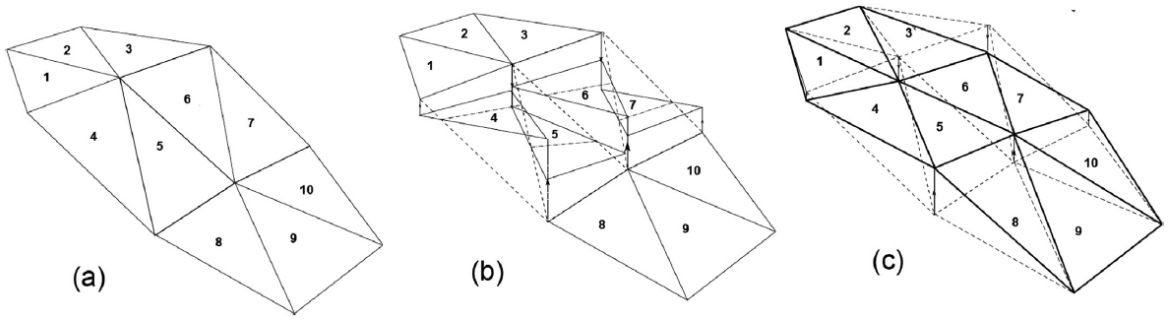

Figure 5-10 The bank failure algorithm of 'Maxslope' mode in Gaia. (a) the initial bank conditions. (b) unstable elements (4, 5, 6, 7) are rotated around the axis. (c) The final surface is created based on the average height of adjacent elements (El Kadi Abderrezzak et al., 2016).

- Sediment composition

The sediment composition is another crucial point that will influence the erosion and deposition process. In Gaia, we define the different compositions of sediment for replenishment sites and active channels. To simplify our model, only four types of non-cohesive sediment with different grain sizes are considered in the Naka River (Table 5-4). The percentages of replenished material are obtained

from the sample collected in 2021. While the percentages of the riverbed are roughly estimated from the previous report of the field survey conducted by the Naka River office.

Table 5-4 The composition of sediment at the replenishment site and riverbed in the Gaia.

	Sediment size (mm)			
	40	10	3	0.5
Replenishment site (%)	17	45	28	10
Riverbed (%)	15	60	20	5

The input geometry for the coupled model is 2017 DEM, which is the only bathymetric data we have. Then, several cross sections (CS-1 to CS-4 in Figure 5-1) that were measured in 2019 are utilized to roughly calibrate our results. In addition, CS-SR is included to see the variation of the replenishment site. Model validation can not be conducted due to the limit of available data.

5.5.2. Initial and boundary conditions

The two boundary conditions have already been illustrated in the single TELEMAC-2D model. The upstream boundary is the releasing flow from Nagayasuguchi dam, while the downstream boundary is the hourly water level simulated from HEC-RAS. Due to the limitation of data, we do not have any information on hourly sediment concentration in the Nagayasuguchi dam, and clear water input is assumed.

As mentioned before, we need to simulate two years period to calibrate our results (from December 2017 to December 2019), which significantly increases our computational time (7 days for 1 trial). To reduce the simulated time and test more trails, we selected 5 crucial flood events during the 2 years and combined them into our simulated hydrograph (Figure 5-11). It means that we assume the sediment movement during the low flow period is small and can be neglected. The final simulated period is reduced to 600 hours and the computational time is decreased to 10 hours for 1 trial.

Regarding the initial condition, the same pre-simulation of 7 days, utilizing constant water level and flow discharge, was implemented to reach the stable condition of the flow regime. Then, it was used as the hot-start for the real simulation.

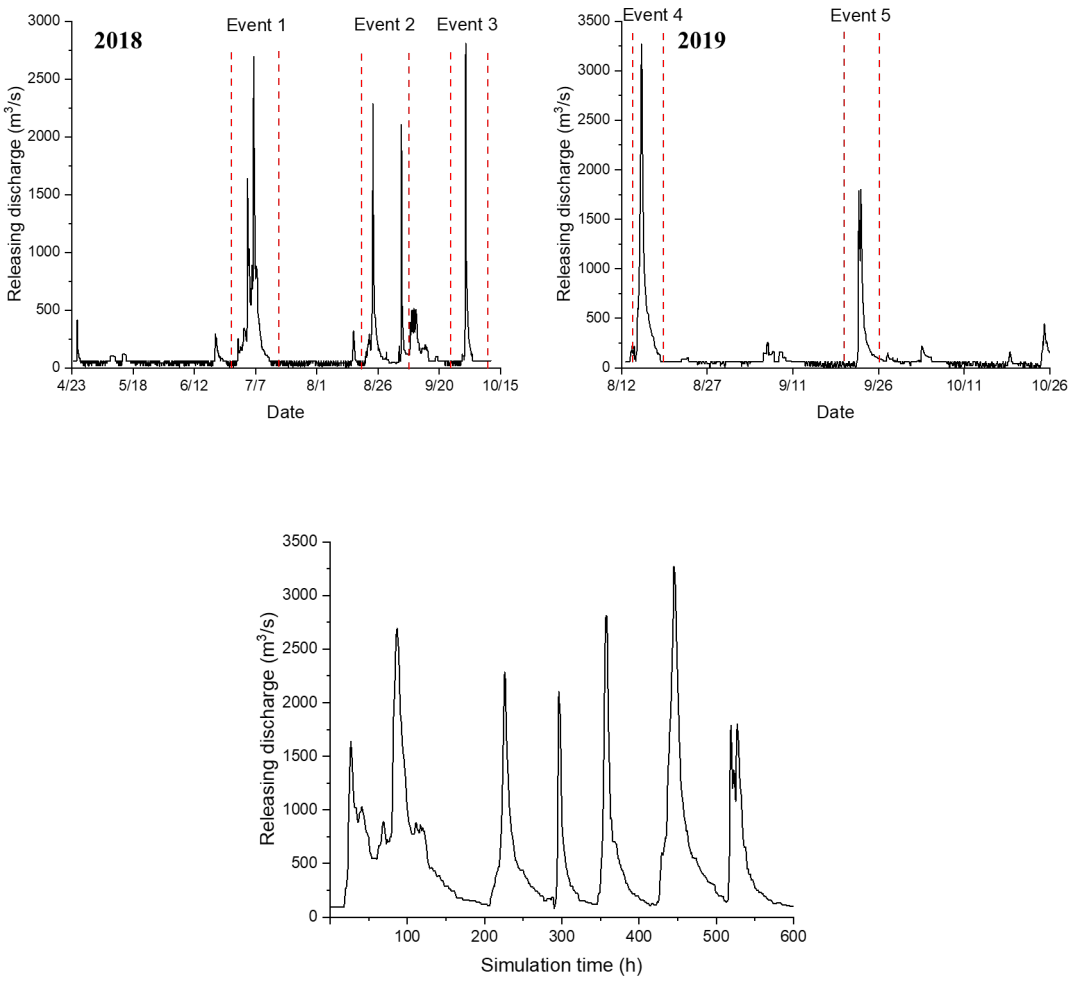

Figure 5-11 Top figure: the hydrograph during the release period in 2018 and 2019. Bottom figure: the combined hydrograph for the upstream boundary.

5.5.3. Sensitivity analysis

Different numerical parameters for sediment transport and bed evolution modes are tested for sensitivity analysis, including time step (Δt), transport formulas for bedload and suspended load, critical classes shield parameter (θ_{cr}), the formula for slope effect, the parameter for deviation (β_2), secondary currents effect and its associated coefficient (α_{sc}), the ratio of roughness height (α_s), active layer thickness (d_a), settling velocity (ω_s), and angle of repose (φ). The time step (Δt) is the crucial parameter to influence the stability of the model. The classes shield parameter (θ), the ratio of

roughness height (α_s), and settling velocity (ω_s) affect the erosion and deposition flux. The angle of repose (φ) is the key parameter for erosion at the replenishment site. The analysis of these sensitivity parameters is depicted below.

- Effects of time step on model stability

Previously, we utilize the constant time step (0.5 seconds) to simulate the single TELEMAC-2D model. However, the coupled model is more complicated and the releasing flow from the upstream boundary is extremely increasing from 900 m^3/s to 3000 m^3/s. Significant fluctuation of flow velocity can be observed if we keep using the constant time step (Figure 5-12). Such instability is mainly due to the higher courant number during the high flow period (greater than 2). To tackle it, the variable time step function is utilized, which can alter the time step based on the maximum courant number during the simulation. It means that a smaller time step is applied for a high flow period, while a larger time step is used for a low flow period. A stable flow velocity profile can be observed and the computational time is also reduced by 20% using the variable time step (Figure 5-12).

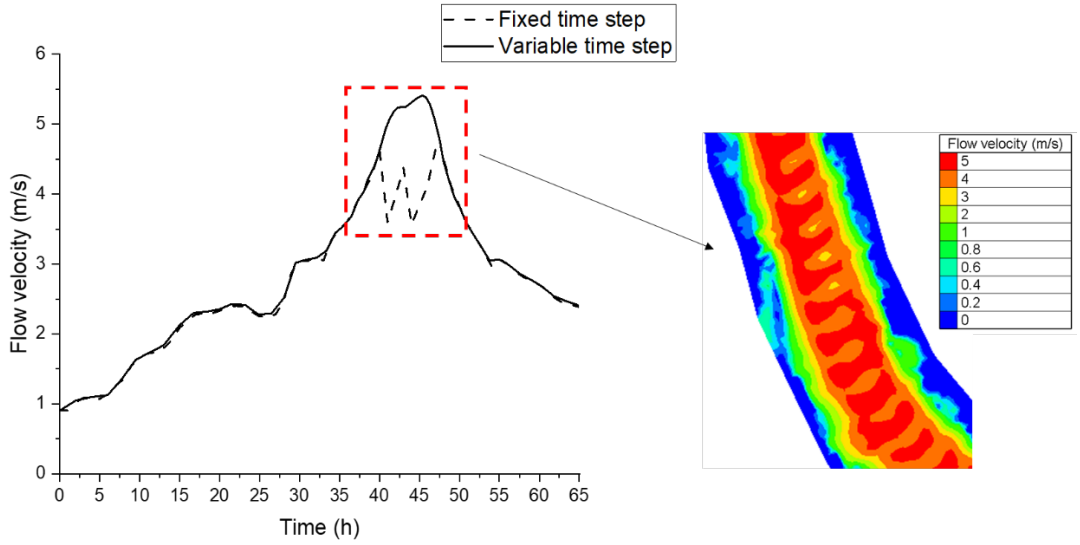

Figure 5-12 Left figure: The comparison of flow velocity between the fixed time step and variable time step. Right figure: the fluctuation of flow velocity occurred when using a fixed time step.

- Effect of classes shield parameters on riverbed evolution

Previous research illustrated that θ_{cr} can be varied from 0.04 to 0.15 with different shear Reynolds numbers (Cao, Pender, & Meng, 2006). In our study, a range from 0.05 to 0.1 is tested. It can be founded that it is very sensitive to controlling the erosion and deposition process. As shown in Figure 5-13, the sediment is more difficult to be transported when increasing the θ, hence, less erosion can be observed. The optimal value of θ_{cr} is 0.08.

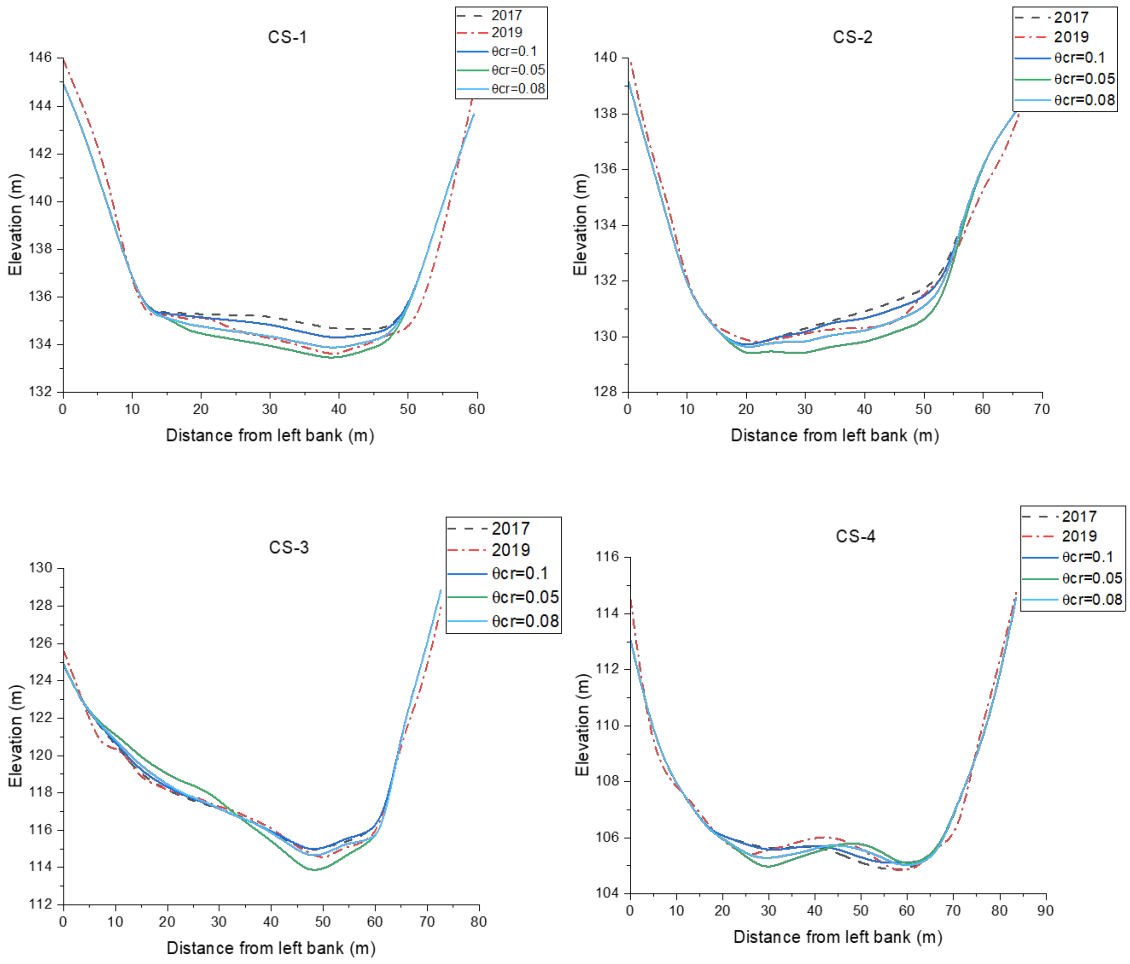

Figure 5-13 Effect of classes shield parameters on riverbed evolution at CS-1 to CS-4

- Effects of the ratio of roughness height on riverbed evolution

In Gaia, the roughness height of sediment is calculated by:

Eq. 5-4 $$k_s' = \alpha_s d_{50}$$

Where k_s' is the roughness height, and d_{50} is the mean diameter of sediment. Mendoza et al. (2017) revealed that α_s has an extremely large of value range ($\alpha_s = 3.6$ for bars and $\alpha_s = 37$ for dunes) and should be calibrated carefully when simulating geomorphological changes. In our study, a value range from 2.5 to 3.8 is tested. Increasing the α_s will increase the roughness height, and lead to more erosion happened (Figure 5-14). The suitable value for α_s is 3.2.

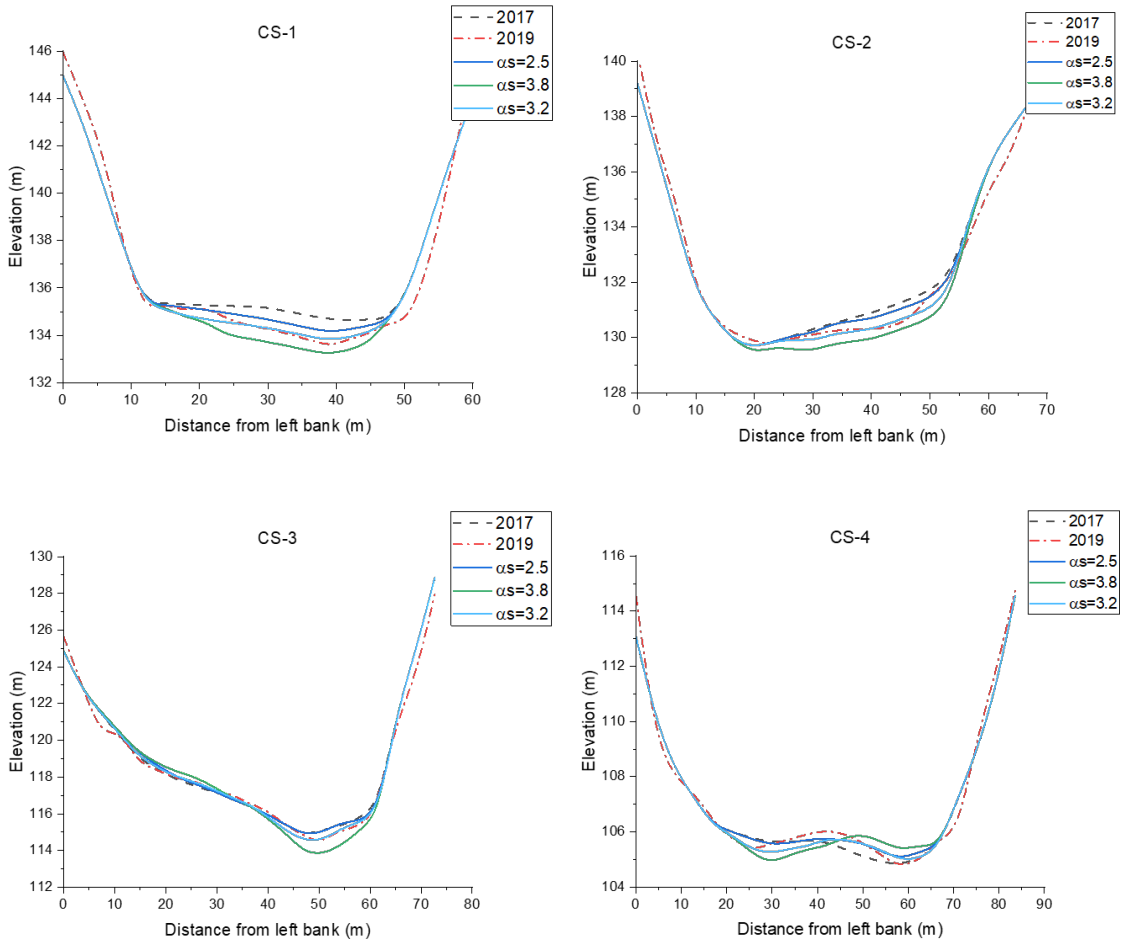

Figure 5-14 Effect of ratio of roughness height on riverbed evolution at CS-1 to CS-4.

- Effects of settling velocity on riverbed evolution

For non-cohesive sediment, the ω_s directly influence the erosion and deposition flux in the model. Here we calibrated the value of ω_s for median sediment (10 mm and 1 mm) between 6×10^{-4} to 1×10^{-2}. The results reveal that decreasing the settling velocity will promote the deposition of sediment, then the riverbed becomes less eroded (Figure 5-15). The optimal value of ω_s is 2×10^{-3}.

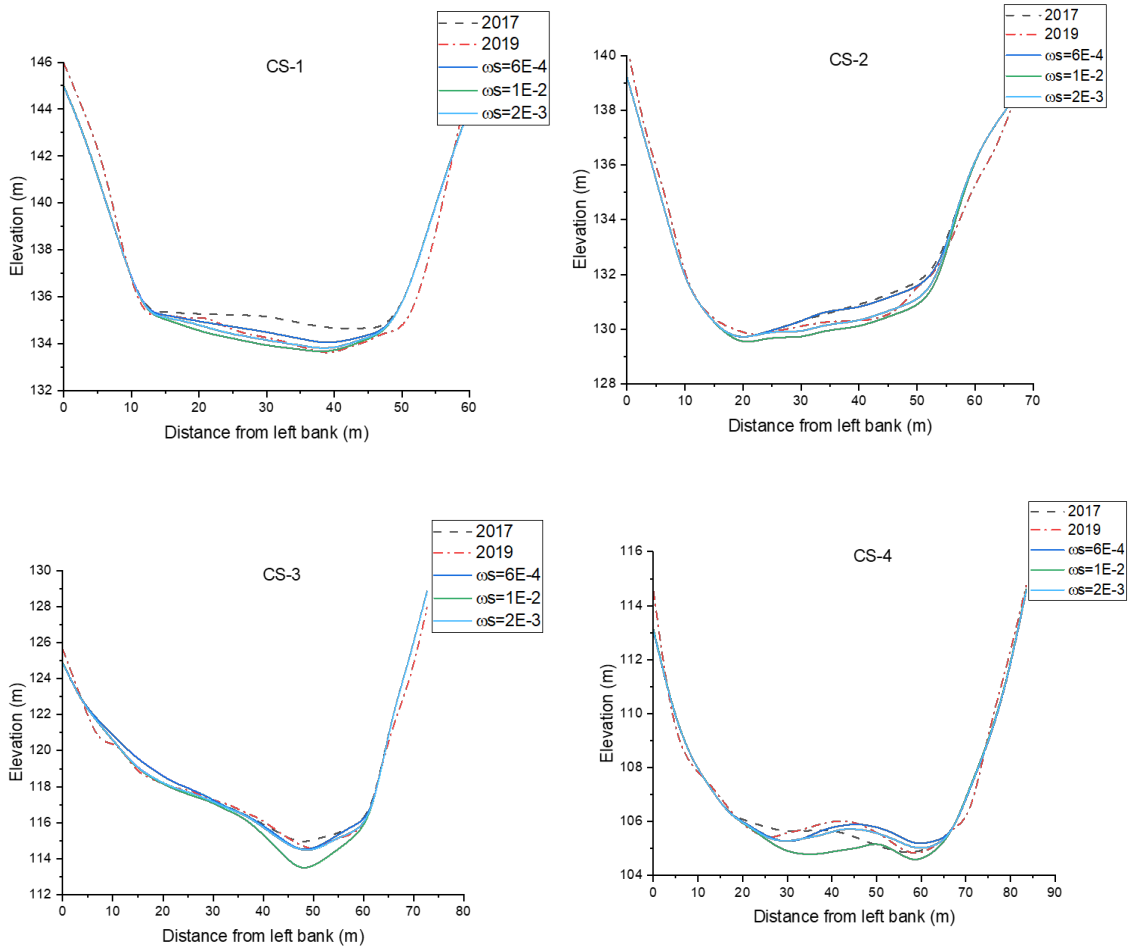

Figure 5-15 Effect of settling velocity on riverbed evolution at CS-1 to CS-4.

- Effects of the angle of repose on replenishment site erosion and deposition

The φ was spatially defined in the domain. According to the bathymetric survey, the Naka River is located in the deep valley. Unreasonable bank failure occurs when utilizing the same φ for the whole

domain area. Hence, $\varphi = 90^{\circ}$ was defined for the domain except the replenishment site to avoid such bank movement. Regarding the replenishment site, φ was tested from 25° to 40°. It can be observed that decreasing the φ lead to more erosion at the top area and more deposition at the bottom area (Figure 5-16). Because we do not have any data to calibrate the erosion and deposition at the replenishment site, a median value of 30° is selected.

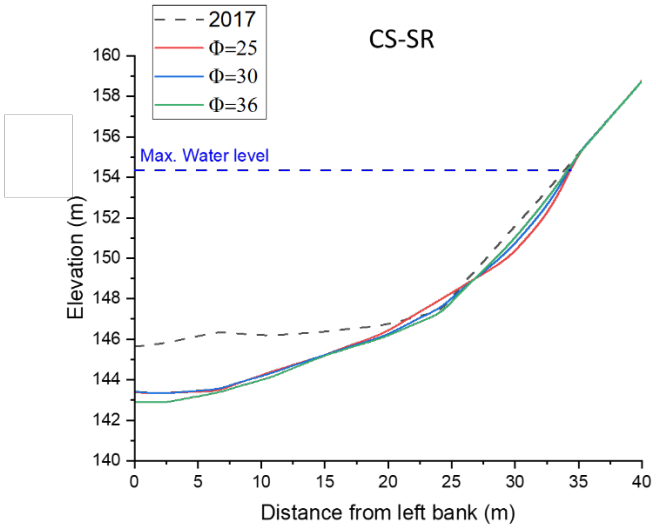

Figure 5-16 Effect of angle of repose on replenishment site erosion and deposition at CS-SR.

5.5.4. Best parameters and modes for the coupled model

Around 50 trials were simulated to get the best parameters and modes for the coupled model. Table 5-5 summarizes the best value of parameters and best options of modes. The comparison between measured and simulated riverbed elevation is illustrated in Figure 5-17. And the performance of the model is evaluated in Table 5-6. It can be noticed that all evaluated indicators are in the acceptable range. The final riverbed evolution is shown in Figure 5-18.

Table 5-5 Best parameters and modes for the coupled model

Parameters or modes	Value or options	Parameters or modes	Value or options
Δt	Variable time step	ω_s	2×10^{-3}
θ	0.08	φ	30° for SR site 90° for rest area
β_2	2.0	Turbulence model	Constant viscosity
α_{sc}	1.0	Bedload formula	Van Rijn
α_s	3.2	Suspended load formula	Van Rijn
d_a (m)	1.0	Slope effect formula	Talmon

Table 5-6 The evaluation of model performance based on four cross-sections

Cross section	RMSE (m)	NSE	BSS
CS-1	0.702	0.967	0.435
CS-2	0.481	0.976	0.312
CS-3	0.542	0.978	0.275
CS-4	0.518	0.969	0.129

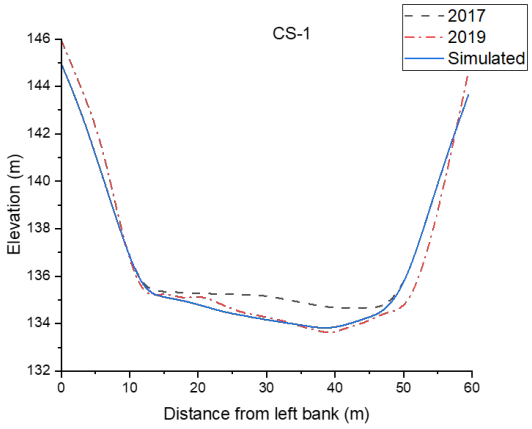

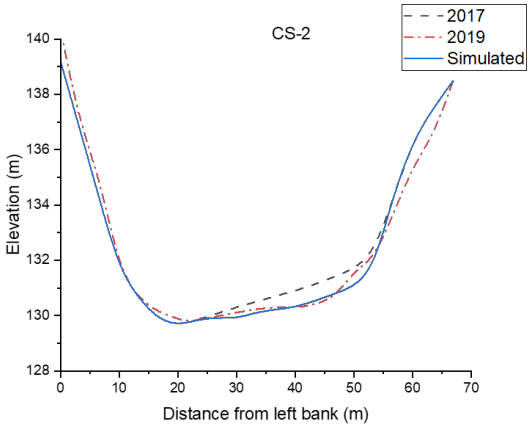

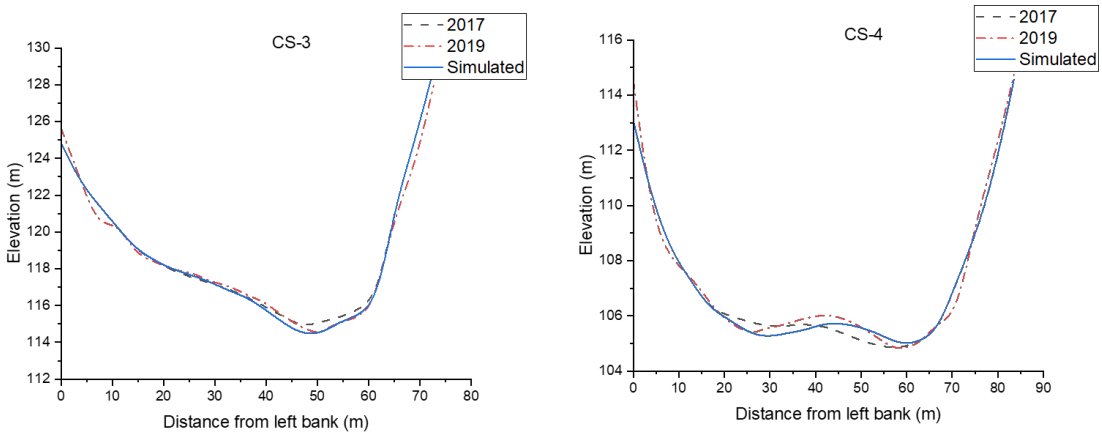

Figure 5-17 The comparison between measured and simulated riverbed elevation in CS-1, CS-2, CS-3, and CS-4.

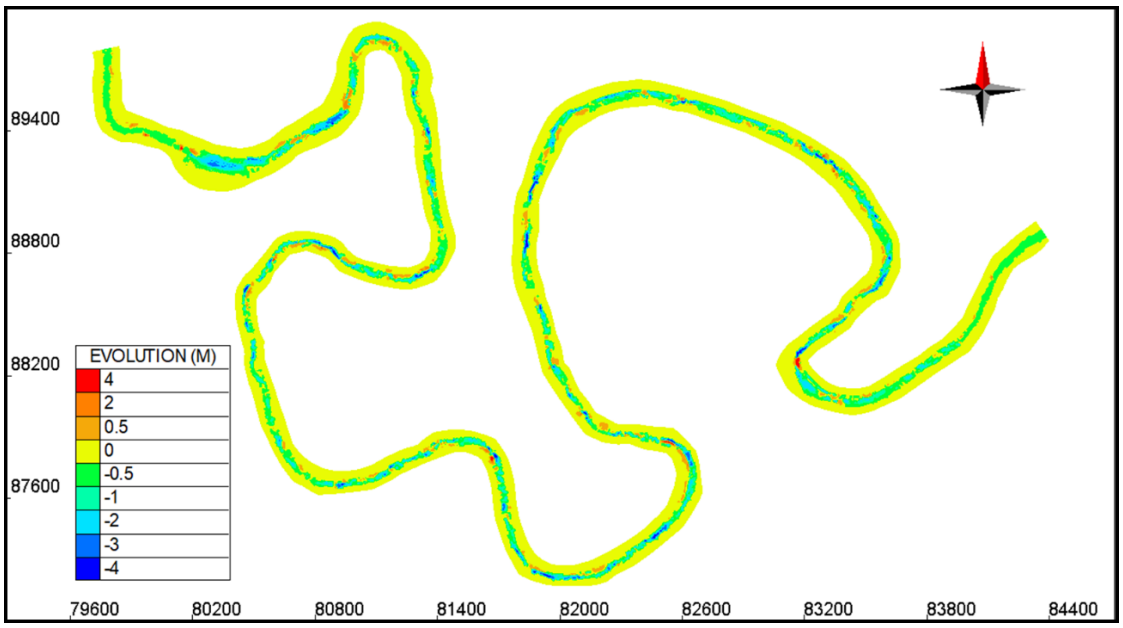

Figure 5-18 The final riverbed evolution after calibrating the model.

5.6. Conclusion

In this chapter, we established a TELEMAC-2D model coupled with Gaia to simulate the hydrodynamics and sediment transport in the Naka River. The expected results including flow

velocity, water depth, and bed evolution, can be utilized to calculate some of the assessment indicators we have already developed in Chapter 4, for instance, TR, HMID, and BCI. Those indicators are the crucial criteria to evaluate the various designed scenarios in Chapter 7 to investigate the optimization strategies of SR in the Naka River.

Due to the extreme lack of available data, the model can not be calibrated and validated accurately and completely. Several limitations are summarized:

- The HEC-RAS is not reliable for water level simulation without calibration, which leads to the instability of the downstream boundary during the high flow period.
- It is not scientific to use 2017 DEM to calibrate and validate the model based on 2021 measured flow velocity.
- The shortening of the simulated period by only considering high flood events may affect the suspension of sediment, and the final results can not present the actual situation.
- The assumption of clear water at the upstream boundary may lead to an underestimation of deposition in some areas.
- In the Naka River, continuous sediment is transported and placed at the replenishment site, and the volume of the stockpile is changing within a year. Such alterations can not be considered in the model if we simulate 2 years period.
- The bank failure mode in the TELEMAC-2D can not define the φ for submerged and unsubmerged areas separately, which leads to an underestimation of eroded volume at the replenishment site.

In the future, the model should be further modified if we can collect sufficient data from the DEM survey, SSC information, flow patterns, riverbed substrates, and replenishment stockpile.

Chapter 6. Sediment replenishment strategies considering stockpile erosion and downstream responses

6.1. Introduction

The erosion process of the replenished stockpile and the downstream responses are two main aspects of SR evaluation that have already been discussed in Chapter 4. The flushing frequency and magnitude, size of replenished sediment, and replenished locations are key characteristics that influence stockpile erosion. Such variation in SR characteristics may lead to different downstream hydro-geomorpho-ecological responses. To mitigate the SR strategies, we need to comprehensively consider the SR erosion and downstream responses.

A 2D numerical model was established in Chapter 5 to simulate the SR erosion and downstream sedimentation and geomorphological changes based on TELEMAC-2D coupled with Gaia. In this Chapter, we would like to investigate the effects of different SR characteristics (flushing flow, replenished sediment sizes, and replenished locations) on stockpile erosion and the downstream hydro-geomorphological changes. To reach it, several scientific scenarios are developed, and part of the assessment approaches in Chapter 4 are utilized for evaluation, including TR, BCI, and HMID.

The flow chart of the designed scenarios and assessment methods utilized in Chapter 6 is shown in Figure 6-1. Regarding the designed scenarios, we analyze the influence of flushing flow and replenished sediment sizes based on the current replenishment arrangement (single stockpile at the right bank with a placed volume around 150,000 m^3). The single flushing pulse with different flushing magnitudes combined with various replenished sediment sizes is investigated at first. Then, we move to the double-flushing pulses by keeping the same increasing water volume and replenished sediment sizes. Different flushing duration and magnitudes of the second pulse are considered. After that, we design several new possibilities for replenishment arrangements to promote the erosion process of replenished sediment. Finally, we make recommendations for optimization strategies of replenishment works in the Naka River based on the assessment results.

Considering the assessment of results, we divide the study area into several semi-zones. The SR site is an independent area where we calculate the BCI value and TR based on the eroded volume of replenished sediment. For the downstream reaches, 13 zones are distinguished based on the distance from the SR site, and the BCI value and HMID value are determined respectively. Moreover, 6 cross

sections (CS-1k, CS-2.5k, CS-5.5k, CS-7k, CS-9.5k, and CS-12k) are selected to investigate the deposition and erosion process at the meandering area. The detailed distribution of semi-zones and cross-sections for assessment is shown in Figure 6-2.

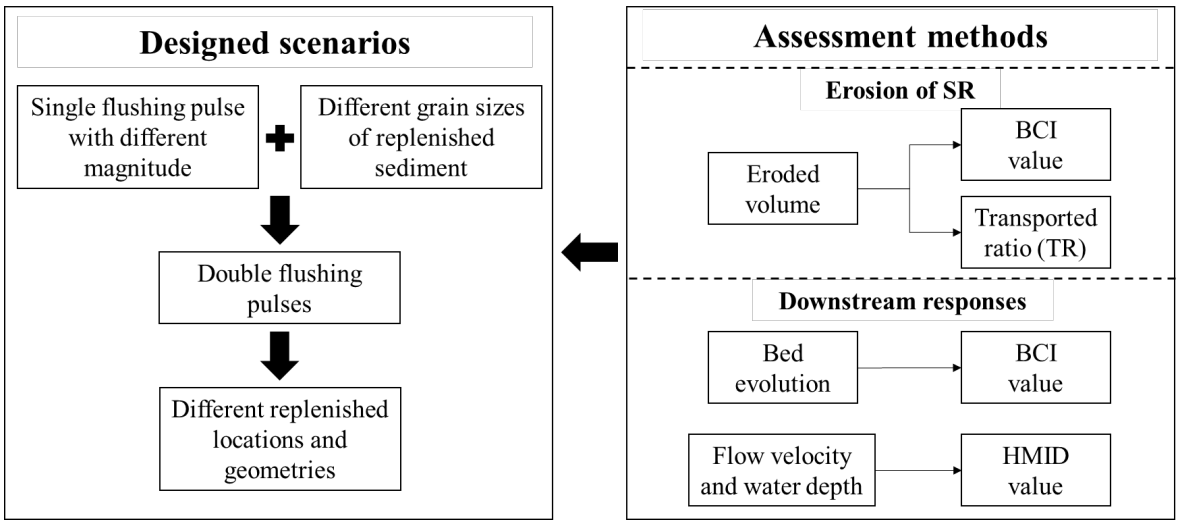

Figure 6-1 The flow chart of designed scenarios and assessment methods utilized in Chapter 6.

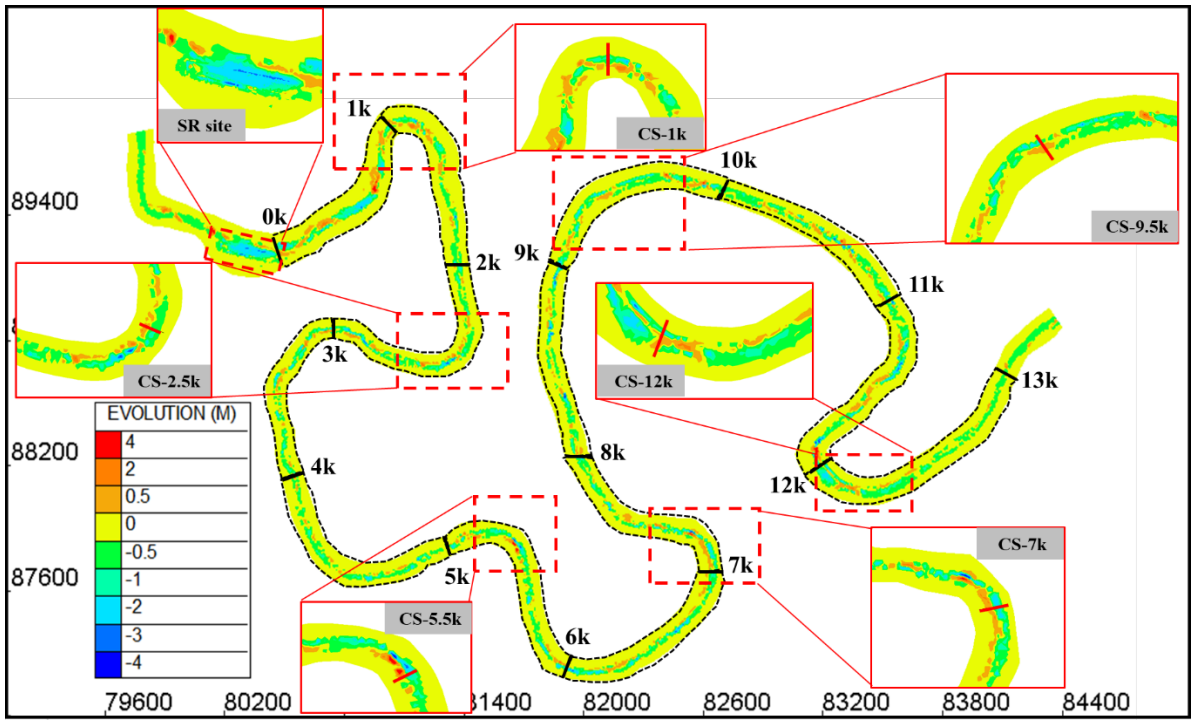

Figure 6-2 The areas and cross sections for assessment of different scenarios considering SR site and downstream reaches.

6.2. Results on current replenishment arrangement: Influence of flushing flow and replenished sediment sizes

6.2.1. The scenarios of a single flood pulse combined with different replenished sediment sizes

6.2.1.1. Introduction of scenarios

As mentioned before, the higher-releasing flow from the Nagayasuguchi dam during flood seasons is the main driving force of SR erosion in the Naka River. In this section, we select a typical hydrograph in 2018, which is a single flood pulse with a duration of 2 days and a peak discharge of 2000 m^3/s (Q0). Then, we add the flushing magnitude by increasing flow discharges by 20%, 40%, 60%, 80%, and 100%. This increasing volume is designed based on the peak releasing flow from 2010 to 2020 in Table 3-2. The simulated hydrograph and the increased discharge are shown in Figure 6-3.

Another variable we add is the grain sizes of replenished material. The current D50 of replenished sediment in the Naka River is around 7 mm. Here we consider another two types of sediment, fine sediment, which D50 is around 1 mm, and coarse sediment, which D50 is around 14 mm. The selection of the grain sizes is based on the D50 of replenished sediment in Japan, where the finer sediment size is around 0.4 mm to 1mm, and the coarser sediment size is around 10 mm to 25 mm (Figure 2-4).

Table 6-1 shows the summary of scenarios for evaluation of the impacts on different flushing magnitudes and replenished sediment sizes. In the section, we have a total of 18 scenarios with different hydrographs and grain sizes of replenished sediment. The base case (SC-B) considers the current size of replenished sediment (D50=7 mm) and the base hydrograph (Q0) and is utilized to calculate the BCI value in this section.

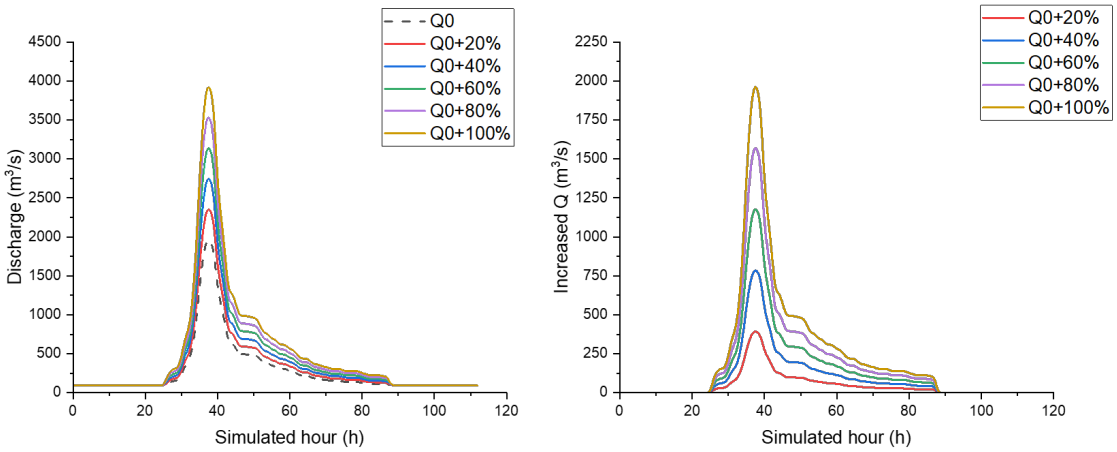

Figure 6-3 The simulated hydrograph and increased discharge for single flood pulse scenarios.

Table 6-1 The simulated scenarios for a single flood pulse combined with different replenished sediment sizes.

Hydrograph	Size of replenished sediment		
	Finer (1 mm)	Medium (7 mm)	Coarser (14 mm)
Q0	SC0-F	SC-B	SC0-C
Q0+20%	SC1-F	SC1-M	SC1-C
Q0+40%	SC2-F	SC2-M	SC2-C
Q0+60%	SC3-F	SC3-M	SC3-C
Q0+80%	SC4-F	SC4-M	SC4-C
Q0+100%	SC5-F	SC5-M	SC5-C

6.2.1.2. Effects on the SR erosion

The bed evolution at the SR site under 3 different flushing flow with the same grain sizes of replenished sediment is shown in Figure 6-4. It can be noticed that with the increase of flushing flow, erosion is increasing significantly at the tail area. Furthermore, a longer scouring stripe can be founded near the edge of the replenishment area, which is mainly due to the increase of bed shear stress here. Regarding the bed elevation of the cross-section, we can see that erosion at the bottom area of the SR is significantly promoted from SC0-F to SC2-F, while no further promotion occurs from SC2-F to SC5-F. Nevertheless, additional erosion can be observed at the top area of the stockpile in SC5-F. The results reveal that increasing the flushing flow can increase erosion at the bottom at

the beginning. If the flushing flow is extremely high, additional erosion occurs at the top area since the water level is increasing dramatically.

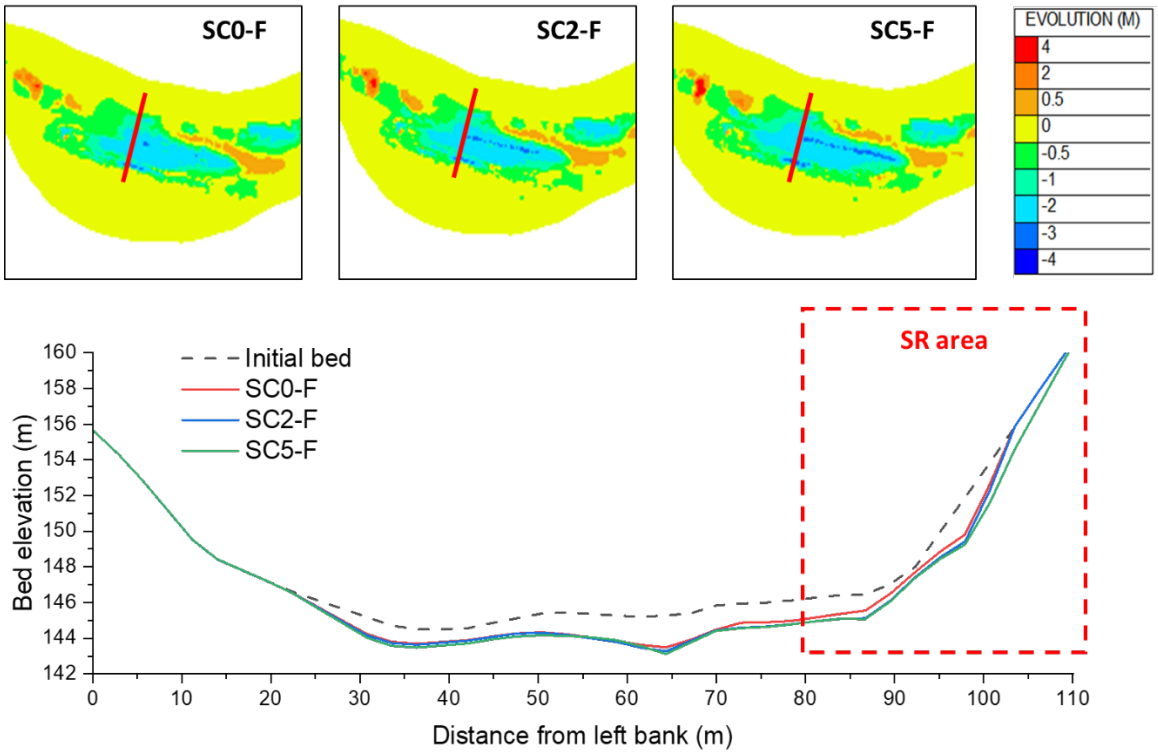

Figure 6-4 The analysis of SR erosion under different flushing flows. Top figure: the bed evolution at the SR site under different flushing flows. Bottom figure: the bed elevation at the selected cross-section (red line).

For different grain sizes and the same flushing flow, the alteration of SR erosion is more prominent. Based on the scalar figures in Figure 6-5, the eroded volume is reduced from fine sediment to coarse sediment. It is obvious that finer sediment is easier to be eroded and transported since the critical shear stress is smaller. Such an increasing rate of erosion may be decreased with the increasing of sediment sizes as the difference between medium sediment and coarse sediment is much smaller.

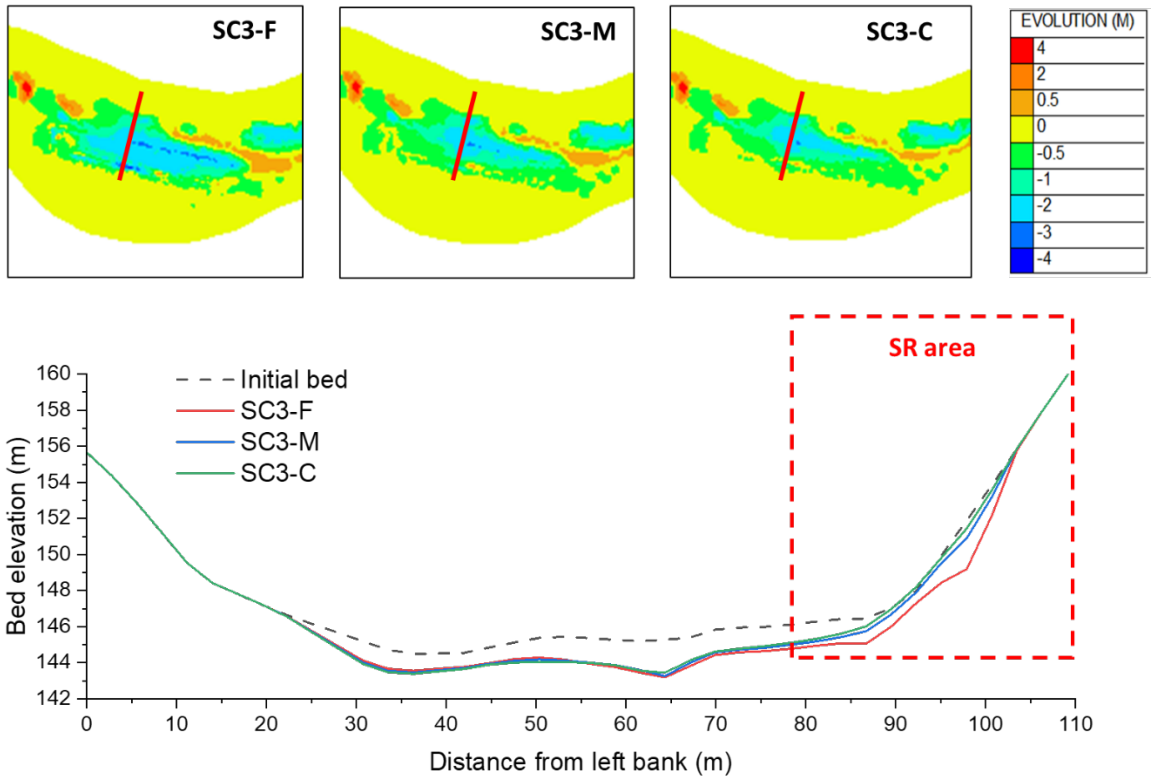

Figure 6-5 The analysis of SR erosion under different replenished sediment sizes. Top figure: the bed evolution at the SR site under different flushing flows. Bottom figure: the bed elevation at the selected cross-section (red line).

The variations of TR value and eroded volume at the SR site with the increase of flushing flow for different grain sizes of replenished sediment are shown in Figure 6-6. The TR values for the fine sediment are varied from 13% to 15%. For medium and coarse sediment, the TR values are similar, which are varied from 3% to 5%. Considering the promotion of erosion by flushing flow, increasing the flushing magnitudes from 0% to 100% leads to a 2% raise in TR value and 3000 m^3 raise in eroded volume for all types of replenished sediment. Nevertheless, different increasing rates of TR values can be observed when increasing the flushing magnitude from 20% to 100%. The relationship between these two factors for different replenished sediment is shown in Figure 6-7. For fine sediment, the TR alteration peaked at the 40% increase of flushing magnitude, with a value of 1%. The increasing rate significantly decreases with a further increase in flushing flow. The same phenomenon can be observed for medium sediment, while the peak value is only half of the fine sediment (0.5%). Moreover, the decreasing rate of TR alteration is not significant as the fine sediment when further

increasing the flushing flow. Nevertheless, the TR alteration is fluctuant for coarse sediment and no obvious optimal discharge (turning point) can be founded. It can be expected that the optimal flushing discharge is higher than the current designed range (100% of Q0) since a further increasing tendency can be seen from 60% of Q0.

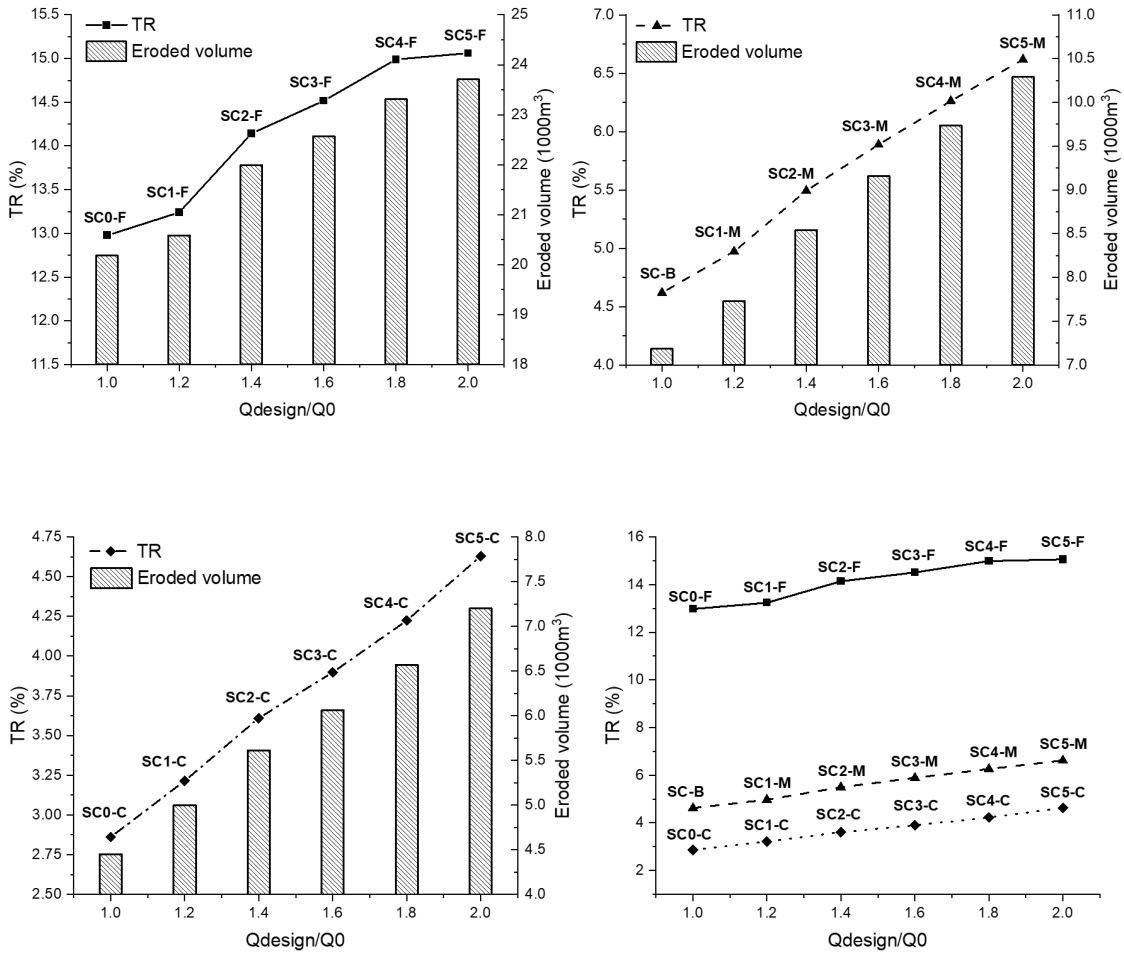

Figure 6-6 The variation of TR value and eroded volume at the SR site with the increase of flushing flow for different grain sizes of replenished sediment.

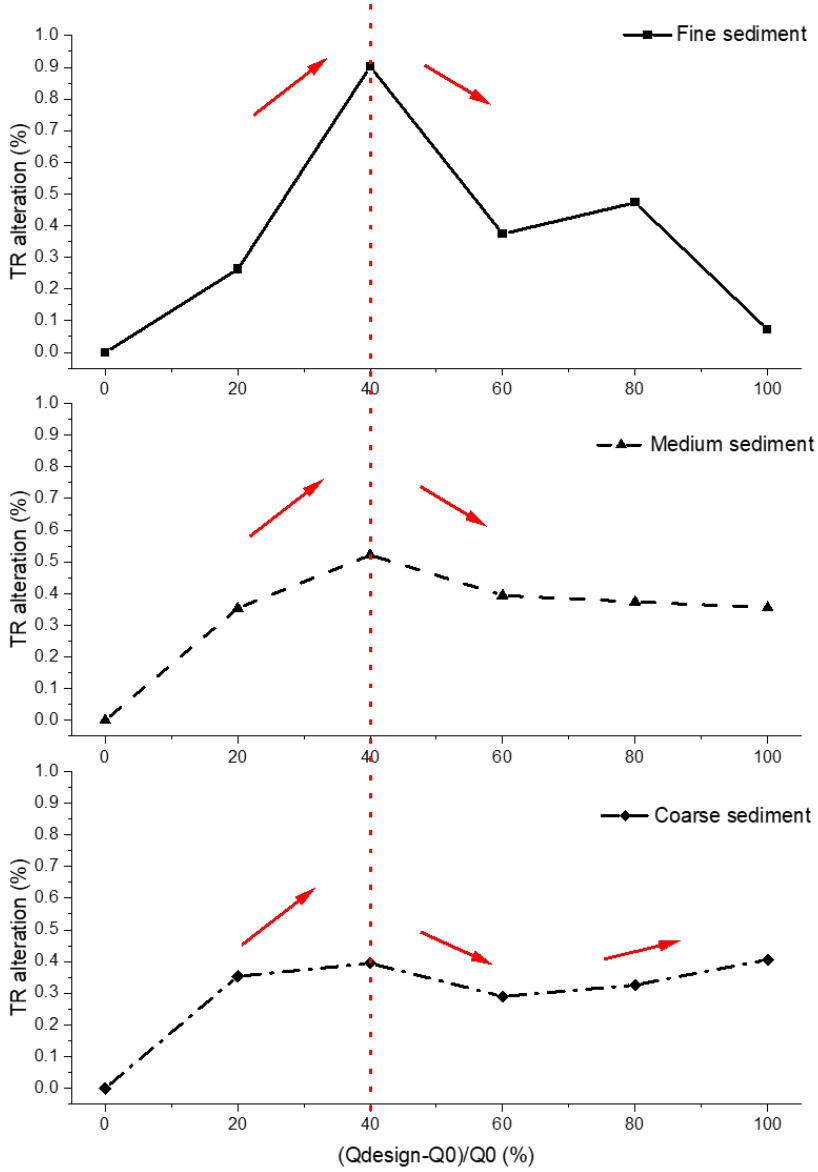

Figure 6-7 The relationship between TR alteration and the increasing percentage of flushing magnitudes.

The calculated BCI value and TR for each scenario are summarized in Table 6-2. It can be noticed that for fine sediment, the BCI value is minus with a greater value than medium and coarse sediment, which means that more erosion happened and the average bed level is reduced significantly. More importantly, though increasing the magnitude of a single flood can promote the erosion process of SR, it can not be considered an efficient way since the variation of BCI and TR is limited. The

sediment size of replenished material is the dominant factor. It can be expected if the current D50 of replenished sediment is reduced by 50% (7 mm to 3.5 mm), the replenishment efficiency may increase by 100% or more.

Table 6-2 The summary of calculated BCI and TR in the SR site for each scenario

Scenario	**SC0-F**	**SC1-F**	**SC2-F**	**SC3-F**	**SC4-F**	**SC5-F**
BCI (m)	-0.358	-0.369	-0.408	-0.424	-0.444	-0.447
TR (%)	12.98%	13.24%	14.14%	14.52%	14.99%	15.06%
Scenario	**SC-B**	**SC1-M**	**SC2-M**	**SC3-M**	**SC4-M**	**SC5-M**
BCI (m)	-	-0.015	-0.037	-0.054	-0.070	-0.086
TR (%)	4.62%	4.97%	5.49%	5.89%	6.26%	6.62%
Scenario	**SC0-C**	**SC1-C**	**SC2-C**	**SC3-C**	**SC4-C**	**SC5-C**
BCI (m)	0.075	0.060	0.043	0.031	0.017	0.000
TR (%)	2.86%	3.21%	3.61%	3.90%	4.22%	4.63%

6.2.1.3. Effects on the downstream responses

The different transported volume from SR combined with different magnitudes of flushing flow causes various riverbed aggradation and degradation phenomenon at downstream reach. Considering the same grain size of replenished material under different flushing flows, the calculated results of evolution volume and mean evolution depth is shown in Figure 6-8. The higher flushing flow (SC5-F) can promote the erosion process at the eroded area, for instance, 6k-7k, 8k-9k, 10k-11k, and 12k-13k. Moreover, we can notice that the higher flushing flow also enhances the deposition at 1k-4k, 7k-8k, and 11k-12k areas. However, based on the comparison of thalweg elevation between SC0-F and SC5-F, the higher flushing flow leads to more erosion happening at the entire study reach (Figure 6-9). These different results between thalweg elevation and bed evolution are mainly because more sediment is accumulated deposited at the convex bend area. This is a very common geomorphological phenomenon for meandering rivers, where sediment is more likely to be deposited at the convex bend to promote the formation of a point bar, while more erosion happens at the thalweg line (concave bend) since the different distribution of flow velocity and water depth during flood period (Hagstrom, Leckie, & Smith, 2018). According to the 2D scalar maps of bed evolution at 6 typical meandering areas (Figure 6-10), we can observe that more deposition is happened at the convex area under higher

flushing flow, while on the contrary, more erosion also occurs at the concave bend. Hence, it can be expected that for higher flushing flow, more sediment is eroded from the SR site or the original riverbed. Such sediment is more likely to be deposited at the convex area to format the point bars, which we have already detected during our field survey of 4 typical gravel bars in Chapter 3. Simultaneously, the higher erosion at the concave area is also beneficial for the formation of riffles and pools. The diversity of the geomorphic units (GUSI-D) will increase since the number of habitat structures increase.

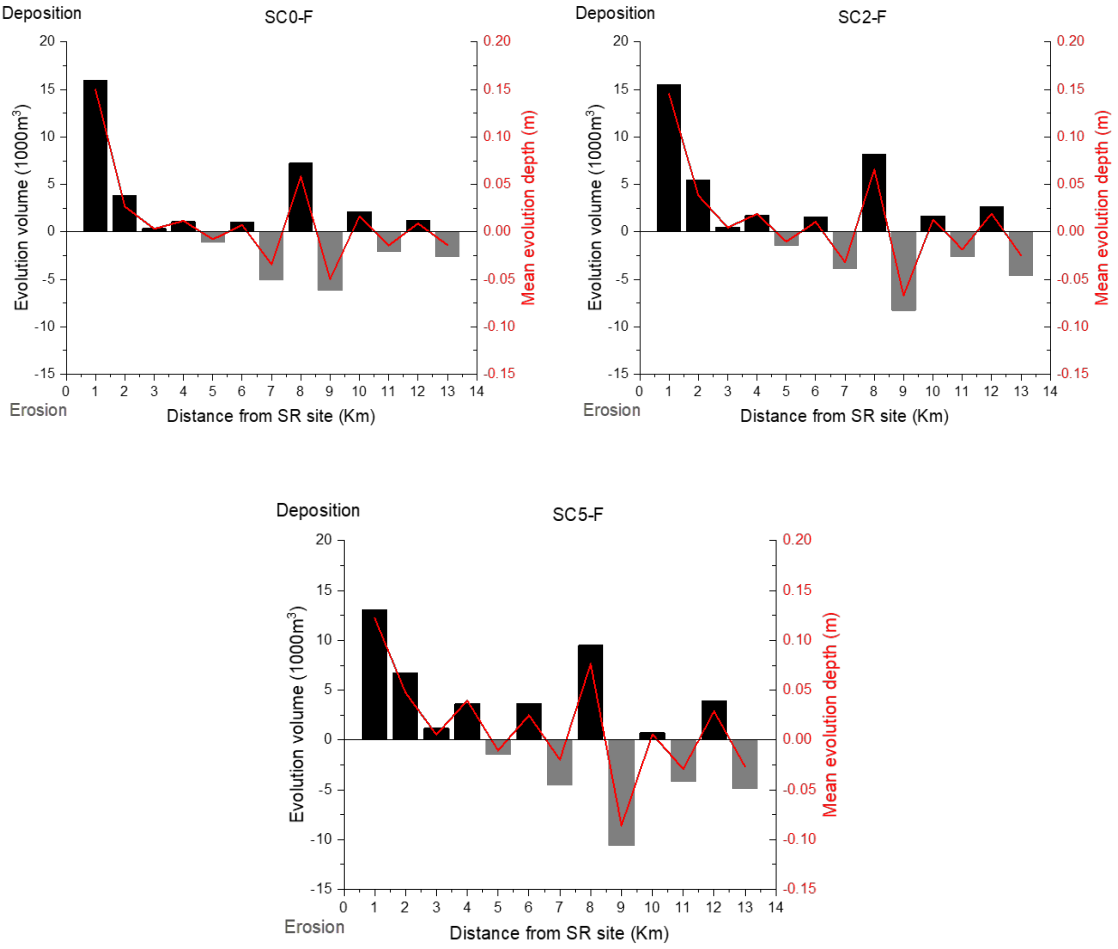

Figure 6-8 The evolution volume and mean evolution depth for same grain size of replenished sediment under different flushing flow.

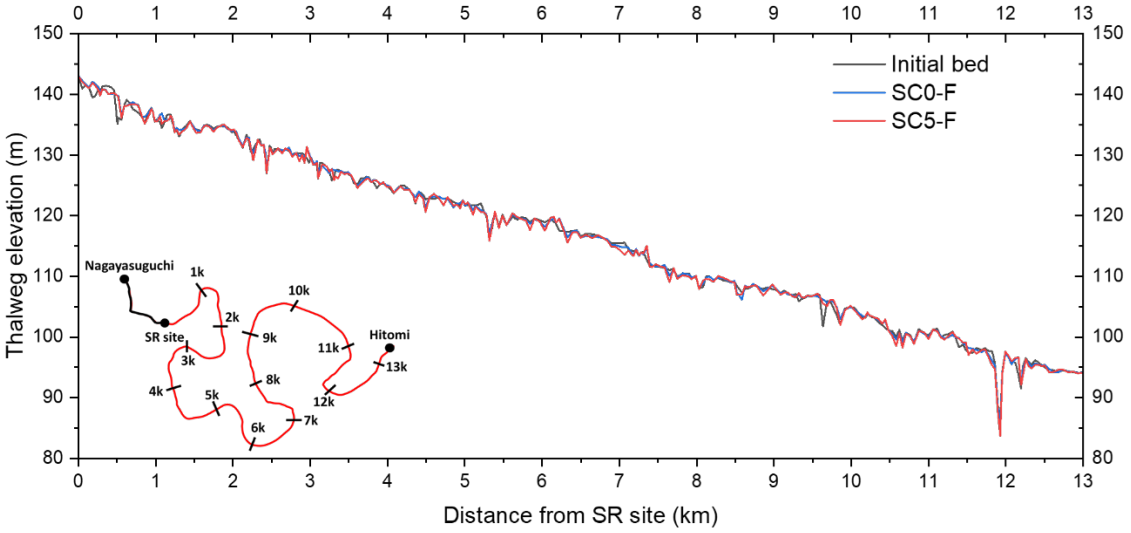

Figure 6-9 The thalweg elevation between initial bed, SC0-F, and SC5-F at 13 km downstream of SR site.

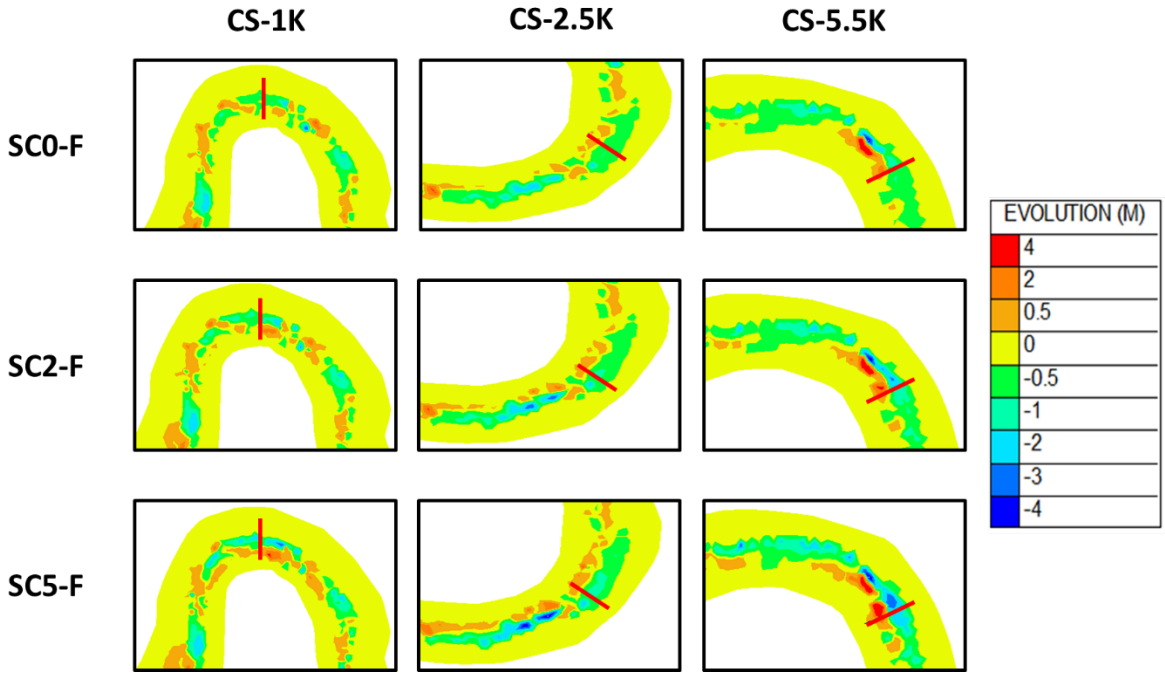

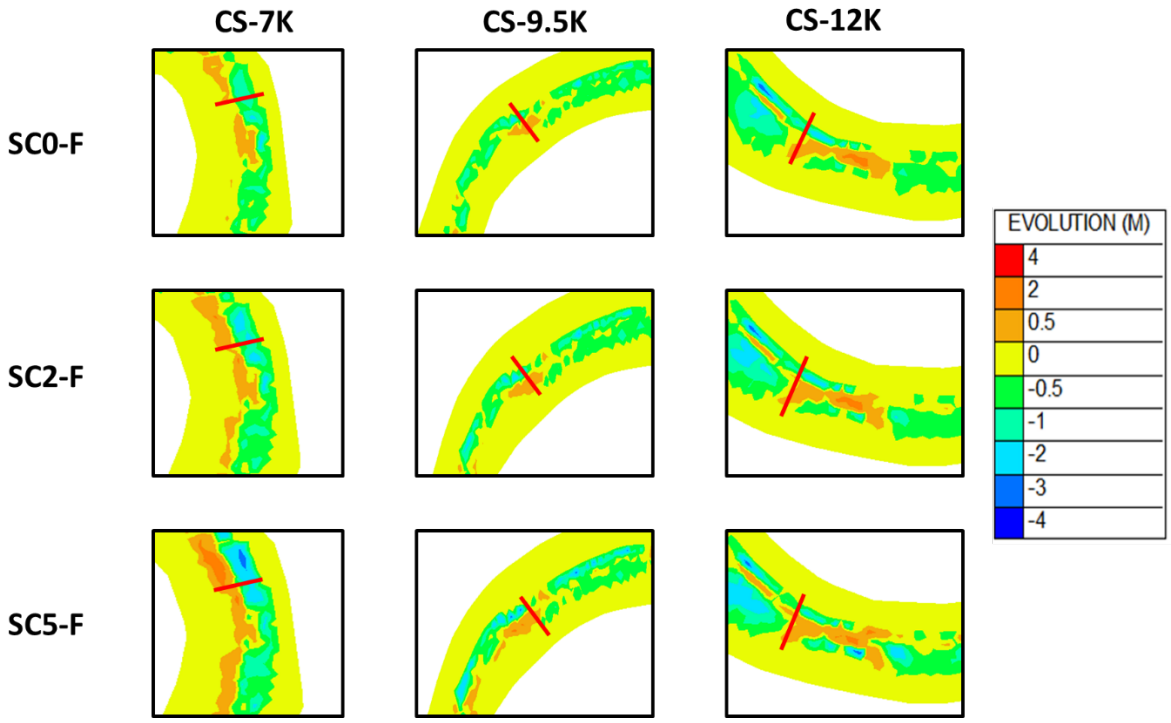

Figure 6-10 The 2D scalar maps of bed evolution at 1k, 2.5k, 5.5k, 7k, 9.5k, and 12k downstream of the SR site under three different flushing flow combined with the same replenished sediment.

The detailed distribution of bed evolution and flow velocity at 6 cross sections in the meandering areas are shown in Figure 6-11. We can see that the flow velocity is lower at the higher eroded area since the water depth is greater. In contrast, the flow velocity at the deposited area is smaller or nearly zero at the deposited area since the original elevation of the riverbed at this area is higher. The newly accumulated sediment transfers the area from submerged to unsubmerged during the normal flow period, and thus the corresponding flow velocity is reduced significantly. Such variation in flow velocity and submerged-unsubmerged areas are the main hydrological consequences of geomorphological alterations. The HMID value can further investigate the downstream hydro-geomorphological changes statistically.

CS-1k

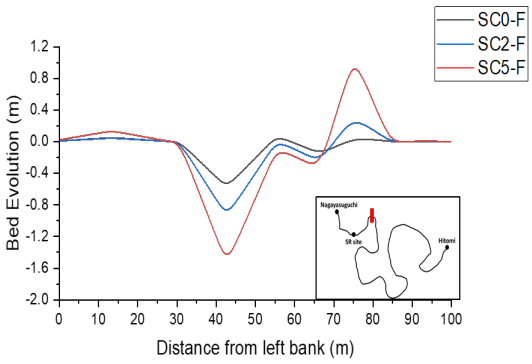

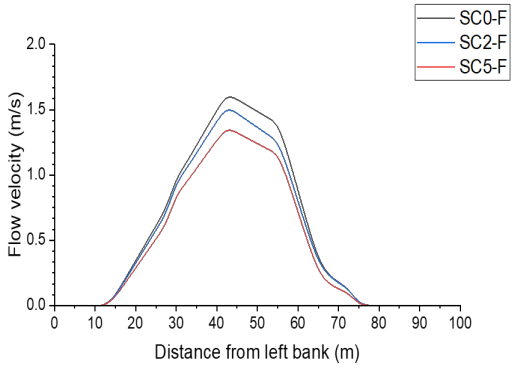

CS-2.5k

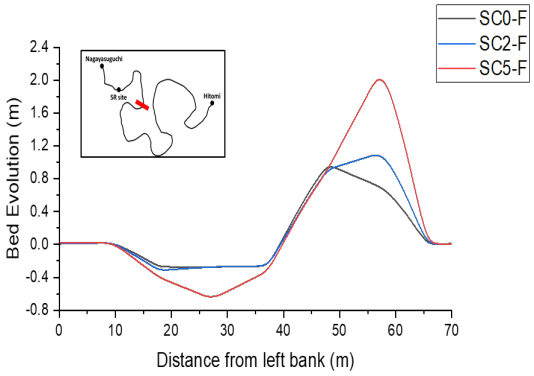

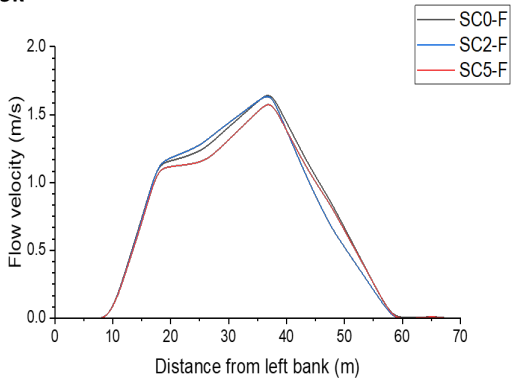

CS-5.5k

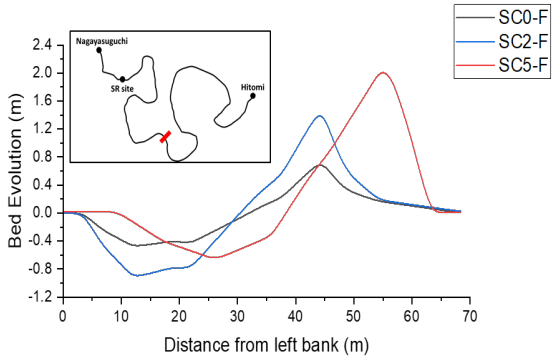

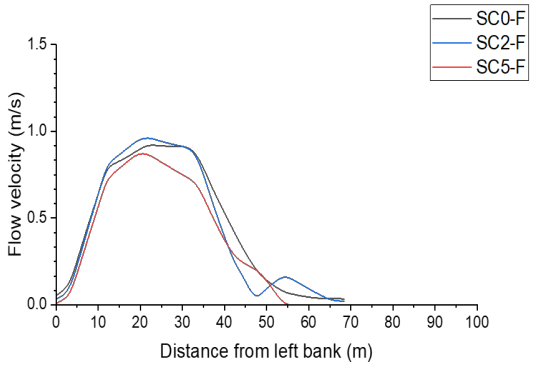

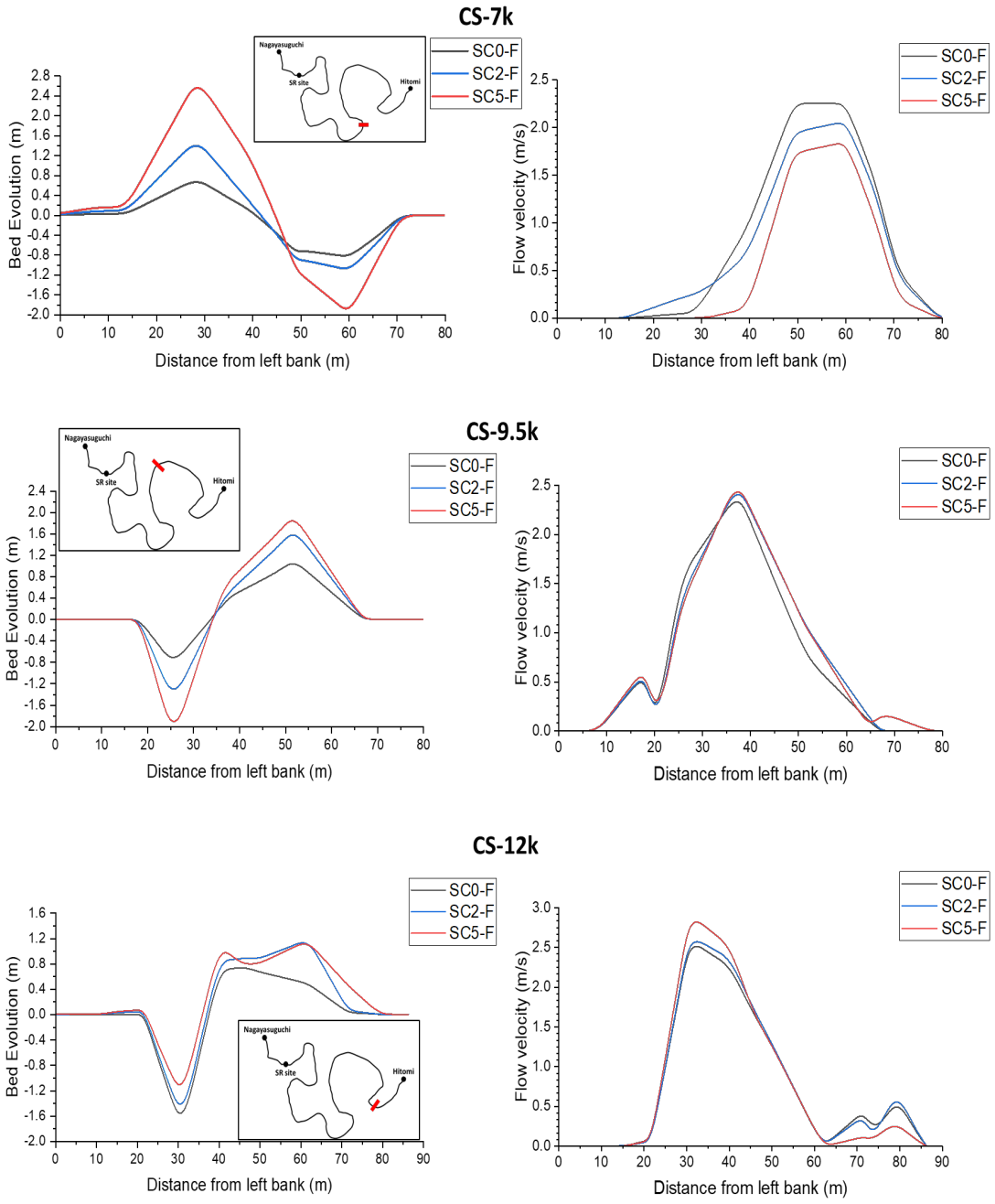

Figure 6-11 The distribution of bed evolution and flow velocity at 6 typical cross sections located at 1k, 2.5k, 5.5k, 7k, 9.5k, and 12k for different flushing flow combined with the same replenished material.

Regarding the different types of replenished sediment under the same flushing flow, the evolution volume and mean evolution depth at downstream reach are shown in Figure 6-12. Significant differences in evolution performance can be observed near the SR site (0k-2k), where more sediment is deposited for the finer sediment scenario (SC3-F). Such significant deposition is mainly due to the higher transported volume of sediment from the SR site for SC3-F compared to SC3-M and SC3-C (higher TR value and eroded volume in Figure 6-6). Based on the 2D scalar map of bed evolution, we can observe that the additional sediment supply from the SR site enhances the formation of a point bar at the meandering area near the SR site (Figure 6-13). Due to the fact that the simulated period is short, we can not investigate the long-term impacts of such additional sediment supply. If we consider a longer period, the finer sediment may be transported entirely and no enhancement of downstream geomorphology occurs. However, the medium and coarse sediment may be deposited in the study area since they need a greater driving force (flushing flow) for transportation.

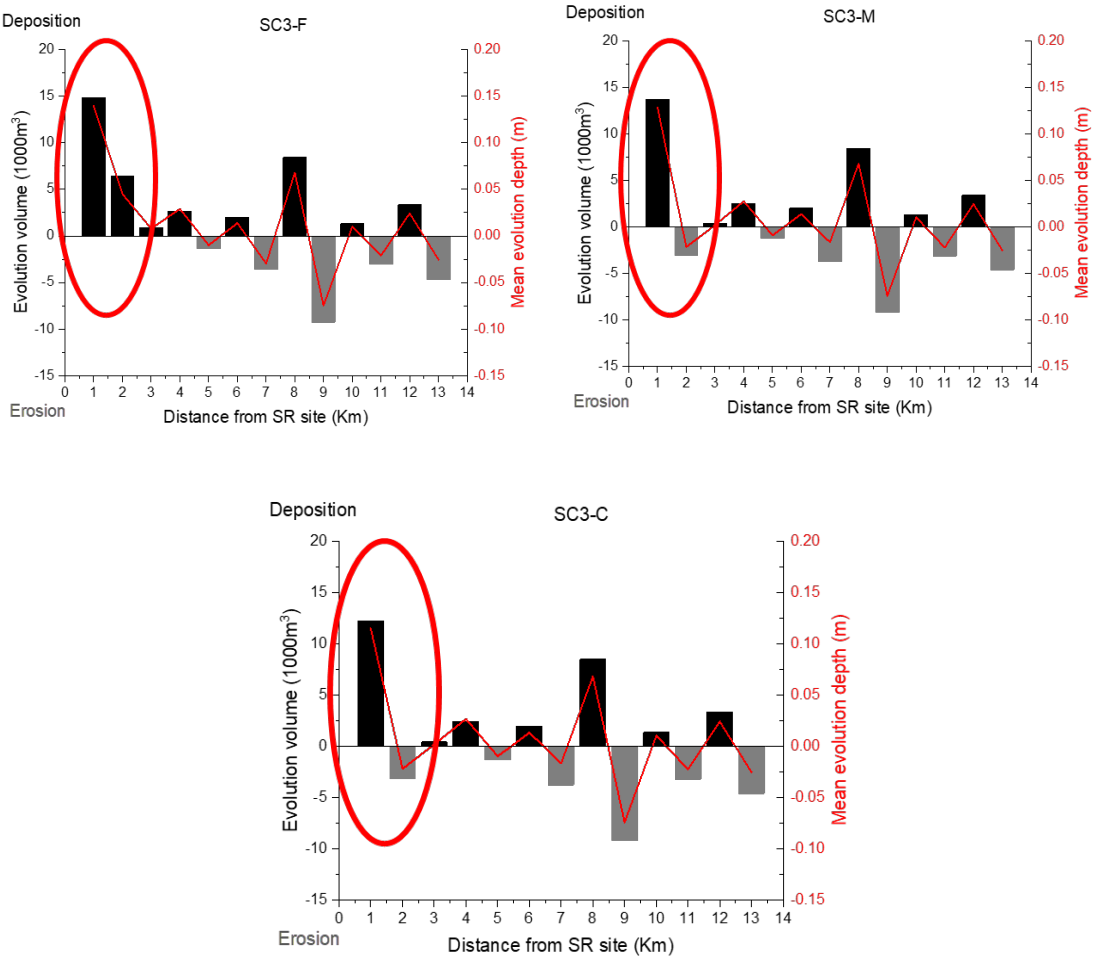

Figure 6-12 The evolution volume and mean evolution depth for different grain sizes of replenished sediment under the same flushing flow.

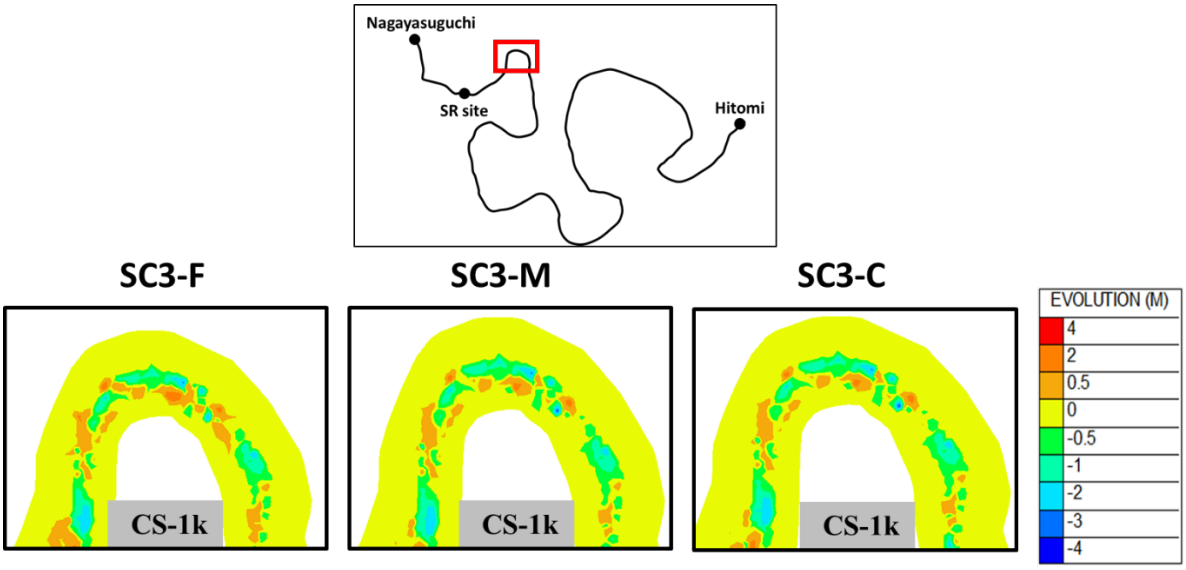

Figure 6-13 The 2D scalar maps of bed evolution at 1k downstream of the SR site under the same different flushing flow combined with different replenished sediment.

The assessments of downstream responses are then conducted based on the previous indicators, BCI and HMID. To be specific, BCI is calculated by the differences in average bed level changes between selected scenarios and base scenarios (SC-B). Considering the impacts of flushing flow, higher flushing magnitude can promote riverbed aggradation in some areas, for instance, 1k-2k, 3k-4k, 5k-8k, and 11k-12k, where the BCI value is positive (left figure, Figure 6-14). Meandering channels or deep pools exist in these areas, which lead to more deposition of upstream sediment from the SR site or original riverbed. Nevertheless, more erosion can be observed at 8k-11k and 12k-13k since the river channel here is straighter and less meandering. The higher flushing flow enhances the sediment movement and more riverbed degradation is expected. Despite this, an interesting phenomenon can be founded at the 0k-1k area, where the BCI value is positive and higher flushing flow gives rise to a lower BCI value. It means that the higher flushing flow can assist more accumulated sediment to be transported downstream. Based on the thalweg elevation (Figure 6-9), we can observe a deep pool located at 0k-1k area. Before the flood occurred, there are already amounts of sediment deposited here, which leads to a positive bed evolution around 4 m. During the flood, a higher magnitude of

flow can promote sediment transportation here and more sediment is derived downstream, which results in the reduction of the BCI value. Regarding the impacts of replenished sediment, we can observe higher BCI values near the SR site (0k-3k), while similar values at the rest area (right figure, Figure 6-14). Compared to medium and coarse sediment, more sediment supply from the SR site is expected for fine sediment (higher TR and eroded volume), which leads to more sediment deposition here, for instance, the meandering channel at 1k (Figure 6-13). It can be expected that the BCI value will reduce at the area near the SR site and increase at the further downstream area if we simulate a long-term period due to the further movement of accumulated sediment.

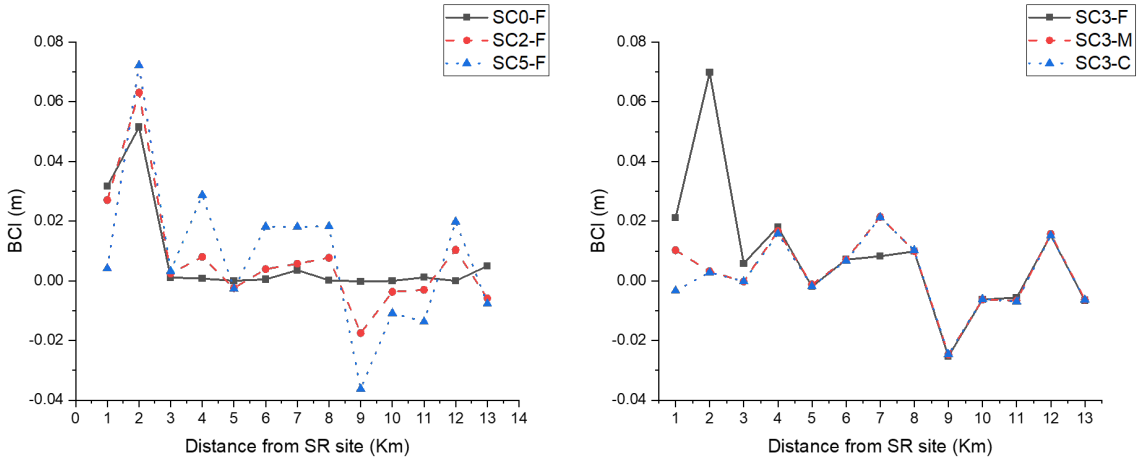

Figure 6-14 The BCI value for different single flood pulse scenarios at 13 km downstream of the SR site. Left figure: The comparison of BCI value between different flushing flows. Right figure: The comparison of BCI value between different sizes of replenished sediment.

The HMID is calculated based on the mean and deviation of water depth and flow velocity (Eq. 4-5), which means that it is correlated to the flow condition. In order to implement the comparison between each scenario, the HMID is determined based on the flow condition at the last time step, where the inflow from the Nagayasuguchi dam is 90 m^3/s. The results of HMID calculation for different scenarios are shown in Figure 6-15. Considering the impacts of flushing flow, higher magnitude (SC5-F) can increase 5% to 10% of HMID value at the entire reach, which is mainly due to the facilitation of pool and bar formations at the meandering areas. Such alterations of river geomorphology will influence the distribution of the flow regime (flow velocity in Figure 6-11) and

finally contributes to the variation of HMID value. Regarding the impacts of replenished sediment, fewer differences can be observed between different sizes of sediment (right figure, Figure 6-15). Based on the results of bed evolution (Figure 6-12) and BCI value (Figure 6-14), more deposition occurs at the meandering area at 1k-2k (Figure 6-13). However, the sediment is accumulated at the bank side which is unsubmerged during the normal flow, which means that the differences in flow velocity and water depth can be ignored when we calculate the HMID value. That is one limitation of HMID since the hydrological variations can not entirely represent the geomorphological changes. It is predicted that more significant differences in HMID will happen if we consider a long-term simulation since the geomorphological alterations between each SR sediment are more obvious.

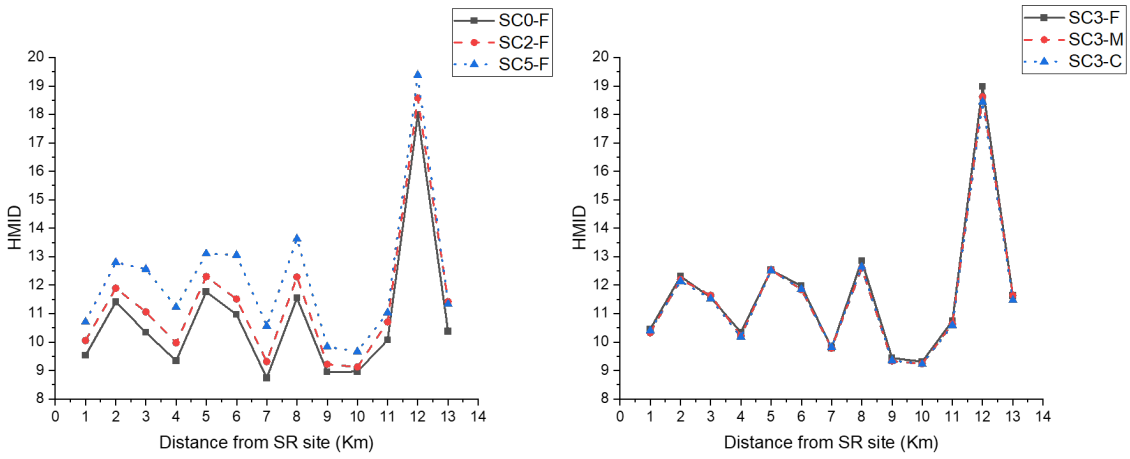

Figure 6-15 The HMID value for different single flood pulse scenarios at 13 km downstream of SR site. Left figure: The comparison of HMID value between different flushing flow. Right figure: The comparison of HMID value between different sizes of replenished sediment.

Table 6-3 The mean values of BCI and HMID for the 13 km study reach downstream of the SR site (all scenarios of single flood pulse).

Scenario	**SC0-F**	**SC1-F**	**SC2-F**	**SC3-F**	**SC4-F**	**SC5-F**
BCI (m)	0.00733	0.00631	0.00737	0.00843	0.00945	0.00858
HMID	10.766	11.007	11.341	11.687	11.944	12.224
Scenario	**SC-B**	**SC1-M**	**SC2-M**	**SC3-M**	**SC4-M**	**SC5-M**
BCI (m)	-	0.00145	0.00190	0.00301	0.00323	0.00346
HMID	10.770	11.151	11.333	11.585	11.873	12.163
Scenario	**SC0-C**	**SC1-C**	**SC2-C**	**SC3-C**	**SC4-C**	**SC5-C**
BCI (m)	0.00086	0.00074	0.00071	0.00173	0.00212	0.00208
HMID	10.793	10.977	11.228	11.549	11.792	12.163

The summarized results of mean BCI and HMID values for the 13 km study reach are shown in Table 6-3. We can observe that the flushing flow is the main factor that influences the downstream hydro-geomorphological responses. From the base flow (Q0) to the highest flow (Q0+100%), the BCI value increases by 17% for fine sediment, 130% for medium sediment, and 140% for coarse sediment. The fine sediment has less sensitive to the increase of flushing flow since it is the required driving force to reach the incipient motion is smaller than the medium and coarse sediment. Moreover, we can also observe that the overall BCI value increases with the decrease of SR sediment sizes since more sediment supply from the SR site promotes the riverbed aggradation at the downstream reach. The solid relationship generated between TR and downstream BCI can prove the viewpoint (Figure 6-16). A higher TR value represents a greater volume of transported sediment from the SR site, and such additional sediment facilitates the downstream aggradation, which has already been proved in the previous investigation in Chapter 4 (Figure 4-16).

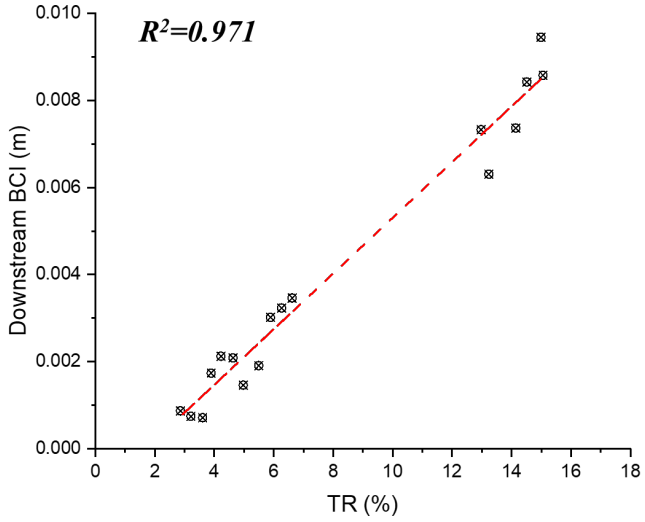

Figure 6-16 The relationship between downstream BCI and TR considering all scenarios for single flood pules.

In summary, the magnitude of flushing flow and sizes of replenished sediment are both essential for SR erosion and downstream geomorphological alterations. Considering the SR sediment, the fine size can promote the overall TR and HMID (Table 6-2 and Table 6-3). While for the flushing flow, a higher magnitude is beneficial for TR and HMID promotion. However, considering the increasing rate of TR (Figure 6-7) and the limitation of releasing flow from Nagayasuguchi dam, an increase of 40%-60% in flushing flow is more efficient for fine sediment. At the same time, extremely higher HMID is not beneficial for the GUSI-D and H values since the number of riffles may decrease. Thus, SC2-F and SC3-F should be the most efficient cases for the single flood pulse scenarios.

6.2.2. The scenarios of a double flood pulses

6.2.2.1. Introduction of scenarios

In the previous section, the flushing magnitude is the main factor discussed to investigate the impacts of flushing flow. Despite this, the flushing frequency and duration are two significant aspects that are usually considered in the enhancement of sediment movement. Esmaeili et al. (2017) investigated that the double flood pulses are more efficient than the single flood pulse for sediment flushing. Since SR and sediment flushing both consider the sediment erosion and deposition processes, we can expect

the double flood pulses can also promote the SR erosion and downstream hydro-geomorphology as well.

In this section, we design three scenarios that have double flood pulses based on one of the efficient cases we have already investigated in the single flood pulse (SC2-F). The first flood pulse is the same as the base flow (Q0), while we add a second flood pulse with a different magnitude and duration. The total flushing water volume during flushing (TFWV) is the same for all scenarios, which means that the longer duration has a longer time of flushing, but the peak magnitude is lower, while the shorter duration has a shorter time of flushing, but the peak magnitude is higher. The designed scenarios and hydrograph for double flood pulses are shown in Table 6-4 and Figure 6-17. The hours represent the duration of the second flood pulse (20h, 16h, and 12h). The flow is smoothly increasing and decreasing during the second flood pulse for consideration of model stability.

Table 6-4 The designed scenarios for double flood pulses

Hydrograph	**Size of replenished sediment**
	Finer (1 mm)
Q0+40%-20h	SC2-F-20h
Q0+40%-16h	SC2-F-16h
Q0+40%-12h	SC2-F-12h

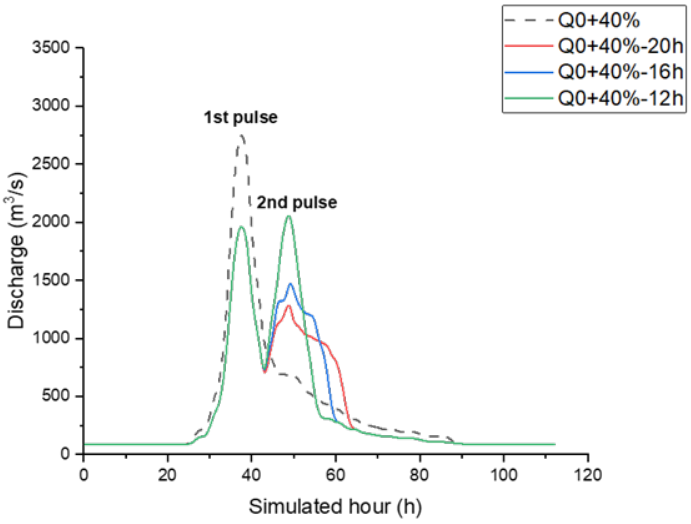

Figure 6-17 The designed hydrograph for double flood pulses scenarios

6.2.2.2. Effects on the SR erosion

The comparison of bed evolution between the single (SC2-F) and double (SC2-F-16H) flood pulses at the SR site are shown in Figure 6-18. The erosion process is promoted by the implementation of a second flood pulse, especially at the head and tail area of the SR stockpile. The cross-sectional bed elevation from the stockpile head to the stockpile tail is shown at the bottom of Figure 6-18. It can be noticed that the eroded depth increases around 1 m at the head area and 0.5-2 m at the tail area for the SC2-F-16H. The velocity magnitude near the SR site is similar between SC2-F and SC2-F-16H at the first flood peak (Figure 6-19), which means that the influence of flow magnitude is not crucial. The second flood pulse can provide an additional process of flushing, and thus facilitates the SR erosion. However, the erosion in the middle area is similar and no promotion occurs. The flow velocity in the middle area is higher and the erosion is almost finished after the first flood pulse (Figure 6-19). During the second pulse, erosion is more likely to occur at the head and tail areas since the accumulated sediment is greater here.

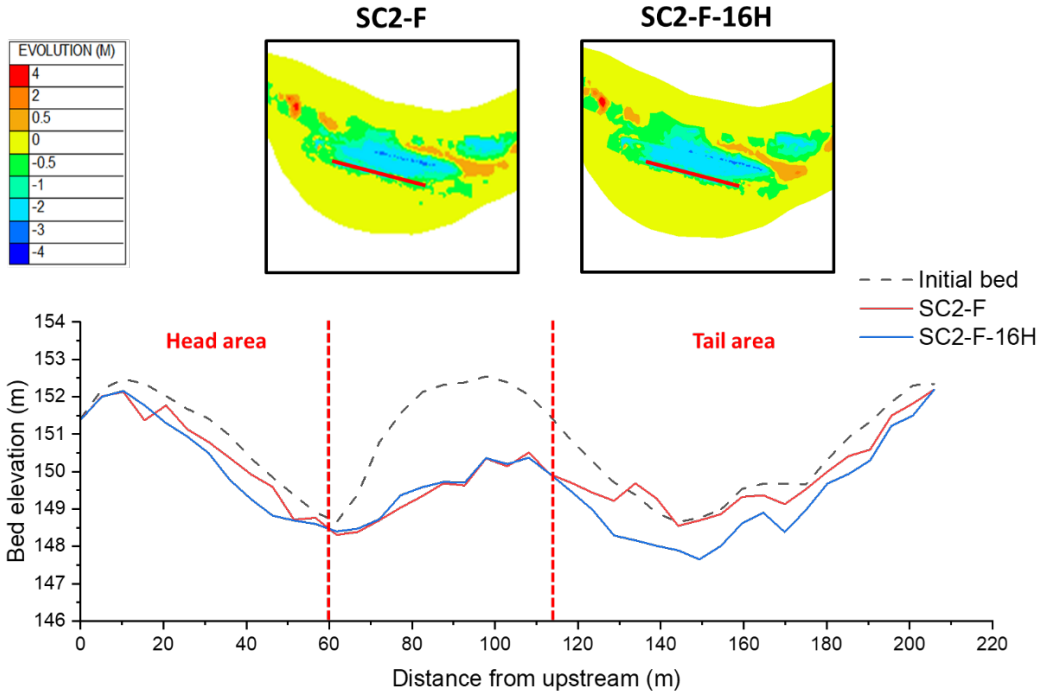

Figure 6-18 The comparison of SR erosion between single and double flood pulses at the SR site. Top figure: the 2D scalar maps of bed evolution. Bottom figure: the cross-sectional bed elevation near the SR site from upstream.

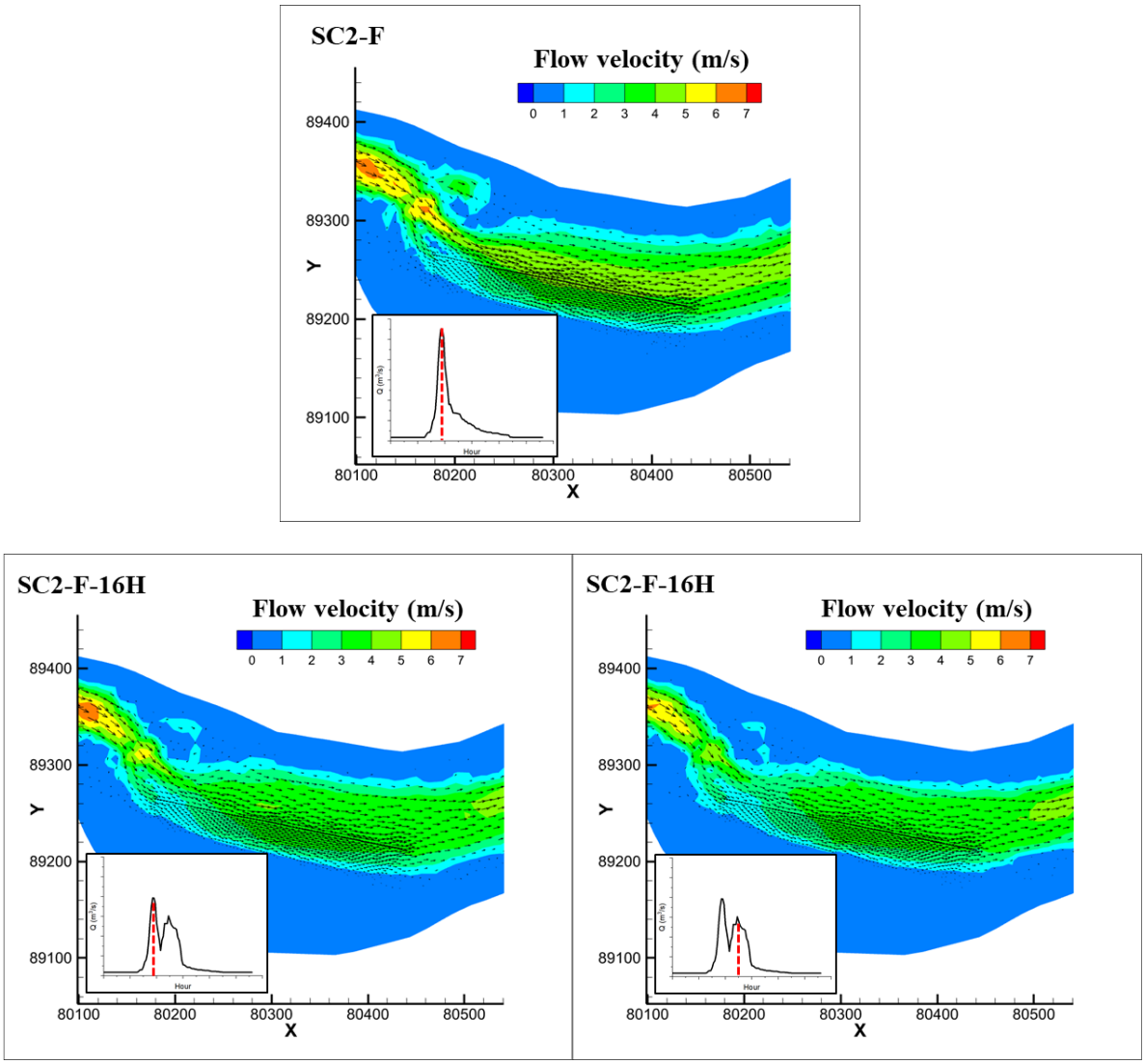

Figure 6-19 The 2D scalar maps of flow velocity distribution during the flood peak between single and double flood pulses. Top figure: the flow velocity at 38h for SC2-F. Bottom figure: the flow velocity at 38h and 49h for SC2-F-16H.

The assessment results of TR and eroded volume between single and double flood pulses are shown in Figure 6-20. Considering all scenarios of double flood pulses, the TR increases by about 1%, and the eroded volume increases by about 2000 m^3, which is mainly due to the additional erosion that happened at the head and tail areas (Figure 6-18). Moreover, compared to the flushing duration and magnitude of the second pulse, higher TR can be observed for SC2-F-16H. It is crucial to weigh the advantages and disadvantages between the flushing magnitude and duration. Higher magnitude can

promote erosion at the area with higher flow velocity (middle area), while longer duration can facilitate the area with lower flow velocity (head and tail areas). Thus, the scenario with medium magnitude and duration is efficient for SR erosion.

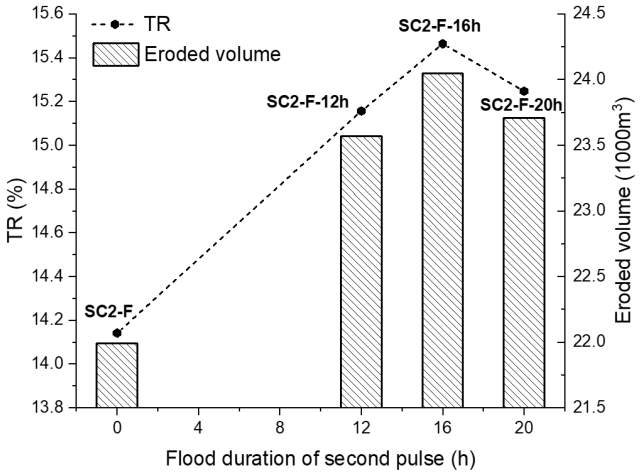

Figure 6-20 The TR and eroded volume at the SR site between single flood pulse (SC2-F) and double flood pulses (SC2-F-12H, SC2-F-16H, and SC2-F-20H).

6.2.2.3. Effects on the downstream responses

The comparison of bed evolution between single flood pulse (SC2-F) and double flood pulses (SC2-F-16H) at downstream reach is shown in Figure 6-21. The deposited volume at the original deposited area is increased, and at the same time, the eroded volume at the original erosion area is reduced for SC2-F-16H. In general, the double flood pulses promote riverbed aggradation and reduce the riverbed degradation at the downstream reach. Such variations of downstream geomorphology have close correlations to the bar, riffle, and pool formations.

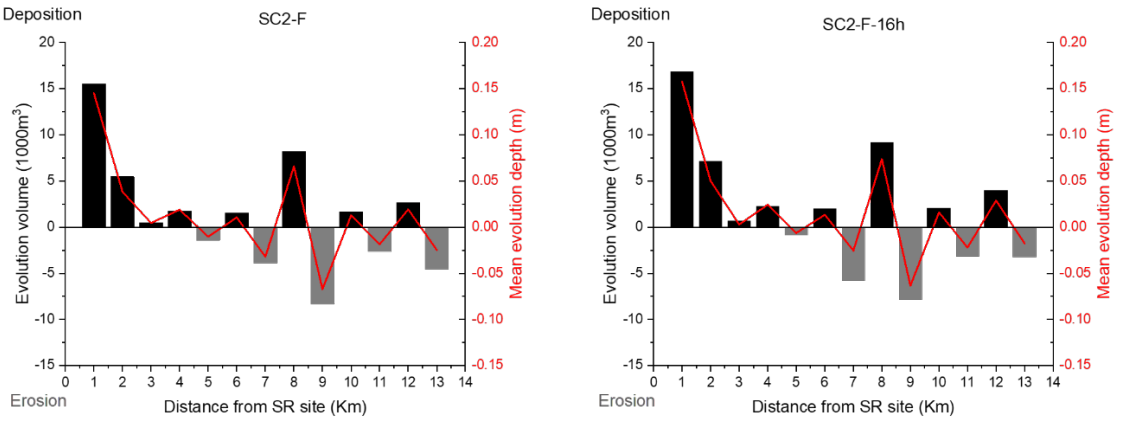

Figure 6-21 The evolution volume and mean evolution depth between single flood pulse (SC2-F) and double flood pulses (SC2-F-16H).

According to Figure 6-22, the impacts of double flood pulses on the downstream geomorphology are varied at different locations due to the different flow regimes. At 1k, the double flood pulses can promote deposition at the convex area while the erosion at the concave area is similar. This area is extremely meandering and near the SR site, which means that the higher sediment supply from the SR site can cause higher deposition here (SC2-F-16H). At 2.5k, the higher flushing magnitude (SC2-F-12H and SC2-F) can lead to more deposition at the convex area. It can be expected that flushing magnitude is the dominant factor that can promote more sediment erosion at the upstream area (lower BCI in 0k-2k). Such additional sediment is then deposited here (higher BCI in 2k-3k). The same phenomenon can be founded at 7k and 12k, where the higher magnitude of the second flood pulse is beneficial for deposition at the convex area. Furthermore, at 5.5k, the double flood pulses can entirely lead to more sediment deposition. The flow velocity is low here and it can be recognized as a deposited area. The greater volume of sediment from the SR site when implementing double flood pulses is more likely to be accumulated here. Nevertheless, at 9.5k, the sediment is easy to be transported at the concave area due to the higher flow velocity, thus the longer flushing duration can promote erosion.

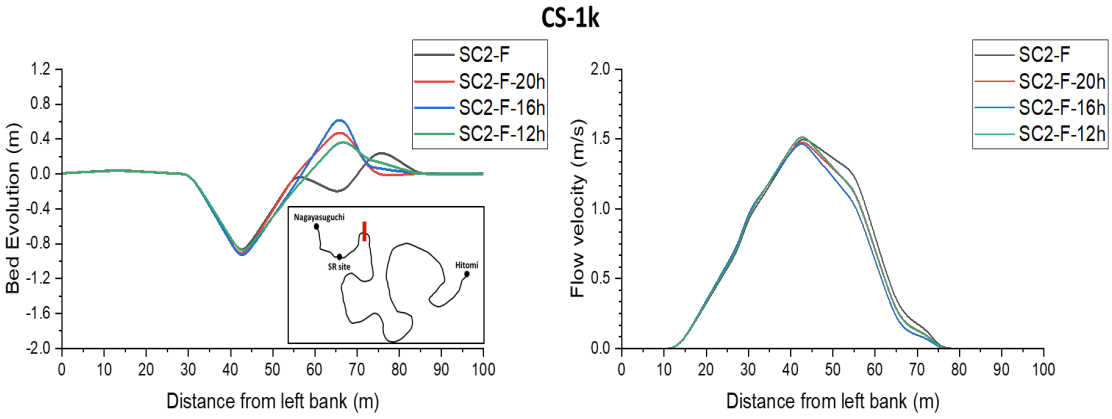
CS-1k
SC2-F
SC2-F-20h
SC2-F-16h
SC2-F-12h
Bed Evolution (m)
Distance from left bank (m)
Nagayasuguchi
SR site
Hitomi
Flow velocity (m/s)
Distance from left bank (m)

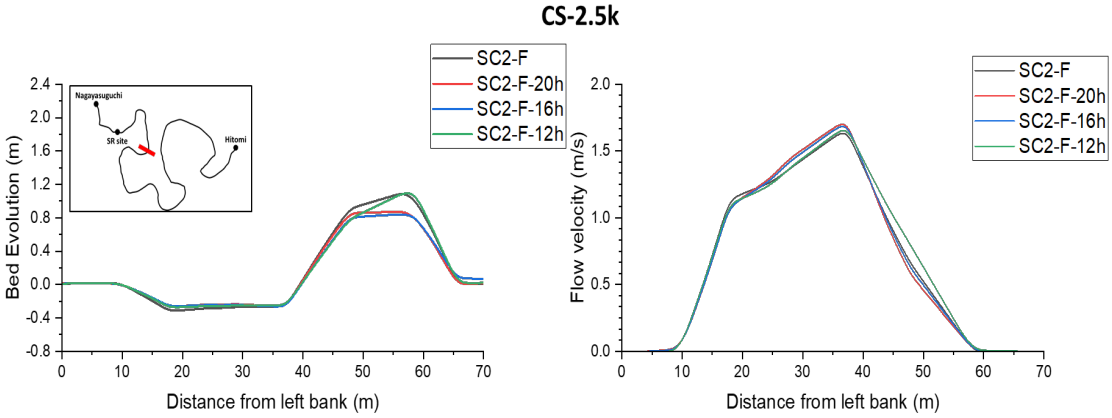
CS-2.5k
SC2-F
SC2-F-20h
SC2-F-16h
SC2-F-12h
Bed Evolution (m)
Distance from left bank (m)
Nagayasuguchi
SR site
Hitomi
Flow velocity (m/s)
Distance from left bank (m)

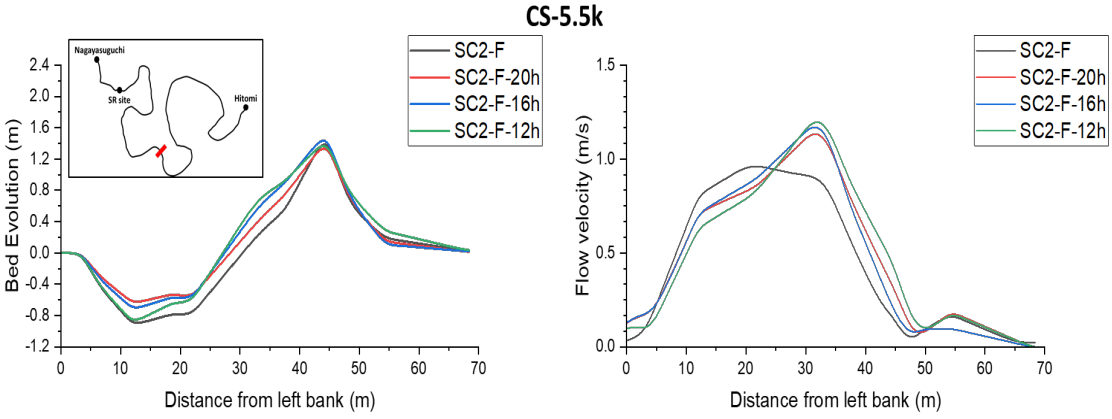
CS-5.5k
SC2-F
SC2-F-20h
SC2-F-16h
SC2-F-12h
Bed Evolution (m)
Distance from left bank (m)
Nagayasuguchi
SR site
Hitomi
Flow velocity (m/s)
Distance from left bank (m)

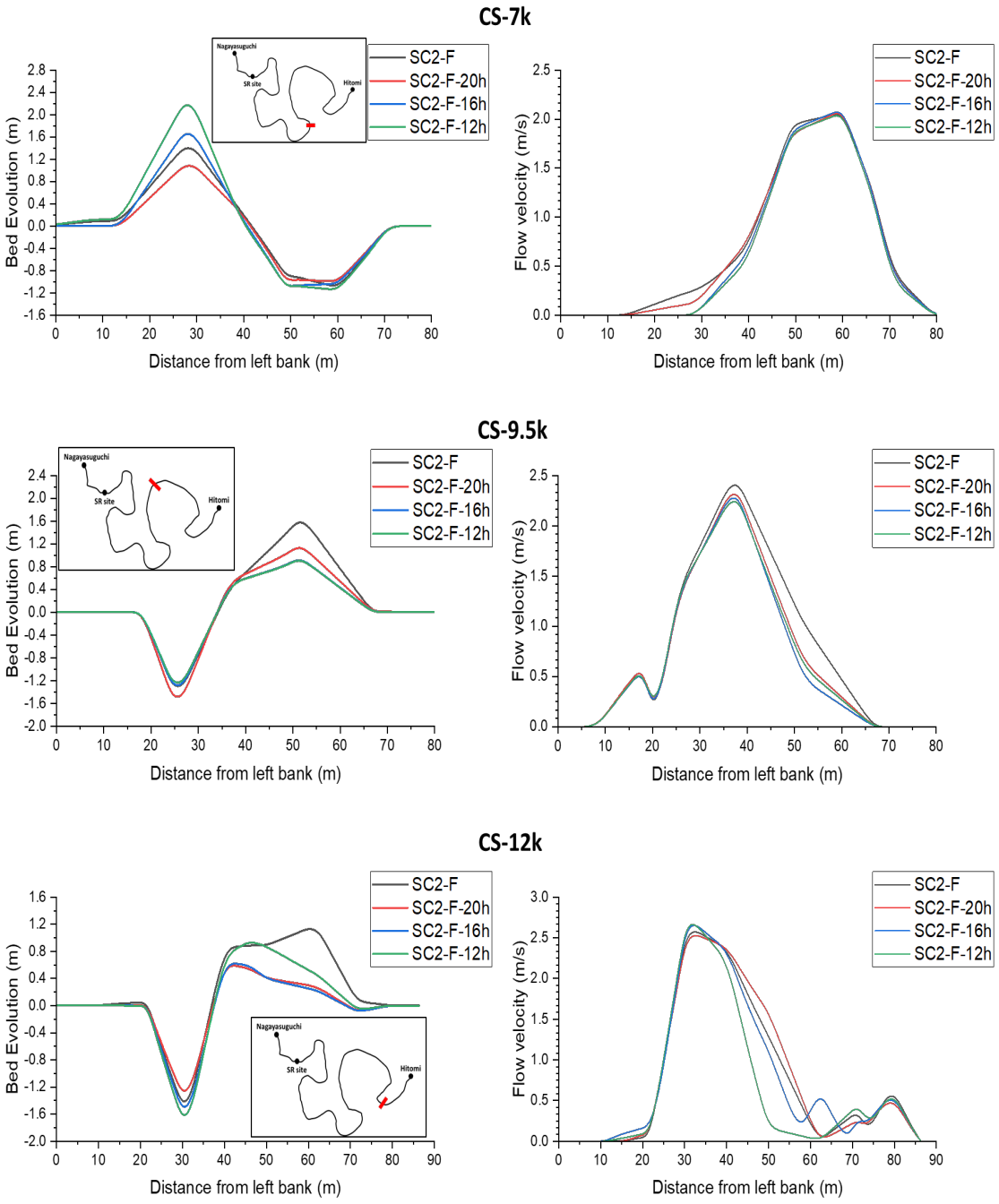

Figure 6-22 The distribution of bed evolution and flow velocity at 6 typical cross sections located at 1k, 2.5k, 5.5k, 7k, 9.5k, and 12k between single flood pulse and double flood pulses.

The results of downstream BCI are calculated in Table 6-5, which considers the SC2-F as the base case. It can be noticed that the bed level is increasing (positive BCI) a majority of the reach for double flood pulses. Decreasing only happened at 8k-11k, where erosion is the dominant process due to the channel being narrow and the flow velocity and bed shear stress being higher. Such variation in bed level is linked to the different erosion and deposition phenomenon at different locations shown in Figure 6-22. Overall, the double flood pulses can further assist the riverbed aggradation at downstream reach (positive of average BCI) due to the increasing volume of sediment from the SR site and the variation of flushing flow.

Table 6-5 The results of downstream BCI for scenarios of double flood pulses

Distance from SR site (Km)	**BCI (m)**		
	SC2-F-20h	**SC2-F-16h**	**SC2-F-12h**
0-1	0.0358	0.0395	0.0281
1-2	0.0798	0.0747	0.0758
2-3	-0.0013	0.0009	0.0033
3-4	0.0162	0.0133	0.0135
4-5	0.0000	0.0017	0.0027
5-6	0.0060	0.0068	0.0087
6-7	0.0109	0.0125	0.0155
7-8	0.0209	0.0156	0.0098
8-9	-0.0161	-0.0138	-0.0154
9-10	-0.0015	-0.0004	0.0000
10-11	-0.0061	-0.0066	-0.0066
11-12	0.0207	0.0199	0.0206
12-13	0.0009	0.0014	-0.0003
Average	0.0128	0.0127	0.0120

Regarding the HMID, the alterations between single and double flood pulses are varied along the reach (Table 6-6). The complicated riverbed responses result in variation in flow velocity (Figure 6-22) and thus impact the water depth as well. For the location where HMID increasing, the double flood pulse can promote the formation of bars and pools but is not beneficial for the protection of existing riffles. The differences in average HMID along the reach are quite small (<0.2) due to the different contributions of the second flood pulse to the river geomorphology.

Table 6-6 The results of HMID for single flood pulse, double flood pulses, and initial condition (before SR). Compared to the SC2-F, the red color represents the increase while the blue color represents decreasing.

Distance from SR site (Km)	HMID							
	Before SR	SC2-F	SC2-F-20h		SC2-F-16h		SC2-F-12h	
			Value	Variation	Value	Variation	Value	Variation
0-1	9.929	10.052	10.421	5.0%	10.420	4.9%	9.698	-2.3%
1-2	11.191	11.892	12.321	10.1%	12.452	11.3%	11.959	6.9%
2-3	9.976	11.060	10.822	8.5%	10.946	9.7%	11.148	11.7%
3-4	9.460	9.971	9.810	3.7%	9.928	4.9%	10.202	7.8%
4-5	11.324	12.300	12.344	9.0%	12.402	9.5%	12.398	9.5%
5-6	11.320	11.512	11.217	-0.9%	11.369	0.4%	11.164	-1.4%
6-7	7.835	9.312	9.640	23.0%	9.687	23.6%	9.741	24.3%
7-8	10.835	12.287	12.357	14.1%	12.303	13.5%	12.406	14.5%
8-9	8.550	9.218	9.604	12.3%	9.658	12.9%	9.659	13.0%
9-10	9.105	9.125	9.079	-0.3%	9.238	1.5%	9.237	1.4%
10-11	9.346	10.708	10.784	15.4%	10.865	16.3%	11.000	17.7%
11-12	15.467	18.578	18.311	18.4%	18.417	19.1%	18.591	20.2%
12-13	10.746	11.418	10.734	-0.1%	10.707	-0.4%	10.858	1.0%
Average	10.468	11.341	11.342	9.2%	11.415	9.9%	11.389	9.6%

6.3. Results on new replenishment arrangement: Influence of replenished locations and geometries

6.3.1. Introduction of scenarios

Despite the original driving force, flushing flow, the replenished locations, and geometries are also crucial to affect SR erosion. The current strategy of replenishment arrangement is to put the sediment at the right bank to build a single stockpile with a great height (around 25 m). Higher flushing flow is required to efficiently transport such a huge stockpile based on the calculated TR in Figure 4-10. Nevertheless, the releasing flow at the Nagayasuguchi dam is significantly reduced due to the lack of precipitations. Therefore, it is worthwhile to consider new strategies of arrangement for promoting sediment erosion at the SR site.

According to the investigated results from Buëch River, 3 directions can facilitate the erosion at the SR site: (1) Alter the geometries by reducing the height and increasing the eroded length; (2) Alter the locations by shifting the stockpiles to the middle of the channel; (3) Arrange an additional stockpile at another side of the bank (Guillaume BROUSSE et al., 2022). Such countermeasures are

designed based on the increase of eroded surface, submerged ratio, and flow velocity. In this section, we designed two new strategies for SR arrangement in the Naka River based on the previous research (Figure 6-23). The SC-SR1 is designed based on the reduction of height, an increase of length, and shifting to the middle, while the SC-SR2 is designed based on the arrangement of the additional stockpile. We keep the total placed volume consistent for scientific analysis. The detailed information of each scenario is shown in Table 6-7. The single and double flood pulses of Q0+40% are both simulated for each SR strategy to investigate the different erosion performances.

Table 6-7 The designed scenarios for the new arrangement of SR

Scenarios	**Hydrograph**	**Stockpile design**					
		Number	**Location**	**Length (m)**	**Height (m)**	**Width (m)**	**Volume (m^3)**
SC2-F (Base case)	Q0+40%	Single	Original location	235	15-25	70	155000
SC2-F-16H (Base case)	Q0+40%-16h						
SC-SR1-S	Q0+40%		20 m shifted to the middle	330	12	70	155000
SC-SR1-D	Q0+40%-16h						
SC-SR2-S	Q0+40%	Double	Left + right	190(L) 235(R)	10	50(L) 70(R)	155000
SC-SR2-D	Q0+40%-16h						

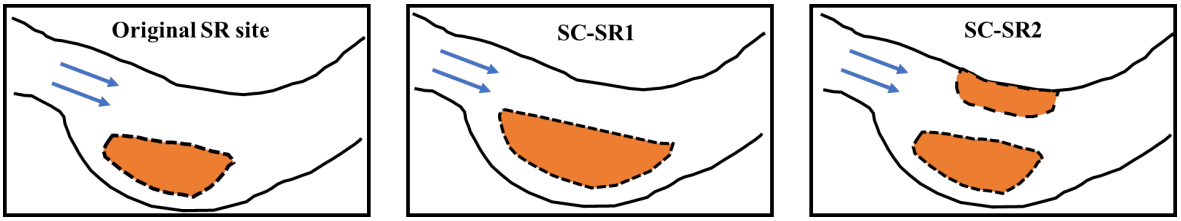

Figure 6-23 The comparison of locations and geometries between original SR site and new design.

6.3.2. Effects on the SR erosion

The bed evolution and the bed elevation at one selected cross-section are shown in Figure 6-24. Considering the two strategies, the SR2 is more efficient to enhance the sediment erosion at the SR

site. According to the flow velocity distribution shown in Figure 6-25, the bank-side flow velocity for SC-SR2 is around 4.5 m/s, which is higher than SC-SR1. The additional stockpile can not only increase the erodible surface but also narrow the river channel to increase the flow velocity and bed shear stress. More erosion can be observed at the head and tail areas of SR1 since we enlarge the length of the stockpile, and it can be expected that the eroded volume is greater than the original design. Nevertheless, sediment deposition also occurs at the bank side near the head and tail areas. The low flow velocity at the head area restricts the movement of eroded sediment. At the tail area, the sediment is deposited due to the effects of the meandering channel. It can be predicted that the eroded sediment may not efficiently be transported downstream for SR1. Regarding the effects of flood pulses, the higher magnitude of a single flood pulse can promote erosion at the top area of the stockpile since the submerged ratio is higher (bottom figure in Figure 6-24). Because we reduce the height of the stockpile, the stockpile may be nearly submerged during higher flushing flow. The flow enters the top surface from the head area during flood peak (SC-SR2-S in Figure 6-25) and we can see some slight erosion occurred here (SC-SR2-S in Figure 6-24).

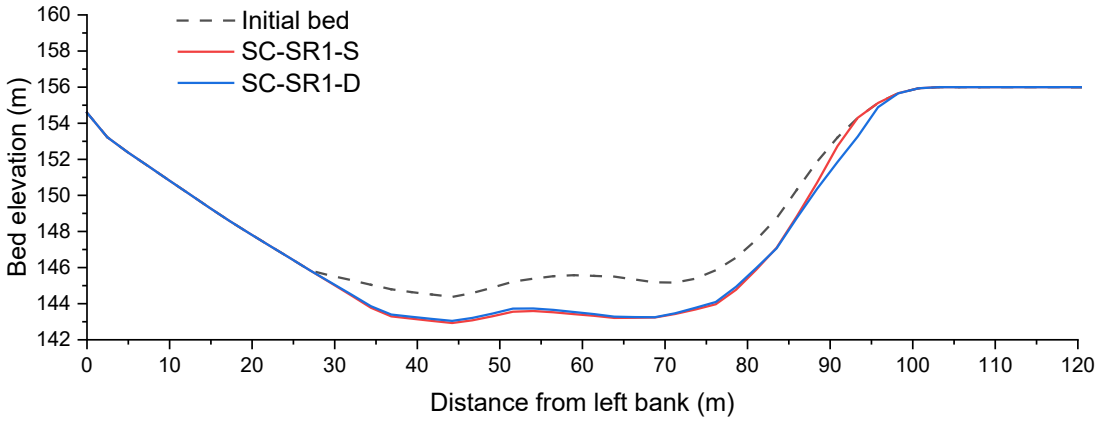

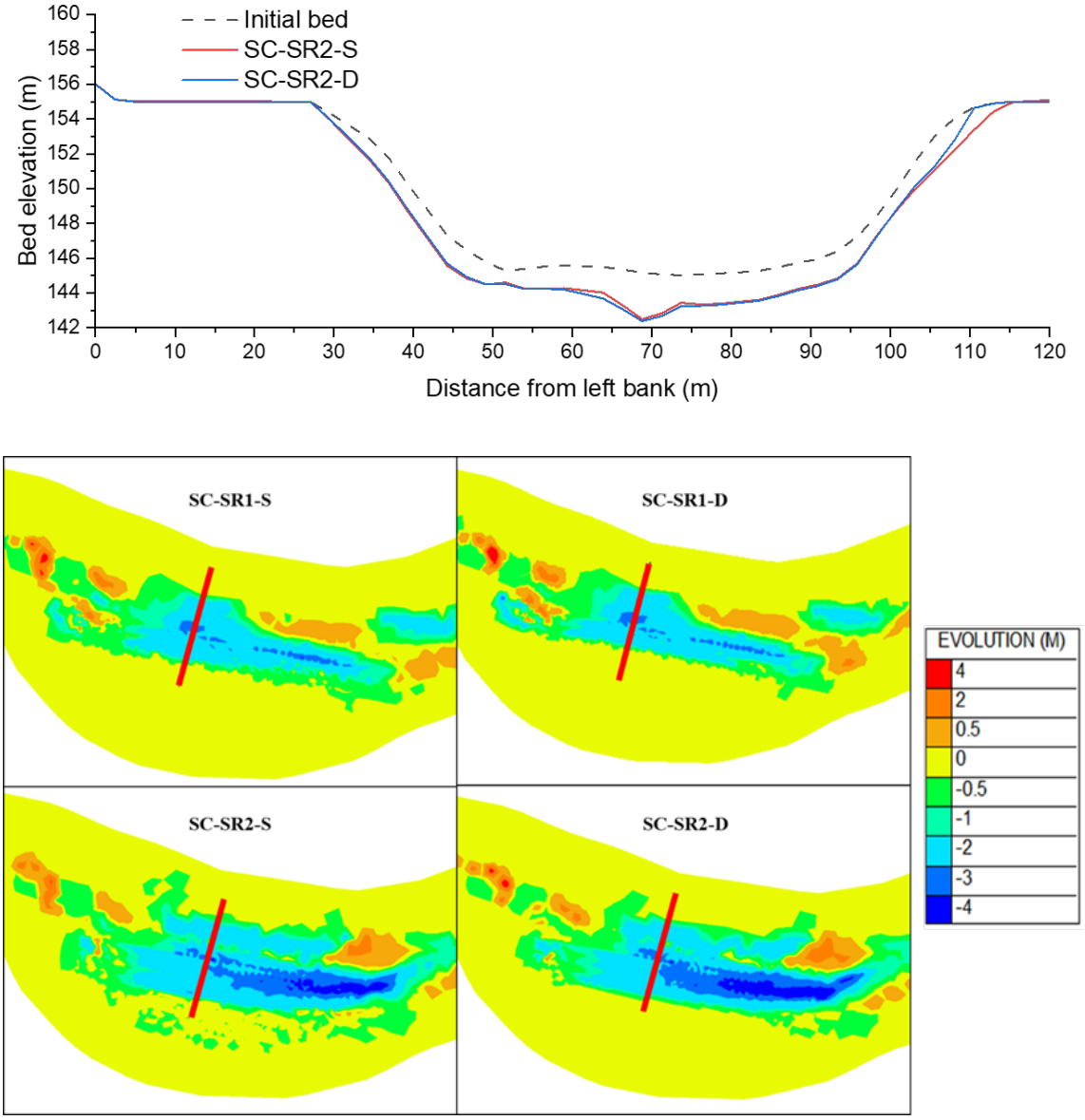

Figure 6-24 The analysis of SR erosion under different arrangement strategies. Top figure: the bed elevation at the selected cross-section (red line). Bottom figure: the bed evolution at the SR site.

SC-SR1-S

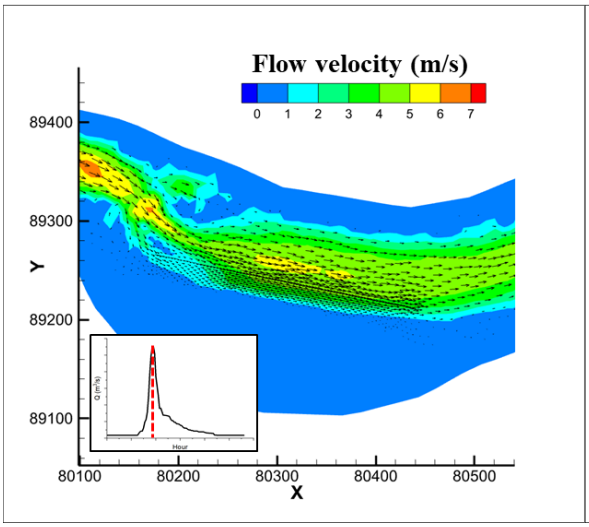

SC-SR2-S

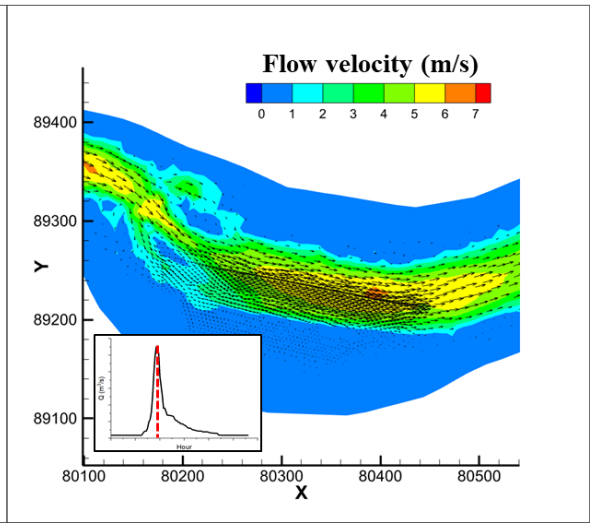

SC-SR1-D

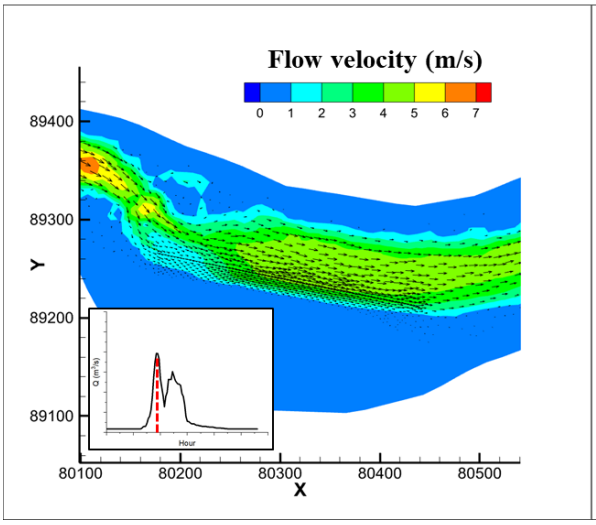

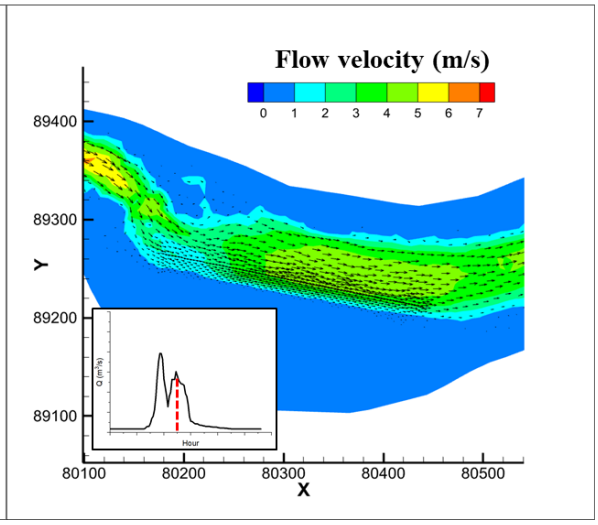

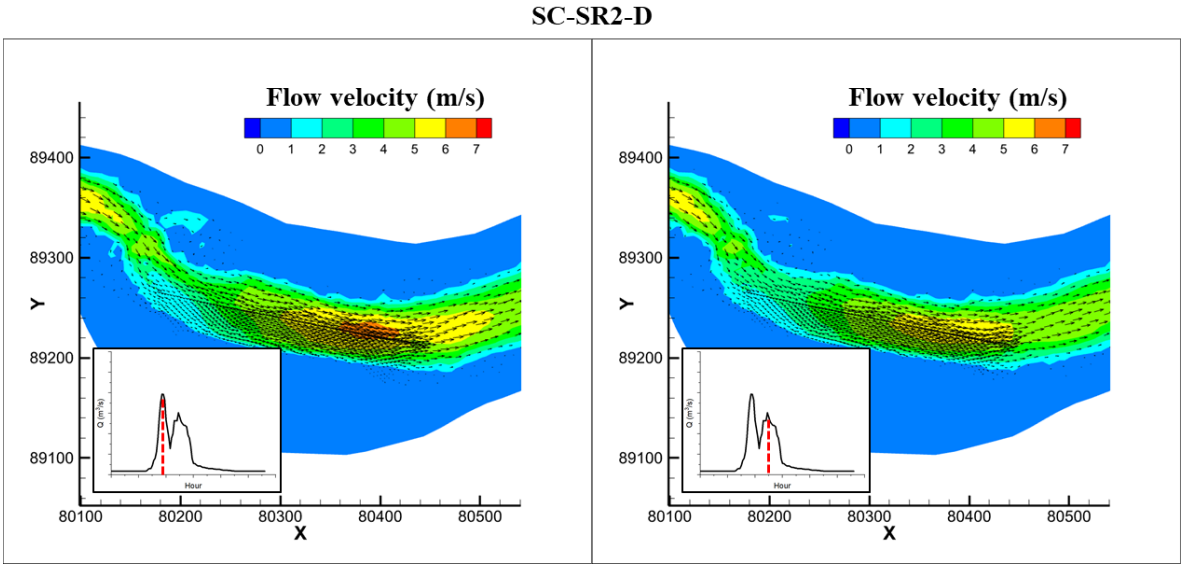

Figure 6-25 The 2D scalar maps of flow velocity distribution during the flood peak of SC-SR1 and SC-SR2. Top figure: the flow velocity at the single peak of SC-SR1-S and SC-SR2-S. Medium figure: the flow velocity at the double peaks of SC-SR1-D. Bottom figure: the flow velocity at the double peaks of SC-SR2-D.

The calculated BCI and TR for the designed scenarios are shown in Table 6-8. For SR1, the TR is increased by around 4% under both flushing flow conditions. Same as the previous results we obtained, the double flood pulses can lead to more erosion, but the increased rate is much lower than at the original site. More sediment is eroded when implemented SR2 and the increase in TR is around 10%. Moreover, the single flood pulse (SC-SR1-D) can result in higher TR than the double flood pulses (SC-SR2-D), which is different from the previous cases. Due to the fact that the height of the stockpile is lower than the original one, a higher magnitude can significantly increase the submerged ratio, which means that more sediment erosion occurred at the top area. Moreover, the double stockpiles further promote such impacts, and we can observe that more erosion happened at the top area of the left stockpile (Figure 6-24).

Considering the BCI, a positive value can be founded for both scenarios of SR1, which means that more sediment is deposited at the SR area compared to the base cases. As mentioned before, sediment deposition occurs at the head and tail areas, and such sediment can not be efficiently transported to the downstream reach. The SSC of replenished material at 0.5 km downstream of the SR site can prove the viewpoint since the values of SC-SR1-S and SC-SR1-D are both lower than the base cases

(Figure 6-26). It can be concluded that put sediment at the tail and head areas are not an adept approach for implementing SR due to the restriction of sediment transportation here.

Table 6-8 The BCI and TR of each scenario in the analysis of the new SR arrangement.

Scenario	SC2-F	SC-SR1-S	SC-SR2-S	SC2-F-16h	SC-SR1-D	SC-SR2-D
BCI (m)	-	0.051	-0.266	-	0.082	-0.217
TR (%)	14.14	17.44	25.33	15.46	17.46	22.46

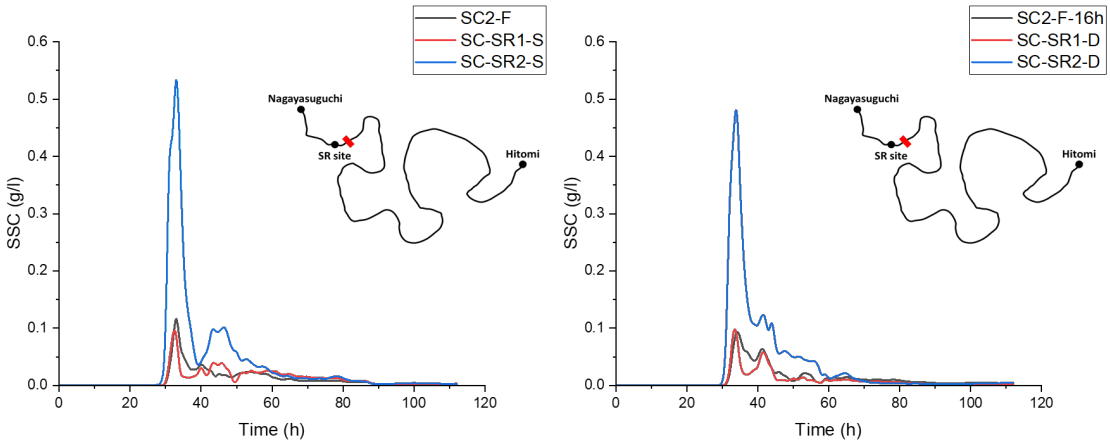

Figure 6-26 The time series of SSC at 0.5 km downstream of the SR site. Left figure: single flood pulse. Right figure: double flood pulses.

6.3.3. Effects on the downstream responses

Due to the differences in transported volume from the SR site, the downstream geomorphological responses are varied in each scenario. The evolution volume and the detail bed elevation between 0k-2k are shown in Figure 6-27. More sediment deposition occurs at the 0k-2k areas for SR2 since the transported sediment is higher than the SR1 based on the previous assessment of SR erosion (Table 6-8). Nevertheless, no significant differences in geomorphological alterations can be founded in the rest area, which means that the SR sediment is mainly accumulated near the SR site (2 km) after one flood event. More riverbed aggradation can be detected in SR2, especially in the pool areas, where sediment accumulation tends to happen. Furthermore, it can also be noticed that though the eroded

volume of the single flood pulse scenario (SC-SR2-S) is higher than the double flood pulse scenarios (SC-SR2-D), the deposited volume at the 0k-2k area is similar. It can be predicted that implementing double flood pulses is more beneficial for the transportation of SR sediment to enlarge the geomorphological responses.

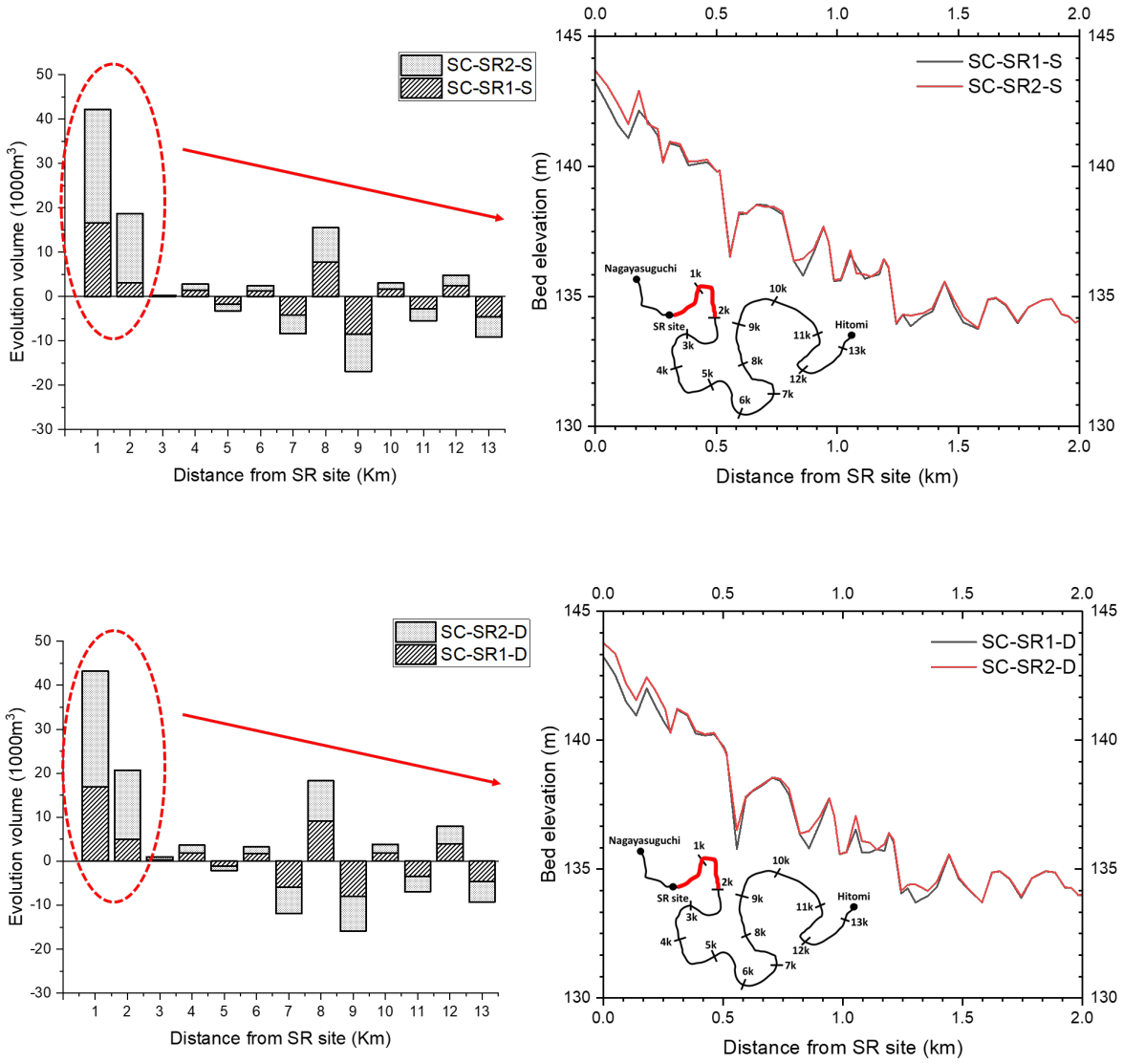

Figure 6-27 The evolution volume and the specific bed elevation at 0k-2k downstream of SR site. Top figure: comparison between scenarios of single flood. Bottom figure: comparison between scenarios of double flood pulses.

The assessment results of downstream BCI are shown in Table 6-9. Compared to the original SR site, the SR2 leads to more bed aggradation downstream, especially at the 0k-2k area, due to the higher volume of SR sediment accumulation. On the contrary, the SR1 can not facilitate the riverbed aggradation (negative BCI) as the eroded sediment can not be efficiently transported downstream. Such deposited sediment may require multiple flushing (long-term period) to assist its movement.

Table 6-9 The results of downstream BCI for scenarios of SR arrangement.

Distance from SR site (km)	**BCI (m)**			
	SC-SR1-S	**SC-SR2-S**	**SC-SR1-D**	**SC-SR2-D**
0-1	**0.010**	**0.095**	**0.000**	**0.089**
1-2	**-0.017**	**0.072**	**-0.015**	**0.061**
2-3	-0.004	-0.003	-0.001	0.000
3-4	-0.003	-0.004	-0.004	-0.004
4-5	-0.002	-0.001	-0.002	-0.001
5-6	-0.002	-0.002	-0.002	-0.003
6-7	0.014	0.014	-0.001	-0.001
7-8	-0.004	-0.003	0.000	0.000
8-9	-0.002	-0.001	-0.001	-0.001
9-10	0.000	-0.001	-0.001	-0.001
10-11	-0.001	-0.001	-0.002	-0.002
11-12	-0.002	-0.002	0.000	0.000
12-13	-0.002	-0.002	-0.009	-0.009
Average	-0.001	0.012	-0.003	0.010

Regarding the HMID (Table 6-10), significant alterations can be founded at 0k-2k, where the differences between SR1 and SR2 are about 10% at 1k and 2% at 2k. The higher SR sediment in SR2 can facilitate the bar and riffle formations, and thus lead to lower HMID than SR1. It can be expected that the GUSI-D and H values will be enhanced in this region.

Table 6-10 The results of HMID for scenarios of SR arrangement. The variation is calculated based on the initial condition (before SR).

Distance from SR site (km)	HMID							
	SC-SR1-S		SC-SR2-S		SC-SR1-D		SC-SR2-D	
	Value	Variation	Value	Variation	Value	Variation	Value	Variation
0-1	**10.118**	**1.9%**	**9.132**	**-8.0%**	**10.680**	**7.6%**	**9.622**	**-3.1%**
1-2	**11.833**	**5.7%**	**12.004**	**7.3%**	**11.780**	**5.3%**	**11.597**	**3.6%**
2-3	11.052	10.8%	11.049	10.8%	11.518	15.5%	11.595	16.2%
3-4	9.919	4.9%	9.879	4.4%	9.877	4.4%	9.827	3.9%
4-5	12.282	8.5%	12.250	8.2%	12.363	9.2%	12.358	9.1%
5-6	11.528	1.8%	11.508	1.7%	11.335	0.1%	11.305	-0.1%
6-7	9.318	18.9%	9.340	19.2%	9.616	22.7%	9.608	22.6%
7-8	12.327	13.8%	12.357	14.0%	12.497	15.3%	12.495	15.3%
8-9	9.215	7.8%	9.202	7.6%	9.685	13.3%	9.687	13.3%
9-10	9.048	-0.6%	9.184	0.9%	9.269	1.8%	9.260	1.7%
10-11	10.704	14.5%	10.707	14.6%	10.882	16.4%	10.895	16.6%
11-12	18.285	18.2%	18.122	17.2%	18.201	17.7%	18.177	17.5%
12-13	11.257	4.8%	11.245	4.6%	11.106	3.4%	11.098	3.3%
Average	11.299	8.7%	11.229	8.1%	11.447	10.2%	11.348	9.2%

6.4. Recommendations for optimization of replenishment works

6.4.1. Recommendations for promoting the SR erosion

Based on the previous results from different scenarios, several factors have significant impacts on SR erosion. The flushing flow as the driving force is the most influenced parameter. Higher flushing magnitude can lead to more SR erosion and promote the transportation of SR sediment. An optimal value of flushing magnitude is existed, which can be considered as the efficient discharge for SR erosion (Figure 6-7). Nevertheless, it is not efficient to increase the magnitude of a single flood pulse for promoting SR erosion since the TR only increases by 2% when the flushing magnitude enlarges 100% (Figure 6-6). There are rare significant floods that occurred recently in the Nagayasuguchi dam, which also indicates that an increase in flushing magnitude is difficult to implement under the consideration of dam management. Alternative countermeasures are developed by adding the frequency of floods instead of increasing the magnitude (multiple flood pulses). The TR is promoted if we utilize the same TFWV during flushing but add another flood pulse (Figure 6-18). Implementing this option is more feasible than the single flood pulse since it is quite similar to one strategy of dam operation called 'Pre-releasing'. The dam operator usually releases some storage water before floods to reduce the flood peak. It is beneficial for dam safety and downstream flood prevention. Despite

this, the releasing magnitude is still crucial since it affects the sediment movement and submerged ratio of the SR stockpile. It is recommended to maintain the same magnitude of both peaks to maximize the SR efficiency.

The grain size of replenished material is also vital for SR erosion. Decreasing the size of SR sediment can significantly promote the TR from 5% to 15%. It is efficient to facilitate SR erosion by increasing the percentage of finer sediment (<7 mm). Nevertheless, such finer sediment may be difficult to obtain from upstream sediment sources, which limits the feasibility of this countermeasure. The managers must deal with the balance between the availability of sediment sources, transported distance from the sediment source, and the cost-benefit of replenishment.

Reshaping and altering the locations of SR stockpiles is an alternative approach for promoting SR erosion which has already been conducted in the Buëch River (Guillaume BROUSSE et al., 2022). Shifting the location to the middle, reducing the height, and increasing the length (SC-SR1) can promote SR erosion, however, the eroded sediment can not efficiently be transported downstream due to the impacts of topography (deep pool and meandering channel). Arranging another stockpile at the left bank (SC-SR2) is more adaptable to increase the erosion rate as shown by the increase of TR (Table 6-8). Re-arranging the existing sediment or placing the new sediment from the downstream source to the left bank should be considered an optimal way to create the additional stockpile. However, reconstruction of the SR site could be complex and expensive since the manager needs to modify the bank at first to make the accessibility of dump trucks and workers. It is worthwhile to evaluate implementing the cost and benefits of downstream restoration.

6.4.2. Recommendations for promoting downstream hydro-geomorpho-ecology

The flushing flow is the main factor that influenced the downstream geomorphological changes. The higher magnitude of flow can promote riverbed aggradation and degradation, and thus facilitate the pool and bar formation while destroying the existing riffles at the meandering area. To maintain the hydro-morphogy and ecology at the same time, the implementation of double flood pulses are recommended since it can protect against the erosion of riffles in some areas where HMID is decreasing.

Due to the fact that the simulated period is short, the downstream impacts of SR sediment are limited. The differences in HMID between each case are limited and only higher BCI can be noticed near the

SR site for fine sediment due to the formation of point bars (Figure 6-13). The medium and coarse sediment cases require long-term simulation to investigate the riverbed responses since they need a higher driving force (flushing flow) for movement. Comparing the riverbed aggradation and degradation, the bed amouring is the dominant problem that river managers should be considered to vary the composition of SR sediment. It is difficult to investigate such issues in the current models and will be considered in the future.

Regarding the new arrangement of the SR site, the SR2 combined with double flood pulses leads to aggradation at 0k-2k, which further reduces the HMID. The higher sediment supply from SR can facilitate the riffles and bars formation and finally give rise to a higher GUSI-D and H value.

6.4.3. Summarized strategies for optimization of SR

Figure 6-28 summarized the strategies for the optimization of SR works in the Naka River. Considering the downstream flood risks and limitation of releasing flow (dry seasons), increasing flushing frequency is more efficient than flushing magnitude for promoting SR erosion and downstream hydro-geomorpho-ecology. Regarding the SR material, increasing the percentage of finer sediment can significantly enhance SR erosion. Nevertheless, the optimal composition of SR sediment requires the consideration of long-term downstream responses and the available sediment sources and will be investigated in the future. The implementation of double stockpiles is more efficient to increase the sediment supply from the SR site and thus beneficial for downstream restoration. However, such a countermeasure needs further evaluation on its feasibility since the requirements of funds and technical support are higher.

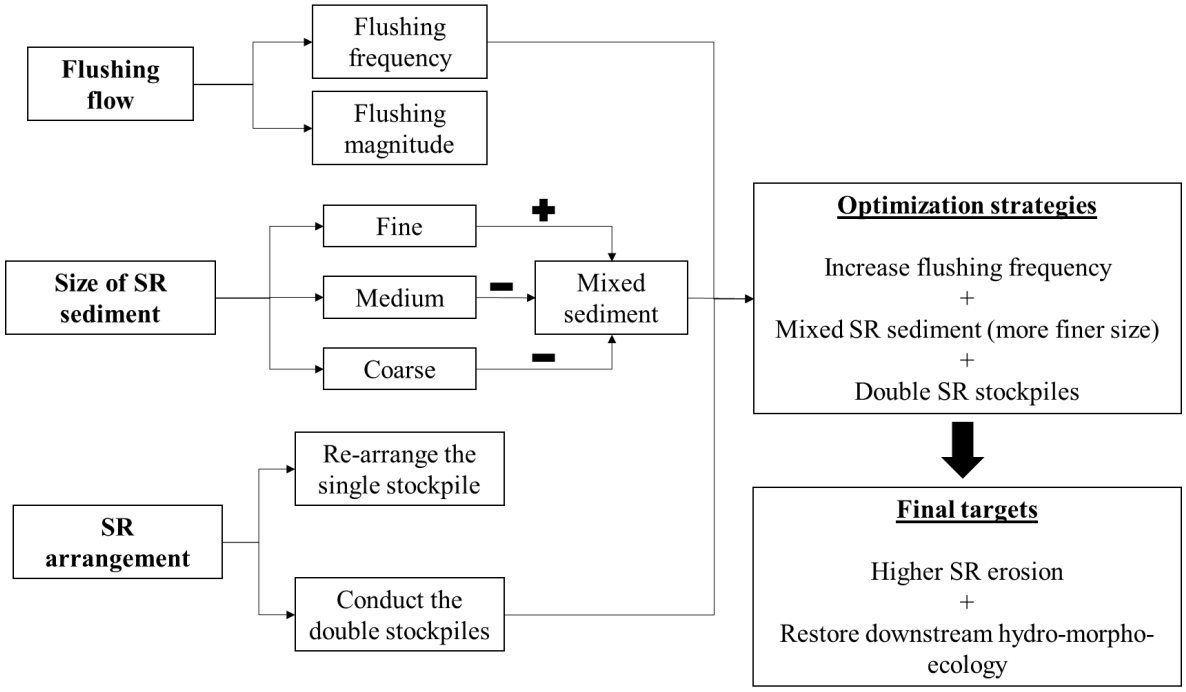

Figure 6-28 The flow chart of recommendations for SR optimization in the Naka River.

An additional long-term simulation was conducted to investigate the effects of the recommended strategies. We utilized the combined hydrograph that created in Chapter 5 as the boundary condition (Figure 5-11), which included all the flood events in 2018 and 2019. The SR site was re-designed to double stockpiles as recommended before. Moreover, we removed the coarsen sediment in the original SR material (D50=40mm), and replaced it into the finer one (D50=3mm) to enhance the SR erosion (Table 6-11).

Table 6-11 The comparison of SR material between original case and modified case

Case	Sediment size (mm)			
	40	**10**	**3**	**0.5**
Original (%)	**17**	45	**28**	10
Modified (%)	**0**	45	**45**	10

Regarding the results, the modified case can efficiently promote the erosion at the SR site. The eroded volume increased from 20375 m^3 to 30550 m^3, and the TR raised from 13% to 20%. The higher supply

of median gravels from SR site can successfully accumulated in the downstream reach, and we can observe that the riverbed of modified case was coarser than the original case (Figure 6-29). Furthermore, the HMID was also varied due to the modify of the SR strategy. Both the original case and the modified case can promote the HMID value at the entire reach Figure 6-29. Higher HMID can be noticed at 0k-1k area under modified case since the higher sediment supply created a bar-pool habitat structure here. At the rest area, the HMID is lower than the original case as the accumulated sediment is higher and more riffles are expected to be formatted. Such hydro-morphological variation can promote the H value of fish diversity and be beneficial for the downstream ecology.

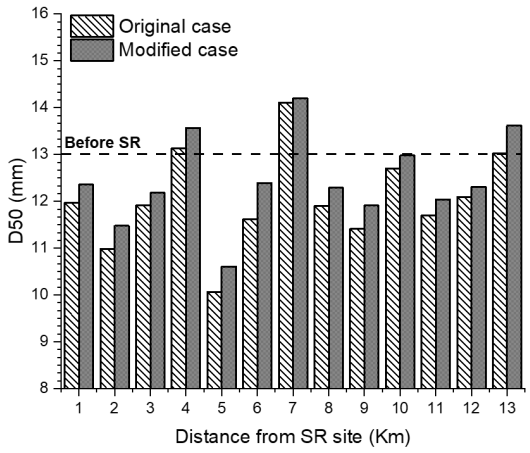

Figure 6-29 The comparison of D50 between original case and modified case after long-term simulation.

Table 6-12 The comparison of HMID between original case and modified case after long-term simulation.

Distance from SR site (km)	HMID			
	Original case		Modified case	
	Value	Variation	Value	Variation
0-1	11.171	13%	11.474	16%
1-2	14.013	25%	13.890	24%
2-3	13.421	35%	13.291	33%
3-4	11.641	23%	11.395	20%
4-5	13.705	21%	13.409	18%
5-6	13.894	23%	13.499	19%
6-7	11.100	42%	10.894	39%
7-8	15.020	39%	14.757	36%
8-9	10.897	27%	10.576	24%
9-10	10.707	18%	10.379	14%
10-11	12.193	30%	11.782	26%
11-12	18.774	21%	17.836	15%
12-13	11.887	11%	11.660	9%
Average	12.956	25%	12.680	22%

Chapter 7. Conclusions and recommendations

In this study, the implementation of SR and its downstream eco-hydro-geomorphological effects were investigated based on the case study in the Naka River, Japan, and the Buëch River, France. Various approaches were utilized for data collection and investigation, including field surveys, statistical analyses, and numerical simulations. Specifically, the image-based approach, BASEGRAIN, was used to estimate the grain size distribution of four gravel bars from high-quality photos taken during field investigation. Two notable non-inclusive velocimetry methods, LSPIV and STIV, were applied to measure the real-time flow patterns near the replenishment sites. Then, by combining the data collected from the field survey and the River office, we conducted the comprehensive assessment of replenishment works in the Naka River and the Buëch River considering the erosion efficiency of replenished sediment and downstream eco-hydro-geomorphological impacts. Several assessment indicators and factors were considered for statistical analysis, including TR, GUSI, HMID, H value, BCI, and riverbed substrates. Regarding the numerical simulation, TELEMAC-2D coupled with Gaia was applied. The established model was then used for simulating the different designed scenarios to investigate the impacts of flushing flow and replenishment characteristics. In the end, recommendations for the optimization of replenishment works were illustrated based on the assessment results of different scenarios.

The main findings of the study can enhance the understanding of relationships between SR implementation and its downstream hydro-geomorpho-ecological impacts. It can further provide references for SR design and arrangement. The key conclusions of the study and a summary of recommendations for future works are demonstrated below.

7.1. Conclusions

The following conclusions were obtained from the field measurement of gravel bars, SSC and flow regime in the Naka River:

- The implementation of SR and the meandering channels leads to spatial and temporal variation of gravel bars in the Naka River. At the convex of the meandering channel, the SR facilitates the construction of multiple point bars, such as gravel bar 2, where a uniform distribution of fine sediment can be observed. Depending on the locations of the bars, varied

coarsening and fining tendencies can be seen from the bar head to the bar tail. Locations with lower flow velocity and bed shear stress may cause increased aggradation of fine sediment from the replenishment site, and as a result, finer tendencies are anticipated in those areas (bar head of gravel bar 1). On the other hand, a greater bed shear stress and higher dissipation area could result in grain coarsening (gravel bar 4). The temporal fluctuation in grain size is also caused by such variations in erosion and deposition area. Since the replenished sediment is the source of the bar, fining or a consistent trend of grain size may always be recognized as those aggraded areas annually. However, the area subject to erosion may be more sensitive to changes in the sediment supply from the SR site.

- A counter-clockwise hysteresis can be observed in the discharge-SSC relationship. The turbidity meter can be utilized to calibrate the numerical model or estimate the missing SSC in the Naka River.
- The LSPIV and STIV can successfully be utilized to measure the real-time surface flow in the Naka River. The LSPIV is helpful for the generation of flow maps and is useful for us to understand the flow regime near the SR site. However, this approach is more intricate and sensitive to the clear surface seedings, and we can observe some errors that occurred in the low-flow areas. The STIV can provide us with an acceptable flow velocity along the cross-section, allowing for a more precise computation of flow discharge than LSPIV.
- The TKE method can not be utilized to accurately estimate the water depth due to several reasons, including: (1) the inaccurate flow velocity estimation by LSPIV; (2) the complex flow conditions near the SR site which can not be assumed as uniform flow; (3) the higher errors when calculating dissipation rate by LOW in deep water areas; (4) The lack of calibration of several model parameters, including model constant, manning value, and the ratio of depth-average velocity.

The following conclusions were achieved regarding the assessment of SR works in the Naka River and the Buëch River:

- Regarding the SR erosion, the current location and geometry of the SR stockpile in the Naka River are not efficient (TR less than 50%) and the remaining sediment is higher. The placement of huge amounts of sediment at one site is not efficient and requires higher flushing flow to promote erosion. It is recommended to divide the single-placed location into multiple sites to accelerate SR erosion.

- The SR sediment can be efficiently transported in the Buëch River (TR greater than 65 %) due to the adaptable management of stockpiles. Moving the sediment from the low erosion area (left bank) to the high erosion area (middle of the channel) can enhance SR erosion and transportation (TR increase of 13%). The lack of sufficient flushing flow from the upstream dam is the main reason that restricts the further erosion of SR sediment.
- The implementation of SR contributes to the restoration of downstream hydro-geomorpho-ecology in the Naka River and the Buëch River. The additional sediment supply combined with flushing flow can assist the generation of new geomorphic units, especially the riffles (higher GUSI-D). However, no new types of units are detected which leads to the reduction of GUSI-R. Such newly formatted riffles are beneficial for the habitat quality and thus lead to a promotion of H value. Yet, it can be noticed that the HMID has a negative correlation with the GUSI-D, which means that the riffles may not suitable for enhancing the hydro-geomorphological quality. Moreover, the amouring issues can be efficiently resolved as more medium-sized gravels from the SR site were accumulated to enrich the sediment compositions of the riverbed. In addition, the SR sediment can promote the riverbed aggradation downstream (higher BCI). It can be expected more riffles and bars are generated, which is beneficial for habitat quality and diversity. Nevertheless, the increase in riverbed level will also intensify the flood risk at downstream reach, and further discussion should be conducted to balance the impacts. Considerable amounts of SR sediment may result in adverse impacts on habitat quality and an annual transported volume of around 100,000 m^3 is optimal for continuous restoration in the Naka River.

The following conclusion was obtained based on the 2D numerical simulation of SR in the Naka River:

- The TELEMAC-2D model coupled with Gaia can be successfully utilized to simulate the hydrodynamics and sediment transport in the Naka River. However, the model can not be fully calibrated and validated due to the lack of data, and limitations still occur in the simulation of the bank erosion process.
- The higher magnitude of flushing flow can promote the erosion of SR sediment. However, it is not an efficient way since the increasing rate of TR is only about 2% if the flushing magnitude is enlarged by 100%. The higher magnitude can only increase the eroded volume at the top area of the stockpile due to the increase in the submerged ratio. The

promotion of near bank erosion is limited since the flow velocity and corresponding shear stress are not dramatically increasing. In terms of downstream responses, higher flushing flow can promote the sediment erosion and deposition processes, and we can observe more riverbed aggradation and degradation along the reach. In the meandering areas, more erosion can be observed in the concave area to promote the formation of pools, while more deposition can be detected in the convex area to facilitate the formation of bars. Such geomorphological changes increase the variation of flow velocity and water depth, and thus, contribute to the increase of HMID. Nevertheless, extremely higher flushing flow may not beneficial for the maintenance of riffles, which means that the GUSI-D and H values may be reduced and it is harmful to the habitat quality.

- Considering the same volume of flushing flow, introducing an additional flood pulse can efficiently facilitate SR erosion, and the eroded volume and TR are enhanced by about 1.5% compared to the case of a single flood pulse. More erosion can be detected at the head and tail areas where the second flood pulse can further promote the transportation of deposited sediment after the first pulse. Moreover, it can be noticed that a medium flow combined with a medium duration can result in the highest SR erosion, which reveals the importance of balance between magnitude and duration. In terms of downstream responses, overall, the double flood pulses increase the deposited volume of sediment along the reach (positive BCI), especially near the SR site, where SR sediment is mainly accumulated. Different geomorphological responses can be observed in different areas since the shear stress and corresponding sediment movement are varied. Such alterations give rise to less promotion of average HMID (less than 5%)
- Adding the percentage of fine sediment in the composition of SR material can significantly enhance SR erosion. The greater amounts of SR sediment can assist in the formation of bars near the SR site. However, it can not be concluded that medium and coarse sediment is not beneficial for SR implementation as they need a long-term period to affect the downstream reach. The size of SR material mainly depends on the upstream sediment sources and the requirements of habitat structures establishment downstream. Further discussion should be conducted to investigate the best composition of SR material.
- The erosion rate of SR is promoted by reducing the height, increasing the length, and shifting the locations of the current stockpile (higher eroded volume and TR).

Nevertheless, the eroded sediment can not be efficiently transported downstream since the existing pool at the head area and the meandering channel at the tail area restricts the sediment movement. Constructing an additional stockpile at the left bank is the most efficient countermeasure. It not only narrows the channel to increase the flow velocity and submerged ratio but also provides an additional replenishment source. Despite this, it can also be noticed that a single flood pulse can further promote SR erosion instead of the double one. The stockpiles are nearly submerged during peak discharge, which significantly increases the eroded volume at the top area. However, considering the downstream responses, the case of double flood pulses combined with double stockpiles is recommended as it can not only keep the HMID in an optimal range but also avoid the higher erosions of riffles. The second pulse can further promote sediment transportation, which is beneficial for the enhancement of habitat suitability away from the SR site.

7.2. Recommendations for future works

According to the results and limitations that concluded before, some general recommendations for future works and developments are summarized, including:

- A comprehensive monitoring system is crucial for the investigation and research of river restorations. In the Naka River, the types of field surveys and measurements are extensive, which are helpful for our assessment of downstream impacts. Nevertheless, some survey was not conducted continuously, which means that it is difficult for us to investigate the time-varied responses of SR. It is recommended to establish a systematic program of field surveys to further assist the understanding of downstream hydro-geomorpho-ecology in the Naka River. Regarding the Buëch River, the research mainly focused on SR erosion and downstream geomorphological alterations. It is recommended to conduct additional measurements related to aquatic habitats to evaluate the ecological impacts of SR.
- The image-based approach was successfully utilized in the Naka River to monitor the real-time flow patterns. Additional calibration should be implemented to enhance the accuracy of the results if we can collect field measurement data of bathymetry, flow velocity, water depth, and GCPs. In the future, this approach can be expanded to be utilized in the investigation of the erosion process of SR. New cameras have already been installed in May 2022, which

provide additional angles to assist the construction of the DEM model by the SFM approach (Structure from motion). The time-varied erosion and deposition of the SR stockpile are able to be investigated by comparison of different DEM models at different times.

- Although the 2D numerical model was established by TELEMAC-2D coupled with Gaia in the Naka River, model calibration and validation should be further implemented in the future. Specifically, the erosion process of SR should be calibrated if we can measure the DEM of the SR site before and after one flood event. The eroded volume, the erosion and deposition areas, as well as the cross sections of the SR stockpile can assist us to adjust the angle of repose, the active layer thickness, and the critical shied parameter to present a more similar erosion process of SR. Regarding the hydrodynamics and geomorpho-dynamics, it is recommended to construct some monitoring gauges downstream of the SR site to provide more measured data of flow velocity, water depth, or SSC, which helps stabilize the boundary conditions and calibrate the model parameters.
- The downstream geomorpho-ecology requires optimal flushing flow combined with optimal volume and sediment supply from the SR site to maintain its positive functionality. In the Naka River, owing to the lack of flood events recently, the downstream reach is expected to be 'hungry' of environmental flow and sediment. According to the current situation, it is recommended to reduce the magnitudes but increase the flushing frequency of flow, which can not only facilitate SR erosion but also maintain the positive impacts toward downstream geomorpho-ecology. Furthermore, finer SR material is also recommended to promote SR efficiency. However, the dam owner should consider the availability of sediment sources and the adverse impacts of downstream reach (higher turbidity). Regarding the arrangement of the SR site, separating the placed locations of SR sediment (multiple SR sites) is recommended to facilitate the sediment supply under lower flow. The double stockpiles at Kohama can be considered a feasible plan to be discussed. In the future, potential SR locations downstream will be investigated if the dam owners aim to restore the geomorpho-ecology at specific areas.
- Owing to the adaptable arrangement of the SR site, the accumulated sediment was efficiently transported downstream and resulted in positive impacts on geomorpho-ecology in the Buëch River. Nevertheless, the SR works have already been stopped recently due to the lack of sediment sources and the consideration of higher costs. Such one-time SR is not beneficial for maintaining the positive responses at downstream reach as the sediment transportation

and the geomorphological alterations are a long-term process. If the stakeholders aim to restore the long-term effects of dam construction, it is recommended to continuously implement the SR works by maintaining the current SR site annually (add sediment and reshape the stockpile) in the Buëch River.

References

Aguirre, D., Bui, M., Giehl, S., Reisenbüchler, M., & Rutschmann, P. (2020). *Development of a hydro-morphodynamic Model for Sediment Management in the Rosenheim Reservoir*.

Al-mamari, M., Kantoush, S., Kobayashi, S., Sumi, T., & Saber, M. (2019). Real-Time Measurement of Flash-Flood in a Wadi Area by LSPIV and STIV. *Hydrology, 6*(1). doi:10.3390/hydrology6010027

Alemu, M. M. (2016). Integrated watershed management and sedimentation. *Journal of Environmental Protection, 7*(4), 490-494.

Arcement, G. J., & Schneider, V. R. (1989). Guide for selecting Manning's roughness coefficients for natural channels and flood plains.

Ashworth, P. (1996). Mid-Channel bar growth and its relationship to local flow strength and direction. *Earth Surface Processes and Landforms, 21*, 103-123. doi:10.1002/(SICI)1096-9837(199602)21:2<103::AID-ESP569>3.0.CO;2-O

Audouin, Y., Benson, T., Delinares, M., Fontaine, J., Glander, B., Huybrechts, N., . . . Walther, R. (2019). *Introducing GAIA, the brand new sediment transport module of the TELEMAC-MASCARET system*.

Babej, J., Máčka, Z., Ondrejka, P., & Peterova, P. (2016). Surface grain size variation within gravel bars: A case study of the River Opava, Czech Republic. *Geografia Fisica e Dinamica Quaternaria, 39*, 3-12. doi:10.4461/GFDQ.2016.39.1

Batalla, R. J. (2003). Sediment deficit in rivers caused by dams and instream gravel mining. A review with examples from NE Spain. *Cuaternario y geomorfología: Revista de la Sociedad Española de Geomorfología y Asociación Española para el Estudio del Cuaternario, ISSN 0214-1744, Vol. 17, Nº. 3-4, 2003, pags. 79-91, 17*.

Battisacco, E. (2016). *Replenishment of sediment downstream of dams: erosion and transport processes*. Retrieved from

Battisacco, E., Franca, M. J., & Schleiss, A. J. (2016). Sediment replenishment: Influence of the geometrical configuration on the morphological evolution of channel-bed. *Water Resources Research, 52*(11), 8879-8894. doi:10.1002/2016wr019157

Bel, C., Jodeau, M., Tassi, P., Claude, N., & Haddad, H. (2019). *Calibration and validation strategy for 2D hydrodynamic modelling: application to morphodynamics of a gravel-bed river with*

suspended sediments. Paper presented at the XXVIth TELEMAC-MASCARET User Conference, 15th to 17th October 2019, Toulouse.

Belletti, B., Rinaldi, M., Comiti, F., Nardi, L., Mao, L., & Bussettini, M. (2015). *The Geomorphic Units survey and classification System (GUS).* Paper presented at the Proceedings IS Rivers, 2nd International Conference.

Binh, D. V., Kantoush, S. A., Ata, R., Tassi, P., Nguyen, T. V., Lepesqueur, J., . . . Sumi, T. (2022). Hydrodynamics, sediment transport, and morphodynamics in the Vietnamese Mekong Delta: Field study and numerical modelling. *Geomorphology, 413*, 108368. doi:10.1016/j.geomorph.2022.108368

Bosa, S., Petti, M., & Pascolo, S. (2018). Numerical Modelling of Cohesive Bank Migration. *Water, 10*(7). doi:10.3390/w10070961

Brevis, W., Niño, Y., & Jirka, G. (2011). Integrating cross-correlation and relaxation algorithms for particle tracking velocimetry. *Experiments in Fluids, 50*(1), 135-147.

Brousse, G., Arnaud‐Fassetta, G., Liébault, F., Bertrand, M., Melun, G., Loire, R., . . . Borgniet, L. (2019). Channel response to sediment replenishment in a large gravel‐bed river: The case of the Saint‐Sauveur dam in the Buëch River (Southern Alps, France). *River Research and Applications, 36*(6), 880-893. doi:10.1002/rra.3527

BROUSSE, G., Jodeau, M., & CORDIER, F. (2022). Replenishment study in gravel bed rivers by 2D numerical morphodynamic modelling. *TSMR*. Retrieved from https://www.barrages-cfbr.eu/IMG/pdf/j4_colloque_tsmr-cfbr_2022_brousse.pdf

Cajot, S., Schleiss, A., Sumi, T., & Kantoush, S. (2012). *Reservoir sediment management using replenishment: a numerical study of Nunome Dam.* Paper presented at the Proceedings (on CD) of the International Symposium on Dams for a changing world-80th Annual Meeting and 24th Congress of CIGB-ICOLD.

Cao, Z., Pender, G., & Meng, J. (2006). Explicit Formulation of the Shields Diagram for Incipient Motion of Sediment. *Journal of Hydraulic Engineering-asce - J HYDRAUL ENG-ASCE, 132*. doi:10.1061/(ASCE)0733-9429(2006)132:10(1097)

Chardon, V., Piasny, G., & Schmitt, L. (2021). Comparison of software accuracy to estimate the bed grain size distribution from digital images: A test performed along the Rhine River. *River Research and Applications*. doi:10.1002/rra.3910

Cordier, F., Tassi, P., Claude, N., Crosato, A., Rodrigues, S., & Pham Van Bang, D. (2019). Numerical Study of Alternate Bars in Alluvial Channels With Nonuniform Sediment. *Water Resources Research, 55*(4), 2976-3003. doi:https://doi.org/10.1029/2017WR022420

Creutin, J., Muste, M., Bradley, A., Kim, S., & Kruger, A. (2003). River gauging using PIV techniques: a proof of concept experiment on the Iowa River. *Journal of Hydrology, 277*(3-4), 182-194.

Dal Sasso, S., Pizarro, A., Samela, C., Mita, L., & Manfreda, S. (2018). Exploring the optimal experimental setup for surface flow velocity measurements using PTV. *Environmental monitoring and assessment, 190*(8), 1-14.

Detert, M., & Weitbrecht, V. (2013). User guide to gravelometric image analysis by BASEGRAIN.

Die Moran, A., el Kadi Abderrezzak, K., Mosselman, E., Habersack, H., Lebert, F., Aelbrecht, D., & Laperrousaz, E. (2013). Physical model experiments for sediment supply to the old Rhine through induced bank erosion. *International Journal of Sediment Research, 28*, 431–447. doi:10.1016/S1001-6279(14)60003-2

Dottori, F., Martina, M., & Todini, E. (2009). A dynamic rating curve approach to indirect discharge measurement. *Hydrology and Earth System Sciences, 13*(6), 847-863.

El Kadi Abderrezzak, K., Die Moran, A., Tassi, P., Ata, R., & Hervouet, J.-M. (2016). Modelling river bank erosion using a 2D depth-averaged numerical model of flow and non-cohesive, non-uniform sediment transport. *Advances in Water Resources, 93*, 75-88. doi:https://doi.org/10.1016/j.advwatres.2015.11.004

Esmaeili, T., Sumi, T., Kantoush, S. A., Kubota, Y., Haun, S., & Rüther, N. (2017). Three-Dimensional Numerical Study of Free-Flow Sediment Flushing to Increase the Flushing Efficiency: A Case-Study Reservoir in Japan. *Water, 9*(11), 900. Retrieved from https://www.mdpi.com/2073-4441/9/11/900

Estrany, J., & Garcia, C. (2005). Monitoring suspended sediment fluxes in the Na Borges basin, Mallorca, Spain. *IAHS-AISH Publication*, 117-123.

Fan, J., & Morris, G. L. (1992). Reservoir sedimentation. II: Reservoir desiltation and long-term storage capacity. *Journal of Hydraulic Engineering, 118*(3), 370-384.

Fleet, D. J. (2012). *Measurement of image velocity* (Vol. 169): Springer Science & Business Media.

Flokstra, C., & Koch, F. (1980). *Bed level computations for curved alluvial channels*.

French, R. H., & French, R. H. (1985). *Open-channel hydraulics*: McGraw-Hill New York.

Friedl, F. (2017). *Laboratory experiments on sediment replenishment in gravel-bed rivers.* ETH Zurich,

Fujita, I. (2017). Discharge Measurements of Snowmelt Flood by Space-Time Image Velocimetry during the Night Using Far-Infrared Camera. *Water, 9*(4), 269. Retrieved from https://www.mdpi.com/2073-4441/9/4/269

Fujita, I., KITADA, M., SHIMONO, M., KITSUDA, T., YOROZUYA, A., & MOTONAGA, Y. (2017). Spatial measurements of snowmelt flood by image analysis with multiple-angle images and radio-controlled ADCP. *Journal of JSCE, 5*(1), 305-312.

Fujita, I., & Komura, S. (1994). Application of video image analysis for measurements of river-surface flows. *Proceedings of hydraulic engineering, 38*, 733-738.

Fujita, I., Muste, M., & Kruger, A. (1998). Large-scale particle image velocimetry for flow analysis in hydraulic engineering applications. *Journal of hydraulic Research, 36*(3), 397-414.

Fujita, I., Notoya, Y., & Shimono, M. (2015). *Development of UAV-based river surface velocity measurement by STIV based on high-accurate image stabilization techniques.* Paper presented at the E-proceedings of the 36th IAHR World Congress.

Fujita, I., Notoya, Y., Tani, K., & Tateguchi, S. (2019). Efficient and accurate estimation of water surface velocity in STIV. *Environmental Fluid Mechanics, 19*(5), 1363-1378.

Fujita, I., Watanabe, H., & Tsubaki, R. (2007). Development of a non‐intrusive and efficient flow monitoring technique: The space‐time image velocimetry (STIV). *International Journal of River Basin Management, 5*(2), 105-114.

Gaeuman, D. (2008). Recommended quantities and gradation for long-term coarse sediment augmentation downstream from Lewiston Dam. *Trinity River Restoration Program, TM-TRRP-2008, 2*.

Gaeuman, D. (2014). *Analyses to support gravel augmentation recommendations for the Trinity River, California*. Retrieved from Weaverville, California:

Gaeuman, D., Krause, A. (2013). *Assessment of pool depth changes in the Trinity River between Lewiston Dam and the North Fork Trinity River*. Retrieved from Weaverville, California:

González del Tánago, M., Gurnell, A. M., Belletti, B., & García de Jalón, D. (2015). Indicators of river system hydromorphological character and dynamics: understanding current conditions and guiding sustainable river management. *Aquatic Sciences, 78*(1), 35-55. doi:10.1007/s00027-015-0429-0

Gostner, W., Alp, M., Schleiss, A. J., & Robinson, C. T. (2012). The hydro-morphological index of diversity: a tool for describing habitat heterogeneity in river engineering projects. *Hydrobiologia, 712*(1), 43-60. doi:10.1007/s10750-012-1288-5

Gostner, W., Parasiewicz, P., & Schleiss, A. (2013). A case study on spatial and temporal hydraulic variability in an alpine gravel-bed stream based on the hydromorphological index of diversity. *Ecohydrology, 6*, 652-667. doi:10.1002/eco.1349

Guillaume, B., Bertrand, M., Arnaud-Fassetta, G., Liébault, F., Borgniet, L., Melun, G., . . . Fantino, G. (2018). *Monitoring of a sediment replenishment operation: The case of the Saint-Sauveur dam in the Buëch River (Southern Alps, France)*.

Gunawan, B., Sun, X., Sterling, M., Shiono, K., Tsubaki, R., Rameshwaran, P., . . . Fujita, I. (2012). The application of LS-PIV to a small irregular river for inbank and overbank flows. *Flow Measurement and Instrumentation, 24*, 1-12.

Hagstrom, C. A., Leckie, D. A., & Smith, M. G. (2018). Point bar sedimentation and erosion produced by an extreme flood in a sand and gravel-bed meandering river. *Sedimentary Geology, 377*, 1-16. doi:https://doi.org/10.1016/j.sedgeo.2018.09.003

Harpold, A., Mostaghimi, S., Vlachos, P. P., Brannan, K., & Dillaha, T. (2006). Stream discharge measurement using a large-scale particle image velocimetry (LSPIV) prototype. *Transactions of the ASABE, 49*(6), 1791-1805.

Hauet, A., Creutin, J.-D., & Belleudy, P. (2008). Sensitivity study of large-scale particle image velocimetry measurement of river discharge using numerical simulation. *Journal of Hydrology, 349*(1-2), 178-190. doi:10.1016/j.jhydrol.2007.10.062

Heckmann, T., Haas, F., Abel, J., Rimböck, A., & Becht, M. (2017). Feeding the hungry river: Fluvial morphodynamics and the entrainment of artificially inserted sediment at the dammed river Isar, Eastern Alps, Germany. *Geomorphology, 291*, 128-142. doi:10.1016/j.geomorph.2017.01.025

Hiroshi, M., & Parker, G. (2012). Numerical simulation of low-flow channel evolution due to sediment augmentation. *International Journal of Sediment Research, 27*(3), 351-361.

Hyodo, M. (2015). Ecological Evaluation of Shifting Habitat History for Riverbed Management.

Ioana-Toroimac, G., Zaharia, L., & Minea, G. (2015). Using Pressure and Alteration Indicators to Assess River Morphological Quality: Case Study of the Prahova River (Romania). *Water, 7*(12), 2971-2989. doi:10.3390/w7062971

Ishigaki, T. (2004). Scouring and flow structure around an attracting groin. *River Flow 2004, 1*, 521-525. Retrieved from https://cir.nii.ac.jp/crid/1573105975504413312

Izumi, N., & Aoki, A. (2012). Linear stability analysis of river meander with gradual bed aggradation/degradation. *Journal of Japan Society of Civil Engineers, Ser. A2 (Applied Mechanics (AM)), 68*(2), I_609-I_616. doi:10.2208/jscejam.68.I_609

Javed, A., Hamshaw, S., Rizzo, D., & Lee, B. (2019). *Analysis of Hydrological and Suspended Sediment Events from Mad River Wastershed using Multivariate Time Series Clustering*.

Jin, T., & Liao, Q. (2019). Application of large scale PIV in river surface turbulence measurements and water depth estimation. *Flow Measurement and Instrumentation, 67*, 142-152.

Johnson, E. D., & Cowen, E. A. (2017). Estimating bed shear stress from remotely measured surface turbulent dissipation fields in open channel flows. *Water Resources Research, 53*(3), 1982-1996.

Juez, C., Battisacco, E., Schleiss, A. J., & Franca, M. J. (2016). Assessment of the performance of numerical modeling in reproducing a replenishment of sediments in a water-worked channel. *Advances in Water Resources, 92*, 10-22. doi:10.1016/j.advwatres.2016.03.010

Kantoush, S., & Schleiss, A. J. (2009). Large-scale PIV surface flow measurements in shallow basins with different geometries. *Journal of Visualization, 12*(4), 361-373.

Kantoush, S., & Sumi, T. (2011). *Sediment replenishing measures for revitalization of Japanese rivers below dams.* Paper presented at the Proceedings of the 34th World Congress of the International Association for Hydro-Environment Research and Engineering: 33rd Hydrology and Water Resources Symposium and 10th Conference on Hydraulics in Water Engineering.

Kantoush, S., & Sumi, T. (2016). The aging of Japan's dams: Innovative technologies for improving dams water and sediment management. In (pp. 1030-1037).

Kantoush, S., Sumi, T., & Kubota, A. (2010). Geomorphic response of rivers below dams by sediment replenishment technique. *River Flow 2010*, 1155-1164.

Kantoush, S., Sumi, T., Kubota, A., & Suzuki, T. (2010). Impacts of sediment replenishment below dams on flow and bed morphology of river.

Kantoush, S., Sumi, T., Suzuki, T., & Murasaki, M. (2010). Impacts of sediment flushing on channel evolution and morphological processes: Case study of the Kurobe River, Japan. *River Flow 2010*, 1165-1176.

Kantoush, S. A., & SUMI, T. (2010). River morphology and sediment management strategies for sustainable reservoir in Japan and European Alps. *京都大学防災研究所年報. B= Disaster Prevention Research Institute Annuals. B, 53*(B), 821-839.

Kantoush, S. A., Suzuki, T., Takemon, Y., Abderrezzak, K. E. k., Ata, R., Sumi, T., & Saber, M. (2018). *Numerical study on reservoir sediment management through adding excavated sediment downstream of dams in Japan*.

Kiku, M., Nakamura, T., & Mizutani, N. (2017). ESTIMATION OF GRAVEL GRAIN SIZE FROM AERIAL PHOTOS USING UAV AT SHICHIRI-MIHAMA COAST. *Journal of Japan Society of Civil Engineers, Ser. B3 (Ocean Engineering), 73*(2), I_588-I_593. doi:10.2208/jscejoe.73.I_588

Kim, Y., Muste, M., Hauet, A., Krajewski, W. F., Kruger, A., & Bradley, A. (2008). Stream discharge using mobile large‐scale particle image velocimetry: A proof of concept. *Water Resources Research, 44*(9).

Kobayashi, S., Kantoush, S. A., Al-Mamari, M. M., Tazumi, M., Takemon, Y., & Sumi, T. (2022). Local flow convergence, bed scour, and aquatic habitat formation during floods around wooden training structures placed on sand-gravel bars. *Science of The Total Environment*, 152992.

Kondolf, G. M. (1997). PROFILE: Hungry Water: Effects of Dams and Gravel Mining on River Channels. *Environ Manage, 21*(4), 533-551. doi:10.1007/s002679900048

Kondolf, G. M., J. Toby Minear. (2004). *Coarse Sediment Augmentation on the Trinity River Below Lewiston Dam:*

Geomorphic Perspectives and Review of Past Projects. Retrieved from California, USA:

Kondolf, G. M., & Wolman, M. G. (1993). The sizes of salmonid spawning gravels. *Water Resources Research, 29*(7), 2275-2285.

Koshiba, T., Miura, S., & Sumi, T. (2022). Study on the Koshibu Dam sediment bypass tunnel operation based on sediment transport monitoring in upstream reaches. *E3S Web of Conferences, 346*, 03013. doi:10.1051/e3sconf/202234603013

Krause, A. (2012). *History of Mechanical Sediment Augmentation and Extraction on the Trinity River, California, 1912 – 2011.* Retrieved from Weaverville, California:

Lageweg, W. I., Schuurman, F., Cohen, K., Van Dijk, W., Shimizu, Y., & Kleinhans, M. (2015). Preservation of meandering river channels in uniformly aggrading channel belts. *Sedimentology*, n/a-n/a. doi:10.1111/sed.12229

Lakra, W. S., Sarkar, U. K., Kumar, R. S., Pandey, A., Dubey, V. K., & Gusain, O. P. (2010). Fish diversity, habitat ecology and their conservation and management issues of a tropical River in Ganga basin, India. *The Environmentalist, 30*(4), 306-319. doi:10.1007/s10669-010-9277-6

Le Coz, J., Hauet, A., Pierrefeu, G., Dramais, G., & Camenen, B. (2010). Performance of image-based velocimetry (LSPIV) applied to flash-flood discharge measurements in Mediterranean rivers. *Journal of Hydrology, 394*(1-2), 42-52.

Leitão, J. P., Peña-Haro, S., Lüthi, B., Scheidegger, A., & de Vitry, M. M. (2018). Urban overland runoff velocity measurement with consumer-grade surveillance cameras and surface structure image velocimetry. *Journal of Hydrology, 565*, 791-804.

Lewis, Q. W., & Rhoads, B. L. (2015). Resolving two‐dimensional flow structure in rivers using large‐scale particle image velocimetry: An example from a stream confluence. *Water Resources Research, 51*(10), 7977-7994.

Ligon, F. K., Dietrich, W. E., & Trush, W. J. (1995). Downstream Ecological Effects of Dams: A geomorphic perspective. *BioScience, 45*(3), 183-192. doi:10.2307/1312557

Lin, J., Kantoush, S. A., Sumi, T., & Takemon, Y. (2021). COMPREHENSIVE ASSESSMENT OF SEDIMENT REPLENISHMENT IN NAKA RIVER: HYDROLOGICAL, MORPHOLOGICAL, AND ECOLOGICAL PERSPECTIVES. *土木学会論文集 B1（水工学）, 77*(2), I_379-I_384. doi:10.2208/jscejhe.77.2_I_379

Linares, M. (2007). Two-dimensional numerical modelling of bed load transport and fluvial morphology. Validation on two sites on the Loire river and on the Arc river.

Lo, T. S., L'Vov, V. S., Pomyalov, A., & Procaccia, I. (2005). Estimating von Kármán's constant from homogeneous turbulence. *Europhysics Letters (EPL), 72*(6), 943-949. doi:10.1209/epl/i2005-10323-8

Maddock, I. (1999). The importance of physical habitat assessment for evaluating river health. *Freshwater biology, 41*(2), 373-391.

Matsushima, K., Hyodo, M., Shibata, N., & Shimizu, Y. (2018). Effectiveness of Flexible Dam Operation and Sediment Replenishment at Managawa Dam, Japan. *Journal of Disaster Research, 13*(4), 691-701.

McCuen, R., Knight, Z., & Cutter, A. (2006). Evaluation of the Nash–Sutcliffe Efficiency Index. *Journal of Hydrologic Engineering - J HYDROL ENG, 11*. doi:10.1061/(ASCE)1084-0699(2006)11:6(597)

Mendoza, A., Abad, J. D., Langendoen, E. J., Wang, D., Tassi, P., & Abderrezzak, K. E. K. (2017). Effect of Sediment Transport Boundary Conditions on the Numerical Modeling of Bed Morphodynamics. *Journal of Hydraulic Engineering, 143*(4), 04016099. doi:doi:10.1061/(ASCE)HY.1943-7900.0001208

Miyagawa, Y., Sumi, T., Takemon, Y., & Kobayashi, S. (2017). Effects of sediment replenishment on riverbed material size distribution and attached algal biomass in the downstream reaches of a dam. *Hydrological Research Letters, 11*(2), 114-120. doi:10.3178/hrl.11.114

Molon, D. A. M. (2019). HyMoCARES Project.

Morgan, J. A. (2018). *Effects of sediment supply, width variations, and unsteady flow on riffle-pool dynamics, The.* Colorado State University,

Mörtl, C., & De Cesare, G. (2021). Sediment Augmentation for River Rehabilitation and Management—A Review. *Land, 10*(12), 1309. Retrieved from https://www.mdpi.com/2073-445X/10/12/1309

Ock, G., Gaeuman, D., McSloy, J., & Kondolf, G. M. (2015). Ecological functions of restored gravel bars, the Trinity River, California. *Ecological Engineering, 83*, 49-60.

Ock, G., Kondolf, G., Takemon, Y., & Sumi, T. (2013). Missing link of coarse sediment augmentation to ecological functions in regulated rivers below dams: Comparative approach in Nunome River, Japan and Trinity River, California, US. *Advances in River Sediment Research*, 1531-1538.

Ock, G., Sumi, T., & Takemon, Y. (2013). Sediment replenishment to downstream reaches below dams: implementation perspectives. *Hydrological Research Letters, 7*(3), 54-59. doi:10.3178/hrl.7.54

Ock, G., & Takemon, Y. (2010). Estimation of transport distance of fine particulate organic matter in relation to channel morphology in tailwaters of the Lake Biwa and reservoir dams. *Landscape and Ecological Engineering, 6*(2), 161-169. doi:10.1007/s11355-009-0099-y

Okano, M., Kikui, M., Ishida, H., & Sumi, T. (2004). *Reservoir sedimentation management by coarse sediment replenishment below dams.* Paper presented at the Proceedings of the Ninth International Symposium on River Sedimentation.

Overzee, H., & Rijnsdorp, A. (2014). Effects of fishing during the spawning period: implications for sustainable management. *Reviews in Fish Biology and Fisheries, 25*. doi:10.1007/s11160-014-9370-x

Panel, G. A. (2005). Key uncertainties in gravel augmentation: geomorphological and biological research needs for effective river restoration.

Paquier, A., Chardon, V., Schmitt, L., Piégay, H., Arnaud, F., Serouilou, J., . . . Rivière, N. (2018). Geomorphic effects of gravel augmentation on the Old Rhine River downstream from the Kembs dam (France, Germany). *E3S Web of Conferences, 40*. doi:10.1051/e3sconf/20184002028

Pasternack, G. B., Wang, C. L., & Merz, J. E. (2004). Application of a 2D hydrodynamic model to design of reach-scale spawning gravel replenishment on the Mokelumne River, California. *River Research and Applications, 20*(2), 205-225. doi:10.1002/rra.748

Pavlíček, M., & Bruland, O. (2019). *Numerical modelling of flash flood event in steep river using Telemac 2D and Sisyphe.* Paper presented at the XXVIth TELEMAC-MASCARET User Conference, 15th to 17th October 2019, Toulouse.

Rinaldi, M., Mengoni, B., Luppi, L., Darby, S. E., & Mosselman, E. (2008). Numerical simulation of hydrodynamics and bank erosion in a river bend. *Water Resources Research, 44*(9). doi:10.1029/2008wr007008

Rinaldi, M., Surian, N., Comiti, F., & Bussettini, M. (2013). A method for the assessment and analysis of the hydromorphological condition of Italian streams: The Morphological Quality Index (MQI). *Geomorphology, 180-181*, 96-108. doi:10.1016/j.geomorph.2012.09.009

Schleiss, A. J., Franca, M. J., Juez, C., & De Cesare, G. (2016). Reservoir sedimentation. *Journal of Hydraulic Research, 54*(6), 595-614. doi:10.1080/00221686.2016.1225320

Shannon, C. E. (2001). A mathematical theory of communication. *ACM SIGMOBILE mobile computing and communications review, 5*(1), 3-55.

Sheng, J., Meng, H., & Fox, R. (2000). A large eddy PIV method for turbulence dissipation rate estimation. *Chemical engineering science, 55*(20), 4423-4434.

Sklar, L., Fadde, J., Venditti, J., Nelson, P., Wydzga, M., Cui, Y., & Dietrich, W. (2009). Translation and dispersion of sediment pulses in flume experiments simulating gravel augmentation below dams. *Water Resour. Res, 45*. doi:10.1029/2008WR007346

Sklar, L. S., Fadde, J., Venditti, J. G., Nelson, P., Wydzga, M. A., Cui, Y., & Dietrich, W. E. (2009). Translation and dispersion of sediment pulses in flume experiments simulating gravel augmentation below dams. *Water Resources Research, 45*(8). doi:https://doi.org/10.1029/2008WR007346

Staentzel, C., Kondolf, G. M., Schmitt, L., Combroux, I., Barillier, A., & Beisel, J.-N. (2020). Restoring fluvial forms and processes by gravel augmentation or bank erosion below dams: A systematic review of ecological responses. *Science of The Total Environment, 706*, 135743. doi:https://doi.org/10.1016/j.scitotenv.2019.135743

Stahly, S., Franca, M. J., Robinson, C. T., & Schleiss, A. J. (2019). Sediment replenishment combined with an artificial flood improves river habitats downstream of a dam. *Sci Rep, 9*(1), 5176. doi:10.1038/s41598-019-41575-6

Stoesser, T., Ruether, N., & Olsen, N. R. B. (2010). Calculation of primary and secondary flow and boundary shear stresses in a meandering channel. *Advances in Water Resources, 33*(2), 158-170. doi:https://doi.org/10.1016/j.advwatres.2009.11.001

Sumi, T., & Kantoush, S. (2011). Sediment management strategies for sustainable reservoir. In *Dams and Reservoirs under Changing Challenges* (pp. 353-362).

Sumi, T., & Kantoush, S. A. (2010). *Integrated management of reservoir sediment routing by flushing, replenishing, and bypassing sediments in Japanese river basins.* Paper presented at the Proceedings of the 8th International Symposium on Ecohydraulics, Seoul, Korea.

Sun, X., Shiono, K., Chandler, J. H., Rameshwaran, P., Sellin, R., & Fujita, I. (2010). *Discharge estimation in small irregular river using LSPIV.* Paper presented at the Proceedings of the Institution of Civil Engineers-Water Management.

Takechi, H., Aragaki, S., & Irie, M. (2021). Differentiation of River Sediments Fractions in UAV Aerial Images by Convolution Neural Network. *Remote Sensing, 13*(16), 3188. Retrieved from https://www.mdpi.com/2072-4292/13/16/3188

Talmon, A., Struiksma, N., & Van Mierlo, M. (1995). Laboratory measurements of the direction of sediment transport on transverse alluvial-bed slopes. *Journal of Hydraulic Research, 33*(4), 495-517.

Vonwiller, L., Vetsch, D., & Boes, R. (2018). Modeling Streambank and Artificial Gravel Deposit Erosion for Sediment Replenishment. *Water, 10*(4). doi:10.3390/w10040508

Wheaton, J. M., Pasternack, G. B., & Merz, J. E. (2004). Spawning habitat rehabilitation - II. Using hypothesis development and testing in design, Mokelumne river, California, U.S.A. *International Journal of River Basin Management, 2*(1), 21-37. doi:10.1080/15715124.2004.9635219

Xiao, Y., Zhou, G., & Yang, F. (2016). 2D numerical modelling of meandering channel formation. *Journal of Earth System Science, 125*(2), 251-267.

Xu, J., Ling, Y., & Zheng, X. (2015). *Forensic detection of Gaussian low-pass filtering in digital images.* Paper presented at the 2015 8th International Congress on Image and Signal Processing (CISP).

Yassine, R., Cassan, L., Roux, H., Frysou, O., & Pérès, F. (2022). Numerical modelling of the evolution of a river reach with a complex morphology to help define future sustainable restoration decisions. *Earth Surf. Dynam. Discuss., 2022*, 1-31. doi:10.5194/esurf-2021-91

List of Publications

Journal papers:

Lin, J., Kantoush, S. A., Sumi, T., & Takemon, Y. (2021). Comprehensive Assessment of Sediment Replenishment in Naka River: Hydrological, Morphological, and Ecological Perspectives. Journal of Japan Society of Civil Engineers, Ser. B1 (Hydraulic Engineering), 77(2), I_379-I_384.

Lin, J., Kantoush, S. A., Sumi, T., & Al-mamari, M. (2022). Real-time measurements of surface flow velocity, turbulence, and depth distribution during sediment replenishment implementation in the Naka River, Japan. Journal of Flow Measurement and Instrumentation. (under review)

International conference:

Sumi, T, Lin, J., & Kantoush, S. A. (2021). Comprehensive Assessment Approach on Sediment Replenishment below dams in Japan. International Symposium on Bedload Management, online, Nov 8-10 , 2021.

Domestic conference:

Lin, J., Kantoush, S. A., Sumi, T., & Takemon, Y. (2021). Comprehensive Assessment of Sediment Replenishment in Naka River: Hydrological, Morphological, and Ecological Perspectives. 第66回水工学講演会, Session of Flood Damage Risk of River Channel, December, 9, 2021.

Lin, J., Kantoush, S. A., Sumi, T., & Takemon, Y. (2022). Comprehensive Assessment of Sediment Replenishment in Naka River: Hydrological, Morphological, and Ecological Perspectives. DPRI Annual Meeting 2022.

Appendix A: Background of TELEMAC-2D and Gaia

A.1 Background of TELEMAC-2D

A.1.1 Governing equations

- Continuity equation

$$\frac{\partial h}{\partial t} + u \cdot \nabla(h) + h div(u) = S_h \qquad (A-1)$$

- Momentum equations

Along x direction:

$$\frac{\partial u}{\partial t} + u \cdot \nabla(u) = -g\frac{\partial Z}{\partial x} + S_x + \frac{1}{h} div(h v_t \nabla u) \qquad (A-2)$$

Along y direction:

$$\frac{\partial v}{\partial t} + u \cdot \nabla(v) = -g\frac{\partial Z}{\partial y} + S_y + \frac{1}{h} div(h v_t \nabla v) \qquad (A-3)$$

- Tracer conservation

$$\frac{\partial T}{\partial t} + u \cdot \nabla(T) = S_T + \frac{1}{h} div(h v_T \nabla T) \qquad (A-4)$$

In which:

- h is water depth (m),
- u, v are velocity components (m/s),
- T is passive (non-buoyant) tracer (g/l, ℃ or no unit),
- g is gravity acceleration (m/s^2),
- v_t, v_T are momentum and tracer diffusion coefficients (m^2/s),
- Z is free surface elevation (m),
- t is time (s),
- x, y are horizontal space coordinates,
- S_h is source or sink of fluid (m/s),

- S_T is source or sink of tracer (g/l/s),
- S_x, S_y are source terms representing the wind, Coriolis force, bottom friction, a source or a sink of momentum within the domain.

A.1.2 Friction law

- Equation of friction velocity

$$\mathrm{US} = \sqrt{\frac{1}{2} C_f (u^2 + v^2)} \qquad (A-5)$$

in which, the C_f can be calculated based on different friction laws. In this study, we utilized Manning friction law:

$$C_f = \frac{2gn^2}{H^{\frac{1}{3}}} \qquad (A-6)$$

In which, n is the Manning coefficient.

A.1.3 Time step management

In TELEMAC-2D, the time step can be defined as fixed or variable.

For fixed mode, the time step maintains the same during the computation.

For variable mode, the time step is varied, which is controlled by the desired courant number (CFL):

$$\mathrm{CFL} = \mathrm{V}\frac{\Delta t}{\Delta x} \qquad (A-7)$$

In which, V is the velocity magnitude, Δt is the time step, and Δx is the mesh size. The desired courant number is set to 1 to maintain the model's stability.

A.2 Background of Gaia

A.2.1 Bedload transport

The dimensionless current-induced sediment transport rate Φ_b is expressed by:

$$\Phi_b = \frac{Q_b}{\sqrt{g(s-1)d^3}} \qquad (A-8)$$

In which $s = \rho_s/\rho$ the relative density; ρ_s is the sediment density (kg/m^3); ρ is the water density (kg/m^3); d is the sand grain diameter (m) (equals to D50).

The Φ_b can be calculated based on different bedload transported formulas. In this study, we selected van Rijin's formula:

$$\Phi_b = 0.053 D_*^{-0.3} \left(\frac{\theta - \theta_{cr}}{\theta_{cr}}\right)^{2.1} \qquad (A-9)$$

In which, the D_* is the non-dimensional diameter:

$$D_* = \mathrm{d}\left[\frac{\left(\frac{\rho_s}{\rho} - 1\right) g}{\upsilon^2}\right]^{\frac{1}{3}} \qquad (A-10)$$

In which, the υ is the water viscosity.

The θ_{cr} is the critical shield parameter, which is defined manually. And the θ is the shields number:

$$\theta = \frac{\mu\tau_b}{(\rho_s - \rho)gd} \qquad (A-11)$$

In which τ_b is the bed shear stress, which can be calculated based on the friction velocity in Eq. A-5:

$$\tau_b = \rho \cdot US^2 \qquad (A-12)$$

The μ is the correction factor for skin friction, which is explained later.

A.2.2 Modification of the magnitude and direction of bedload

- Correction of the direction of the sediment transport

The angle α is the angle between the sediment transport direction and the x-axis direction will deviate from that of the shear stress by the combined action of a transverse slope and secondary currents:

$$\tan\alpha = \frac{sin\delta - \frac{1}{f(\theta)}\frac{\partial z_b}{\partial y}}{cos\delta - \frac{1}{f(\theta)}\frac{\partial z_b}{\partial x}} \qquad (A-13)$$

In which, the $\frac{\partial z_b}{\partial x}$ and $\frac{\partial z_b}{\partial y}$ represent the transverse and longitudinal slopes respectively. z_b is the bottom elevation.

δ is the angle between the sediment transport vector and the flow direction. In the curved channel, the direction of the sediment transport will not flow the direction of bed shear stress, due to the effect of secondary flows:

$$\delta = \tan^{-1}\left(\frac{v}{u}\right) - tan^{-1}\left(\frac{A}{r_s}h\right) \qquad (A-14)$$

In which, the r_s is the local radius of curvature, and A is the spiral flow coefficient, which is equal to 7 in this study.

$f(\theta)$ is the sediment shape function, which can be calculated by shields parameter θ based on Talmon, Struiksma, and Van Mierlo (1995):

$$f(\theta) = \beta_2\sqrt{\theta} \qquad (A-15)$$

Where β_2 is the empirical coefficient for deviation.

- Correction of the magnitude of the sediment transport

The correction of the magnitude is derived based on the modification of the bedload transport rate Q_b by a factor (Flokstra & Koch, 1980):

$$Q_b^* = Q_b\left[1 + \beta\left(\frac{\partial z_b}{\partial x}cos\alpha + \frac{\partial z_b}{\partial y}sin\alpha\right)\right] \qquad (A-16)$$

Where β is an empirical factor accounting for the streamwise bed slope effect (=1.3).

A.2.3 Influence of the roughness on sediment transport processes

The influence of the roughness on sediment transport processes is considered by the skin friction factor μ that is illustrated in Eq. A-11, which equals to:

$$\mu = \frac{C_f'}{C_f} \qquad (A-17)$$

Where C_f' is the friction coefficient due to skin friction:

$$C_f' = 2\left(\frac{\kappa}{\log\left(\frac{12h}{k_s'}\right)}\right)^2 \qquad (A-18)$$

In which κ is the von Kármán coefficient (=0.40). The roughness height $k_s' = \alpha_{k_s} d_{50}$, where α_{k_s} is the ratio between skin friction and mean diameter.

A.2.4 Suspended sediment transport

The suspended sediment transport is calculated by solving the 2D advection-diffusion equation:

$$\frac{\partial hC}{\partial t} + \frac{\partial hUC}{\partial x} + \frac{\partial hVC}{\partial y} = \frac{\partial}{\partial x}\left(h\varepsilon_s \frac{\partial C}{\partial x}\right) + \frac{\partial}{\partial y}\left(h\varepsilon_s \frac{\partial C}{\partial y}\right) + \mathrm{E} - \mathrm{D} \qquad (\mathrm{A}-19)$$

Where $\mathrm{C} = \mathrm{C}(\mathrm{x}, \mathrm{y}, \mathrm{t})$ is the depth-averaged concentration (g/l), (U,V) are the depth-averaged components of the velocity in the x and y directions. ε_s is the turbulent diffusivity of the sediment, which is related to the eddy viscosity $\varepsilon_s = v_t/\sigma_c$, with σ_c the Schmidt number.

The E and D are the erosion and deposition rate. For the non-cohesive sediment:

$$\mathrm{E} = \omega_s C_{eq} \qquad (A-20)$$

$$\mathrm{D} = \omega_s C_{z_{ref}} \qquad (A-21)$$

In which ω_s is the settling velocity. C_{eq} is the equilibrium near-bed concentration, which is determined by the van Rijn formula in this study:

$$C_{eq} = 0.015 d_{50} \frac{\left(\frac{\mu\theta}{\theta_{cr}} - 1\right)^{\frac{3}{2}}}{z_{ref} D_*^{0.3}} \qquad (A-22)$$

Where z_{ref} is the reference elevation, which is equal to $0.5 \times k_s$. k_s is the total roughness.

$C_{z_{ref}}$ is the near-bed concentration, which can be calculated by the depth-averaged concentration from a Rouse profile:

$$C_{z_{ref}} = FC \tag{A-23}$$

$$\mathrm{F}^{-1} = \begin{cases} \dfrac{1}{(1-Z)} B^{R}(1 - B^{1-R}) & if\ R \neq 1 \\ -BlogB & if\ R = 1 \end{cases} \tag{A-24}$$

$$\mathrm{R} = \frac{\omega_s}{\kappa u_*} \tag{A-25}$$

$$\mathrm{B} = \frac{z_{ref}}{h} \tag{A-26}$$

A.2.5 Bed evolution

The bed evolution is determined by solving the mass conservation equation for sediment:

$$(1-\lambda)\frac{\partial(z_b)}{\partial t} + \nabla \cdot Q_b + E - D = 0 \tag{A-27}$$

In which λ is the sediment porosity. z_b is the bed elevation.

Appendix B: Results of designed scenarios for SR optimization

B.1 Results of a single flood pulse combined with different grain sizes of SR material

Table B.1 The bed evolution volume in m^3 (a positive value means deposition, and a negative value means erosion).

Distance from SR site (km)	SC0-F	SC1-F	SC2-F	SC3-F	SC4-F	SC5-F
0-1	16008	15455	15510	14877	14721	13065
1-2	3804	4355	5460	6420	6903	6759
2-3	352	348	500	878	1185	1196
3-4	1073	1194	1740	2665	3042	3649
4-5	-1072	-1194	-1405	-1346	-1301	-1443
5-6	1047	1197	1551	2026	2506	3656
6-7	-5055	-4220	-3906	-3601	-3807	-4494
7-8	7245	7626	8182	8451	9016	9498
8-9	-6146	-7239	-8283	-9245	-9881	-10595
9-10	2141	1697	1662	1319	839	730
10-11	-2044	-2302	-2636	-3003	-3554	-4154
11-12	1224	2127	2658	3334	3608	3959
12-13	-2554	-4100	-4545	-4667	-4742	-4832

Distance from SR site (km)	SC-B	SC1-M	SC2-M	SC3-M	SC4-M	SC5-M
0-1	12621	13122	13762	13717	14134	14243
1-2	-3538	-3437	-3233	-3082	-3053	-3142
2-3	226	142	181	408	870	756
3-4	1003	1192	1669	2538	2866	3588
4-5	-1078	-1198	-1346	-1244	-1327	-1634
5-6	977	1151	1418	2031	2467	3575
6-7	-4602	-4244	-4013	-3735	-3947	-4430
7-8	7224	7561	8140	8469	8894	9173
8-9	-6122	-7211	-8249	-9168	-9920	-10619
9-10	2144	1773	1644	1335	975	792
10-11	-2207	-2368	-2736	-3145	-3741	-4421
11-12	1228	2111	2408	3387	3649	4028
12-13	-3467	-4002	-4645	-4622	-4718	-4892

Distance from SR site (km)	SC0-C	SC1-C	SC2-C	SC3-C	SC4-C	SC5-C
0-1	12179	12391	12301	12264	12750	12650
1-2	-3644	-3515	-3291	-3135	-3079	-3167
2-3	194	93	189	419	908	883
3-4	921	1167	1617	2453	2919	3486
4-5	-1075	-1296	-1400	-1327	-1388	-1671
5-6	1033	1169	1487	1965	2166	3457
6-7	-4617	-4292	-4107	-3771	-3644	-4319
7-8	7264	7529	8022	8499	8795	9023
8-9	-6114	-7176	-8241	-9162	-9927	-10732
9-10	2210	1841	1616	1345	1029	891
10-11	-2263	-2431	-2624	-3197	-3842	-4640
11-12	1213	2089	2366	3317	3644	4170
12-13	-3497	-4104	-4640	-4631	-4653	-4895

Table B.2 The BCI value

Distance from SR site (km)	SC0-F	SC1-F	SC2-F	SC3-F	SC4-F	SC5-F
0-1	0.0317	0.0265	0.0271	0.0211	0.0197	0.0042
1-2	0.0515	0.0553	0.0631	0.0698	0.0732	0.0722
2-3	0.0011	0.0011	0.0024	0.0058	0.0032	0.0032
3-4	0.0008	0.0021	0.0080	0.0181	0.0222	0.0288
4-5	0.0001	-0.0008	-0.0024	-0.0020	-0.0016	-0.0027
5-6	0.0005	0.0015	0.0039	0.0071	0.0104	0.0182
6-7	0.0036	0.0031	0.0057	0.0082	0.0211	0.0181
7-8	0.0002	0.0032	0.0077	0.0099	0.0144	0.0183
8-9	-0.0002	-0.0090	-0.0175	-0.0253	-0.0305	-0.0362
9-10	0.0000	-0.0034	-0.0037	-0.0063	-0.0100	-0.0108
10-11	0.0012	-0.0007	-0.0030	-0.0056	-0.0095	-0.0137
11-12	0.0000	0.0065	0.0104	0.0153	0.0173	0.0198
12-13	0.0050	-0.0035	-0.0059	-0.0066	-0.0070	-0.0077

Distance from SR site (km)	SC-B	SC1-M	SC2-M	SC3-M	SC4-M	SC5-M
0-1	-	0.0047	0.0107	0.0103	0.0142	0.0152
1-2	-	0.0007	0.0021	0.0032	0.0034	0.0028
2-3	-	-0.0014	-0.0012	-0.0002	0.0018	0.0013
3-4	-	0.0021	0.0072	0.0167	0.0203	0.0281
4-5	-	-0.0009	-0.0020	-0.0012	-0.0018	-0.0041
5-6	-	0.0012	0.0030	0.0071	0.0101	0.0176
6-7	-	0.0192	0.0202	0.0214	0.0205	0.0183
7-8	-	0.0027	0.0074	0.0100	0.0134	0.0157
8-9	-	-0.0088	-0.0172	-0.0247	-0.0308	-0.0364
9-10	-	-0.0028	-0.0038	-0.0062	-0.0090	-0.0104
10-11	-	-0.0011	-0.0037	-0.0066	-0.0108	-0.0156
11-12	-	0.0064	0.0086	0.0157	0.0176	0.0203
12-13	-	-0.0029	-0.0064	-0.0063	-0.0068	-0.0078

Distance from SR site (km)	SC0-C	SC1-C	SC2-C	SC3-C	SC4-C	SC5-C
0-1	-0.0041	-0.0021	-0.0030	-0.0033	0.0012	0.0003
1-2	-0.0007	0.0002	0.0017	0.0028	0.0032	0.0026
2-3	-0.0012	-0.0016	-0.0012	-0.0002	0.0020	0.0019
3-4	-0.0009	0.0018	0.0067	0.0158	0.0208	0.0270
4-5	0.0000	-0.0016	-0.0024	-0.0018	-0.0023	-0.0044
5-6	0.0004	0.0013	0.0035	0.0067	0.0081	0.0168
6-7	0.0175	0.0189	0.0198	0.0212	0.0218	0.0188
7-8	0.0003	0.0025	0.0064	0.0102	0.0126	0.0145
8-9	0.0001	-0.0085	-0.0172	-0.0246	-0.0308	-0.0374
9-10	0.0005	-0.0023	-0.0041	-0.0061	-0.0085	-0.0096
10-11	-0.0004	-0.0016	-0.0029	-0.0070	-0.0115	-0.0172
11-12	-0.0001	0.0062	0.0083	0.0152	0.0175	0.0214
12-13	-0.0002	-0.0035	-0.0064	-0.0064	-0.0065	-0.0077

Table B.3 The HMID value

Distance from SR site (km)	SC0-F	SC1-F	SC2-F	SC3-F	SC4-F	SC5-F
0-1	9.529	9.902	10.052	10.460	10.499	10.707
1-2	11.407	11.583	11.892	12.307	12.530	12.802
2-3	10.336	10.668	11.060	11.566	12.124	12.561
3-4	9.337	9.610	9.971	10.342	10.511	11.228
4-5	11.765	12.003	12.300	12.527	12.937	13.107
5-6	10.965	11.055	11.512	11.973	12.599	13.055
6-7	8.740	9.094	9.312	9.791	10.097	10.560
7-8	11.548	11.874	12.287	12.858	13.491	13.631
8-9	8.948	8.992	9.218	9.440	9.556	9.837
9-10	8.961	9.108	9.125	9.310	9.437	9.667
10-11	10.067	10.364	10.708	10.743	10.800	11.036
11-12	17.984	18.017	18.578	18.985	19.121	19.383
12-13	10.373	10.825	11.418	11.628	11.573	11.334

Distance from SR site (km)	SC-B	SC1-M	SC2-M	SC3-M	SC4-M	SC5-M
0-1	9.901	10.049	10.063	10.328	10.606	10.779
1-2	11.459	11.793	11.926	12.200	12.474	12.773
2-3	10.385	10.871	11.175	11.642	12.097	12.555
3-4	9.310	9.783	9.996	10.215	10.337	11.192
4-5	11.729	12.161	12.346	12.532	12.860	13.061
5-6	10.681	11.262	11.544	11.845	12.466	12.933
6-7	8.748	9.280	9.424	9.786	10.067	10.460
7-8	11.491	12.023	12.308	12.601	13.243	13.578
8-9	8.976	9.090	9.220	9.332	9.511	9.762
9-10	8.950	9.062	9.176	9.236	9.436	9.634
10-11	10.029	10.445	10.632	10.637	10.739	10.952
11-12	18.112	18.153	18.184	18.618	18.896	19.141
12-13	10.239	10.985	11.333	11.638	11.614	11.294

Distance from SR site (km)	SC0-C	SC1-C	SC2-C	SC3-C	SC4-C	SC5-C
0-1	9.781	9.922	10.113	10.400	10.483	10.681
1-2	11.452	11.593	11.843	12.137	12.383	12.644
2-3	10.408	10.641	11.055	11.520	12.088	12.462
3-4	9.316	9.557	9.882	10.175	10.345	11.169
4-5	11.726	11.996	12.216	12.508	12.859	13.039
5-6	10.963	11.038	11.405	11.861	12.109	12.787
6-7	8.743	9.095	9.298	9.815	10.033	10.395
7-8	11.400	11.746	12.160	12.635	13.106	13.348
8-9	8.973	8.965	9.097	9.355	9.470	9.711
9-10	8.962	9.063	9.067	9.224	9.444	9.552
10-11	10.021	10.274	10.574	10.592	10.658	10.859
11-12	18.061	17.979	18.006	18.438	18.720	18.890
12-13	10.507	10.828	11.247	11.473	11.602	11.304

B.2 Results of a double flood pulses

Table B.4 The bed evolution volume in m^3 (a positive value means deposition, and a negative value means erosion).

Distance from SR site (km)	SC2-F-20h	SC2-F-16H	SC2-F-12H
0-1	16441	16842	15616
1-2	7839	7117	7275
2-3	163	663	1204
3-4	2489	2224	2247
4-5	-1083	-849	-707
5-6	1859	1982	2260
6-7	-6130	-5768	-5081
7-8	9818	9170	8438
8-9	-8104	-7823	-8025
9-10	1943	2089	2140
10-11	-3071	-3141	-3138
11-12	4082	3969	4059
12-13	-3311	-3220	-3517

B.3 Results of the new replenishment arrangement

Table B.4 The bed evolution volume in m^3 (a positive value means deposition, and a negative value means erosion).

Distance from SR site (km)	SC-SR1-S	SC-SR1-D	SC-SR2-S	SC-SR2-D
0-1	16562	16853	25603	26341
1-2	3057	4936	15671	15767
2-3	-4	323	251	697
3-4	1464	1829	1339	1838
4-5	-1687	-1125	-1527	-1042
5-6	1240	1686	1250	1574
6-7	-4151	-5983	-4198	-5952
7-8	7705	9174	7828	9113
8-9	-8484	-7964	-8419	-7941
9-10	1603	1924	1483	1938
10-11	-2722	-3451	-2740	-3468
11-12	2419	3977	2388	3991
12-13	-4572	-4644	-4593	-4624